Predictive Model for a PV/Thermal Impinging Jet Solar Collector

by

Sébastien Athanase Brideau

A thesis
presented to the University of Waterloo
in fulfillment of the
thesis requirement for the degree of
Master of Applied Science
in
Mechanical Engineering

Waterloo, Ontario, Canada, 2010

AUTHOR'S DECLARATION

I hereby declare that I am the sole author of this thesis. This is a true copy of the thesis, including any required final revisions, as accepted by my examiners.

I understand that my thesis may be made electronically available to the public.

ABSTRACT

This thesis is a study of impinging jet PV/Thermal collectors. More specifically, the thesis deals with the development of a model for this type of collector and its validation.

The model developed for this thesis consists of a series of energy balances at every layer of the collector. The transient effects due to thermal mass of the different layers were taken into account. The resulting differential equations were solved using the backwards Euler method in an iterative manner.

The validation of the model was done using a prototype of the collector. The aperture area of the collector was 0.78m^2 and the PV cells covered 0.27m^2. The collector was tested on 8 different days between January 30th and March 31st 2010. The experiments were conducted with various weather conditions, and parameters (such as mass flow rate and inlet temperature). The data was taken every 0.5 seconds and averaged over 5 minutes.

In general, the model was found to work very well. For March 31st, the total modeled heat gain for the day was found to be within 2.1% of the experimental data. The PV electrical energy was found to be within 4.4% of the experimental results.

The model was also found to work well with longer time steps than 5 minutes. Furthermore, the model seemed to work relatively well without accounting for the transient effects due to thermal mass.

ACKNOWLEDGEMENTS

I am forever indebted for the help and support from many people.

To Christie, who has for the last few years been an ear to my frustrations, a foot to my behind and an incredible partner. Thank you for the support, and your help with building the collector.

To my supervisor, Pr. Michael Collins, who always was ready to help when I needed it. Thank you for giving me the great opportunity of doing research independently, and for trusting me. Thank you for letting me figure it out. I made mistakes, but I learned so much.

To Pr. Kyle Daun who granted me the status of honorary student in his lab. Thanks for your help, advice, and friendship.

To Andrew who never ceases to amaze me with great use of scholarly vocabulary and appropriate behaviour. Thank you for bringing the average IQ of this lab to immeasurable levels.

To all the members of the solar lab. Thanks for making this a fun place to work.

To Andy Barber who's helped a lot with different electrical and sensor problems I had. Thank you for always being willing to help.

À Véronique Deslisle, merci pour ton aide extraordinaire. Par ta thèse, ou par communication directe, tu m'as grandement simplifié la vie à plusieurs occasions.

DEDICATION

À ma famille. Votre support est toujours précieux.

TABLE OF CONTENTS

LIST OF FIGURES

LIST OF TABLES

NOMENCLATURE

A	Area, Nusselt number correlation coefficient
B	Nusselt number correlation coefficient
C	Specific heat (J/kg K)
C_D	Jet plate discharge coefficient
D	Diameter of holes (m)
g	Gravity (9.8 m/s^2)
G_c	Cross flow mass velocity on channel cross-sectional area (kg/s·m^2)
G_j	Jet mass velocity based on jet hole area (kg/s·m^2)
h	Heat transfer coefficient (W/m^2 K)
k	Conductivity of air (W/m K)
L_c	Characteristic length (m)
L	Length of collector (m)
$\dot{m}$	Air mass flow rate (kg/s)
m	Nusselt number correlation exponent
n	Nusselt number correlation exponent
N	Amount of discrete elements in x direction
Nu	Nusselt number
P	Electrical Power per collector area (W/m^2)
Pr	Prandtl number
r_r	Average recovery factor
Ra	Raleigh number
Re	Reynold's number
S	Incident solar radiation (W/m^2)
t	Time (s)
T	Temperature (K)
T_i	Impingement surface temperature (K)
T_j	Jet plenum temperature (K)
$T_{m,n}$	Mixed-mean total temperature over channel cross section (K)
U	Conductance (W/m^2)
w	Width of collector (m)
x	Distance along flow direction (m)
X_n	Distance between holes (m)

Z_{b1}	Distance between back plate and P_1 (m)
Z_n	Distance between P_1 and P_2 (m)
Z_{gP2}	Distance between glass cover and P_2 (m)
α	Absorptivity (solar spectrum), Thermal diffusivity (m^2/s)
α_n	Measured cell solar absorptivity at normal incidence
ß	Collector tilt angle (radians)
ß'	Inverse of average temperature of two parallel plates (K^{-1})
ε	Emissivity
η	Efficiency
η_r	Average fluid temperature difference influence factor
$\mu_{p,mp}$	PV max. power point temperature coefficient (%efficiency/°C)
μ	Dynamic viscosity (kg/m·s)
ρ	Density (kg/m^3), reflectivity
ρ_d	Reflectance of system for diffuse radiation from absorber plate
ν	Kinematic viscosity (m^2/s)
σ	Stefan-Boltzmann constant
τ	Transmissivity (solar spectrum)
(τα)	Transmittance-absorptance product
Φ	Nusselt number correlation coefficient

Subscripts and Superscripts

a	Ambient
B	Back of collector
beam	Beam solar radiation
c	Convection, Collector aperture
cond	Conduction
diffuse	Sky diffuse solar radiation
elec	PV electrical
f_2	Fluid between P_2 and P_1
f_1	Fluid between back and P_1
g	glass cover

ground	Ground reflected solar radiation
in	Air entering discrete element
mp	Maximum power point
out	Air leaving discrete element
P_2	Plate on which impinging takes place
P_1	Perforated plate
p	Power
pref	Reference power
pv	Photovoltaic cells
r	Radiation
s	PV cells
side	Side insulation
sky	Long-wave sky radiation
STC	Standard test conditions
w	Ambient wind or free convection
”	Previous element

Chapter 1
BACKGROUND INFORMATION

1.1 ENERGY AND ENVIRONMENTAL CONCERNS

In 2007, the Intergovernmental Panel on Climate Change (IPCC, 2007) published a report that stated that "warming of the climate system is unequivocal" and that "most of the global average warming over the past 50 years is *very likely* due to anthropogenic GHG increases". It also warned that "unmitigated climate change would, in the long term, be *likely* to exceed the capacity of natural, managed and human systems to adapt." In order to lower the amount of green house gases in the atmosphere, it is imperative to look for ways to reduce our energy consumption or move consumption to less polluting or more benign sources.

Another incentive to reducing our energy consumption is the rising cost of most forms of energy. In Canada, 16% of all energy used and 59% of the total residential energy consumption is spent on space heating (Natural Resources Canada, 2009). Small reductions in energy demands in this field can yield significant results in the overall reduction of energy use, and at the same time, green house gases. From Natural Resources Canada data on energy use, and knowing the approximate cost of the different types of energy, it can be calculated that approximately 16 billion dollars is spent every year in Canada on space heating for residential and commercial buildings. This means that even a small reduction in heating energy demand could yield hundreds of millions of dollars in savings.

Many things can be done to limit the space heating energy demand in buildings. Adequate insulation, an air tight enclosure, and keeping the window coverage to between 25%-40% ensure that the heat losses to the environment are minimal. However, no matter what is done, buildings in Canada will always need some energy for space heating.

One way to further reduce the energy demand from traditional, non-renewable sources is to employ solar thermal and solar electric technologies. Solar radiation can be converted to electricity with photovoltaic cells, or thermal energy with the use of solar collectors. Photovoltaic systems are expensive and much less efficient

than thermal systems, but they produce electricity, which is more valuable (versatile) than low temperature thermal energy.

At the end of 2007, it was estimated that there was a total of 0.544 km^2 of solar collectors installed in Canada, 0.385 km^2 of which was being used for residential pools heating (SAIC Canada, 2008). This accounts for 627×10^{12} J of energy produced by thermal systems. Unfortunately, this is equivalent to only 0.04% of the total space and water heating demand in Canada. In 2006, solar PV systems produced 76×10^{12} J of electricity, even less than the amount produced by thermal system. (International Energy Agency, 2009) In Canada, the potential for solar energy is still not exploited to the level it should be.

1.2 SOLAR ENERGY

1.2.1 SOLAR ENERGY FUNDAMENTALS

The earth is bombarded with an incredible 173×10^{15} W of solar radiation at every moment. Figure 1.1 shows a schematic of what happens to the sun's radiation when it reaches the earth. Roughly 55% (95×10^{15} W) of the total energy hitting the upper atmosphere directly reaches the oceans or land (51% is absorbed, 4% is reflected). Over a full year, this is equivalent to 3×10^{24} Joules of energy reaching the surface of the earth (land or water) with 900×10^{21} Joules hitting land. The Energy Information Administration (EIA) in the United States predicts a worldwide energy demand of 536×10^{18} Joules for year 2010. This means that there is 1680 times more solar energy hitting land in a year than there is demand for energy worldwide.

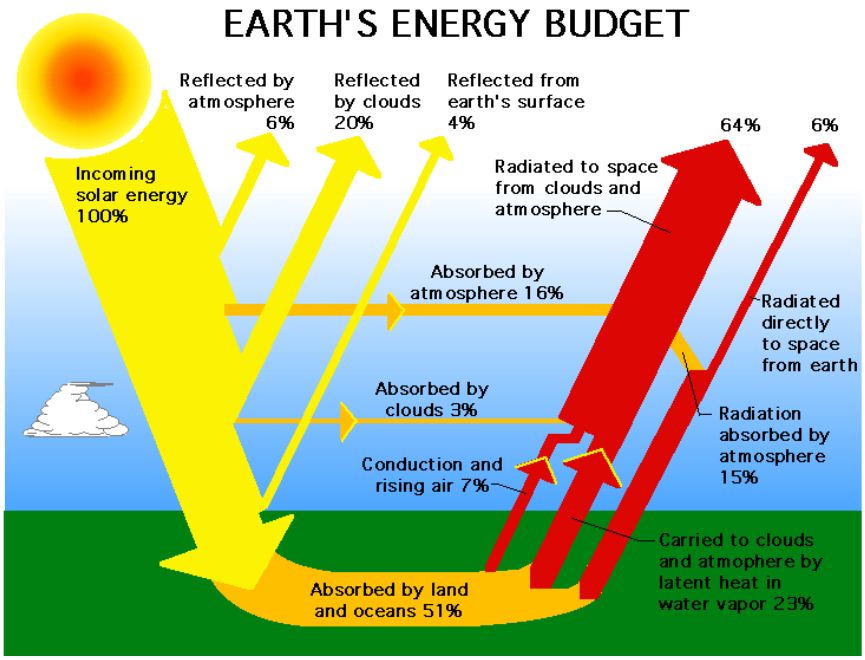

FIGURE 1.1 SCHEMATIC OF EARTH'S ENERGY BUDGET, SOURCE: NASA ASDC (2010)

1.2.2 THERMAL COLLECTORS

Solar thermal collectors are a means to convert sun radiation into thermal energy. There are many different types of solar collectors, each with different pros and cons.

Concentrating collectors, as seen in Figure 1.2, use mirrors to concentrate the solar radiation falling on a large area (the aperture) onto a small absorber plate. It is therefore possible to have a much smaller absorber plate area. They normally use a liquid as the heat transfer fluid, and it is possible to achieve very high temperatures. Concentrating collectors are very expensive and are normally used for special tasks, such as electricity production (through a turbine).

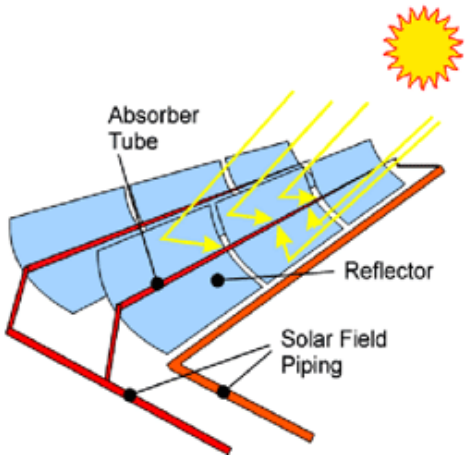

FIGURE 1.2 CONCENTRATING COLLECTORS, SOURCE: NREL (2010)

Flat plate collectors consist of a large absorber plate that is the same size as the aperture. Flat plate collectors are the simplest, cheapest, and most used type of collectors. This type of collector can use air or a liquid as the working fluid and they normally achieve moderate temperatures (up to 100°C above ambient temperature). Figure 1.3 and 1.4 show examples of water flat plate collectors and air flat plate collector.

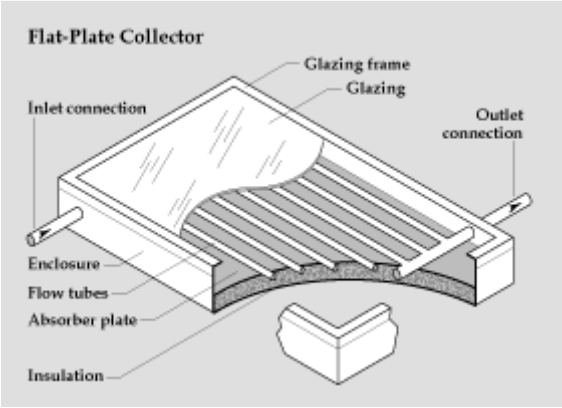

FIGURE 1.3 WATER FLAT PLATE COLELCTOR, SOURCE: U.S. DEPARTMENT OF ENERGY (2010)

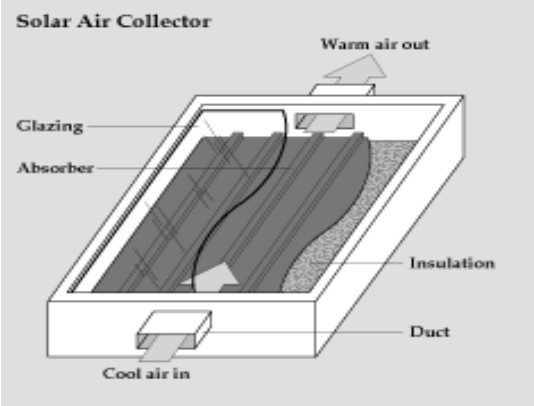

FIGURE 1.4 AIR FLAT PLATE COLLECTOR, SOURCE: U.S. DEPARTMENT OF ENERGY (2010)

Evacuated tube collectors, seen in Figure 1.5, consist of evacuated glass tubes in which absorbers are located. The heat transfer fluid is normally water with glycol. The evacuated glass tubes eliminate convective heat losses between the absorber and the cover, resulting in very low thermal losses, and they can therefore be very effective in cold weather or low sun radiation or for high temperature applications. In warmer weather, their efficiency can be slightly less than that of flat plate collectors.

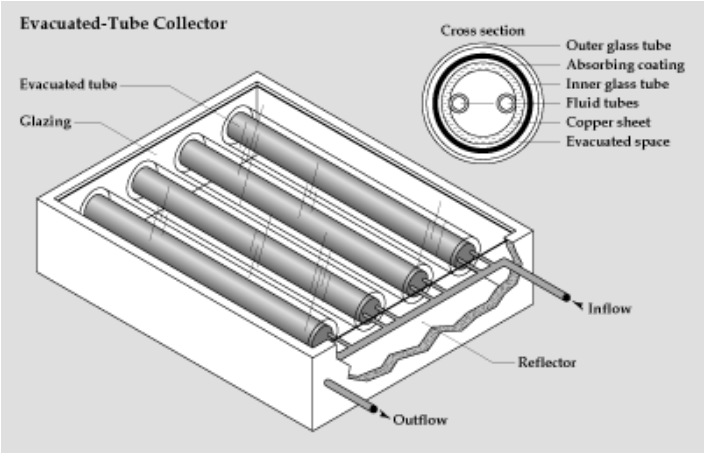

FIGURE 1.5 EVACUATED TUBE COLLECTOR, SOURCE: U.S. DEPARTMENT OF ENERGY (2010.A)

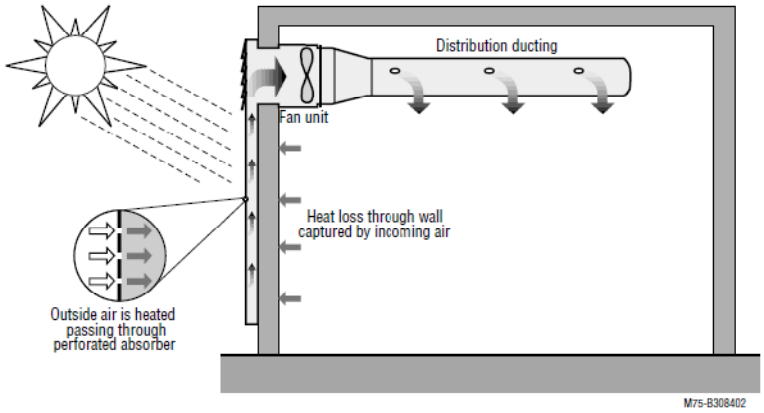

FIGURE 1.6 TRANSPIRED COLLECTOR, SOURCE: U.S. DEPARTMENT OF ENERGY (2010.B)

Transpired collectors (Figure 1.6) are large panels of dark, perforated, corrugated metal and are used like a cladding on a building. Air is driven by negative pressure, through the holes in the collector, between the wall and the cladding. The air picks up the heat from the collector, and is then blown through a HVAC system where it is either further heated, or blown directly in the space.

The type of solar thermal collector that this research focuses on is an air based flat plate collector.

1.2.3 FLAT PLATE AIR SOLAR COLLECTOR

Air based collectors are some of the most viable collectors available. They do not have the freezing, overheating or corrosion problems associated with water based collectors. Further, warm air from a collector can be used for crop drying, HVAC preheating, or space heating, and they can be installed fairly easily as a retrofit on a building's existing HVAC system or furnace ducts (in a house). They are, however, less efficient than water based collectors, and heat storage can be problematic.

A schematic of a typical air collector can be seen in Figure 1.7. Air flows between the back insulation and the absorber plate. The parallel flow air collectors have been studied extensively and a thorough discussion of how to analyze them can be found in Duffie and Beckman (2006). Figure 1.8 shows an impinging jet collector. The air comes in between the back insulation and the perforated plate, flows through the perforated plate, impinges on the absorber, and then flows out the rest

of the way between the absorber and the perforated plate. The latter configuration can achieve much higher heat transfer coefficients than parallel flow for the same flow rate. A simple impinging jet collector model was developed by Choudhury and Garg (1991) and Rask et al. (1977) were the first to experimentally study such collectors. Both studies showed an increase in efficiency compared to parallel plate collector, between 10 and 20% depending on the configuration, test conditions, and flow rate. Belusko et al (2007) modeled and tested an unglazed impinging collector where the jet impingement was induced by negative pressure and the absorber plate was corrugated. They found an increase of 21% in efficiency under typical conditions.

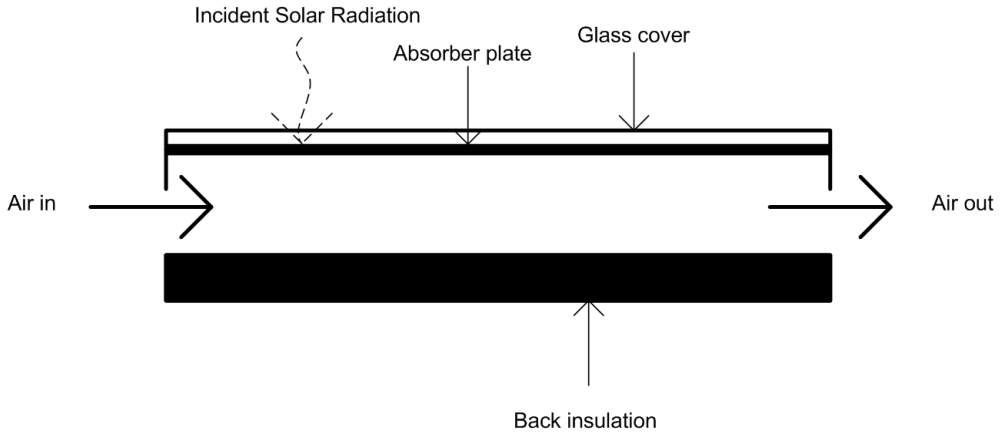

FIGURE 1.7 AIR PARALLEL FLOW COLLECTOR

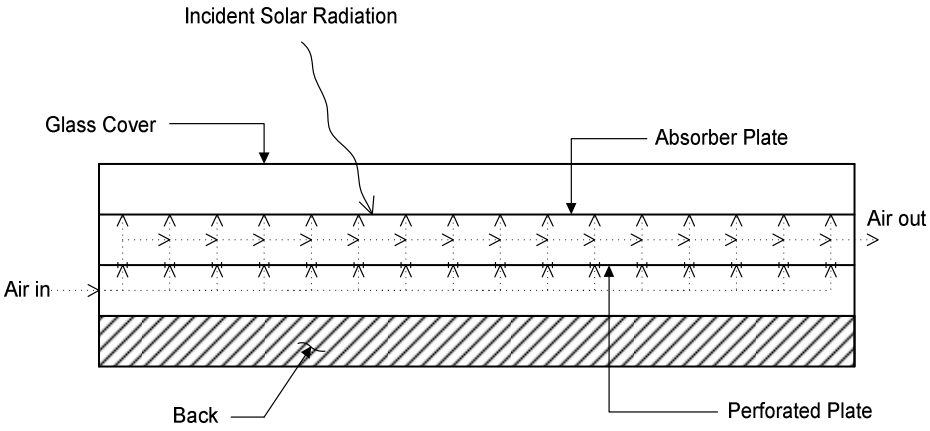

FIGURE 1.8 AIR IMPINGING JET COLLECTOR

1.2.4 PHOTOVOLTAIC (PV) CELLS

Photovoltaics convert the sun radiation to electricity. There are many types of PV cells; mono-crystalline silicon, poly-crystalline silicon, amorphous silicon, cadmium sulphite, dye sensitive etc. This research will focus on mono or poly-crystalline (Si) PVs.

Crystalline silicon photovoltaics are made of two semi conductors; an N-type and a P-type. When silicon is in a crystalline form, every silicon atom shares its four valence electrons with its four neighbours so that its outer shell becomes full with 8 electrons. By doping silicon with phosphorous atoms (which has 5 valence electrons) we obtain excess electrons, not in a bond, which are only held in place by the phosphorus nuclei. Those electrons are easily knocked loose from their nuclei. They are called free electrons. The result of doping silicon with phosphorus atoms is called an N-type semi-conductor.

If we instead dope the silicon with boron atoms, we get "holes". Boron atoms only have three valence electrons. There is one electron missing to complete the bonds with the four silicon atoms around the boron atom. The result of doping silicon with boron atoms is called a P-type semi-conductor.

When we put a N-type and a P-type semiconductor together, the free electrons close to the interface in the N-type, jump to the free holes, close to the interface in the P-type. This process forms a "barrier" making it difficult for the electrons to jump all the way over where there is a free hole. An electric field is created because the charge is imbalanced on both side of the junction.

When a photon enters the cell, it knocks loose an electron that had previously jumped from the N-type to the P-type. This electron jumps back to the N-type (leaving a hole in the P-type). Because of the electric field, the electron cannot jump back to the P-type. The electric field only allows electrons to flow from the P-type to the N-type. If you connect a load (a wire and a light bulb for example) from the N-type to the P-type, the electron will flow through it to get back in the hole on the P-type.

The current and voltage outputs of a photovoltaic cell are dependent on the load applied to the cell. This can be seen in Figure 1.9. Typically, the characteristics of PV cells and panels are plotted on a current vs. voltage graph (I-V curve). For different solar radiation intensity, the I-V curve will shift. Figure 1.9 shows three typical curves for a 65W panel at different radiation intensity. At every solar flux curve, it is possible to find the open circuit voltage, and the short circuit current of the panel. The open circuit voltage (V_{OC}) is the voltage at the point where the curve crosses the Voltage axis (when the current is 0). The short circuit current (I_{SC}) is the current at the point where the curve crosses the Current axis (where the voltage is 0).

The straight lines corresponding to different resistances dictate at what current and voltage the panel will operate at a given radiation intensity. For example, if a 4.18 ohm load is applied to the panel, it will operate at around 16V and 4A with a flux of 1000 W/m^2, 11V and 2.5A at 600W/m^2, and 4V and 0.9A at 200W/m^2. To maximize the power output of a PV panel, the perceived load by the panel must be equal to the ratio of V_{OC} over I_{SC}. This is called the maximum power point. In Figure 1.9 the maximum power points for 1000, 600, and 200 W/m^2 occur with loads of 4.18, 7.02, and 20.55 ohm respectively.

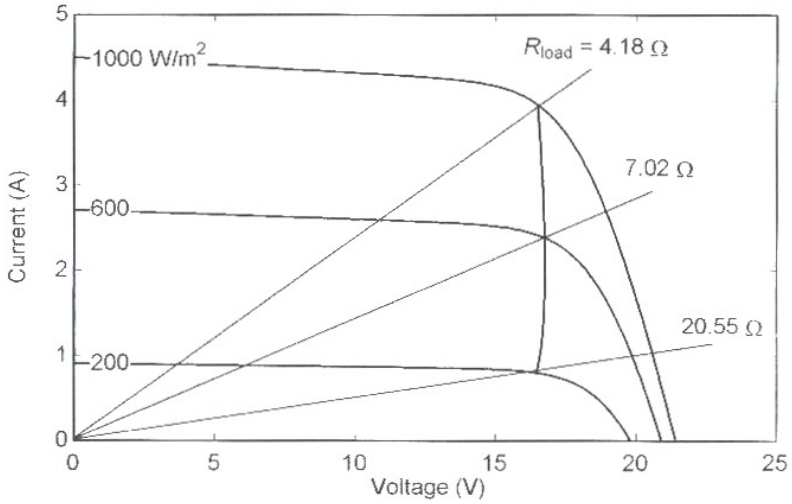

FIGURE 1.9 CURRENT VS VOLTAGE CURVE FOR PHOTOVOLTAIC MODULE, SOURCE: DUFFIE AND BECKMAN (2006)

Also affecting the performance of photovoltaic panels is the temperature of the panel. When the temperature of the panel increases, V_{OC} decreases, and I_{SC} increases slightly resulting in a lower maximum power point.

1.2.5 PV/THERMAL COLLECTORS

The next generation of solar thermal systems incorporates photovoltaic (PV) technologies. By replacing or augmenting absorber plates with photovoltaic cells, it may be possible to increase total solar conversion efficiency. When photovoltaic panels are exposed to the sun, they produce electricity. Due to their relatively low conversion efficiency, however, they also heat up. If this heat energy is collected, thereby cooling the PV cells, it is possible to increase the PV efficiency. The heat removed is then used in the same way as with a conventional collector. The PV/Thermal system can achieve better PV efficiency, but at a reduced thermal efficiency.

1.2.6 IMPINGING JET PV/THERMAL COLLECTOR

The impinging jet PV/Thermal flat plate collector studied in this thesis is very similar to an impinging jet thermal collector described earlier. It consists of five different layers (Figure 1.10): the glass cover, the PV, the layer on which the PV is glued (Plate 2 or P_2), the perforated plate (Plate 1 or P_1), and the back insulation. Depending on the configuration of the collector (PV coverage, opaque or transparent P_2), the designation of "absorber" could be given to P_1, P_2, or the PV cells. It will therefore be easier to refer to the different layers by the names given above and in Figure 1.10.

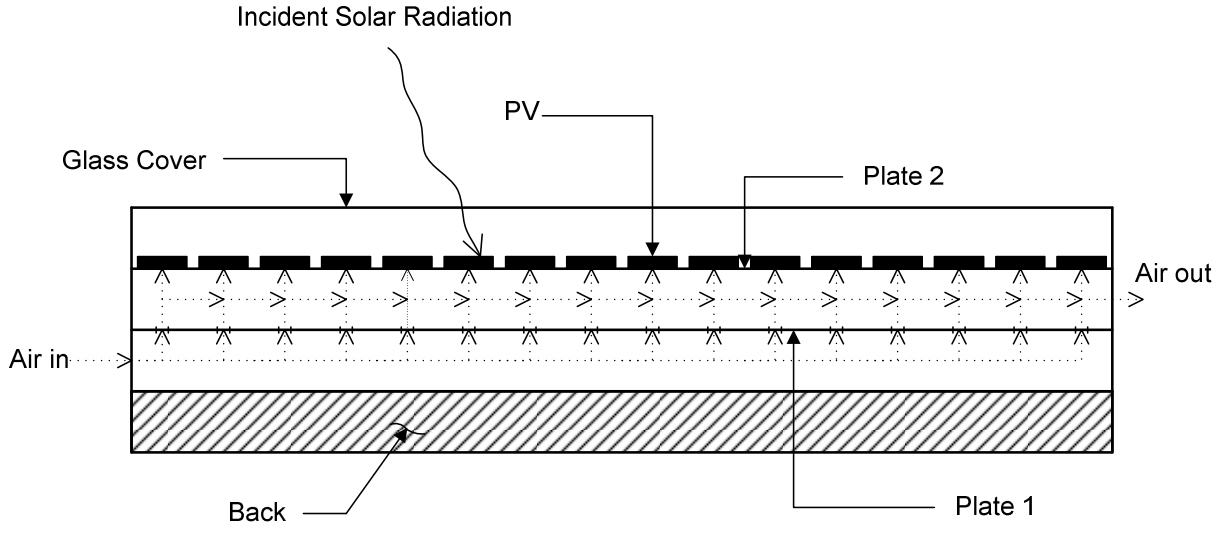

FIGURE 1.10 IMPINGING JET PV/THERMAL COLLECTOR

1.3 MOTIVATION AND OBJECTIVES

This research was motivated by Task 35 from the International Energy Agency (IEA). The task's objectives were to study PV/Thermal collectors and to help the market introduction of competitive PV/Thermal systems. Task 35 started in January 2005 and ended in December 2007. This research was inspired by the need to have more PV/Thermal models available to designers, and to get a better understanding of different types of PV/Thermal collectors.

The objectives of this research are:

- To develop a model for an impinging jet PV/Thermal air collector in TRNSYS,
- To build a prototype of this collector and test it, and
- To validate the model with experimental data.

1.4 OUTLINE

This thesis is divided in 6 chapters. Chapter 1 is the introduction.

Chapter 2 contains a literature review of relevant research. Models of thermal collectors are reviewed, as well as relevant heat transfer coefficients, and PV performance models.

Chapter 3 presents the mathematical model of the PV/Thermal impinging jet collector. The energy balance equations that make up the model are stated and a detailed explanation of the heat transfer coefficients used in the model is given.

Chapter 4 presents the experimental setup. Chapter 5 presents and compares results from the model and experiment. Chapter 6 contains the conclusion

Chapter 2
LITERATURE REVIEW

2.1 INTRODUCTION

Many books, papers, and technical reports that can be used to study impinging jets PV/Thermal collectors have been published. The following chapter is a review of the most applicable information found in the literature to this particular project.

Section 2.2 is a review of different studies on heat transfer modes applicable to impinging jet collectors. Section 2.3 looks at PV modeling studies. Section 2.4 is a review of studies on hybrid collectors. Section 2.5 looks at the few studies available on impinging jet thermal collectors. Finally, Section 2.6 reviews studies on transient effects in thermal collectors.

2.2 HEAT TRANSFER

2.2.1 IMPINGING HEAT TRANSFER

Heat transfer coefficients for an array of impinging jets have been studied extensively (Florschuetz et al. 1981, Kercher and Tabakoff 1970, Florschuetz and Su 1987, Metzger et al. 1979, Gao et al. 2005). These studies were primarily focused on impinging jets applications to cool down turbine blades. Figure 2.1 shows impinging jets with crossflow. In that figure, T_c is the crossflow temperature, T_j is the jet temperature, and T_s is the impinging surface temperature. When Nusselt number correlations were given, it was assumed that the temperature of the impinging fluid, and of the cross flow, were equal due to the fact that the impinging surface was of much higher temperature. If T_s is much larger than T_c and T_j, it can be assumed that T_c and T_j are the same. In collector applications, however, it is possible that T_s, T_j, and T_c, are all of similar value. This may cause errors because the basic assumptions used to formulate the aforementioned correlations are not correct.

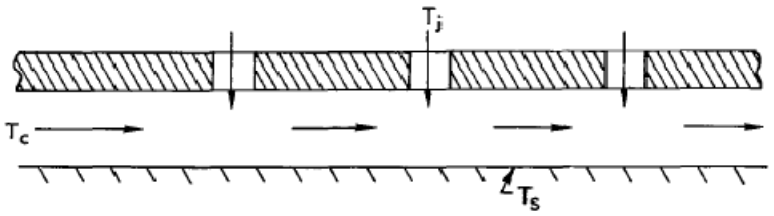

FIGURE 2.1 IMPINGING JET WITH CROSSFLOW, FLORSCHUETZ ET AL. (1982)

Florschuetz et al. (1981) studied heat transfer characteristics of impinging jets with crossflow. The impinged plate consisted of an array of rectangular electrical plate heaters arranged in the streamwise direction. Every heater was adjusted to give the proper amount of power so that the plate temperature was constant. Knowing the power, a heat transfer coefficient could be calculated. Most of the configurations provided a streamwise resolution of at least one streamwise hole spacing. In other words, there was at least one electrical plate heater per row of holes. Figure 2.2 shows a schematic of the apparatus with a resolution of one plate heater per row of holes. Figure 2.3 shows the same schematic with a resolution of three plate heaters per row of holes.

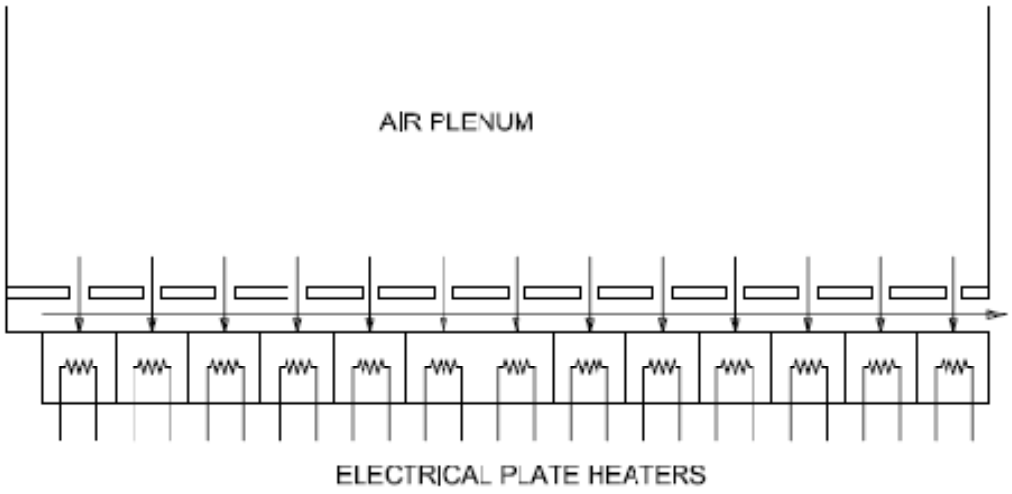

FIGURE 2.2 APPARATUS WITH RESOLUTION OF ONE PLATE HEATER PER ROW OF HOLES

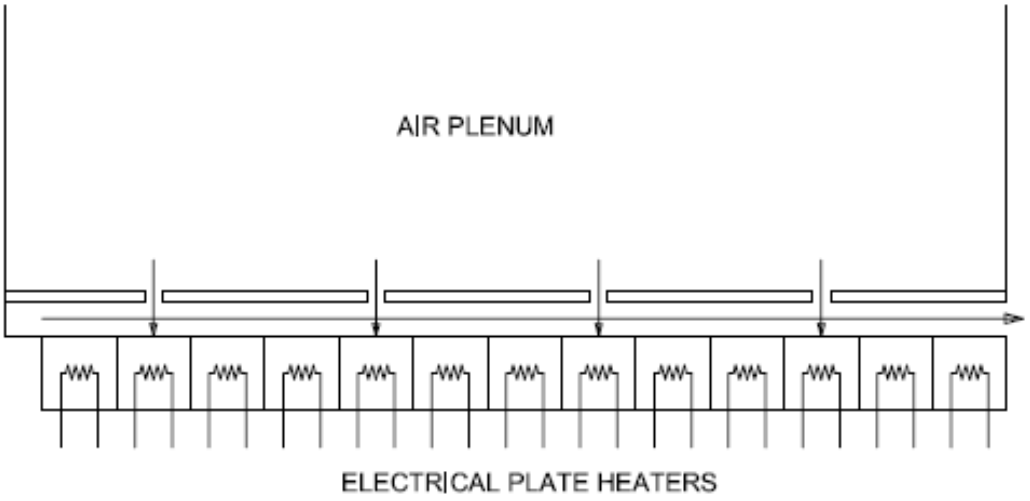

FIGURE 2.3 APPARATUS WITH RESOLUTION OF THREE PLATE HEATERS PER ROW OF HOLES

A Nusselt number correlation for inline and staggered jet patterns was derived based on experimental data, and a flow distribution model was derived analytically. The Nusselt number correlation is found to be

$$Nu = A\,Re_j^{\,m}\left\{1 - B\left[(Z_n/\mathrm{D})\left(G_c/G_j\right)\right]^n\right\}Pr^{1/3} \qquad (2.1)$$

Where A, m, B, and n can be found using tabulated data.

The derived flow distribution equation is

$$\frac{G_c}{G_j} = \frac{1}{\sqrt{2}\,C_d}\,\frac{\sinh\beta(x/X_n - 1/2)}{\cosh\beta(x/X_n)} \qquad (2.2)$$

Where $\beta = \frac{C_D\sqrt{2}(\pi/4)}{[(y_n/d)(z/d)]}$ and C_D is the hole discharge coefficient, and can be assumed to be roughly 0.8 for in-line pattern.

Kercher and Tabakoff (1970) conducted a similar experiment and gave their Nusselt number results in the form showed in Equation 2.3. They used a similar method as Florschetz et al., but the streamwise resolution was not as good. The variables in that equation are given graphically. The flow distribution was not studied analytically.

$$Nu = \phi_1 \phi_2 {Re_D}^m Pr^{1/3} \left(\frac{Z_n}{D}\right)^{0.091} \tag{2.3}$$

Useful conclusions were given:

- As the ratio of total hole area to total heat transfer area increases, the heat transfer coefficient also increases.
- The heat transfer is dominated by the hole diameter Reynolds number and the hole spacing to hole diameter ratio.
- Decreasing hole diameter with increasing number of holes (everything else being equal) improves heat transfer performances.

Florschuetz and Su (1987) studied the effects of crossflow temperatures on heat transfer and formulated the problem analytically. They also studied the effects of Reynolds number, crossflow to jet mass flux ratio, and geometric parameters on a fluid temperature difference factor and Nusselt number. They defined the problem with the following equation:

$$\bar{q} = \left(\frac{k}{D}\right) Nu \left[\left(T_i - T_j\right) - \eta_r \left(T_{m,n} - T_j\right) + (1 - r_r) \frac{\left(\frac{G_j}{\rho}\right)^2}{2c_p} \right] \tag{2.4}$$

Where η_r can be calculated by setting $\bar{q}$ to zero and r_r can be assumed to be 0.9. η_r was found by running an experiment with impingement surface insulated. The three temperatures were measured, and Equation 2.4 was applied to solve for η_r. The Nusselt number was then found by using electrical resistance heaters instead of insulated plates. This method can only be applied if an experiment has been conducted to solve for η_r.

Metzger et al. (1979) studied heat transfer characteristics for inline and staggered arrays of circular jets with crossflow of spent air. They experimentally studied first 10 rows of impinging jets and found local Nusselt numbers. They found that local Nusselt numbers varies periodically for the first 10 rows with the Nusselt number being highest in line with the holes, and the lowest halfway between two holes. The effects were diminished after about 10 rows.

More recently, Gao et al. (2005) used correlations by Florschuetz et al. and Kercher and Tabakoff on an array of linearly stretched holes (hole spacing changes streamwise). Gao found that the correlations matched experimental data fairly well, but that they over predict the Nusselt number at the first row of impinging holes, but underestimate at high Reynolds numbers or with large crossflow.

2.2.2 OTHER CONVECTIVE HEAT TRANSFER

The other types of convective heat transfer present in an impinging jet collector have also been studied extensively, and many correlations can be found in the literature.

From data by Kays and Crawford (1980), Duffie and Beckman (2006) derived a correlation for internal fully developed turbulent channel flow (between two plates) with one side heated and the other insulated (Equation 2.5). This correlation under predicts the actual Nusselt number when the ratio of the distance from the leading edge to the hydraulic diameter is less than 100 because of the effects of the entrance region. The correlation is normally used in air collectors when parallel flows are present.

$$Nu = 0.0158Re^{0.8} \tag{2.5}$$

Hollands et al. (1976) provided a correlation (based on experimental results) for free convection between two inclined plates (Equation 2.6). The correlation has 5% error between 0 and 60 degrees, 10% at 75 degrees. This correlation is normally used in collector analysis to calculate the heat transfer between the glass cover and the absorber plate, or between two covers.

$$Nu = \left[1 + 1.44\left[1 - \frac{1708(\sin 1.8\beta)^{1.6}}{Ra\cos\beta}\right]\left[1 - \frac{1708}{Ra\cos\beta}\right]^{+} + \left[\left(\frac{Ra\cos\beta}{5830}\right)^{\frac{1}{3}} - 1\right]^{+}\right] \qquad 2.6)$$

Duffie and Beckman (2006) have proposed equations for heat transfer between the cover and the surroundings. Sartori (2006) reviewed many correlations and papers on external flow over flat plate, including those found in Duffie and Beckman, and

found that flat plate collectors are generally subjected to fully turbulent flow because of the turbulent nature of the wind. Figure 2.4 shows the many different correlations that have been proposed and used to analyse thermal and PV collectors. The values for h differ greatly between certain correlations. Based on analytical (boundary layer theory) and experimental data, Sartori suggested correlations and compared them with other correlations found in the literature. Correlations were given for laminar, mixed, and turbulent regimes.

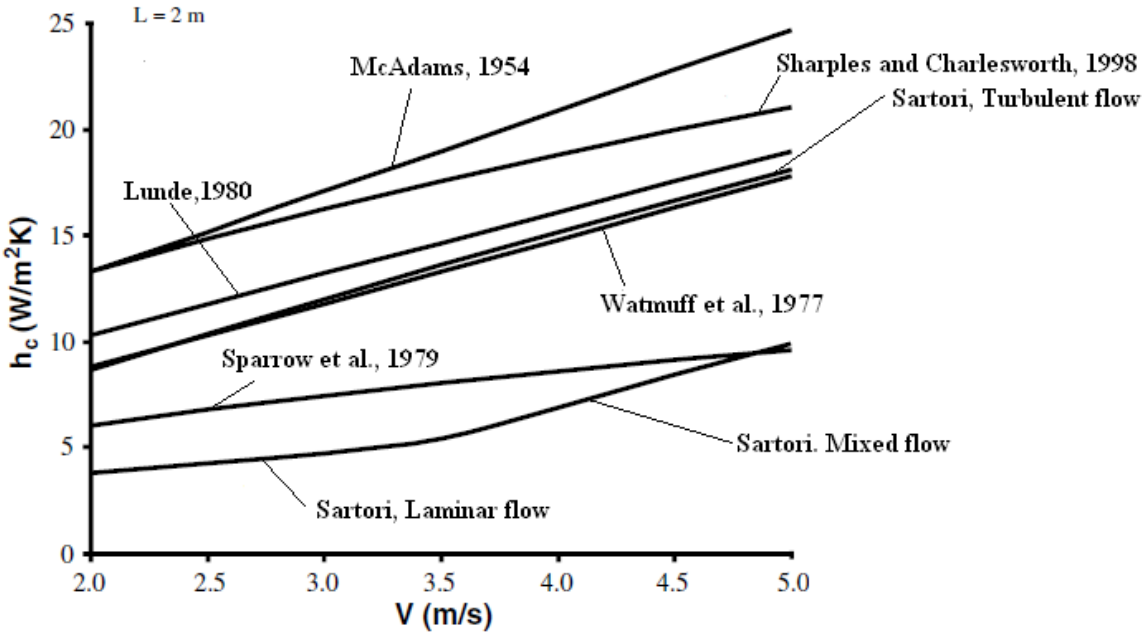

FIGURE 2.4 HEAT TRANSFER COEFFICIENTS COMPARISON (ORIGINAL FIGURE BY SARTORI, 2006)

The following equation is the fully turbulent correlation suggested by Sartori for use with collectors.

$$h_{forced\ conv} = 5.74V^{0.8}L^{-0.2} \tag{2.7}$$

Where V is the wind velocity in m/s and L is the length of the path of the wind on the collector. Sartori also found that the angle of the collector has very little effect on the heat transfer coefficient.

In the absence of significant wind, free convection will dominate the convective losses from the cover. This can be approximated by a correlation by Lloyd and Moran (1974) for a horizontal plate.

$$h_{free\ conv} = \frac{\overline{Nu}_{L_c} \cdot k}{L_c} = \frac{0.15 {Ra_{L_c}}^{1/3} \cdot k}{L_c} \tag{2.8}$$

2.3 PV CELLS MODELING

Some PV cell modeling approaches and assumptions can give very accurate results, while providing a more easily implemented solution methodology.

Duffie and Beckman (2006) explain that the maximum power point efficiency of a cell can be assumed to be linearly dependent on the temperature of the cell. A temperature coefficient of maximum power efficiency is easily approximated by knowing the reference efficiency, the maximum power point voltage, and the temperature coefficient of open circuit voltage.

In order to determine how much radiation is absorbed by the PV cells or modules, it is important to know the optical characteristics of the cells at different angles.

An analytical approach was used by Sjerps-Koomen et al. (1996) to model reflection losses of PV panels by taking into consideration every layer of the cover (three slab model, see Figure 2.5). They then compared the results with simplified modeling methods. These simplified methods include an air-glass approximation (where only the reflection losses at the air-glass interface are taken into account), the air-glass-air approximation developed for thermal collectors, but sometimes erroneously used for PV modules, and a model developed by ASHRAE (Standard 93) which is closer to a line fit than an analytical solution. It was found that the air-glass model and the three slab model give very similar results.

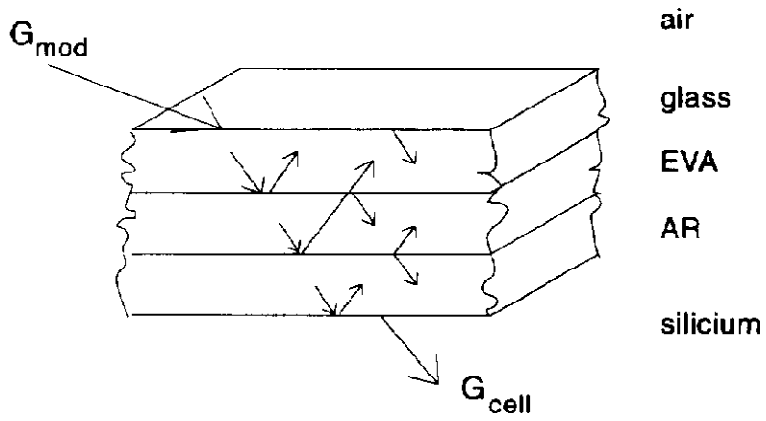

FIGURE 2.5 THREE SLAB MODEL SCHEMATIC (SJERPS-KOOMEN ET AL. 2006)

Parretta et al. (1999a) characterized the reflectivity of PV modules (mono-crystalline) experimentally at different angle of incidence with the use of an integrating sphere. The modules had flat or textured glass cover, anti-reflective coatings or not, and textured or flat silicon. The interface between the glass and EVA (encapsulant) was not taken into consideration, but when available, there was a mention of whether the interface was textured or not. They found that a relative transmittance (the ratio of transmittance at a given angle to transmittance at 0 degrees) can be approximated by that of a homogeneous semi-infinite dielectric material with a refractive index ranging between 2.5 and 3. The transmittance is taken as the transmittance of the module's cover. These models were derived by reflectance measurements on roughly 20 PV modules with incidence angles ranging between 0 and 70 degrees at a wavelength of 633 nm. Figure 2.6 shows the relative transmittance of different modules, while Figure 2.7 shows the relative transmittance for an air/dielectric interface at different dielectric refractive indices. It is possible to superimpose the dielectric curves with those of the different modules to look at the best fit.

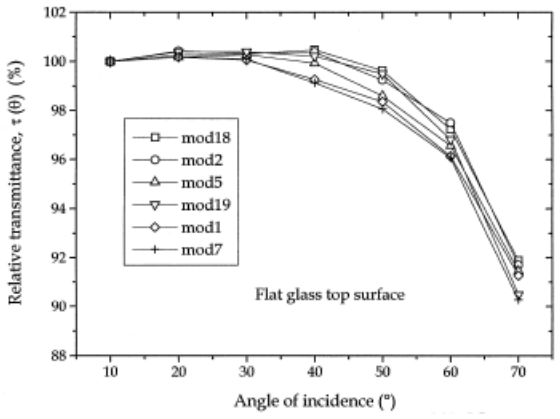

FIGURE 2.6 RELATIVE TRANSMITTANCE OF DIFFERENT MODULES (PARRETA ET AL. 1999A)

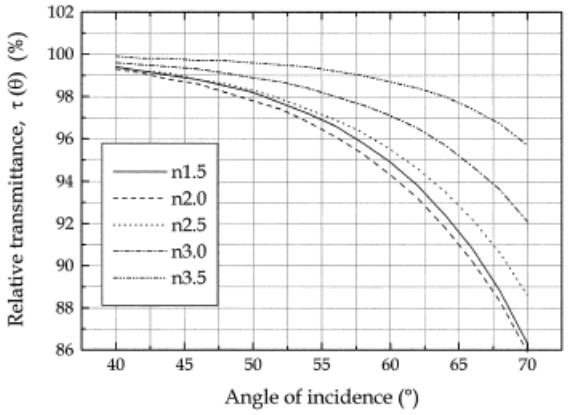

FIGURE 2.7 RELATIVE TRANSMITTANCE OF AIR-DIELECTRIC MATERIAL INTERFACE (PARRETA ET AL. 1999A)

Parretta et al. (1999b) characterized PV cells in the same manner as described above. The effect of the wire grid was removed so that only the silicone cell was characterized. Various silicon materials and solar cells were characterized: mono-Si samples of different surface treatments, screen printed monocrystalline silicon (c-Si) solar cells, PERL (passivated emitter, rear locally-diffused) cells, multicrystalline silicon honeycomb solar cells, and an encapsulated c-Si solar cell used to compare the effects of the glass cover. Anti reflective coatings were also considered. A silicon wafer with a TiO_2/SiO_2 - (450/950 Å) coating, and a textured (pyramids) silicon cell with anti reflective coating of TiO_2 (400 Å) were studied. Figure 2.8 shows experimental results for different silicon cells. From the data in this research, it is possible to calculate an approximate equivalent refractive index for all of these cells.

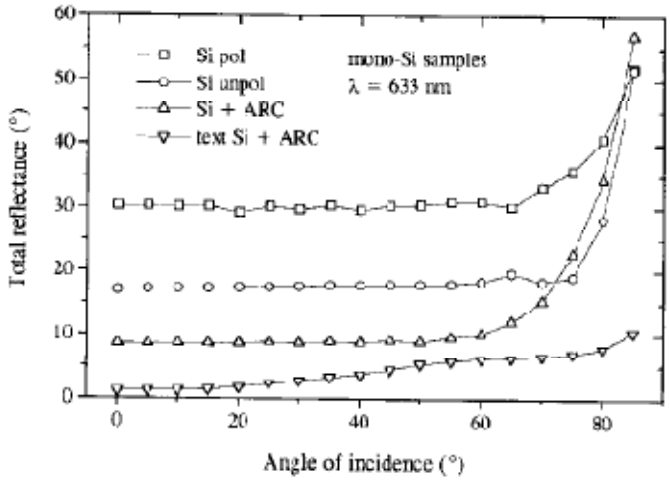

FIGURE 2.8 REFLECTANCE VS ANGLE OF INCIDENCE FOR DIFFERENT CELLS (PARRETA ET AL. 1999B)

De Soto et al. (2005) derived a model for PV modules based on equivalent electrical circuit, and optical properties modeled as a dielectric material with a thin glass cover. It uses data normally given by the manufacturer to model the performance of the cells. This model is more accurate but much more complex than the other models discussed here.

Parretta et al. (1998) analyzed and modeled the losses due to irradiation conditions compared to standard test conditions. The losses that were estimated are the reflection of unpolarized light, the spectrum, the intensity of the incident radiation, and the temperature of the module. They modeled some of these effects in a similar fashion as De Soto et al. Paretta et al. also recognized the effect of the polarization of incident radiation as another loss mechanism but could not easily model it as the polarization of light in the field is not known. Figure 2.9 shows the ratio of the actual efficiency over the efficiency at standard test condition (STC) for a monocrystalline cell vs. the irradiance. It can be seen that an irradiance level of 500 W/m^2 lowers the cell efficiency by roughly 5%, and 200 W/m^2 by 15%. If a very accurate model is needed, this effect should be taken into consideration. PV/Thermal collectors do not normally require extremely accurate models, especially at low irradiance levels.

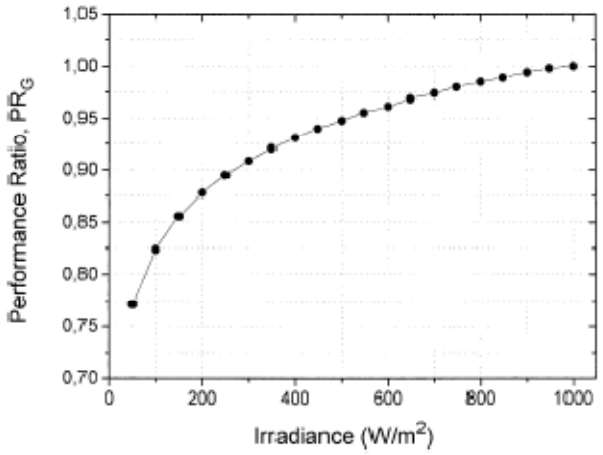

FIGURE 2.9 RELATIONSHIP BETWEEN EFFICIENCY AND INCIDENT RADIATION, PARRETTA ET AL. (1998)

Most hybrid collector models found in the literature only take into consideration the effect of the temperature on the efficiency of the PV cells (Assoa et al. 2007, Aste et al. 2008, Bhargava et al. 1991, Florschuetz 1979, Garg and Adhikari 1997, Othman et al. 2007). In most models, the efficiency of the cells is assumed to be linearly proportional to the cell temperature as suggested by Duffie and Beckman (2006).

2.4 HYBRID COLLECTORS

Garg and Adhikari (1997) modeled a typical (parallel flow) air based hybrid collector assuming no thermal mass. They varied different parameters, and found that the system efficiency increases with collector length, mass flow rate, and cell density and decreases with increased duct depth.

The finding that the system efficiency increases with cell density is misleading as this may not always be the case. The absorptivity and emissivity of the cells were not given in the paper but it is obvious that if the absorptivity of the cell was low relative to the absorber plate, or if the emissivity of the cells was high compared to that of the absorber plate, the system efficiency would most likely decrease with higher cell density.

Based on the above work, the same Garg and Adhikari (1998) modeled a typical (parallel flow) air based hybrid collector including the transient effects of the thermal mass. They looked at the performance over a year in New Delhi, India.

The problem was solved by means of energy balances at each layer of the collector. The resulting simultaneous differential equations were solved with a combination of fourth and fifth order Runge-Kutta method (Runge-Kutta-Fehlberg) with step size control. This method adds an extra calculation to estimate error (by comparing fifth and fourth order together), hence the ability to pick an appropriate step size.

Results were very similar to the steady state study by the same authors. In this paper, the authors gave the values of the emissivity and absorptivity of both the absorber plate and the cells. The absorber plate absorptivity and emissivity were both 0.9, and the PV cells absorptivity and emissivity were 0.9 and 0.1 respectively. This could be the reason why they previously had found that an increase in cell coverage yielded an increase in total efficiency. They may have used a higher than normal cell absorptivity and lower than normal cell emissivity, making the cells retain more heat than they normally would.

2.5 IMPINGING JET COLLECTORS

A simple impinging jet collector model was developed by Choudhury and Garg (1991). They compared effects of geometry on the efficiency of the collector. The model compared the impinging jet collectors with a conventional parallel plate collector. Their model has never been validated experimentally. Although many results were provided, many assumptions and details (e.g. optical properties of plates and insulation properties) were unclear or unspecified. Rask et al. (1977) were the first to experimentally study such collectors. They also looked at the effects of geometry, and produced a model that agreed relatively well with the experimental data, but definitely could have been improved.

Both studies showed an increase in efficiency compared to parallel plate collector, between 10 and 20% depending on the configuration, test conditions, and flow rate. Rask et al. found that parallel flow collectors were slightly better during cold winter conditions than the impinging jet collectors. Figure 2.10 shows efficiency curves for the baseline parallel flow collector and an efficient impinging jet collector studied by Rask et al. The y-intercept efficiency of the impinging jet collector is greater than that of the parallel flow collector, but the slope of the parallel flow collector is flatter. This is most likely due to the fact that the parallel flow collector had more back insulation than the impinging jet collector.

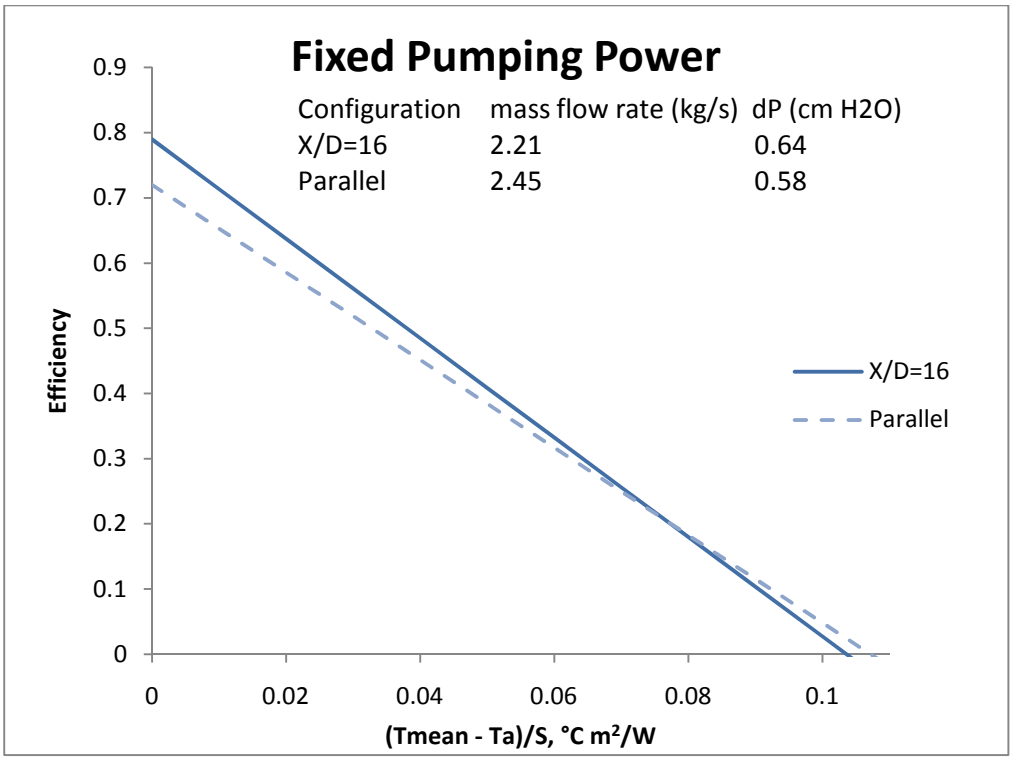

FIGURE 2.10 EFFICIENCY CURVES FOR IMPINGING JET AND PARALLEL FLOW COLLECTORS, DATA BY RASK ET AL. (1977)

Figure 2.11 shows the outlet temperature and thermal efficiency of the collector vs the mass flow rate based on the model by Choudhury and Garg (1991) for four different configurations; parallel plate with two different channel size, jet plate, and jet plate with an initial crossflow.

In both studies, the impinging jet heat transfer coefficient correlation is given by Kercher and Tabakoff (1970). Rask et al. (1977) also measured an increased pressure drop across some configurations of perforated plates (compared with parallel flow) for the same flow rates. Various impinging jet collectors were compared with the parallel flow collector at a constant fan power of 1.95W, and most impinging jet configurations were found to perform better than the parallel flow collector.

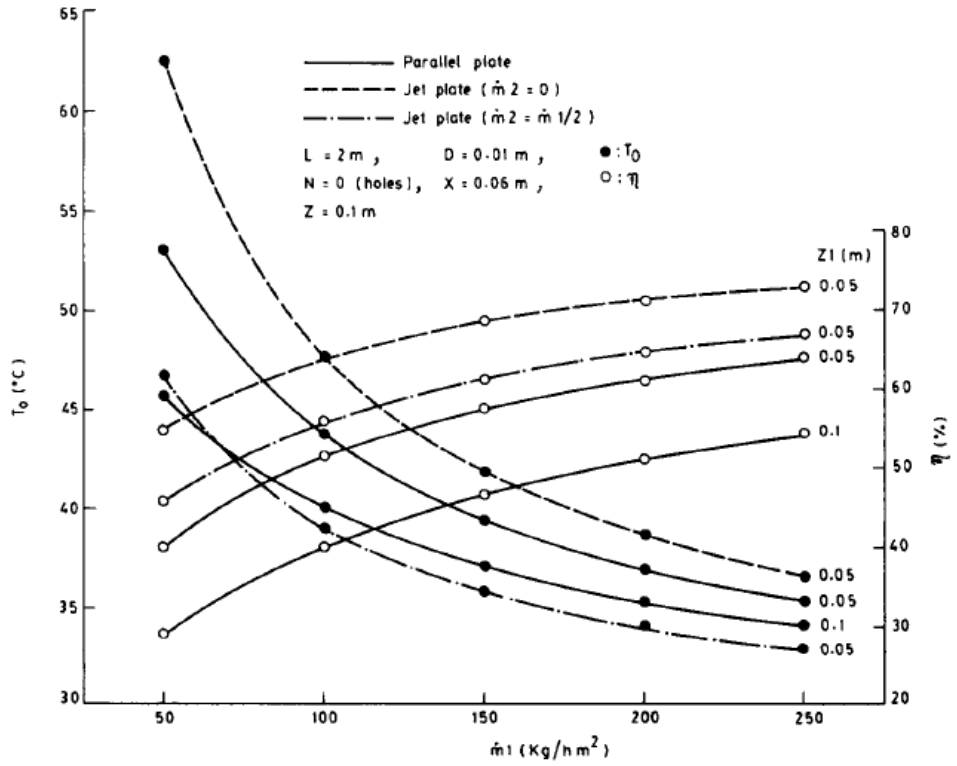

FIGURE 2.11 EFFICIENCY AND TEMPERATURE VS FLOW RATE, CHOUDHURY AND GARG (1991)

Belusko et al. (2007) modeled an unglazed impinging jet air collector. The flow in the collector was driven by a negative pressure, which was found to have a significant effect on the flow distribution in the collector. The model calculates the flow distribution using work by Florschuetz et al. (1981) before solving for the impinging jet heat transfer. They found that there was an increase of 21% in the thermal efficiency at typical conditions compared to unglazed parallel flow collectors.

2.6 TRANSIENT EFFECTS

Klein et al. (1974) modelled the transient effects of collectors. They looked at three different models; the Hottel, Whillier, Blitz model, the one-node capacitance model, and the multi-node model. The Hottel, Whillier, Blitz (HWB) model does not take transient effects in consideration (no thermal mass). The one-node capacitance model lumps the thermal mass of the collector into one equation. It is very similar with the HWB model, in that only one equation is solved. The multi-node model

includes the thermal mass of each layer (or group of layers) of the collector, and is essentially an energy balance across these layers. For example, the covers could be lumped as one node, and the absorber plate would be the other node.

It was found that the time constant of the flat plate collector analyzed was in the order of a few minutes. Use of weather data at much larger intervals than the time constant will not permit full transient effects of collector to be calculated. The results of the study showed that a one-node model is an appropriate model when using weather data at a 1 hour interval and that the zero-capacitance model makes almost as good a prediction as the one-node model. A multi-node approach would only be useful when the data interval was short.

Wijeysundra (1975) looked at the response time of collectors analytically. It was found that the response time increases with the overall mass of the collector, lower emissivity of the absorber plate and higher absorber plate temperature (lower efficiency). The same author (1977) also compared the zero capacitance model, the one-node model by Klein et al. (1974), and a two-node model (modification of the one-node model) with the response time method and found that when hourly weather data is used, the zero capacitance model gives good prediction of the daily useful energy gain. It was of Wijeysundra's opinion that the main usefulness of transient heat transfer models are in the short term study of collectors, and in predicting temperature fluctuations. This can only be done if sufficient data is available.

Chapter 3
MODEL DEVELOPMENT

3.1 INTRODUCTION

3.1.1 STEADY STATE AND TRANSIENT MODELS

Two models were developed for the simulation program TRNSYS (SEL, 2005). The first is a steady state model (zero capacitance), while the second takes the transient effects into account. Both models use the same general equations, but the mass of the plates is neglected in the steady state model. Both models are solved itteratively, and the transient model is solved using the backward Euler method. This method is unconditionally stable, and very simple to implement.

3.1.2 DESCRIPTION OF COLLECTOR

The impinging jet PV/Thermal flat plate collector consists of five different layers (Figure 3.1): the glass cover, the PV, the layer on which the PV is glued (Plate 2 or P_2), the perforated plate (Plate 1 or P_1), and the back insulation. The model was based on an energy balance at each layer of the collector. The collector was also discretised in the flow direction. Figure 3.2 shows a drawing of the collector and Figure 3.3 shows a picture of the collector used in the experiment discussed in Chapter 4. The PV cells can be seen through the cover covering most of the surface of P_2. The slot at the end is the outlet of the collector. A similar slot is located at the inlet of the collector. Figure 3.4 shows a schematic of the heat transfer between all layers.

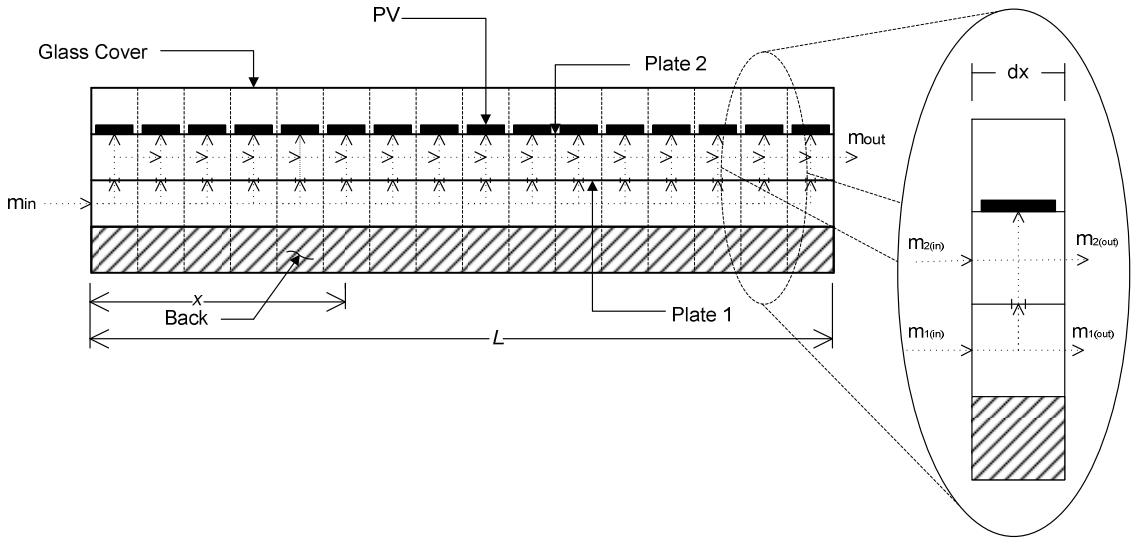

FIGURE 3.1 DISCRETISATION OF COLLECTOR

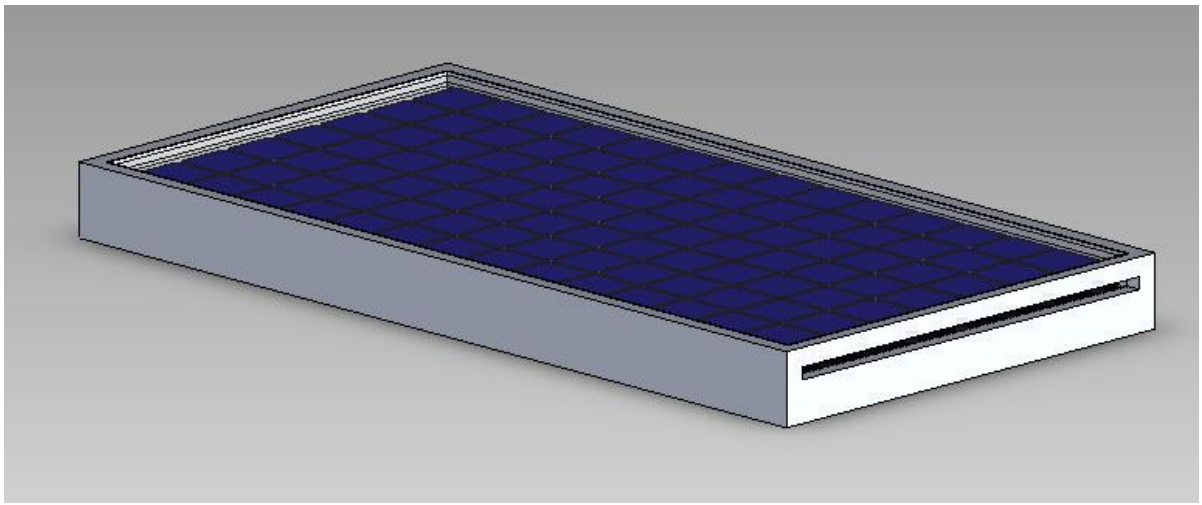

FIGURE 3.2 RENDERING OF COLLECTOR

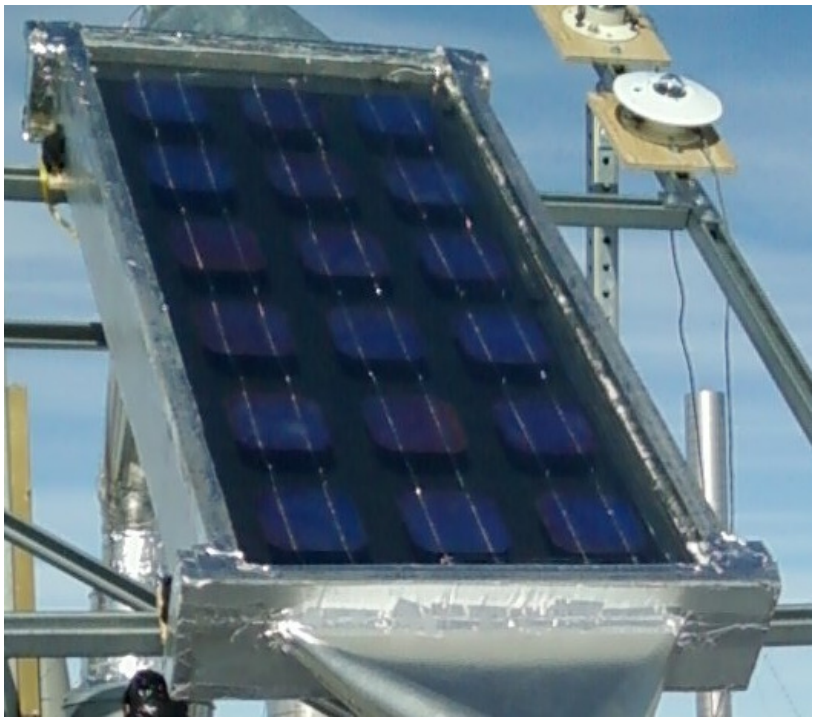

FIGURE 3.3 PICTURE OF COLLECTOR USED IN EXPERIMENT

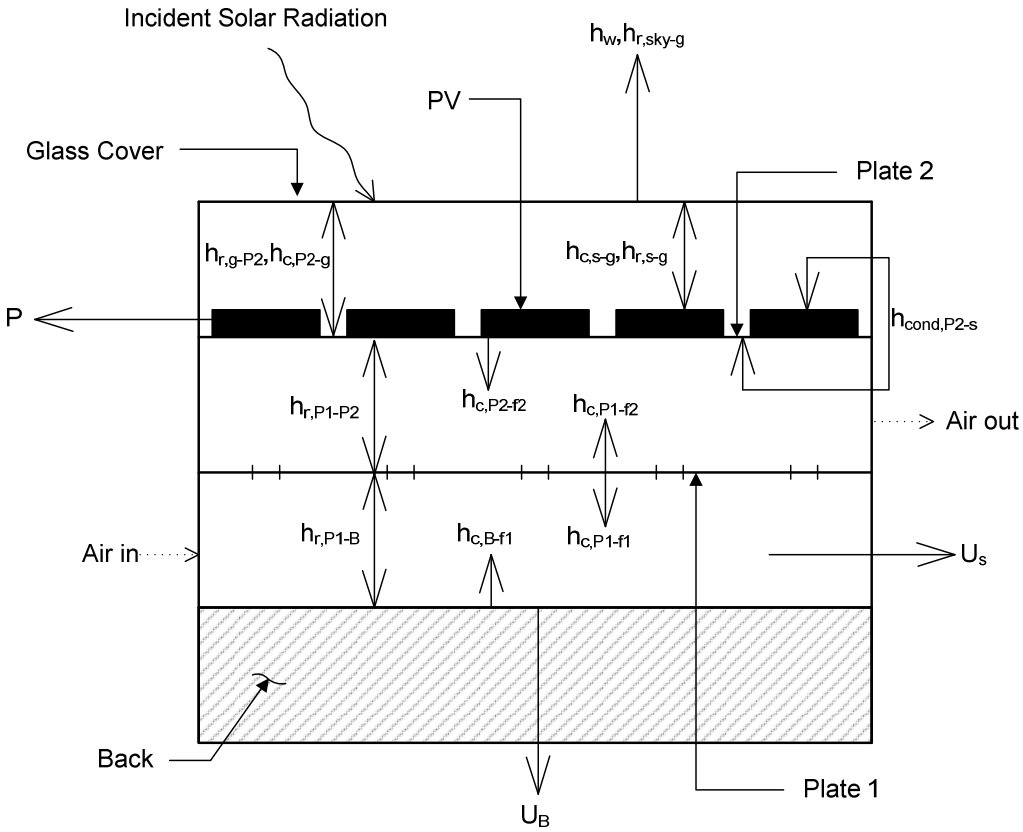

FIGURE 3.4 SCHEMATIC OF HEAT TRANSFER BETWEEN LAYERS

3.1.3 ASSUMPTIONS

Many assumptions were made in developing the model.

- Heat transfer in the x-direction is neglected. Only the fluid carries heat energy between discretised elements.
- The flow rate through the perforated plate is uniformly distributed.
- The mass of the fluid was always assumed to be insignificant and is not shown in the energy balance equations.

3.2 MODEL EQUATIONS AND CORRELATIONS

3.2.1 ENERGY BALANCE

Equations 3.1 through 3.7 show the various energy balances for the collector. For the plate energy balances, the left hand side of the equations is the energy storage term. The right hand side of the equation is the sum of the convective, radiative and conductive heat transfer, and the absorbed solar radiation. For the fluid energy balances, the left hand side of the equation represents the heat gained by the fluid.

- Back:

$$\rho_B \cdot z_B \cdot dx \cdot w \cdot C_B \frac{dT_B}{dt} = \left[h_{r,P_1-B}\left(T_{P_1} - T_B\right) - h_{c,B-f_1}\left(T_B - T_{f_1}\right) - U_B(T_B - T_a)\right] \cdot w \cdot dx \quad (3.1)$$

- Fluid 1 (f_1, between P_1 and the back insulation)

$$\dot{m}_{f_1} \cdot C_{f_1}\left(T_{f_1,out} - T_{f_1,in}\right) = \left[h_{c,B-f_1}\left(T_B - T_{f_1}\right) + h_{c,P_1-f_1}\left(T_{P_1} - T_{f_1}\right) + \frac{U_{side}\left(T_a - T_{f_1}\right) \cdot 2 \cdot Z_{b1} \cdot \frac{(L+w)}{N}}{w \cdot dx}\right] \cdot w \cdot dx \tag{3.2}$$

- Plate 1:

$$\rho_{P_1} \cdot z_{P_1} \cdot dx \cdot w \cdot C_{P_1} \frac{dT_{P_1}}{dt} = \left[-h_{c,P_1-f_1}\left(T_{P_1} - T_{f_1}\right) + h_{c,P_1-f_2}\left(T_{f2} - T_{P_1}\right) - h_{r,P_1-B}\left(T_{P_1} - T_B\right) - h_{r,P_1-P_2}\left(T_{P_1} - T_{P_2}\right) + S_{beam} \cdot (\tau\alpha)_{P_1,beam} + S_{ground} \cdot (\tau\alpha)_{P1,ground} + S_{diffuse} \cdot (\tau\alpha)_{P1,diffuse}\right] \cdot w \cdot dx \tag{3.3}$$

- Fluid 2 (f_2, between P_1 and P_2)

$$\dot{m}_{f_2} \cdot C_{f_2}\left(T_{f_2,out} - T_{f_2,in}\right) = \left[h_{c,f_2-P_1}\left(T_{P_1} - T_{f_2}\right) + h_{c,P_2-f_2}\left(T_{P_2} - T_{f_1}\right) + \frac{U_{side}\left(T_a - T_{f_2}\right) \cdot 2 \cdot Z_n \cdot \frac{(L+w)}{N}}{w \cdot dx}\right] \cdot w \cdot dx \tag{3.4}$$

Where

$$T_{f_{2,in}} = \frac{\dot{m}\left(\frac{x}{L}\right) T_{f_{2,out}}" + \frac{\dot{m}}{N} T_{f_1}}{\dot{m}\left(\frac{x}{L}\right) + \frac{\dot{m}}{N}}$$

- Plate 2:

$$\rho_{P_2} \cdot z_{P_2} \cdot dx \cdot w \cdot C_{P_2} \frac{dT_{P_2}}{dt} = \Bigg[h_{r,P_1-P_2}\left(T_{P_1} - T_{P_2}\right) + \left(S_{beam} \cdot (\tau\alpha)_{P2,beam} + S_{ground} \cdot (\tau\alpha)_{P2,ground} + S_{diffuse} \cdot (\tau\alpha)_{P2,diffuse}\right) \cdot \left(1 - \left(\frac{A_{pv}}{A_c}\right)\right) + h_{cond,P_2-s}\left(T_s - T_{P_2}\right)\left(\frac{A_{pv}}{A_c}\right) - \left(1 - \frac{A_{pv}}{A_c}\right) \cdot h_{r,g-P_2}\left(T_{P_2} - T_g\right) - h_{c,P_2-f_2}\left(T_{P_2} - T_{f_1}\right) - h_{c,P_2-g}\left(T_{P_2} - T_g\right)\left(1 - \frac{A_{pv}}{A_c}\right)\Bigg] \cdot w \cdot dx \quad (3.5)$$

- Photovoltaic:

$$\rho_s \cdot z_s \cdot dx \cdot w \cdot C_s \frac{dT_s}{dt} = \left[h_{r,s-g}\left(T_g - T_s\right) + \left(S_{beam} \cdot (\tau\alpha)_{s,beam} + S_{ground} \cdot (\tau\alpha)_{s,ground} + S_{diffuse} \cdot (\tau\alpha)_{s,diffuse}\right) - h_{cond,P_2-s}\left(T_s - T_{P_2}\right) + h_{c,s-g}\left(T_g - T_s\right) - P\right] \cdot w \cdot dx \quad (3.6)$$

- Glass:

$$\rho_g \cdot z_g \cdot dx \cdot w \cdot C_g \frac{dT_g}{dt} = \left[\left(\frac{A_{pv}}{A_c}\right) h_{r,s-g}\left(T_s - T_g\right) + \left(S_{beam} \cdot \alpha_{g,beam} + S_{ground} \cdot \alpha_{g,ground} + S_{diffuse} \cdot \alpha_{g,diffuse}\right) + \left(1 - \frac{A_{pv}}{A_c}\right) h_{r,g-P_2}\left(T_{P_2} - T_g\right) + h_{r,sky-g}\left(T_{sky} - T_g\right) + h_w\left(T_a - T_g\right) - h_{c,s-g}\left(T_g - T_s\right)\left(\frac{A_{pv}}{A_c}\right) + h_{c,P_2-g}\left(T_{P_2} - T_g\right)\left(1 - \frac{A_{pv}}{A_c}\right)\right] \cdot w \cdot dx \quad (3.7)$$

It is assumed that the resistance to heat transfer across the sides and back is only caused by the insulation. Also, the area of the "top" and "bottom" of the collector are factored in to every element.

By rearranging these equations, the temperature of each plate and fluid can be solved explicitly when the mass of the plate is assumed to be zero (zero capacitance) or with the Euler method for the transient model.

This model does not calculate the location of the sun in the sky, or the three components of incoming solar radiation (beam, sky diffuse, and ground diffuse). TRNSYS already provides other means to accurately get those values.

3.2.2 HEAT TRANSFER COEFFICIENTS

A number of heat transfer coefficients are used in solving Equations 3.1 through 3.7. They are defined in this section.

The conduction between P_2 and the PV cells $\left(h_{cond,P_2-s}\right)$ is taken as:

$$h_{cond,P_2-s} = \left(\frac{k}{z}\right)_{adhesive} \tag{3.8}$$

Typical adhesive should yield numbers between 30 and 100 W/m^2 K.

Kercher and Tabakoff (1970) examined the effect of cross flow on impinging heat transfer coefficient and experimentally derived the following correlation

$$h_{c,f_2-P_2} = \frac{\left(Nu_{D,f_2-P_2}\right)k}{Z_n} = \frac{k}{Z_n}\phi_1\phi_2 {Re_D}^m Pr^{1/3}\left(\frac{Z_n}{D}\right)^{0.091} \tag{3.9}$$

For

$$1 \leq Z_n/D \leq 4.8$$
$$300 \leq Re_D \leq 3 \times 10^4$$
$$3.1 \leq X_n/D \leq 12.5$$

Where m, ϕ_1, and ϕ_2 are given graphically in Figures 3.5 to 3.7.

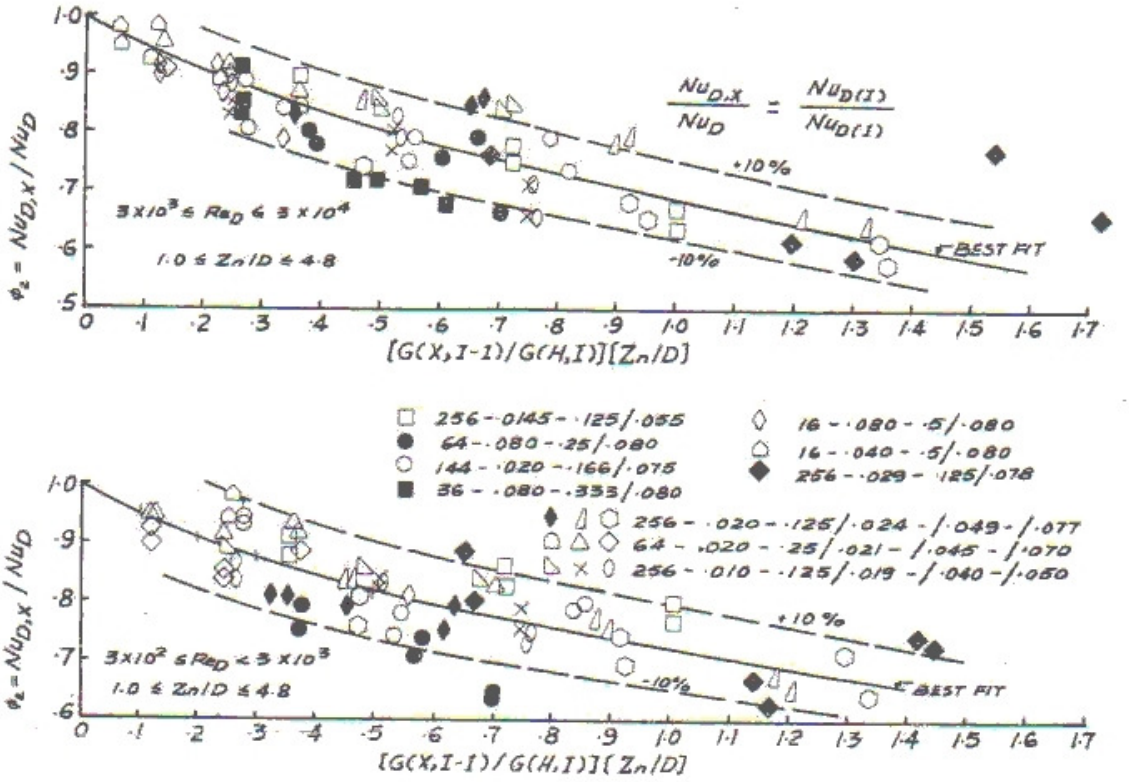

FIGURE 3.5 IMPINGEMENT HEAT TRANSFER DEGRADATION COEFFICIENT SOURCE: KERCHER AND TABAKOFF (1970)

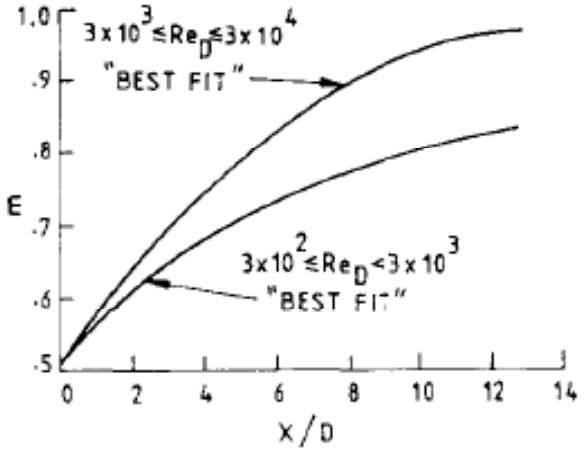

FIGURE 3.6 EXPONENT m VS RATION OF HOLE SPACING AND DIAMETER SOURCE: KERCHER AND TABAKOFF (1970)

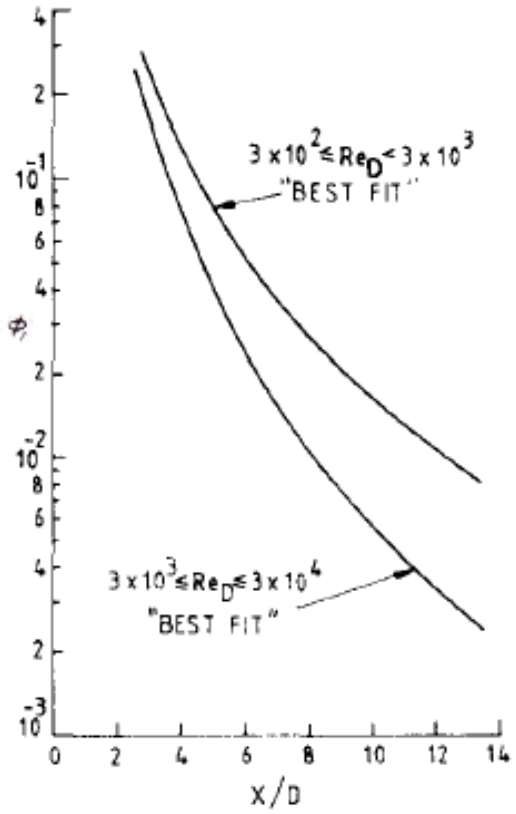

FIGURE 3.7 COEFFICIENT FOR NUSSELT NUMBER CORRELATION FOR AN ARRAY OF IMPINGING JETS WITHOUT CROSSFLOW SOURCE: CHOUDHURY AND GARG (1991) REPRODUCED FROM KERCHER AND TABAKOFF (1970)

Fitting curves through the graphs yields the following equations. These are approximate, but are essential to the model.

$$\phi_2 = \begin{cases} 0.9582e^{-0.302V_{\phi_2}}, & Re_D < 3 \times 10^3 \\ 0.9699e^{-0.363V_{\phi_2}}, & Re_D \geq 3 \times 10^3 \end{cases} \tag{3.10}$$

where

$$V_{\phi_2} = \frac{\left(\frac{\dot{m}}{N}\right)}{\left(\frac{D^2}{4}\pi\right)\left(\frac{w \times \left(\frac{L}{N}\right)}{{X_n}^2}\right)}$$

$$\phi_1 = \begin{cases} 2.8055\left(\frac{X_n}{D}\right)^{-2.255}, & Re_D < 3\times10^3 \\ 3.3588\left(\frac{X_n}{D}\right)^{-2.789}, & Re_D \geq 3\times10^3 \end{cases} \tag{3.11}$$

$$m = \begin{cases} -2.37\cdot10^{-6}\left(\frac{X_n}{D}\right)^4 + 1.61\cdot10^{-4}\left(\frac{X_n}{D}\right)^3 \\ -0.00429\left(\frac{X_n}{D}\right)^2 + 0.0591\left(\frac{X_n}{D}\right) + 0.5, & Re_D < 3\times10^3 \\ -0.00244\left(\frac{X_n}{D}\right)^2 + 0.0696\left(\frac{X_n}{D}\right) + 0.497, & Re_D \geq 3\times10^3 \end{cases} \tag{3.12}$$

Here, the Reynolds number is that of the flow through the holes.

A correlation for forced convection heat transfer between a plate and the fluid in parallel plate channel flow can be found in Duffie and Beckman (2006)

$$h_{c,B-f_1} = h_{c,P_1-f_1} = 0.0158\, Re^{0.8}\left(\frac{k}{D_h}\right) \tag{3.13}$$

where

$$D_h = 4\left(\frac{w\, Z_{b1}}{2(w + Z_{b1})}\right) \tag{3.14}$$

$$Re = \frac{2\dot{m}\left(1 - \frac{x}{L}\right)}{(w+Z)\mu} \tag{3.15}$$

$$h_{c,P_1-f_2} = 0.0158\, Re^{0.8}\left(\frac{k}{D_h}\right) \tag{3.16}$$

where

$$D_h = 4\left(\frac{w\,Z_n}{2(w+Z_n)}\right) \tag{3.17}$$

$$Re = \frac{2\dot{m}\left(\frac{x}{L}\right)}{(w+Z_n)\mu} \tag{3.18}$$

Equations 3.19 to 3.22 represent the radiative heat transfer coefficients between plates. Equation 3.23 is the radiative heat transfer coefficient between the sky and the glass cover.

$$h_{r,P_1-B} = \frac{\sigma\left({T_{P_1}}^2 + {T_B}^2\right)\left(T_{P_1} + T_B\right)}{{\varepsilon_{P_1}}^{-1} + {\varepsilon_B}^{-1} - 1} \tag{3.19}$$

$$h_{r,s-g} = \frac{\sigma\left({T_s}^2 + {T_g}^2\right)\left(T_s + T_g\right)}{\frac{1-\varepsilon_s}{\varepsilon_s} + \frac{\left(1-\varepsilon_g\right)\left(A_{pv}\right)}{\varepsilon_g A_c} + 1} \tag{3.20}$$

$$h_{r,P_1-P_2} = \frac{\sigma\left({T_{P_2}}^2 + {T_{P_1}}^2\right)\left(T_{P_2} + T_{P_1}\right)}{{\varepsilon_{P_1}}^{-1} + {\varepsilon_{P_2}}^{-1} - 1} \tag{3.21}$$

$$h_{r,g-P_2} = \frac{\sigma\left({T_{P_2}}^2 + {T_g}^2\right)\left(T_{P_2} + T_g\right)}{\frac{1-\varepsilon_{P_2}}{\varepsilon_{P_2}} + \frac{\left(1-\varepsilon_g\right)\left(A_c - A_{pv}\right)}{\varepsilon_g A_c} + 1} \tag{3.22}$$

$$h_{r,sky-g} = \sigma\varepsilon_g\left({T_g}^2 + {T_{sky}}^2\right)\left(T_g + T_{sky}\right) \tag{3.23}$$

The losses through the cover are also due to convective heat transfer from the glass to the ambient air. When there is very little wind, free convection is the dominant heat transfer mode. When there is sufficient wind, forced convection is the dominant heat transfer mode. In Equation 3.24, the forced convection equation is

given by Sartori (2005). The Nusselt number correlation of Equation 3.25 can be found in Lloyd and Moran (1974).

$$h_w = max\left(h_{free\ conv}, 5.74V^{0.8}L^{-0.2}\right) \tag{3.24}$$

where

$$h_{free\ conv} = \frac{\overline{Nu}_{L_c} \cdot k}{L_c} = \frac{0.15{Ra_{L_c}}^{1/3} \cdot k}{L_c} \tag{3.25}$$

and L_c is four times the area divided by the perimeter of the collector.

The model does not take into account the wind direction. For this reason, the value of L in Equation 3.24 can be taken as the same as L_c with relatively little effect on the heat transfer coefficient.

The free convection heat transfer coefficient in Equation 3.26 between P_2 (or the PV cells) and the glass cover is given by a correlation by Hollands et al. (1976).

$$\begin{aligned} h_{c,P_2-g} &= \frac{Nu \cdot k}{Z_{gP_2}} \\ &= \left[1 + 1.44\left[1 - \frac{1708(\sin 1.8\beta)^{1.6}}{Ra\cos\beta}\right]\left[1 - \frac{1708}{Ra\cos\beta}\right]^{+}\right. \\ &+ \left.\left[\left(\frac{Ra\cos\beta}{5830}\right)^{\frac{1}{3}} - 1\right]^{+}\right]\frac{k}{Z_{gP_2}} \end{aligned} \tag{3.26}$$

Where;

$$Ra = \frac{g\beta'\Delta T\ {Z_{gP2}}^3}{\upsilon\alpha}$$

ß' is the inverse of the average of the temperatures of the two plates, and ß is the angle of the collector. + denotes that if the value of the term in the brackets is negative, that term becomes zero.

3.2.3 AIR PROPERTIES

The following correlations relating air properties to temperatures were used (all temperatures in °C, property units are in square brackets).

$$C = 0.0006T^2 - 0.0011T + 1005.9;\ \left[\frac{J}{kg\ K}\right] \tag{3.27}$$

$$\alpha = 1.4614 \cdot 10^{-7}T + 1.8343 \cdot 10^{-5};\ \left[\frac{m^2}{s}\right] \tag{3.28}$$

$$k = 7.5714 \cdot 10^{-5}T + 2.4181 \cdot 10^{-2};\ \left[\frac{W}{m\ K}\right] \tag{3.29}$$

$$\upsilon = 9.7506 \cdot 10^{-8}T + 1.3118 \cdot 10^{-5};\left[\frac{m^2}{s}\right] \tag{3.30}$$

$$Pr = -9.8398 \cdot 10^{-10}T^4 + 1.8486 \cdot 10^{-7}T^3 - 8.5713 \cdot 10^{-6}T^2 + 2.2359 \cdot 10^{-4}T + 7.15735 \cdot 10^{-1} \tag{3.31}$$

3.2.4 PV ANALYSIS

The photovoltaic array is assumed to always operate at maximum power point. Its performance is affected by two parameters: incident angle, and temperature.

A linear relationship between the PV efficiency and the temperature of the cell can be assumed

$$\eta_{p,elec} = \eta_{pref,mp} + \mu_{\eta,mp}(T_s - T_{STC}) \tag{3.32}$$

where $\mu_{\eta,mp}$ is the PV temperature coefficient in %efficiency per °C.

The electrical power produced is therefore

$$P = \left[(\tau\alpha)_s \left(\frac{\eta_{p,elec}}{\alpha_s(n)}\right) S\right]_{beam} + \left[(\tau\alpha)_s \left(\frac{\eta_{p,elec}}{\alpha_s(n)}\right) S\right]_{diffuse} + \left[(\tau\alpha)_s \left(\frac{\eta_{p,elec}}{\alpha_s(n)}\right) S\right]_{ground} \quad (3.33)$$

3.3 OPTICAL PROPERTIES

3.3.1 TRANSMITTANCE-ABSORPTANCE PRODUCT

The transmittance-absorptance product for any given plate with a cover system can be found using

$$(\tau\alpha) = \frac{\tau\alpha}{1-(1-\alpha)\rho_d} \quad (3.34)$$

The solar radiation incident on the collector can be divided in three parts. Beam radiation, sky diffuse radiation, and ground diffuse radiation. The incident angle of the beam component is a function of the slope of the collector, the time of year, and the location. TRNSYS provides means of getting the angle of incidence of the beam radiation based on geometry calculations that are described in Duffie and Beckman (2006). The sky diffuse and ground diffuse angle of incidence are functions of the slope of the collector only, and can be approximated with the following equations (all angles in degrees):

$$\theta_{sky} = 59.68 - (0.1388\beta + 0.001497\beta^2) \quad (3.35)$$

$$\theta_{ground} = 90 - (0.5788\beta + 0.002693\beta^2) \quad (3.36)$$

The properties of each transparent plate (glass covers) in the collector are calculated using the following equations:

$$\theta_{2,p} = \sin^{-1}\left(\frac{n_{1,p}\sin\theta_{1,p}}{n_{2,p}}\right) \quad (3.37)$$

$$\tau_{a,p} = e^{-\left(\frac{(KL)_p}{\cos\theta_{2,p}}\right)} \tag{3.38}$$

$$r_{\perp,p} = \frac{\sin^2(\theta_{2,p} - \theta_1)}{\sin^2(\theta_{2,p} + \theta_1)} \tag{3.39}$$

$$r_{\parallel,p} = \frac{\tan^2(\theta_{2,p} - \theta_1)}{\tan^2(\theta_{2,p} + \theta_1)} \tag{3.40}$$

$$\tau_{\perp,p} = \frac{\tau_{a,p}(1 - r_{\perp,p})^2}{1 - (r_{\perp,p}\tau_{a,p})^2} \tag{3.41}$$

$$\rho_{\perp,p} = r_{\perp,p}(1 + \tau_{a,p}\tau_{\perp,p}) \tag{3.42}$$

$$\alpha_{\perp,p} = (1 - \tau_{a,p})\left(\frac{1 - r_{\perp,p}}{1 - r_{\perp,p}\tau_{a,p}}\right) \tag{3.43}$$

The subscript p refers to the fact that these values are for one particular plate (the glass cover, the PVs, or P_2).

Equations 3.41, 3.42 and 3.43 can be used for the parallel component by replacing $\perp$ with $\parallel$. The total values for r, τ, ρ, and α are the average of the parallel and perpendicular components.

3.3.2 CALCULATING ρ_d

To calculate the transmittance-absorptance product, the effective absorber plate must be defined. For the purpose of this exercise, the absorber plate can be defined as the bottom most plate to be exposed to solar radiation. If P_2 is transparent, and the PV coverage is not 100%, then the absorber plate is P_1, otherwise, it is P_2+PV cells. To find the transmittance-absorptance product of the absorber plate, the reflectance of the system for diffuse radiation incident from the absorber plate (ρ_d)

must be calculated. This can be estimated by solving for the reflectance of radiation emitted by the absorber plate at an angle of 60 degrees. Duffie and Beckman (2006) have outlined a method to solve for this. A few complications arise due to the fact that one of the sheets of glass will be partially covered in PV cells.

For the PV cells, the transmittance is zero, and if it is assumed that the absorptivity of the back of the PV cells is close to unity, then the reflectivity of the combination of P_2 and the PV cells can be approximated as the reflectivity of P_2. This assumption can be shown to have a relatively small effect on the ($\tau\alpha$) product for P_1 by looking at Equation 3.34. An absorber plate would most likely have a large α, making the multiplier in front of ρ_d very small. The transmissivity of the combined P_2 and PV cells can be approximated using

$$\tau_{P2s} = \tau_{P2}\left(1 - \frac{A_{pv}}{A_c}\right) \tag{3.44}$$

The total transmittance of the cover system for diffuse radiation (which can be approximated to an equivalent angle of 60°) incident from the bottom can be found with Equation 3.45. Similarly, the reflectance can be found with Equation 3.46.

$$\tau_m = \frac{1}{2}(\tau_\perp + \tau_\parallel) = \frac{1}{2}\left[\left(\frac{\tau_1\tau_2}{1+\rho_1\rho_2}\right)_\perp + \left(\frac{\tau_1\tau_2}{1+\rho_1\rho_2}\right)_\parallel\right] \tag{3.45}$$

$$\rho_d = \frac{1}{2}(\rho_\perp + \rho_\parallel) = \frac{1}{2}\left[\left(\rho_1 + \frac{\tau_m\rho_2\tau_1}{\tau_2}\right)_\perp + \left(\rho_1 + \frac{\tau_m\rho_2\tau_1}{\tau_2}\right)_\parallel\right] \tag{3.46}$$

3.3.3 CALCULATING τ AND α

After solving ρ_d for the perforated plate, τ (total transmittance of the cover system) and α (absorptivity of the plate) need to be calculated. The method laid out by Duffie and Beckman (2006) can be used again knowing that the transmittance of P_2 and the PV cells together is equal the transmittance of P_2 multiplied by the percentage of area not covered by the cells.

Parretta et al. (1999) have measured the reflectance of photovoltaic cells of different configurations at different incident angles. They found that the ratio of the reflectance (at some incident angle) to the normal reflectance of encapsulated PV cells can be modeled as a semi-infinite dielectric material with a refractive index between 2.5 and 3. They also produced data for a cell with no encapsulation (but did not correlate to a refractive index). The closest fit to the data for a PV cell with anti-reflective coating and no encapsulation is that of a semi-infinite dielectric material with a refractive index of 3. A measured normal reflectance of the PV cell can be used to find it's absorptance at any incident angle. Equation 3.47 is used to calculate the absorptivity of the solar cell. θ_1 is the incident angle, $\theta_{2,s}$ is the equivalent angle of refraction and can be calculated with Snell's law. θ_1 and $\theta_{2,s}$ in the denominator are different than in the numerator and are taken as θ_1 approaching zero, and it's corresponding $\theta_{2,s}$.

$$\alpha_s(\theta) = \frac{\alpha_s(n)\left[1 - \frac{1}{2}\left(\frac{\sin^2(\theta_{2,s} - \theta_1)}{\sin^2(\theta_{2,s} + \theta_1)} + \frac{\tan^2(\theta_{2,s} - \theta_1)}{\tan^2(\theta_{2,s} + \theta_1)}\right)\right]}{\left[1 - \frac{1}{2}\left(\frac{\sin^2(\theta_{2,s} - \theta_1)}{\sin^2(\theta_{2,s} + \theta_1)} + \frac{\tan^2(\theta_{2,s} - \theta_1)}{\tan^2(\theta_{2,s} + \theta_1)}\right)\right]\Big|_{\theta_1 \to 0}} \tag{3.47}$$

For P_2 and the PV cells, ρ_d can be taken as the reflectance of the glass cover at 60°. Also the transmittance can be taken as the transmittance of the glass cover at the incident angle. To calculate the temperature of the PV cells, and the power produced, α_s is used in Equation 3.34. For the glass cover, $\tau\alpha = \alpha_g$, and α_{P2} is the calculated absorptivity of P_2 if the material is transparent, or can be prescribed for opaque materials (in which case, no solar radiation reaches P_1).

3.4 SOLVING THE ENERGY BALANCE EQUATIONS

3.4.1 STEADY-STATE SOLUTION

An iterative procedure was used to solve the governing equations. For the steady-state problem, Equations 3.1, 3.3, and 3.5 to 3.7 are simplified by assuming that the left hand side of the equations are equal to zero.

The air temperature is first assumed to be equal to the air inlet temperature, and the plate temperatures are assumed to be equal to the ambient temperature. Next, all heat transfer coefficients are calculated. For those that require temperatures of plates, the initial assumed temperatures are used for the first iteration. The energy balance equations are then solved, and plate and fluid temperatures are determined for the next iteration. Convergence is reached when the fluid temperature between plate 2 and plate 1 (T_{f2}) changes by less than 0.00001 K between two iterations. The next element is then solved, using the previous element temperatures as the guess temperatures.

To solve for the average fluid temperature at a specific element, T_{f1}, the exit temperature is first found using Equation 3.2 by letting T_{f1} be equal to the inlet temperature (of that element). The average of the element exit and inlet temperatures is then used (in T_{f1}) to recalculate the exit temperature. The exit and inlet temperature are once again averaged to find the average temperature of the element. This iterative process yields a more accurate value for the fluid temperature than would be possible if the outlet temperature was solved with no iteration.

T_{f2} is solved with Equation 3.4, using the same method as for T_{f1}.

3.4.2 BACKWARDS EULER

The backwards Euler method is used to solve the differential equations when the transient effects are taken into consideration. The same iterative method is used to solve the system of equations as for the steady state model.

The backwards Euler method is an implicit method, and is unconditionally stable. It is also one of the easiest methods to numerically solve differential equations. Its major drawback is that it is a first order method; therefore its error is orders of magnitude larger than other higher order methods such as the Runge-Kutta methods.

In order to reduce the error, a small time step must be used. By doing so, the model stays very simple, but it is possible to produce a solution accurate enough to be useful.

In a differential equation like Equation 3.48, we can start from a known boundary condition (for example, at t=0, y=0), then take a step forward in time to find y for the next time step (y_{n+1}).

$$\frac{dy}{dt} = f(y, x, z \dots) \tag{3.48}$$

The first step in using the backwards Euler method is to decide in which direction the next y will be. This is done by calculating the gradient $f(y, x, z \dots)$. In the case of the backwards Euler method, the gradient is calculated at the next time step. Equation 3.48 can be turned into Equation 3.49 by forming a linear approximation of the derivative.

$$\frac{y_{(n+1)} - y_{(n)}}{\Delta t} = f(y_{(n+1)}, x_{(n+1)}, z_{(n+1)} \dots) \tag{3.49}$$

Where n+1 represents the times step to solve for, n is the previous time step, y,x, and z are variables, and Δt is the time step.

Rearranging the energy balance equations, we can isolate the appropriate variable. As an example, the general form of the energy balance equations for the different plates is as follow:

$$T_{(n+1)} = \frac{\frac{[\sum h \cdot T_i + \sum S \cdot (\tau\alpha)]_{(n+1)} \cdot \Delta t}{\rho \cdot z \cdot C} + T_{(n)}}{1 + \left(\frac{\Delta t}{\rho \cdot z \cdot C}\right) \cdot (\sum h)_{n+1}} \tag{3.50}$$

3.5 PRELIMINARY RESULTS

Impinging PV/Thermal collectors have never been studied, but impinging thermal collectors have. Choudhury and Garg (1991) produced a model similar to the one developed here and compared effects of geometry on the efficiency of the collector. Their model has never been validated experimentally, and some parameters are unknown or unclear. Nonetheless, it is possible to compare their results to the results from the model presented here. Table 3.1 shows the parameters used in the model to get the results seen in Figures 3.8 through 3.11.

TABLE 3.1 PARAMETERS USED IN FIGURES 3.8 - 3.11

Figure	3.8	3.9 & 3.10	3.11
Width of Collector (m)	1	0.835	0.835
Length of Collector (m)	2	1.67	1.67
%PV coverage	0	0	0
Back insulation thickness (m)	0.05	0.05	0.05
Side insulation thickness (m)	0.05	0.025	0.025
Conductivity of insulation (W/mK)	0.034	0.04	0.04
Distance between glass cover and P2 (m)	0.0254	0.0254	0.0254
Distance between P2 and P1 (m)	0.05	0.0381	0.0127
Distance between holes (m)	0.06	0.0508	0.0762
Diameter of holes (m)	0.01	0.0064	0.0064
Distance between back plate and P1 (m)	0.05	0.0254	0.0254
Back plate emmissivity	0.25	0.25	0.25
Emissivity of P1 up	0.25	0.25	0.25
Emissivity of P1 down	0.25	0.25	0.25
Emissivity of P2 up	0.1	0.91	0.91
Emissivity of P2 down	0.5	0.5	0.5
Asorptivity of P2	0.95	0.95	0.95
Thickness of glass cover	0.0031	0.005	0.005
Extinction coefficient of glass cover (1/m)	4	18	18
Emissivity of glass cover	0.87	0.87	0.87

Figure 3.8 shows a comparison of both models. The inlet and ambient temperatures are 300K. The figure shows efficiency and outlet temperatures for a specific geometry and varying flow rates. The discrepancy between the two models can be attributed to a few things. First, the emissivity of the absorber plate is not given by Choudhury and Garg (1991). When running the model, an emissivity of 0.1 was used. A smaller emissivity would yield less of a difference between the two curves. Also, they made no mention of side losses. As this collector is thicker than a parallel flow collector, the side losses are more significant than in other collectors. Furthermore, different correlations were used for some of the heat transfer coefficients (Equations 3.13, 3.21, and 3.23). Overall, the general trends of the efficiency and temperature curves are fairly good, but have an offset.

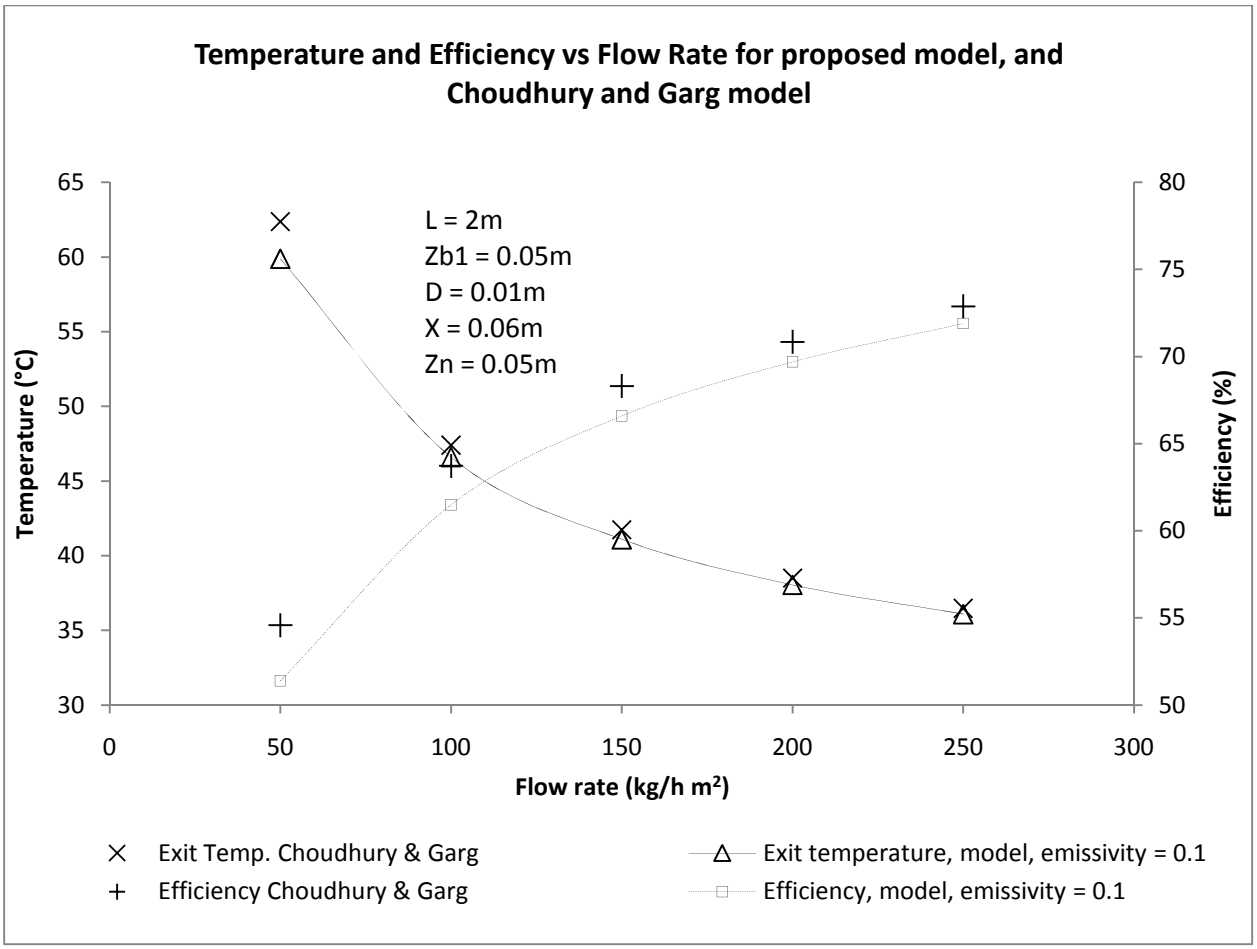

FIGURE 3.8 COMPARISON BETWEEN MODEL AND CHOUDHURY AND GARG

Rask et al (1977) have studied impinging air collectors experimentally. The experimental data did not include an error analysis, and some radiative properties of the plates were not given. Figures 3.9, 3.10 and 3.11 show efficiency curves as found experimentally by Rask et al. (1977) compared to model results. $(T_{in}-T_{amb})/S$ is varied by changing T_{amb}. The model assumed a sky temperature equal to the ambient temperature. It can be seen that a reasonable agreement exists between experimental data and the model. A selective surface would yield a curve with a much smaller slope. All of the comparisons between the model and the experimental data show a tendency to underestimate the efficiency at low $(T_{in}-T_{amb})/S$ and overestimate the efficiency at high $(T_{in}-T_{amb})/S$. It is hard to determine what causes this trend because many factors could be at play.

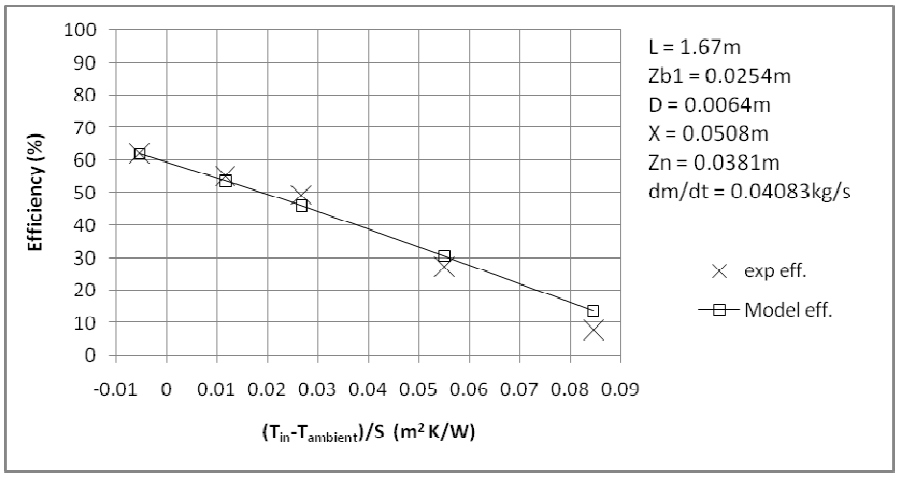

FIGURE 3.9 COMPARISON BETWEEN MODEL AND EXPERIMENTAL DATA

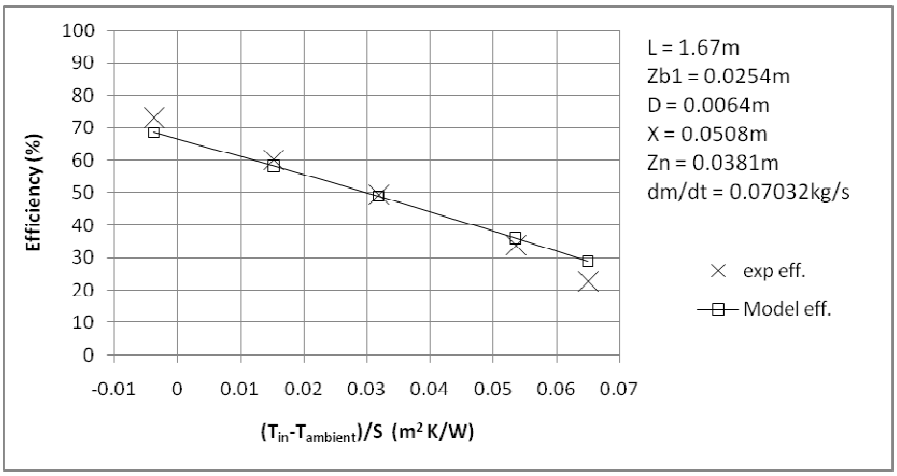

FIGURE 3.10 COMPARISON BETWEEN MODEL AND EXPERIMENTAL DATA

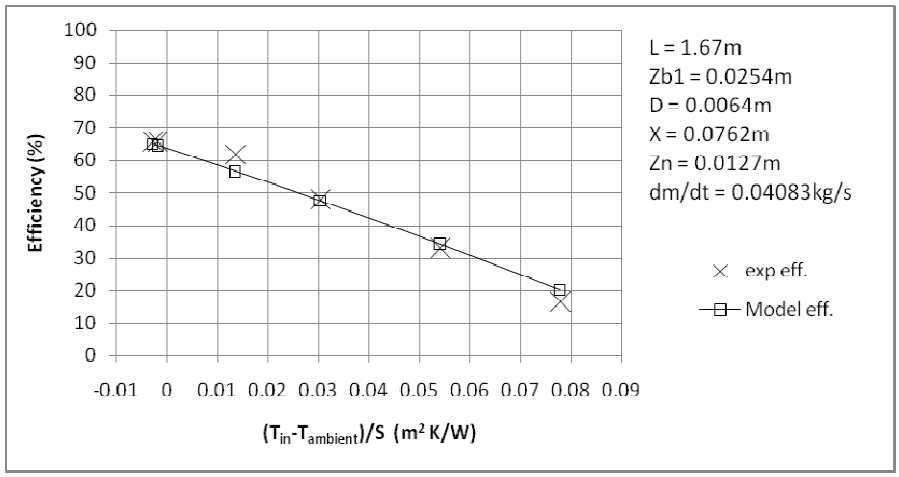

FIGURE 3.11 COMPARISON BETWEEN MODEL AND EXPERIMENTAL DATA

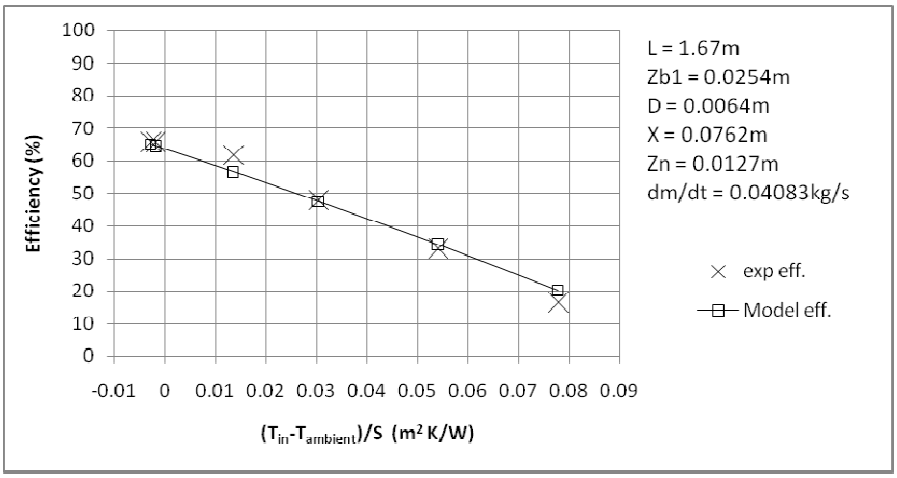

FIGURE 3.12 COMPARISON BETWEEN MODEL AND EXPERIMENTAL DATA

Inputs, and parameters

The following tables show the many inputs, outputs and parameters for the TRNSYS models, and a short description. The source code for the model is shown in Appendix A.

TABLE 3.2 INPUTS FOR TRANSIENT AND STEADY- STATE MODELS

Input	Note	Unit
Flow rate of air		kg/s
Collector inclination		radians
Beam solar radiation on collector		W/m^2
Inlet temperature of air		K
Ambient Temperature		K
Tsky	Equivalent sky temperature	K
V	Wind Velocity	m/s
incidentangle	Incident angle for beam radiation	radians
Sdiffuse	Sky diffuse radiation	W/m^2
Sground	Ground diffuse radiation	W/m^2

TABLE 3.3 OUTPUTS FOR TRANSIENT AND STEADY-STATE MODELS

Output	Note	Unit
Toutofcollector	Air temperature out of collector	K
thermalefficiency	Thermal efficiency of collector	
elecpower	Electrical Power	W
eleceff	Electrical efficiency based on aperature area of collector	
totaleff	Electrical efficiency plus thermal efficiency	
Heat Gain		W

TABLE 3.4 PARAMETERS FOR TRANSIENT AND STEADY-STATE MODEL

Parameters	Note	Unit
Initial temperature guess of collector		K
Amount of elements	Discretized elements in the streamwise direction	
Width of Collector		m
Length of collector		m
Absorber plate area		m^2
PV area		m^2
Thickness of back insulation		m
Back plate emmissivity		
Thickness of perforated plate		m
Perforated plate emissivity up	Emissivity of P_1, towards P_2	
Perforated plate emissivity down	Emissivity of P_1, towards back plate	
Thickness of plate 2		m
Emissivity of plate 2 (glass)	Emissivity of P_2 is it is a transparent material like glass	
Emissivity of glass cover		
Thickness of glass cover		m
Emissivity of PV cell		
Thickness of PV cell		m
Distance between back and plate 1		m
Diameter of holes		m
Distance between holes		m
Distance between plate 1 and plate 2		m
Distance between cover and plate 2		m
Extinction coefficient cover		m^{-1}
Index of refraction of cover		
Extinction coefficient of Plate 2	Extinction coefficient for transparent P_2	m^{-1}
Index of refraction of plate 2	Index of refraction for transparent P_2	
Absorptivity of plate 1	Solar absorptivity of P_1	
Thickness of PV cells		m
Specific heat of air in channel 1		J/kg K
Specific heat of air in channel 2		J/kg K
Conductivity of back insulation		W/m K
Efficiency of PV cell at NOCT	Efficiency between 0 and 1	
Max. power point efficiency temperature coefficient		K^{-1}
AbsorberPlateCheck	Set to 0 for transparent P_2, set to 1 for opaque P_2	
Aborber emissivity facing up	Emissivity for opaque P_2, towards glass cover	
Absorber emissivity facing down	Emissivity for opaque P_2, towards P_1	
Absorber plate absorptivity	Solar absorptivity of P_2	
npv	equivalent PV index of refraction (see Parreta et al. 1999)	
alphapvnormal	Solar absorptivity of PV cell at normal incidence	
kside	Conductivity of side insulation	W/m K
zside	Thickness of side insulation	m

TABLE 3.5 EXTRA PARAMETERS FOR TRANSIENT MODEL

Parameters	Note	Unit
Specific Heat cover		J/kg K
Specific Heat P_1		J/kg K
Specific Heat P_2		J/kg K
Specific Heat Back Plate	Specific heat of back plate in contact with the the fluid (not insulation)	J/kg K
Specific Heat PV cells		J/kg K
density PV cells		kg/m^3
density cover		kg/m^3
density P_1		kg/m^3
density P_2		kg/m^3
density back plate	Specific heat of back plate in contact with the the fluid (not insulation)	kg/m^3

Chapter 4
EXPERIMENTAL SETUP

4.1 INTRODUCTION

To validate the TRNSYS model, a series of experiments were performed on the roof of the ERC building on the University of Waterloo campus. Its coordinates are 43.47 N,-80.54W with an elevation of approximately 330m above sea level. The PV/Thermal collector was constructed, and an apparatus was designed and built to change operating conditions and to monitor the results. The intent was to verify the models accuracy to both steady-state and transient conditions, and its response to parameters such as insolation, inlet temperature, and ambient temperature.

4.2 COLLECTOR DESIGN AND CONSTRUCTION

The collector conceptualized in Chapter 3 was built and tested. Figure 4.1 shows a section of the collector with the location of the different plates.

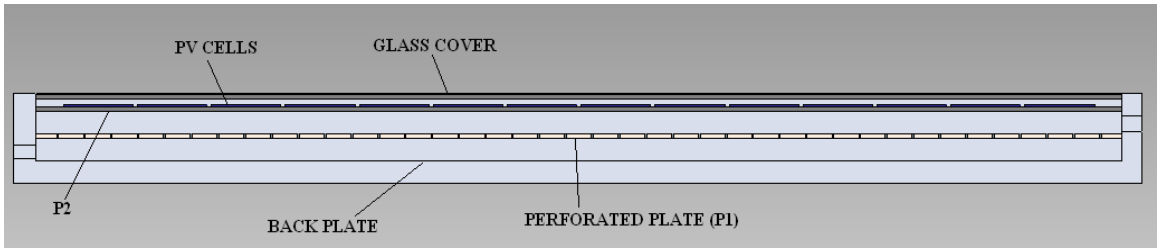

FIGURE 4.1 SECTION VIEW OF COLLECTOR

The collector is made of 5 layers: the glass cover, the PV cells, P_2, the perforated plate (P_1), and the back plate. Refer to Section 1.2.6 for more details.

4.2.1 GLASS COVER AND P_2

A standard sheet of 3.09mm tempered soda lime glass was used for the cover. Standard soda lime glass has been tested extensively so it was not necessary to test

for the properties (Rubin, 1985). According to the International Glazing Database (LBNL, 2010), the solar transmissivity of the glass to the solar spectrum is 0.834, and the reflectivity is 0.075. The infrared emissivity is 0.84 and its index of refraction is 1.526. From this data, it was possible to calculate the extinction coefficient to be $30.9 m^{-1}$.

The sheet of glass on which the PV cells were glued (P_2) was a 3.28mm sheet of ultra-clear glass (PPG, 2010). Its transmissivity was 0.899, reflectivity 0.081, and emissivity 0.84. The extinction coefficient was calculated to be $8.98 m^{-1}$. It was assumed P_2 has a refractive index of approximately 1.526.

4.2.2 PV CELL PROPERTIES

The PV cells used were silicone monocrystaline cells. They were rated at $2.5 W_{peak}$ (5 Amp, 0.5V). The PV cells emissivity was measured to be 0.55 and the absorptivity was 0.8. Tests were conducted on three cells to get the properties of the cells using an Optical Radiation Corporation Solar Simulator 1000. The air mass was set at 1.5, and the solar simulator was calibrated at $1000 W/m^2$. The average efficiency of the three cells at 25.33°C was 11.88%. In order to calculate the effect of temperature on the efficiency of the cells, the cells were heated to tempeartures ranging between 33°C and 39.3°C. The average maximum power point current, voltage, and power temperature coefficients were found to be 0.0086 A/°C, -0.0038 V/°C, and -0.012 W/°C.

The cells were glued to P_2 with Dow Corning 3-6753 thermally conductive adhesive (Dow Corning, 2010) with a conductivity of 1.4 W/m·K and with an approximate thickness of 0.35mm. The adhesive was cured at room temperature. By visual inspection (see Figure 4.2), it was assumed that roughly 75% of the PV was glued to the glass pane. The total area of PV cells was 0.26744 m^2, which was equivalent to 34% of the aperture area.

The solar absorptivity of the cells was measured with a Cary 5000 UV-Vis-NIR spectrophotometer (Varian, 2010). Three cells were measured and the average absorptivity was 0.8.

Eighteen cells were arranged in series in an array of 3 x 6 for a total of 18 cells (See Figures 4.3). According to the data given by the supplier, the peak power (at standard test conditions) of the array was 45W (2.5W per cell). The peak voltage and current were 9V and 5A respectively.

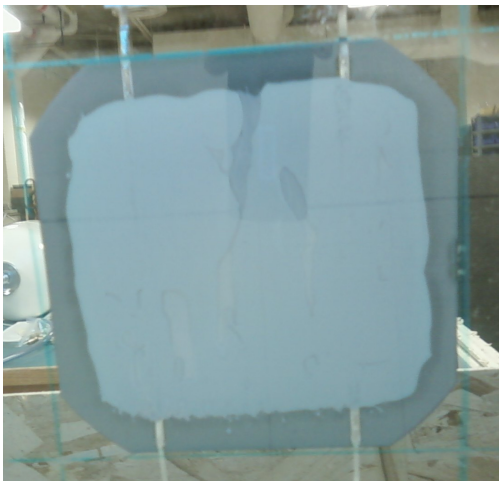

FIGURE 4.2 PV CELL ADHESIVE

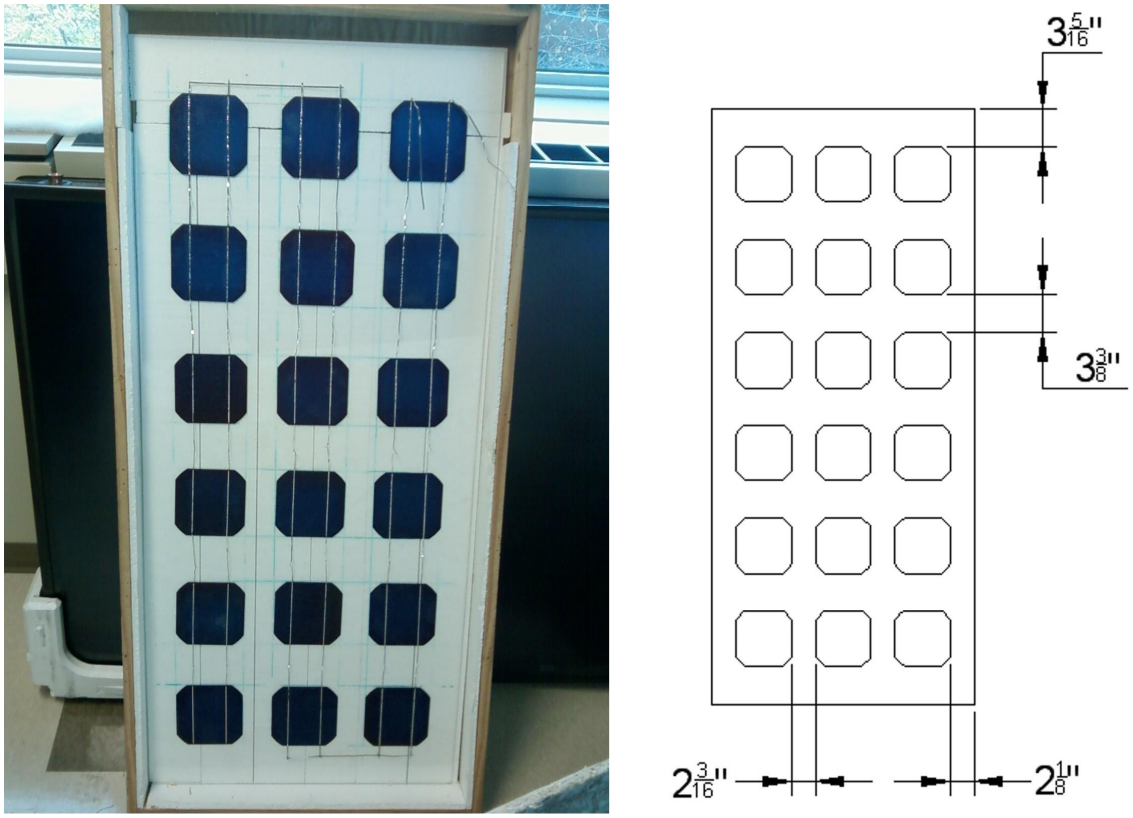

FIGURE 4.3 GLASS PANE WITH PV CELLS AND DIMENSIONS

4.2.3 PERFORATED PLATE (P_1)

The perforated plate was made of 4'-5 1/8" x 1'-11 3/8" x 1/8" aluminum plate. The 0.25" dimater holes were drilled with a distance of 3" between hole. See Figure 4.4 for a drawing of the perforated plate.

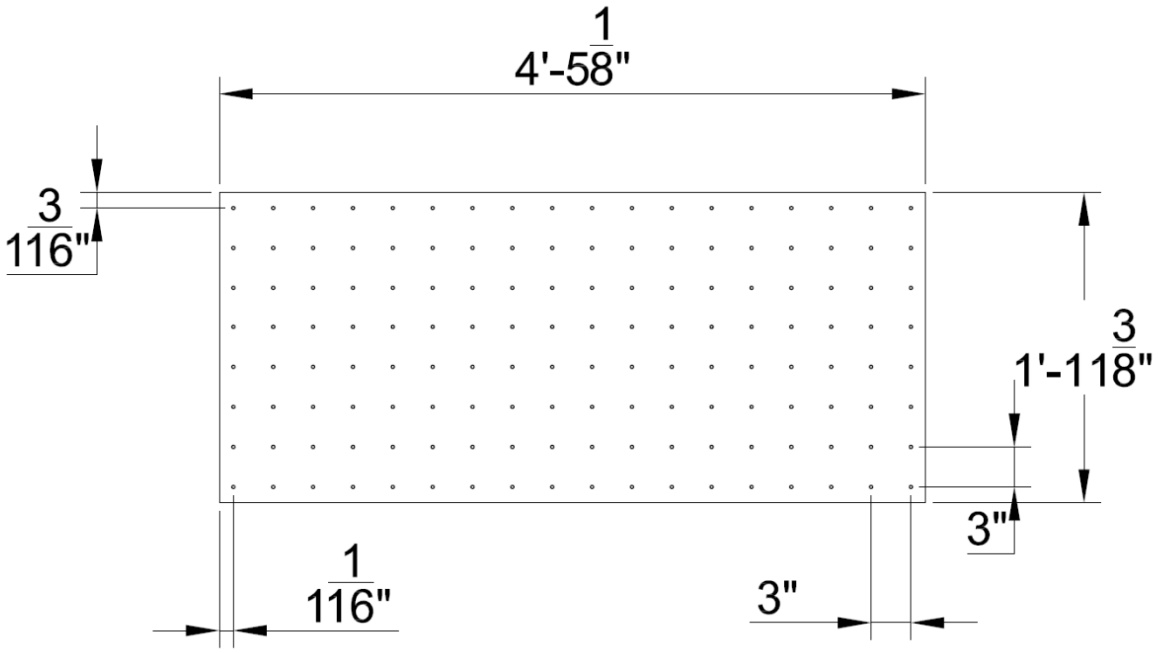

FIGURE 4.4 PERFORATED PLATE DIMENSIONS

A spectrally selective paint, Dampney Thurmalox 250 (Dampney, 2010), was applied on the perforated plate. The optical properties were measured with Gier-Dunkle reflectometers. The perforated plate had an emissivity of 0.68, and a solar absorptivity of 0.91.

4.2.4 BACK PLATE

The back plate of the collector consisted of a 4'-5 1/8" x 1'-11 3/8" x 1/8" aluminum plate. The back plate was also painted with Dampney Thermalox 250. Its emmisivity was measured to be 0.59. The back of the collector was insulated with 0.75" polyisocyanurate with a nominal conductance of 1.27 $W/m^2 K$.

4.2.5 FRAME

The collector frame was made of four 5" x 0.5" aluminum bars. Aluminum was chosen because of its relatively light weight, and because it does not rust. The collector's outer dimensions were 1.37m x 0.686m while the collector aperture dimensions were 1.34m x 0.58m for a total aperture area of 0.78m^2. Detailed construction drawings of the collector frame are shown in Appendix B.

The collector frame was built in such a way that allowed for geometry changes. Slots in the collector frame allowed for changing plates, or moving them so that the space between plates can be varied (Figure 4.5). The top slot would normally be used for the glass cover. One of the next two slots is used for P_2, and the other is left empty. This allows for testing at different distances between the perforated plate (P_1) and P_2. The fourth slot is for the perforated plate, and the last one is for the back plate. To ensure that air would not leak at the interfaces between the aluminum bars, rubber gaskets were used in those areas. The sides of the collector were insulated with 0.75" polyisocyanurate with a nominal conductance of 1.27 W/m^2 K.

FIGURE 4.5 OPENED COLLECTOR SHOWING THE SLOTS IN WHICH THE PLATES ARE INSTALLED

The plates were sealed around the edges with removable weather-strip caulk to prevent transfer of air between layers. The assembled frame, without any other components (such as plates and insulation), is shown in Figure 4.6.

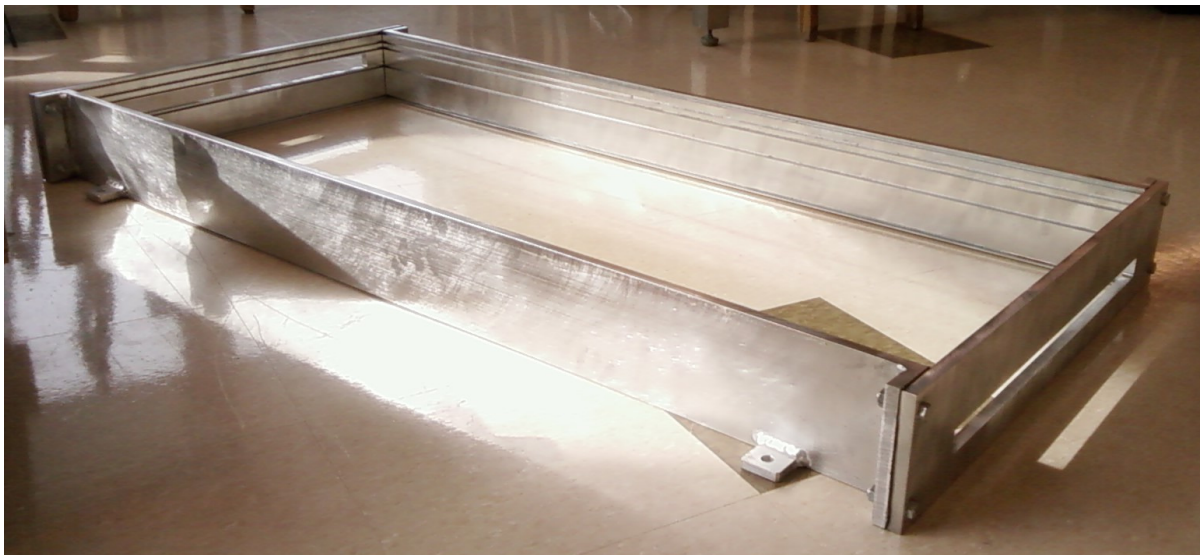

FIGURE 4.6 COLLECTOR FRAME

4.3 EXPERIMENT APPARATUS

In order to meaningfully test the collector, variables had to be monitored, and some controlled. The experiment apparatus was built to monitor all relevant variables, and to control certain other variables. Two variables were necessary to control: the mass flow rate, and the inlet temperature to the collector. Many more variables were monitored: ambient temperature, relative humidity, wind speed, incoming solar radiation, mass flow rate, inlet and outlet temperature. Figure 4.7 is a schematic of the air loop with all of the major components.

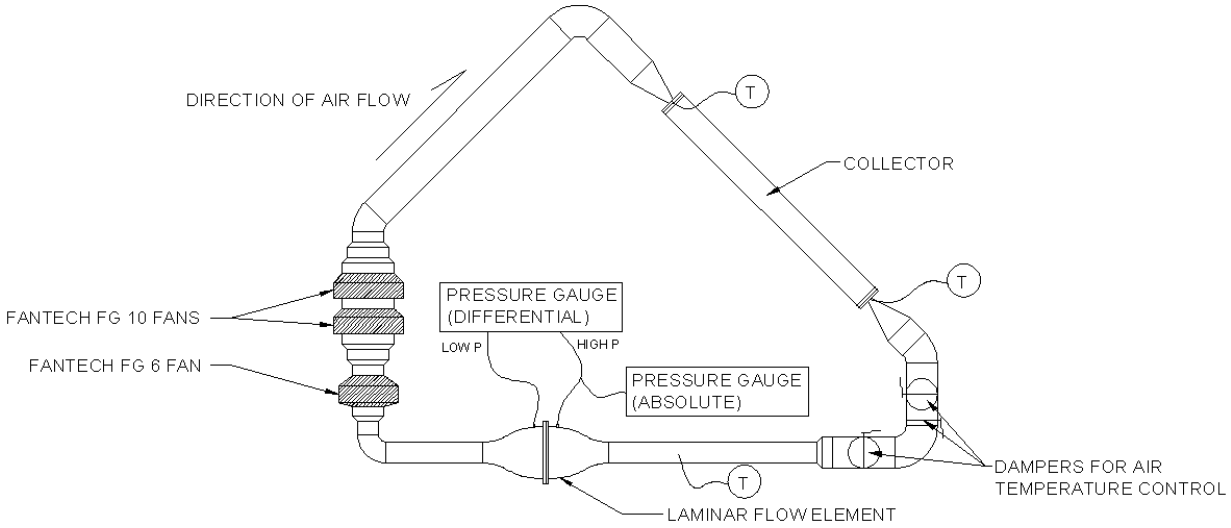

FIGURE 4.7 COLLECTOR LOOP

The collector was set at an angle of 45°, facing 29 degrees East of South.

4.3.1 FANS

The collector was supplied air by positive pressure. Three inline centrifugal fans in series produced a maximum head pressure of 6.6" H_2O (at 0 CFM), and a maximum flow rate of approximately 450 CFM. The fan models were Fantech FG6 (1 unit) and FG10 (2 units) (Fantech, 2010a). Figure 4.8 shows the fan curves of the two models of fan used, and the approximate fan curve when the three fans are in series (the sum of the head of the three fans), and functioning at full capacity. Three Fantech WC15 solid state speed controllers (Fantech, 2010) were used to control the capacity of the fans in order to get the wanted flow rate in the collector. Figure 4.9 is a picture of the three fans in series. For the experiment, the flow rates investigated were between 60 and 140CFM. Most of the head losses occurred in the flow meter, hence the need for the large amount of head at those flow rates.

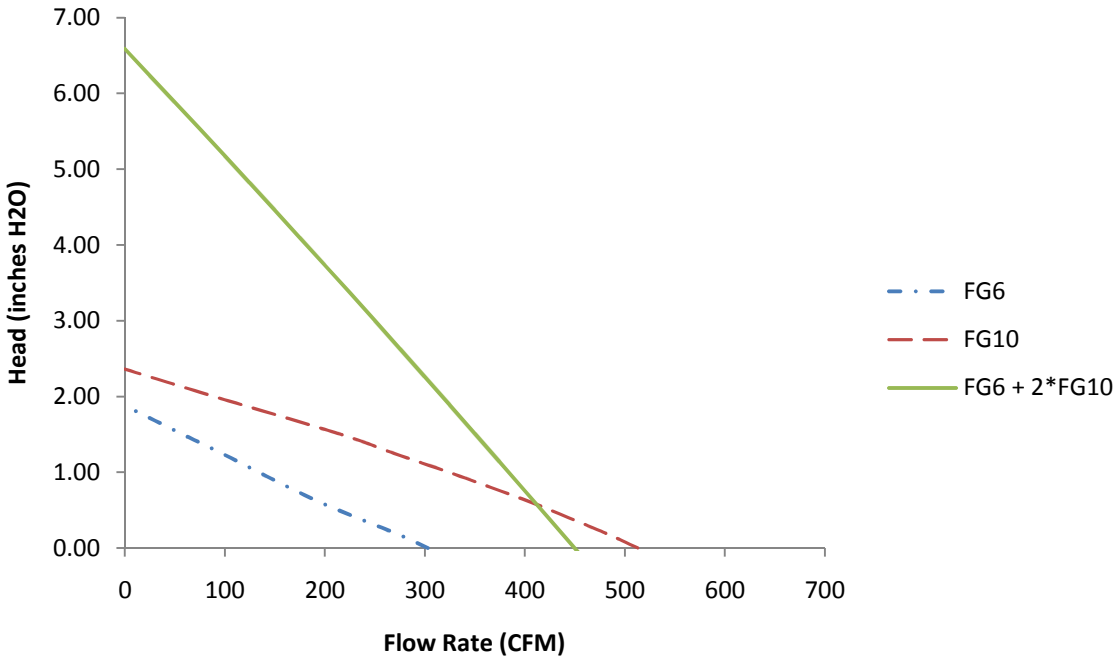

FIGURE 4.8 FAN CURVES

FIGURE 4.9 FANS

4.3.2 LAMINAR FLOW ELEMENT

The mass flow rate measurements were performed using a Meriam Z50MC2-4 (Meriam, 2009) laminar flow element (LFE). A laminar flow element is a flow meter that relates a pressure difference to a flow rate (Figure 4.10). In the case of a

laminar flow element, the flow is passed through an array of capillaries. This forces the flow to the laminar regime, with which, the Hagen-Poiseuille law can be used. The Hagen-Poiseuille relates flow rate with pressure drop across a long tube.

FIGURE 4.10 LAMINAR FLOW ELEMENT

The differential pressure across the LFE is used to calculate the actual volumetric flow rate of dry air. The equation used to calculate the standard volumetric flow rate is in the following form:

$$CFM_{STD} = (B \times DP + C \times DP^2)\left(\frac{\mu_{STD}}{\mu_{wet-air}}\right)\left(\frac{T_{STD}}{T_f}\right)\left(\frac{P_f}{P_{STD}}\right)\left(\frac{\rho_{wet}}{\rho_{dry}}\right) \qquad (4.1)$$

where B and C are given and the properties ratios are specified in graphical form in the user manual for the LFE. The accuracy of the LFE is ±0.72%.

The LFE has been calibrated for differential pressures between 1.007 and 7.997" H_2O, corresponding to flow rates between 53.64 and 420.8 CFM.

The differential pressure transducer is an Omega PX277 (Omega, 2010a) and gives a 0-10VDC output with 0-7.5" H_2O at an accuracy of ±0.075" H_2O. The absolute pressure transducer is an Omega PX209 (Omega, 2010b) and gives a 0-5VDC output with 0-30 PSIA at an accuracy of ±0.0125PSIA. All of the sensors were supplied a constant DC voltage of roughly 15VDC with a Circuit-Test PS-3030 power supply.

The temperatures in the duct were all measured with Omega type T thermocouples. The thermocouples were calibrated to an accuracy of ±0.2°C.

4.3.3 DUCTING AND INLET TEMPERATURE CONTROL

The collector was in a "closed loop" configuration. The air coming out of the collector was sent back to the fans, through the laminar flow elements, and finally, back to the collector. It was possible to vary the temperature of the inlet of the collector by opening and closing three dampers. These dampers (Figure 4.11) will allow air in and out of the loop, so that ambient air can be sent to the collector, or the outlet air (warmer than ambient air) can circulate back in the collector.

A 6" duct was used between the fans and the collector, and between the collector and the 2 dampers. The ducts were connected with the collector inlet and outlet with two transition pieces (from 6" diameter to 20" x 1" rectangle). Approximately 40" of 4" duct was used before the Laminar Flow Element, and 20" after.

FIGURE 4.11 DUCTS FOR TEMPERATURE CONTROL

4.3.4 INLET AND OUTLET TEMPERATURE MEASUREMENTS

The air temperature at the inlet and outlet of the collector were measured with type-T thermocouples. These thermocouples have an accuracy of ±1°C. The thermocouples were attached to a probe in the duct in a way that it was possible to adjust the location of the thermocouple.

4.3.5 PV MAXIMUM POWER POINT TRACKING

To track the maximum power point of the PV panel, a resistor bank was used. The resistance of the bank can be varied between 1-74 Ω. The bank is made of resistors of 1, 5, 10, 20 and 33 Ω and a 5 Ω rheostat. The resistors were all wired in series with switches that allowed bypassing the resistors (Figures 4.12 and 4.13).

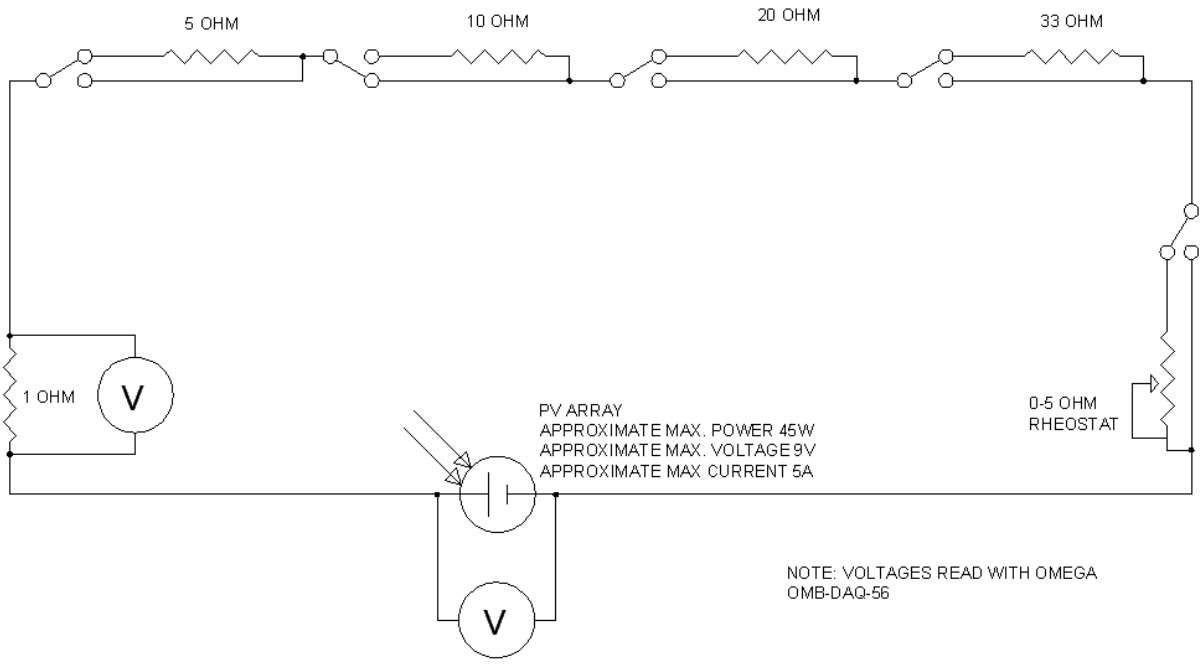

FIGURE 4.12 DIAGRAM OF THE MAXIMUM POWER POINT TRACKER

The 1Ω resistor was used to measure the current through the circuit by measuring the voltage across the resistor. Its quoted accuracy was ±1%. The relationship V=IR can be used to calculate the current. The voltage across the bank of resistor was also measured. With the current and voltage known, the power from the PV cells was calculated with P=VI. The power was measured in real time, and it was therefore possible to manually vary the resistance to find the maximum power point.

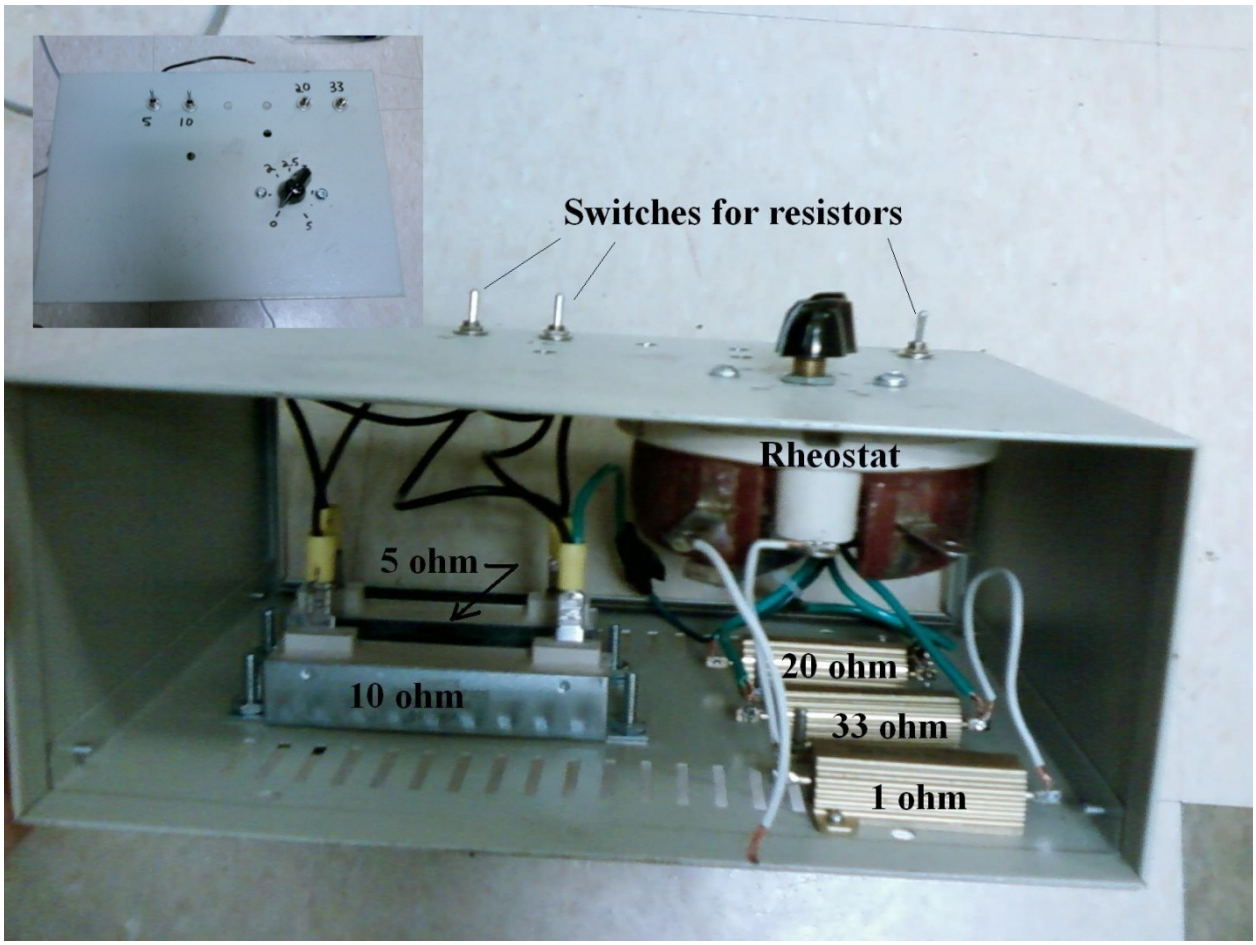

FIGURE 4.13 RESISTOR BANK FOR MAXIMUM POWER POINT TRACKING

4.3.6 WEATHER MEASUREMENTS

The wind speed was measured with an R.M. Young 05103VM (R.M. Young, 2010) anemometer with a range of 0-50m/s at a 0-1VDC output. The accuracy of the anemometer was ±0.3m/s + 1% of reading. The ambient humidity and temperature were measured with a Vaisala HMP155 (Vaisala, 2010) with a Vaisala DTR503 radiation shield. The temperature range of the sensor is -40°C to 60°C at a 0-1 VDC output and the %RH range is 0-100% at a 0-1VDC output. The accuracy of the humidity sensor was ±0.6%RH between 0 and 40%RH and ±0.9%RH between 40 and 97%RH. The temperature sensor accuracy was ±0.1°C. They were located roughly 4 meters west of the collector, at an elevation about 0.6 meters above the top of the collector.

The incoming radiation was measured with an Eppley Lab pyranometer model PSP (Eppley Lab, 2010). The pyranometer was installed on the same plane as the collector and measured the total solar radiation on the collector. The pyranometer has an accuracy of ±5%.

4.4 DATA ACQUISITION AND MONITORING

All sensors were connected to an Omega OMB-DAQ-56 data acquisition board. The readings were taken every 0.5 seconds.

NI LabVIEW was used to provide a graphical user interface allowing monitoring of the different sensors, and calculations (for flow rate measurements), in real time. LabVIEW logged every data point in one file, and a 5 minute average in a separate file.

The graphical user interface also allowed for manual maximum power point tracking. Looking at the instantaneous power output of the PV, it was possible to manually adjust the resistor bank to the appropriate value for maximum power output.

Images of the LabVIEW front panel can be found in Appendix C.

Chapter 5
RESULTS AND DISCUSSION

5.1 INTRODUCTION

As discussed in Chapter 4, experiments were conducted to test the validity of the model described in Chapter 3. The results of this experiment and a discussion of those results make up this chapter.

The thermal mass of the collector and the time step size used in the model are discussed first. The last section of the chapter presents the weather data and the comparison between the model results and the experimental results.

5.2 MODEL VALIDATION

5.2.1 TRNSYS ANALYSIS

Data gathered from the experiment was fed into the TRNSYS transient and steady state models. The following standard TRNSYS types were used:

Type 9c - Data Reader for Generic Data Files
Type 69b - Effective Sky Temperature for Long-Wave Radiation Exchange
Type 33e - Psychrometrics: Dry Bulb and Relative Humidity Known
Type 65c - Online Graphical Plotter with Output File

Type 9c is used to read the weather data gathered during the experiment. Type 69b output generates an effective sky temperature based on ambient and dew point temperatures, and radiation on the horizontal plane. Type 33c generates a dew point temperature, used in type 69b, based on dry bulb temperature and relative humidity. Finally, type 65c generates a file with the experimental and modeling data.

Custom TRNSYS types were also used:

Type 195 – Impinging Jet PV/T Collector Steady State model
Type 196 - Impinging Jet PV/T Collector Transient model
Type 202 – Radiation Converter

Types 195 and 196 are the Impinging Jet PV/Thermal collector models. Type 202 is a component originally written by Ann L. Barrett (1987), and then modified by Véronique Delisle (2007). It is used to convert a single total incident radiation measurement, at a specified angle, into beam, sky diffuse, and ground components.

5.2.2 THERMAL MASS

In Section 2.6, the transient effects of thermal collectors were discussed. The literature on this topic seems to point towards gains in prediction accuracy of thermal collector performances when thermal mass is considered. In order for the more complex transient models to yield better results, weather data should be available at a few minutes interval for a multi-node approach, or every hour for a single node approach. Even at one hour data interval, neglecting the thermal mass results in almost as good results as the single node models.

Typical collectors are built differently than the one built for the present experiment. Typically, the plates are supported by an insulating material with relatively small thermal mass, and the air only exposed to this material. The frame then supports the insulating material. In this experiment, the plates were supported by the aluminum frame, and the warm air was in contact with the frame. This made the construction of the collector much simpler than a typical collector. The drawbacks of this way of building the collector are that the frame plays a part in the thermal mass, and also acts as a thermal bridge between the plates. To see the effects of thermal mass on the model, and the added effect of the frame, data taken on March 31st 2010 was compared to the TRNSYS model for three cases with a time step of 5 minutes.

The first case analyzed was the "zero-capacitance" model. In this model, the transient effects were neglected and the collector plates and frame were assumed to have no mass. The second case was the "standard thermal mass" model. The standard thermal mass model included the thermal mass of the plates, but not the frame. The last case was the "added thermal mass" model. This model accounted for the extra thermal mass of the frame. To account for the thermal mass of the frame, the densities of each plate were increased by 65% in the model. The amount by which to increase the densities of each plate was calculated so that the sum of the thermal mass of the plates used in the model was the same as the total thermal mass of the actual collector (plates and frame) as used in the experiment.

After running all three models, it was found that the best fitting model was the "standard thermal mass" model that accounts only for the mass of the plates. All three models gave almost exactly the same results for the electrical output, but the thermal output yielded more significant differences. This was likely because PV cells outputs are only slightly dependent on temperature. Most of the transient effects on a PV cells are due to irradiance levels. Figure 5.1 shows the experimental results and the model results for the PV electrical output. The PV output difference between the three models was so small that it cannot be seen on a graph. For that reason, only one graph is shown for all three models.

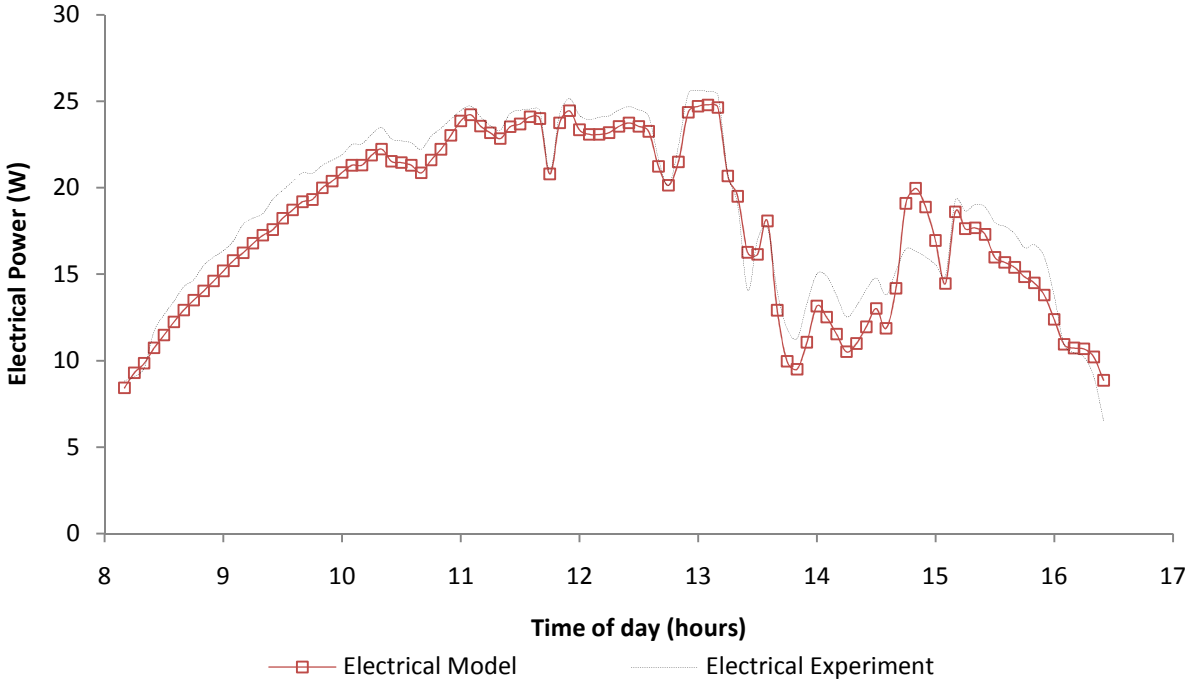

FIGURE 5.1 MARCH 31 ELECTRICAL OUTPUT FOR ZERO-CAPACITANCE MODEL AND TRANSIENT MODELS

Figure 5.2 shows the heat gain results of the "standard" and "added" mass models, and the experimental results for the heat gain. By visual inspection, it is clear that the two models yield very similar results, except that the "standard mass" model response is slightly faster at the beginning of the day.

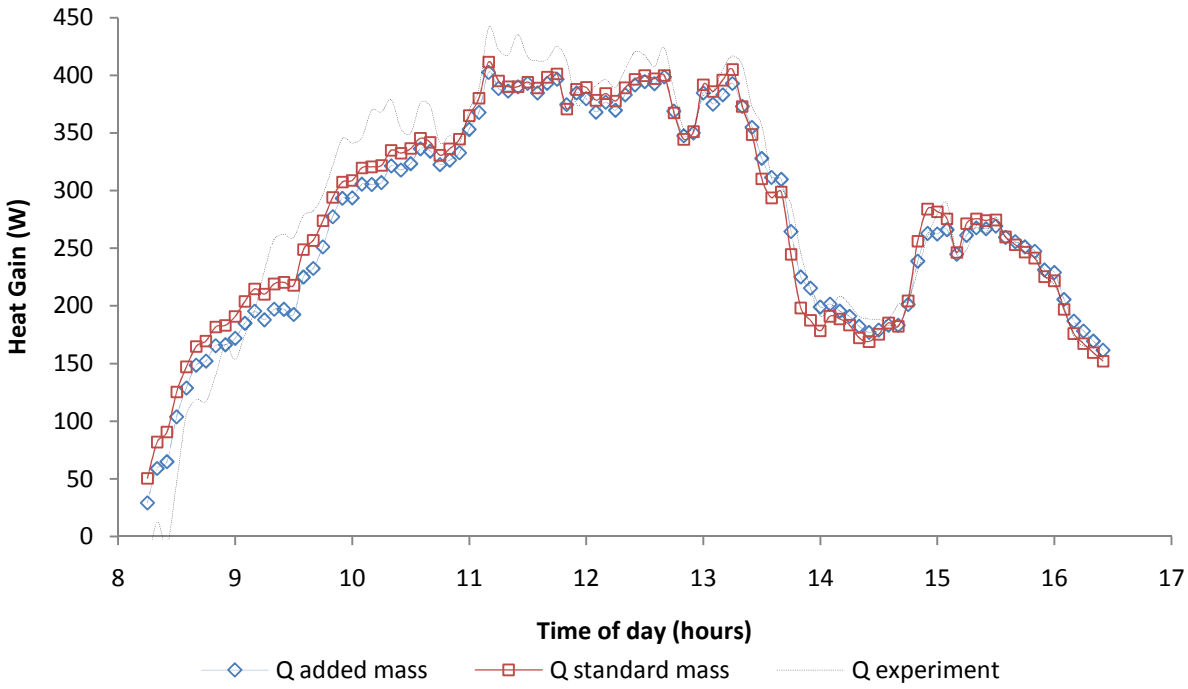

FIGURE 5.2 MARCH 31 THERMAL OUTPUT FOR ADDED MASS AND STANDARD MASS MODELS

Figure 5.3 shows the results of the "standard mass" model, the "zero-capacitance" model, and the experimental results for the heat gain. In this case, there is a much larger difference between the "standard mass" and the "zero-capacitance" models. The zero-capacitance model is much quicker to respond to changing parameters, and this creates large variations in the thermal output in relatively short amounts of time.

The root mean squared deviation (RMSD) between each model and the experimental data was calculated. The RMSD values for the "added mass", "standard mass", and "zero-capacitance" models were found to be 32.4 W, 32.0 W, and 45.5 W respectively. The RMSD is a measure of how well the individual model data points fit the experimental data points. The lower the RMSD, the better the model is at predicting each data point.

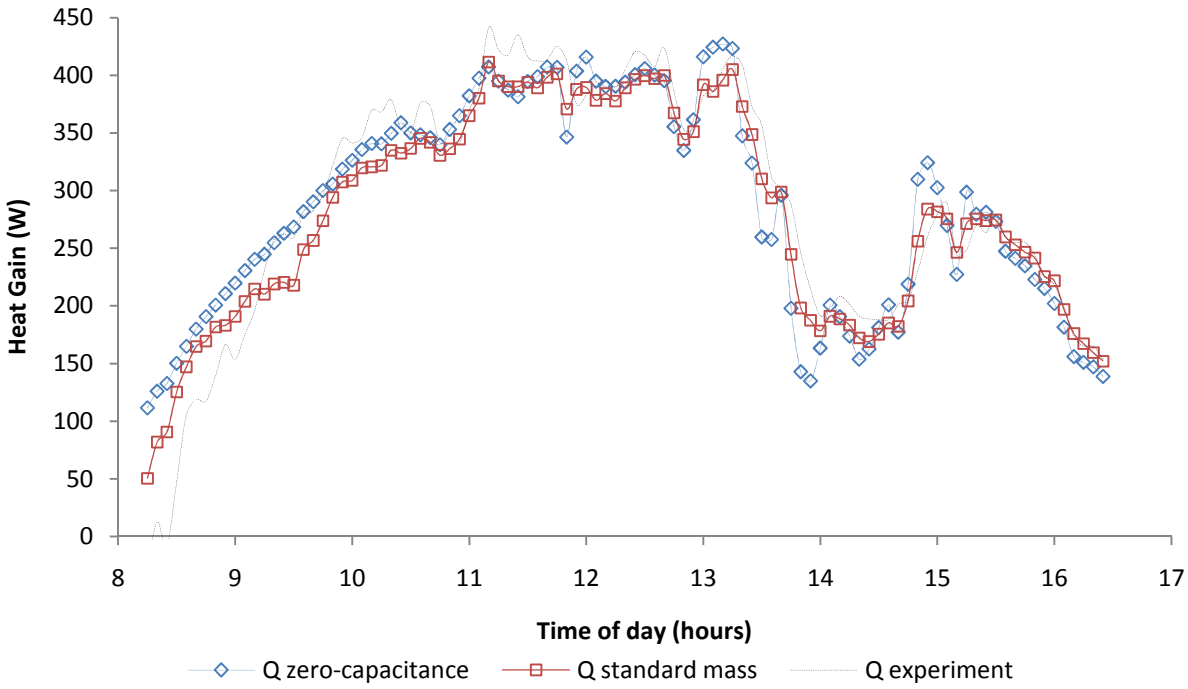

FIGURE 5.3 MARCH 31 THERMAL OUTPUT FOR STANDARD MASS AND ZERO-CAPACITANCE MODELS

Another way of looking at how well the model fits is by looking at the total energy over a certain amount of time. Table 5.1 shows the energy output for the models and the experiment of March 31st. The zero-capacitance model does seem to be the best at predicting the total energy gain for the day. This should, however, not be seen as a proof that the zero-capacitance model is better. For that day, the two other models seem to constantly slightly underestimate the heat gain, but the zero-capacitance model overestimates the heat gain for the first 2 hours of the day. This seems to yields just enough extra heat gain to make up for underestimating the rest of the day. The transient trends are estimated with much better accuracy by the two models with mass as noted by the RMSD.

TABLE 5.1 MARCH 31 TOTAL ENERGY COMPARISONS FOR VARYING THERMAL MASS

	5 minutes time step		% Difference with experiment	
Model	Heat Gain (W·h)	Electrical Energy (W·h)	Heat Gain	Electrical Energy
Standard Mass	2311.5	148.3	-2.1	-4.4
Added Mass	2265.0	148.5	-4.2	-4.3
Zero-Capacitance	2371.4	148.1	0.4	-4.6
Experiment	2361.0	155.0	-	-

5.2.3 TIME STEP

Another important parameter that should be studied is the time step size. For the purposes of this research, a small time step should be used to be able to pick up as much of the transient effects of the collector as possible; however, most of the weather data used in industry is hourly. It is therefore important to make sure that the model yields acceptable results at a small time step and an hourly time step. Three time steps were tested: 1 hour, 30 minutes, and 5 minutes. Figures 5.4 – 5.6 show the heat gain and electrical power results for those time steps. The experimental and weather data was recorded every 0.5 seconds, but averaged over the relevant time step.

Figures 5.4 - 5.6 show very good agreement for all time steps. When looking at the graphs for the different time steps, it becomes quite obvious that some information is lost when using larger time steps. The same general trends are still shown, but the events that happen on a shorter amount of time are averaged out in the longer time steps results.

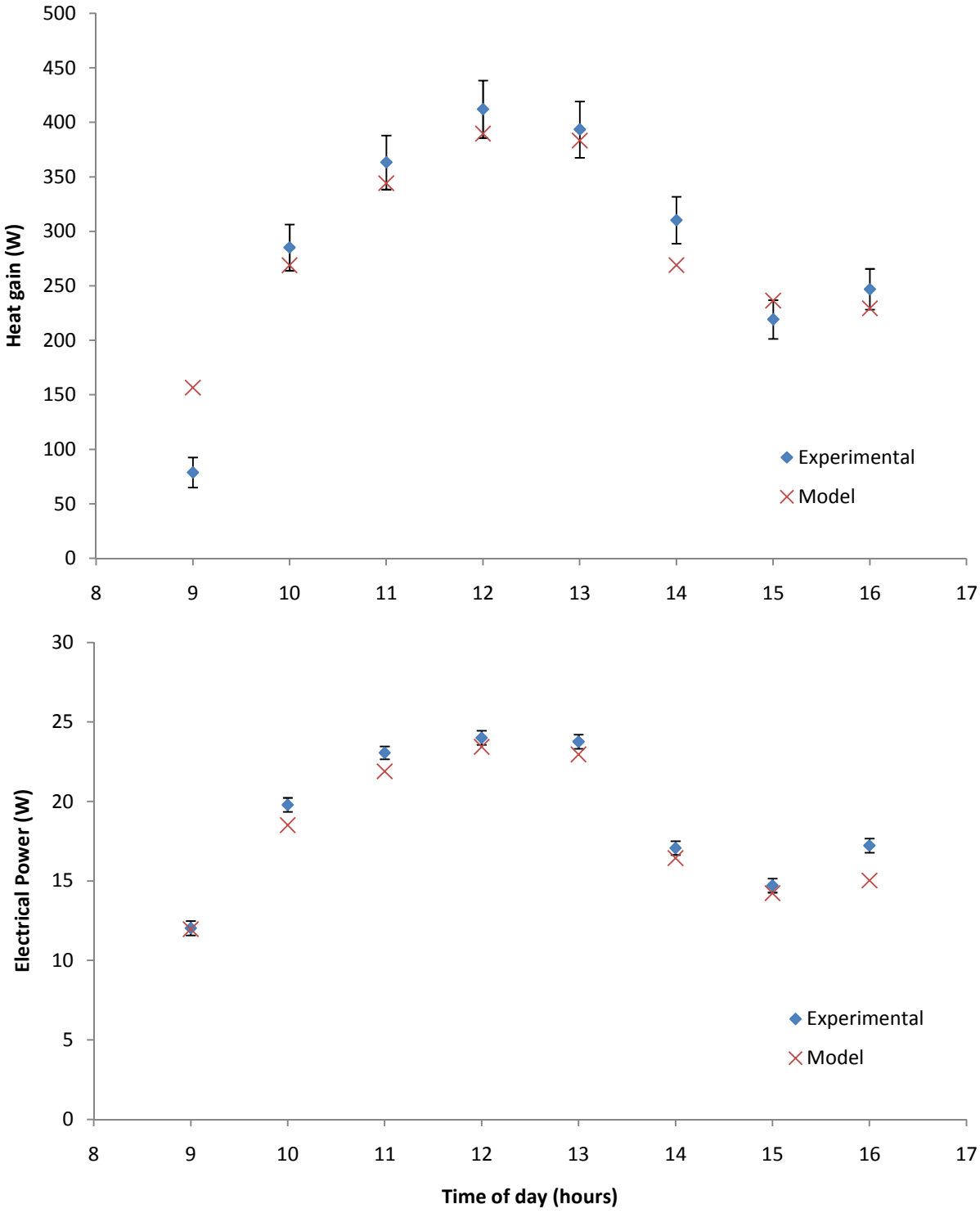

FIGURE 5.4 MARCH 31, 1 HOUR TIME STEP THERMAL AND ELECTRICAL RESULTS

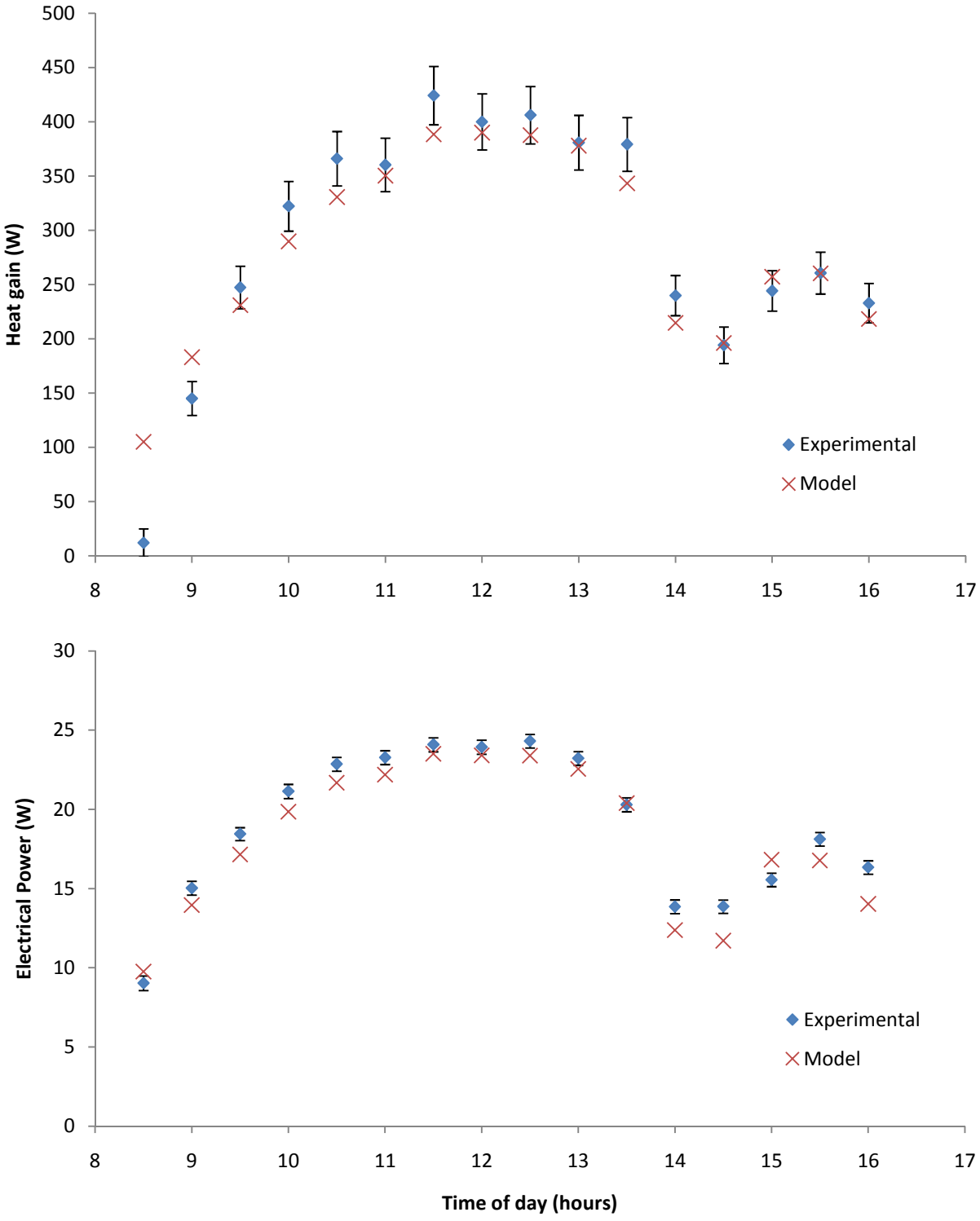

FIGURE 5.5 MARCH 31, 30 MINUTES TIME STEP THERMAL AND ELECTRICAL RESULTS

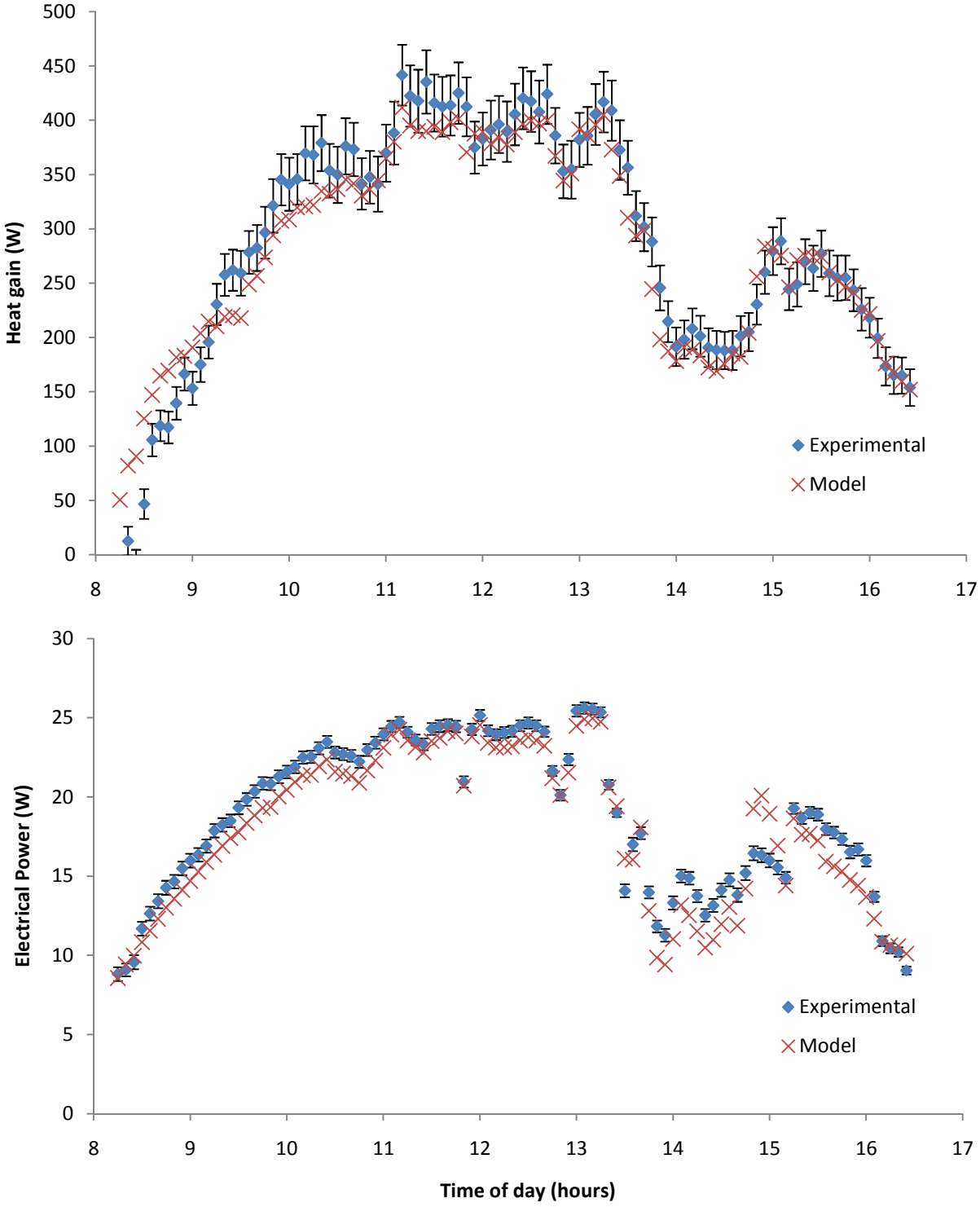

FIGURE 5.6 MARCH 31, 5 MINUTES TIME STEP THERMAL AND ELECTRICAL RESULTS

The total energy output for the first 8 hours of the day at different time steps are shown in Table 5.2. All three time steps show good agreement with the experimental data. Even though the 1 hour time step was slightly better at predicting the total energy output for the day, the 5 minutes time step provides much more information about the collector than the 1 hour time step. Also, one factor to keep in mind is that the initial conditions of the collector fed into the model (at the beginning of the day) are not exact. This may have a small effect on the behavior of the model for the first hour. Overall, the three time steps yield very good results for that particular day.

TABLE 5.2 MARCH 31 TOTAL ENERGY COMPARISONS FOR VARYING TIME STEP

	Standard mass model		Experiment		% Difference with experiment	
Time Step	Heat Gain (W·h)	Electrical Energy (W·h)	Heat Gain (W·h)	Electrical Energy (W·h)	Heat Gain	Electrical Energy
1 hour	2277.3	144.4	2308.8	151.7	-1.4	-4.9
30 min	2262.1	144.8	2307.7	151.7	-2.0	-4.7
5 min	2207.0	145	2306.2	151.6	-4.4	-4.5

5.3 RESULTS

This section compares the model output and the experimental results. All model results are for the standard mass model, and the time step size is 5 minutes.

For each day, a discussion of the results is provided, then figures. The first figure is a graph of the weather data for the day. The second figure is a graph of the experimental inlet and outlet temperatures, the model outlet temperature and the mass flow rate. The third figure is a graph of the model and experimental PV electrical outlet and heat gain calculated with $Q_{gain} = \dot{m}C(T_{out} - T_{in})$.

The experimental error bars were calculated as shown in Appendix D. The experimental error bars are shown for the mass flow rate, heat gain, and PV output for all days. The error bars for the temperature measurements are not shown as they are too small (0.2K) to be clearly visible on the graph. They were however considered in the error analysis for the heat gain graphs. The uncertainty due to the manual maximum power point tracking is not included in the error bars.

The uncertainty in the model also needs to be considered. The input values to the model all have an associated uncertainty, so the output values will also have a

certain amount of uncertainty. To evaluate the uncertainty of the model, a perturbation method (Moffat, 1985) was used. Because of the clutter that would be brought by two different sets of error bars in a graph (experimental and model), only the experimental error bars are shown for all days. An example of the model error bars is shown for March 31 in figure 5.9.

A sample of raw data and TRNSYS simulation results are shown in Appendices E and F respectively.

5.3.1 STEADY OPERATING CONDITIONS

One day of data was taken with a near constant mass flow rate, and a collector inlet temperature almost equal to the ambient temperature. These two conditions are the only ones easily controlled. For all else being equal, the ratio $\frac{T_{in}-T_{ambient}}{S}$ and the mass flow rate are the two most important predictors of performance in a collector. By keeping those constant, the response of the model to weather conditions alone can be evaluated.

On March 31st, the collector was run at steady operating conditions. The dampers in the ducts were opened in such a way that ambient air would flow in the ducts, to the collector. When this was done, it was almost always found that the air at the inlet of the collector was slightly warmer than ambient. This is most likely due to the sun warming the ducts. A small amount of heat given by the fans may also be part of the explanation. The mass flow rate was kept fairly constant at around 0.04kg/s. The weather data for March 31st is shown in Figure 5.7. Figure 5.8 shows the temperatures and mass flow rate. The heat gain and electrical output are shown in Figure 5.9 with experimental and model error bars.

As discussed previously, the model works very well for that particular day. The electrical output seems to consistently be underestimated, while the heat gain is slightly overestimated for the first hour. Most of the model's data points for the heat gain are within the error bars.

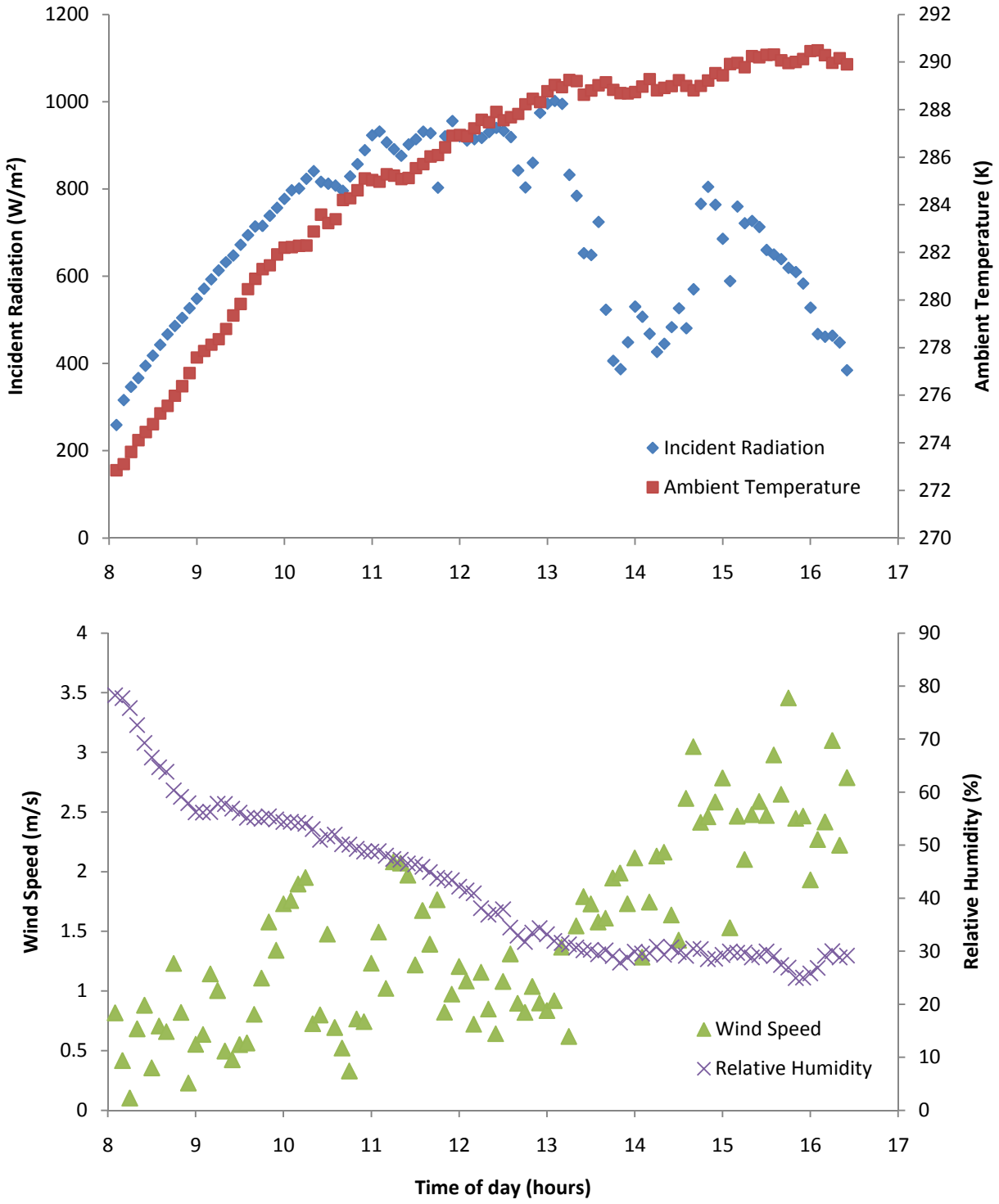

FIGURE 5.7 MARCH 31 WEATHER DATA

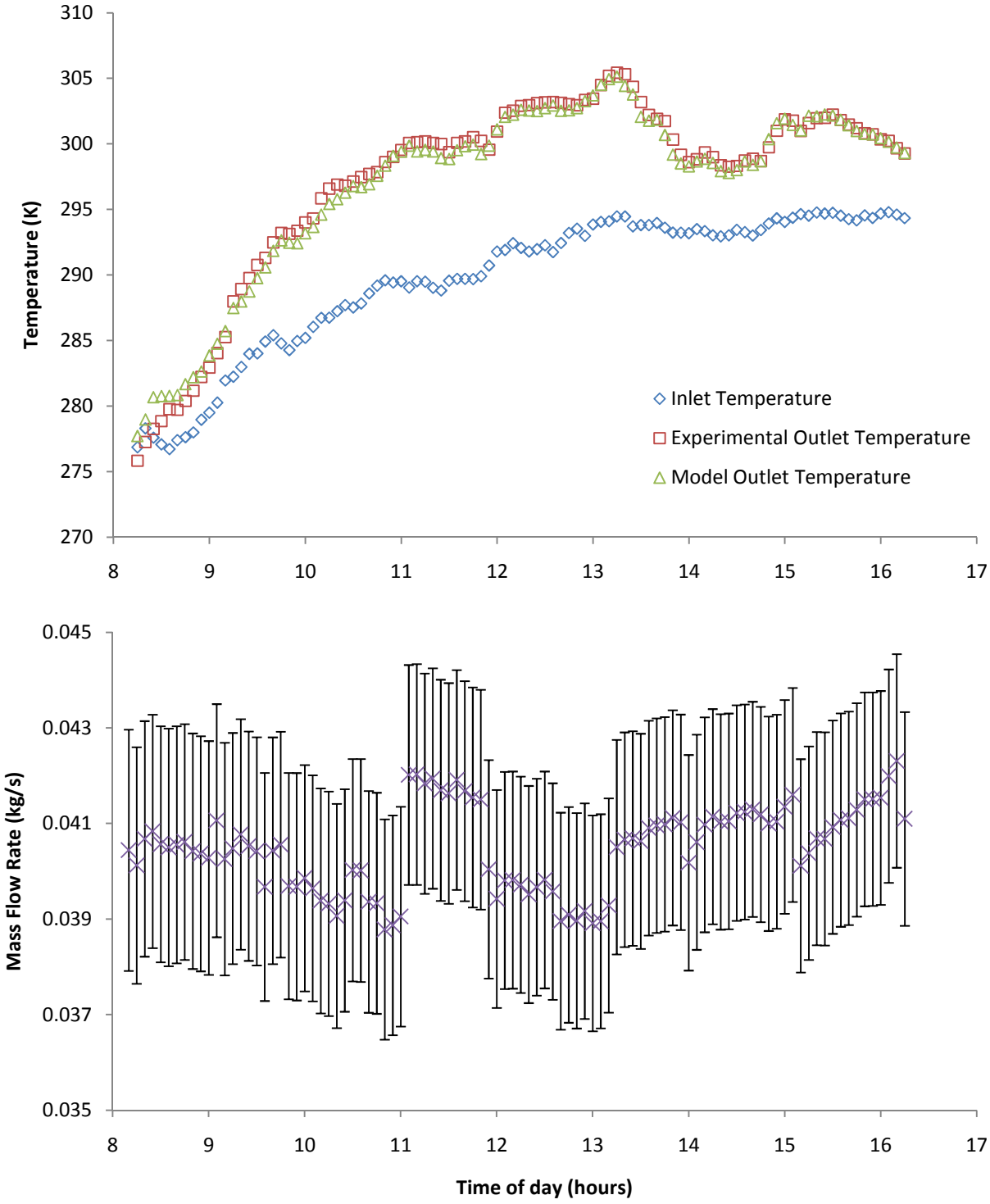

FIGURE 5.8 TEMPERATURES AND MASS FLOW RATE

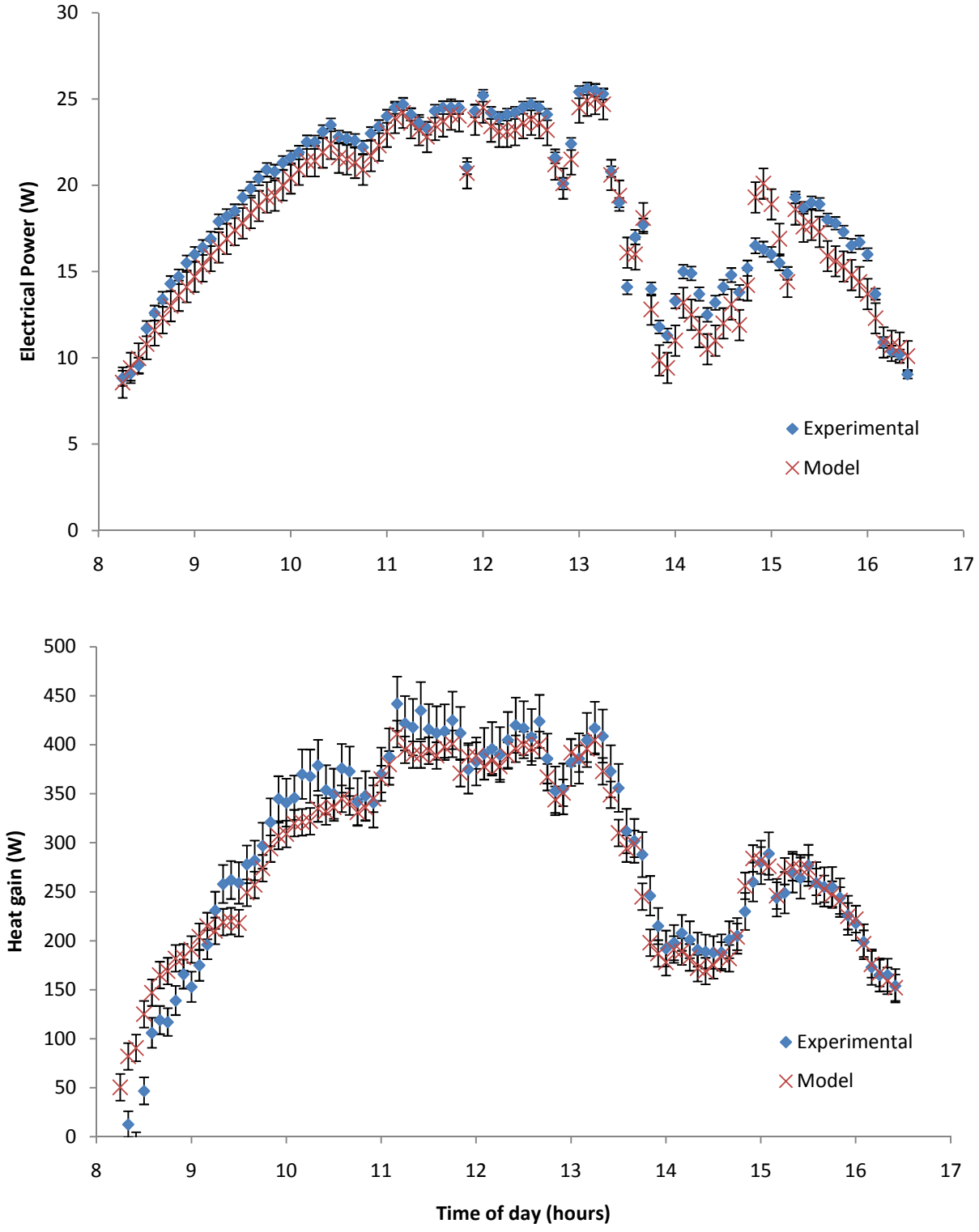

FIGURE 5.9 MARCH 31 MODEL ERROR BARS PV OUTPUT AND HEAT GAIN

5.3.2 VARIATION OF MASS FLOW RATE

To look at the effects of a change in mass flow rate on the collector performance and the ability of the model to accurately evaluate the changes in output, the mass flow rate was varied on two days.

On January 30th, the dampers were arranged in such a way that ambient air was fed to the inlet of the collector. The mass flow rate was kept between roughly 0.030kg/s and 0.035kg/s until noon. At noon, the flow rate was increased to roughly 0.043kg/s and was kept between 0.035kg/s and 0.045kg/s until the rest of the day. Figure 5.12 show that a very good agreement between the model and the experimental results was found for both the electrical and thermal power outputs. The model seems to pick up the transient response of the system fairly well for the whole day. The weather data is shown in Figure 5.10, and the inlet and outlet temperatures and the mass flow rate are shown in figure 5.11.

Due to an equipment problem, data between 10:20AM and 10:50AM on January 30th was not collected. The weather data fed in the models at those points was the same as for 10:15AM. This was needed because the transient models require previous time step data. Those data points were later removed from the results, which is why there is a gap with no data points in the graphs.

On February 8th, the air was recirculated to the collector. The mass flow rate was kept at approximately 0.037kg/s until 12:30PM when it was lowered to approximately 0.025kg/s. The electrical output matches the transient model fairly well but it is under predicted after 1:30PM. The heat gain is slightly under predicted from the beginning of the day until the flow rate is changed. It is afterwards over predicted. The weather data for February 8th is shown in Figure 5.13. Figure 5.14 shows the temperatures and mass flow rate. The heat gain and electrical output are shown in Figure 5.15.

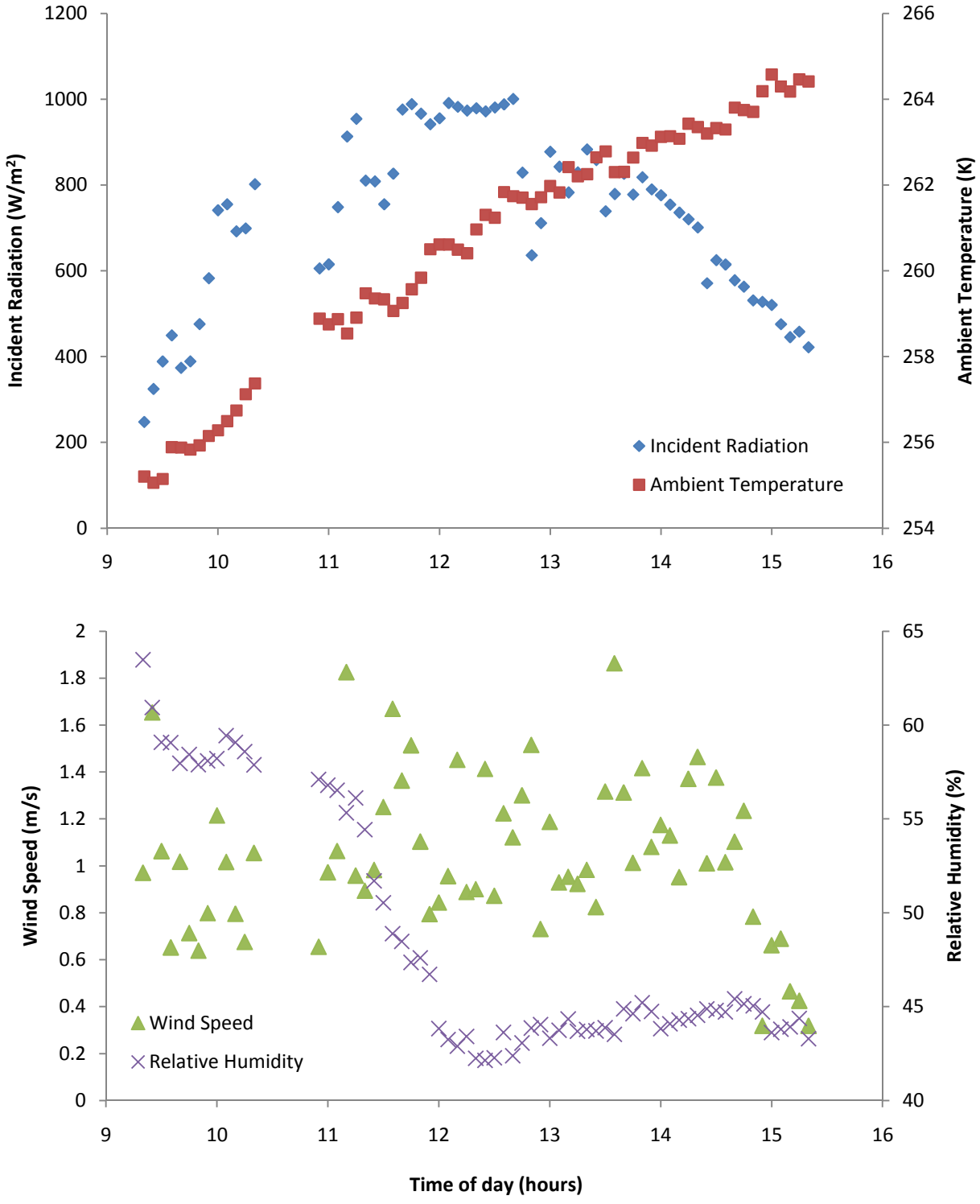

FIGURE 5.10 JANUARY 30 WEATHER DATA

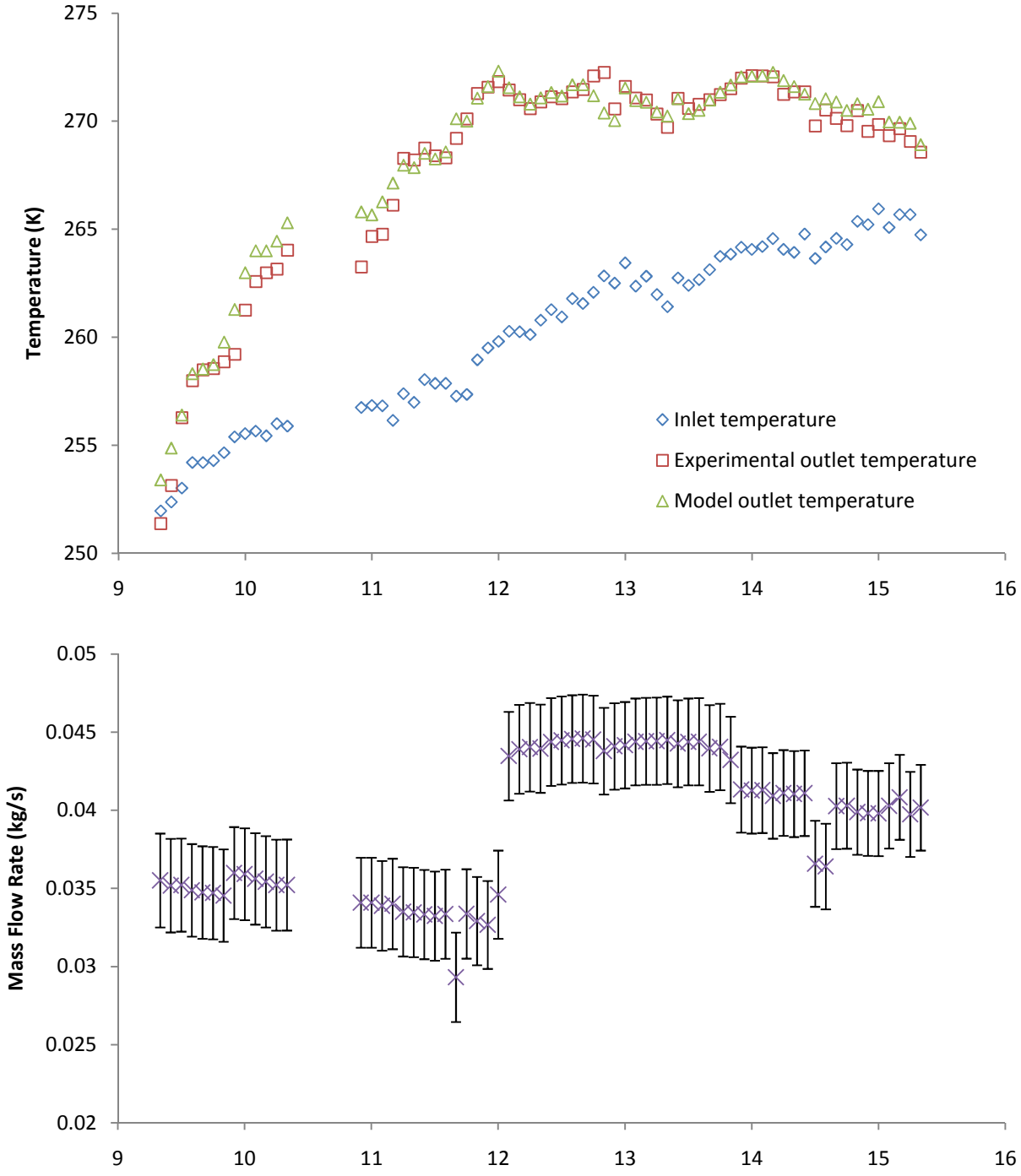

FIGURE 5.11 JANUARY 30 TEMPERATURES AND MASS FLOW RATE

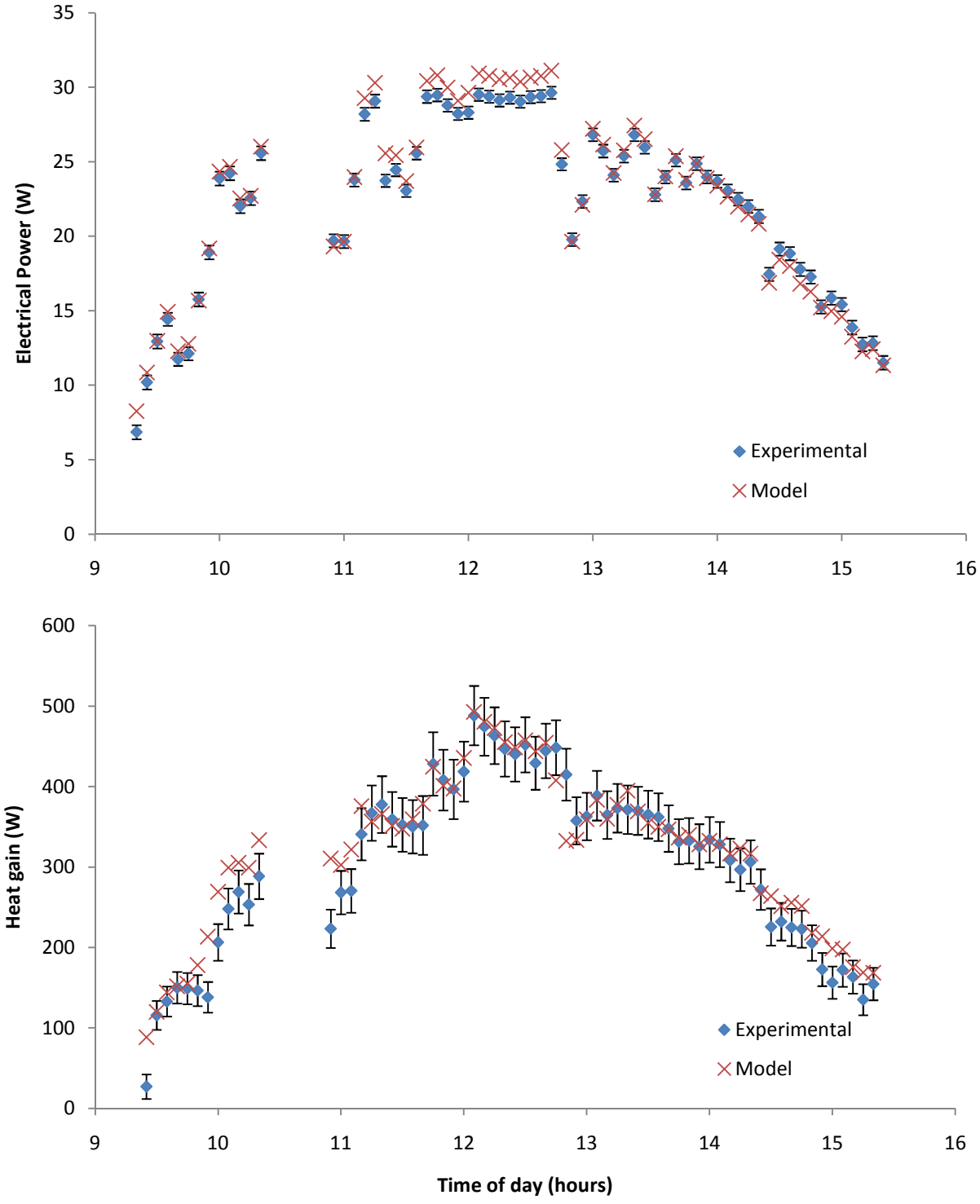

FIGURE 5.12 JANUARY 30 PV OUTPUT AND HEAT GAIN

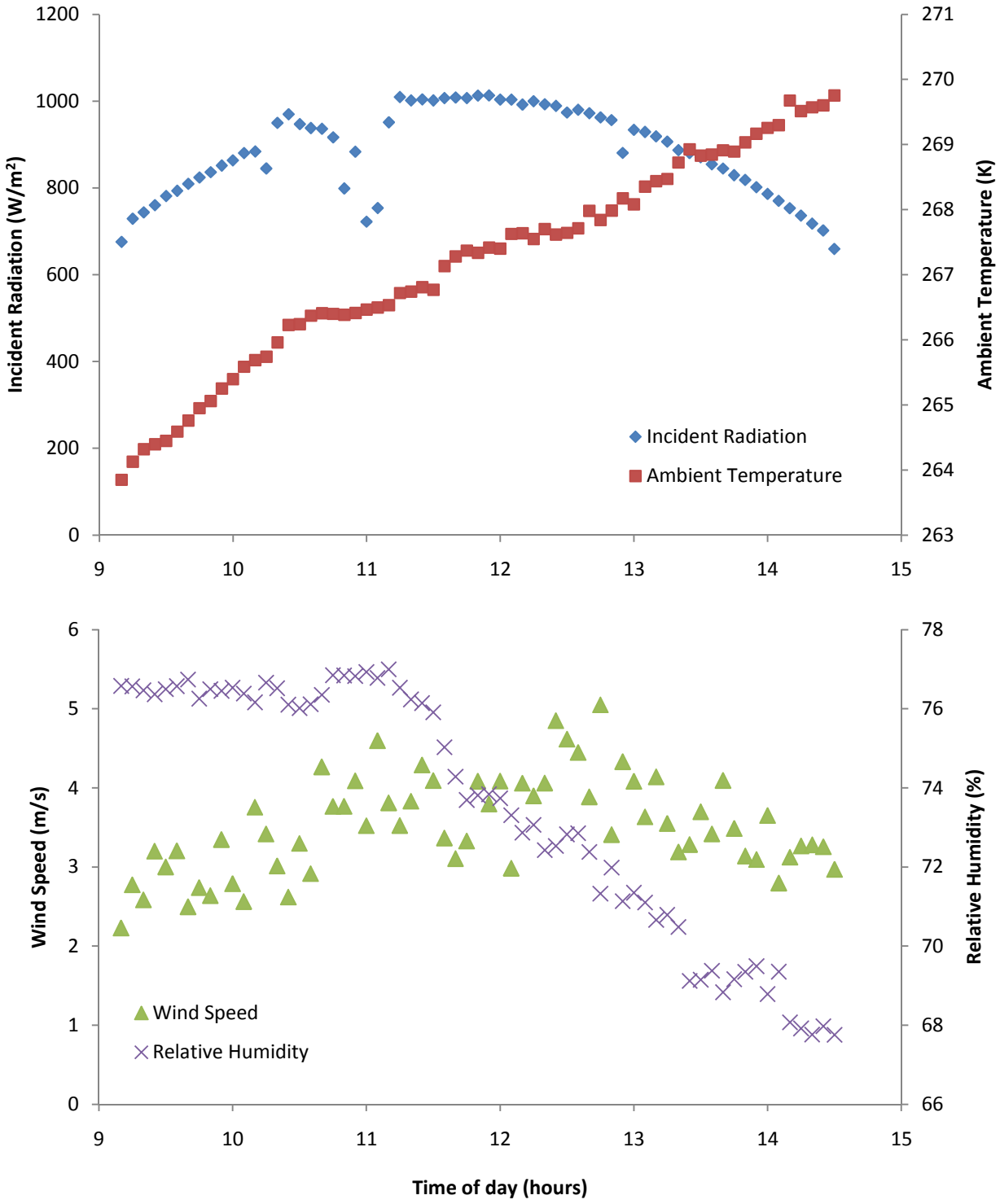

FIGURE 5.13 FEBRUARY 8 WEATHER DATA

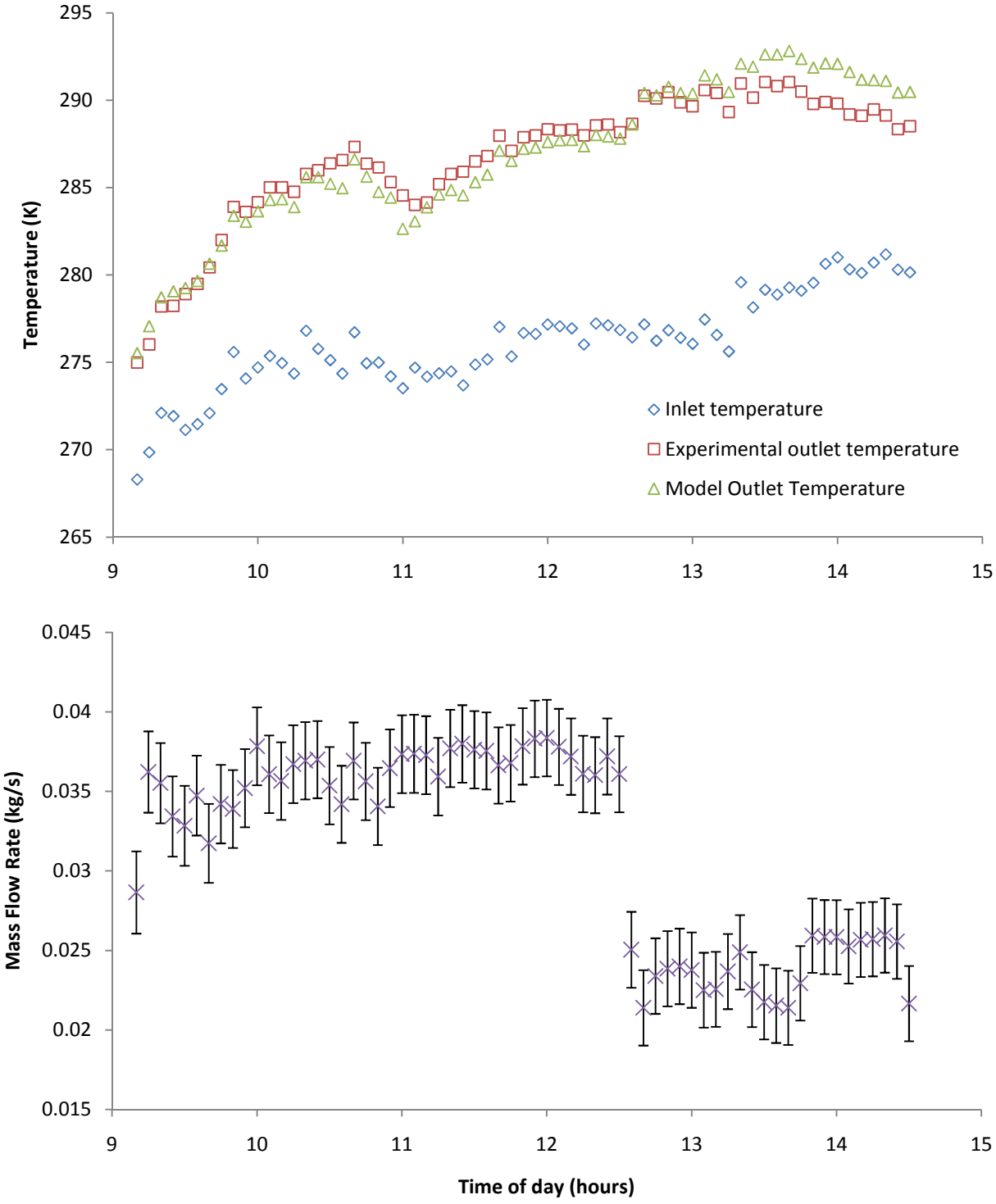

FIGURE 5.14 FEBRUARY 8 TEMPERATURES AND MASS FLOW RATE

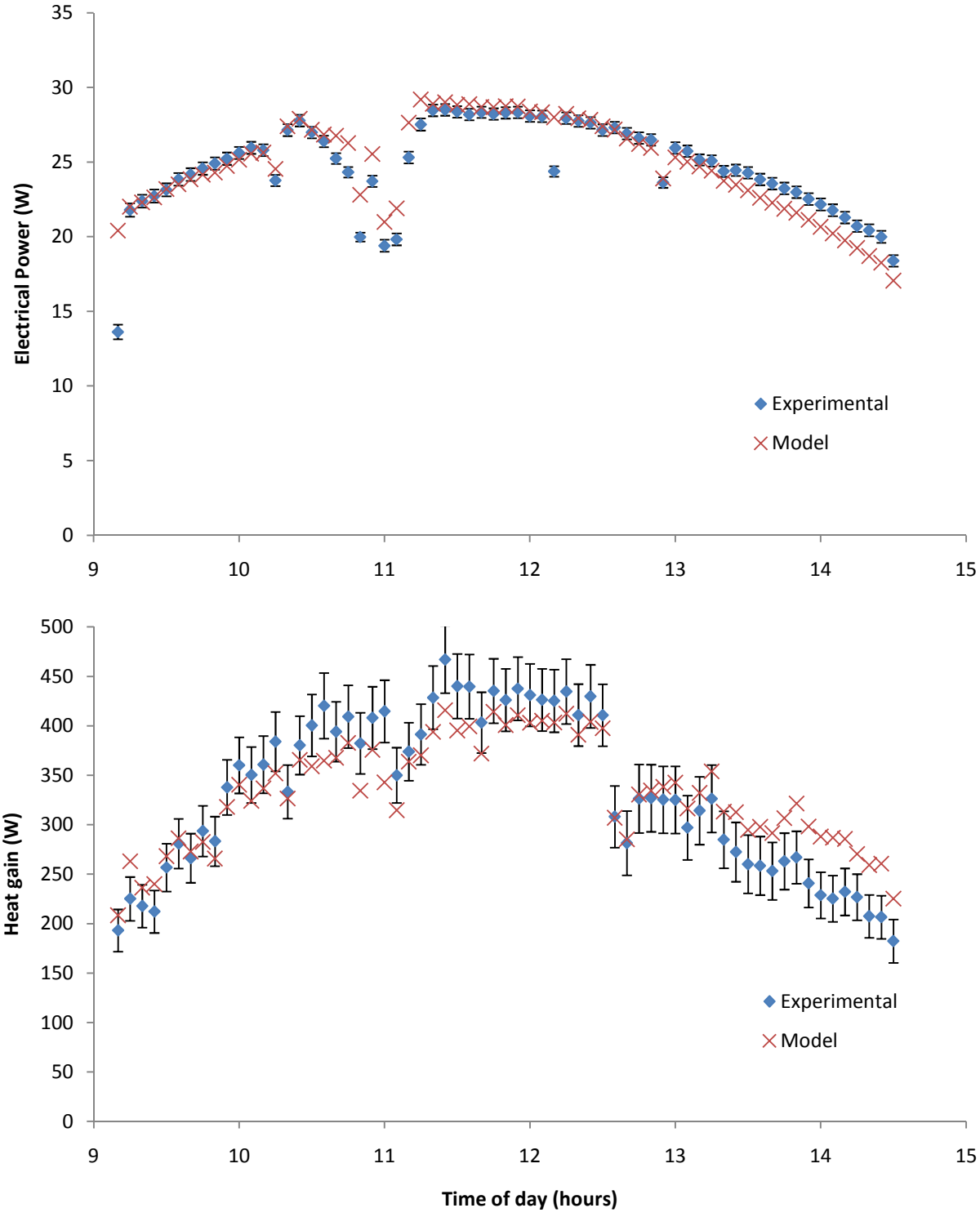

FIGURE 5.15 FEBRUARY 8 PV OUTPUT AND HEAT GAIN

5.3.3 VARIATION OF INLET TEMPERATURE

Similarly to varying the mass flow rate, the inlet temperature can be varied by changing the configuration of the dampers. On February 21st, the flow rate was kept fairly constant at approximately 0.033 kg/s for the whole day. Warm air was recirculated to the collector until 11:30AM after which ambient air was fed to the collector. At 2:25PM, the dampers were adjusted again to allow warm air to flow to the collector again. The thermal model fits well until 11:30AM, but the heat gain is over predicted afterwards. The electrical output is under predicted starting at around 1:00PM. The weather data for February 21st is shown in Figure 5.16. Figure 5.17 shows the temperatures and mass flow rate. The heat gain and electrical output are shown in Figure 5.18.

The missing data points in the experimental electrical output at 14:00 is due to human error while operating the resistor bank for maximum power point tracking. The data points were removed because of this error.

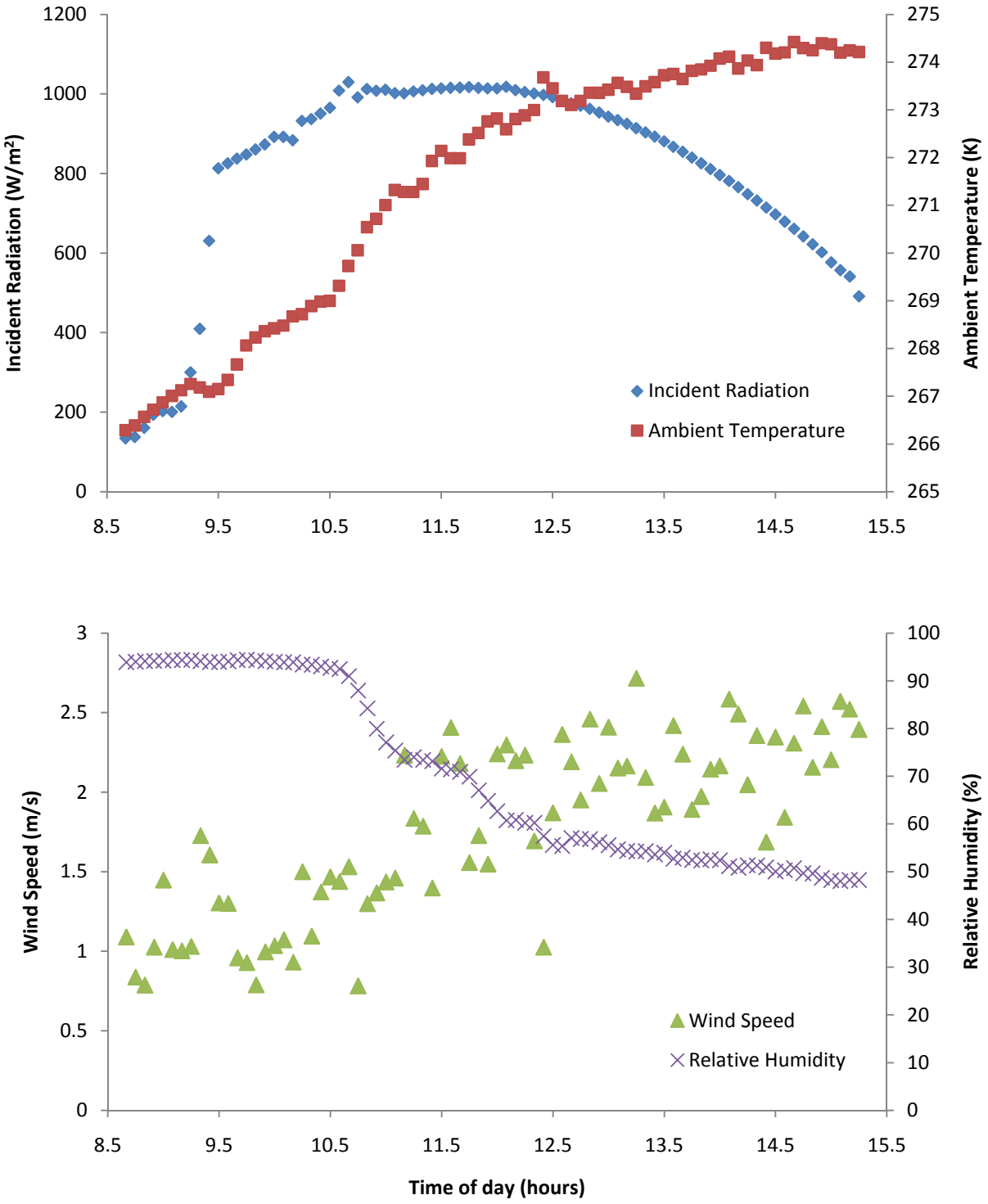

FIGURE 5.16 FEBRUARY 21 WEATHER DATA

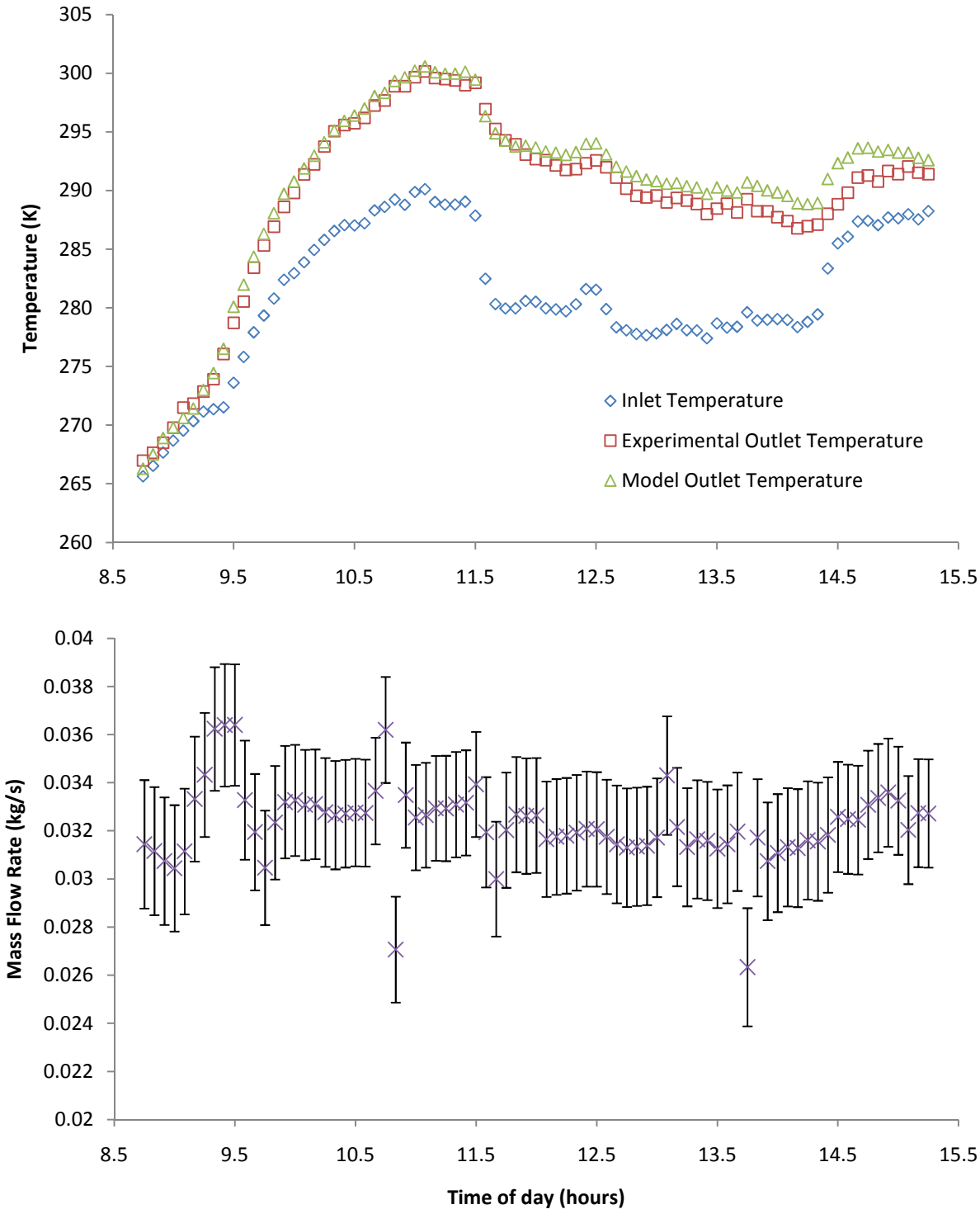

FIGURE 5.17 FEBRUARY 21 TEMPERATURES AND MASS FLOW RATE

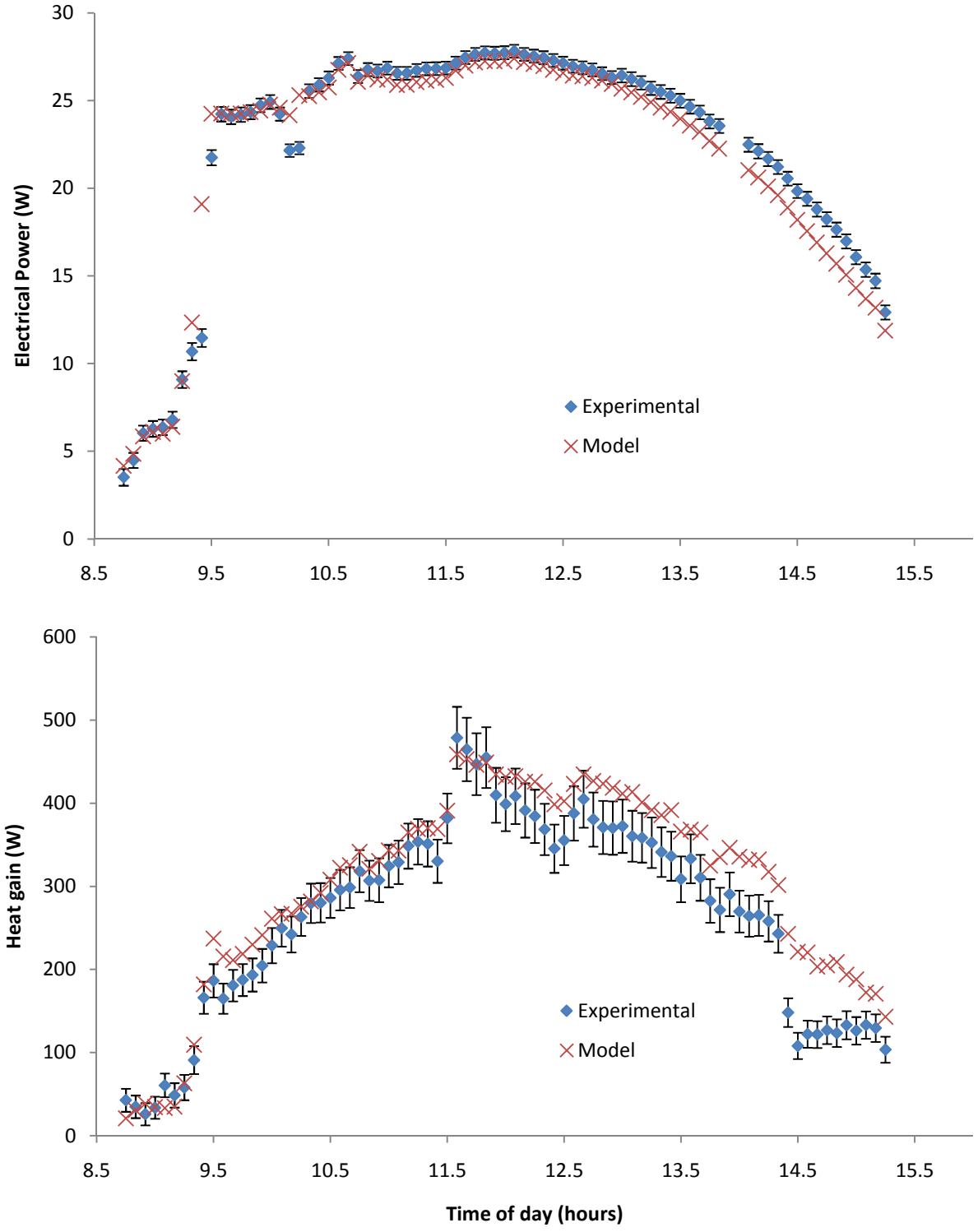

FIGURE 5.18 FEBRUARY 21 PV OUTPUT AND HEAT GAIN

5.3.4 RESPONSE TO STEP INPUT

An interesting method to evaluate the transient response of the collector and the model is to provide the collector with a "step input". This can be done by letting the collector stagnate until the solar radiation is fairly constant (mid-day), then starting the fans, or by covering the collector until midday when it is uncovered.

On March 3rd, the collector was left covered (so that no solar radiation would be incident on the collector) until approximately 11AM. The mass flow rate was left fairly constant at approximately 0.026kg/s for the day and the warm air was fed back to the collector. The sky was cloudy at times, and it was difficult to adjust the resistor bank for the electrical output. A few experimental electrical points are lower than the model value and the inadequacy of the manual maximum power point tracking might be at fault. The thermal output is overestimated by the model for the whole day, but the overall trends are followed. The weather data for March 3rd is shown in Figure 5.19. Figure 5.20 shows the temperatures and mass flow rate. The heat gain and electrical output are shown in Figure 5.21.

On March 4th, the collector was uncovered with no air flow (stagnation) until 10:50AM, and then the fans were turned on. The dampers were arranged so that warm air was fed back to the collector. Both the heat gain and the electrical output are well predicted. . The weather data for March 4th is shown in Figure 5.22. Figure 5.23 shows the temperatures and mass flow rate. The heat gain and electrical output are shown in Figure 5.24.

It is worth noting that between 10:45 and 11:00, the incident solar radiation does not vary a great deal, and that most of the large variation in electrical output in that time period is due to the cooling of the cells by the impinging jets. The PV output goes from roughly 21 W to 30 W in 1 hour. This is a 40% increase in electrical output with only a 4% increase in solar radiation. The reason for this large increase in electrical output is the cooling of the cells by the impinging jets. Starting at 13:45, the electrical data points were deleted as there were problems with the maximum power point tracking.

March 5th was very similar to March 4th except that ambient air was fed into the collector. The thermal and PV output are well predicted by the model. As for

March 4th, the electrical data was deleted after 14:30 due to maximum power point tracking problems. It seems to look like the electrical output would have been underpredicted after that time. . The weather data for March 5th is shown in Figure 5.25. Figure 5.26 shows the temperatures and mass flow rate. The heat gain and electrical output are shown in Figure 5.27.

Like for March 4th, the electrical output increases dramatically in the first hour after the fan is turned on. The increase in PV output on March 5th is roughly 27%. This increase is less than for March 4th because the flow rate in the collector yielding less heat being removed from the cells.

From this data, it is possible to calculate the time constant of the collector. The time constant is defined as the time it takes a system to reach 63% of steady state value when excited by a step input. Because the collector was tested outdoors and all variables cannot be controlled, it is very difficult to get an exact value of the time constant. In this case, the step input was the mass flow rate. If all other variables are assumed to be fairly constant, the collector time constant can be estimated to be roughly15 minutes.

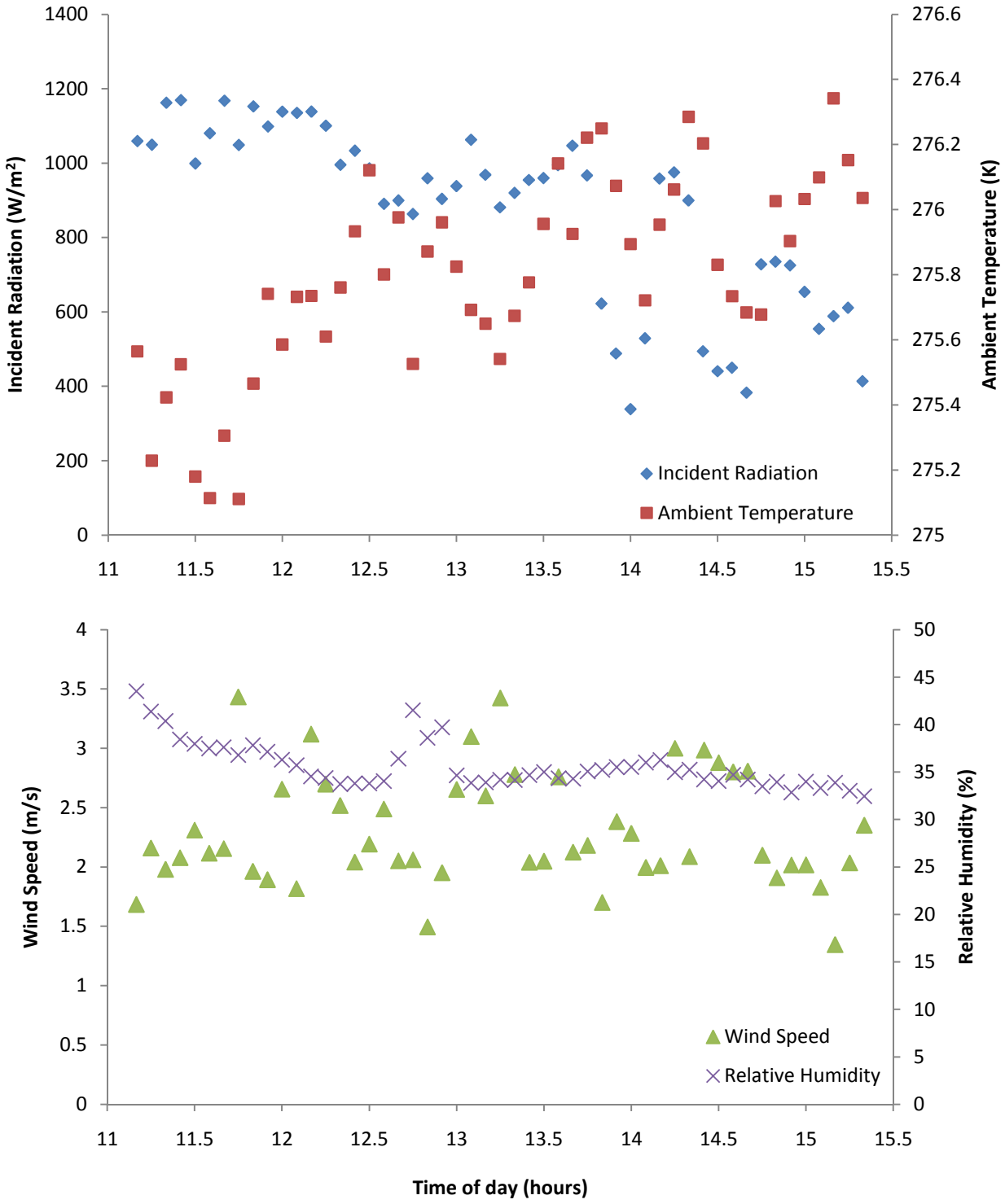

FIGURE 5.19 MARCH 3 WEATHER DATA

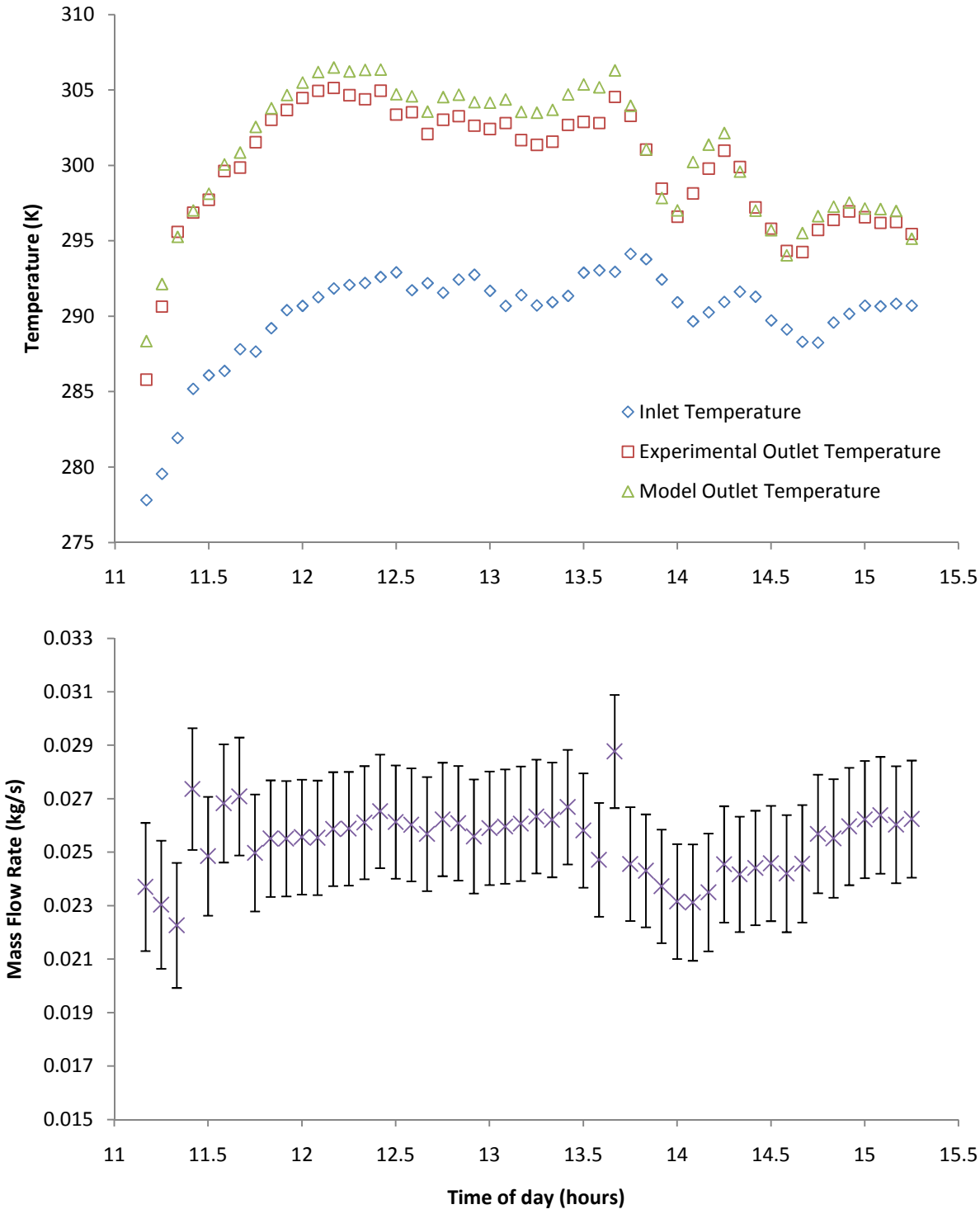

FIGURE 5.20 MARCH 3 TEMPERATURES AND MASS FLOW RATE

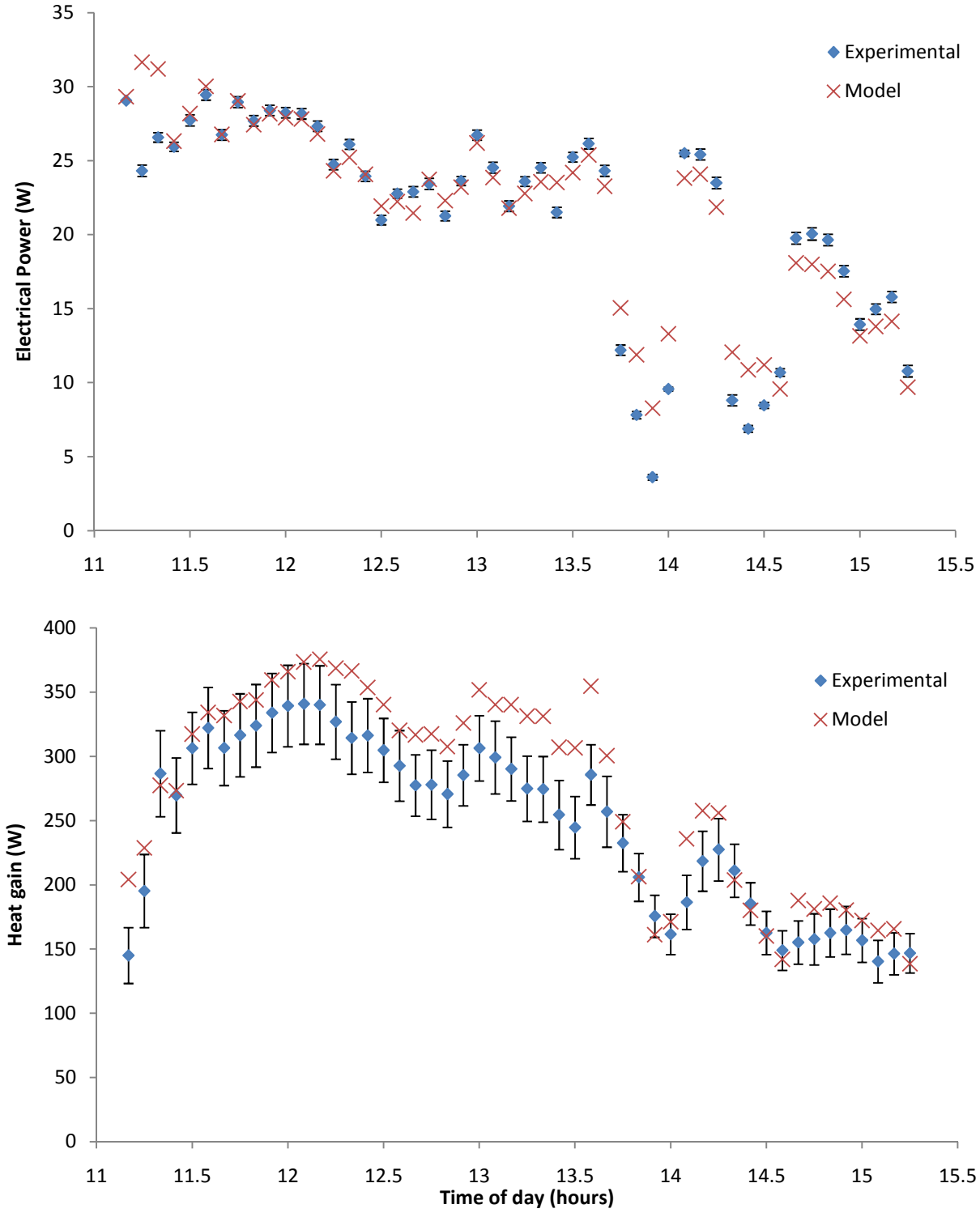

FIGURE 5.21 MARCH 3 PV OUTPUT HEAT GAIN

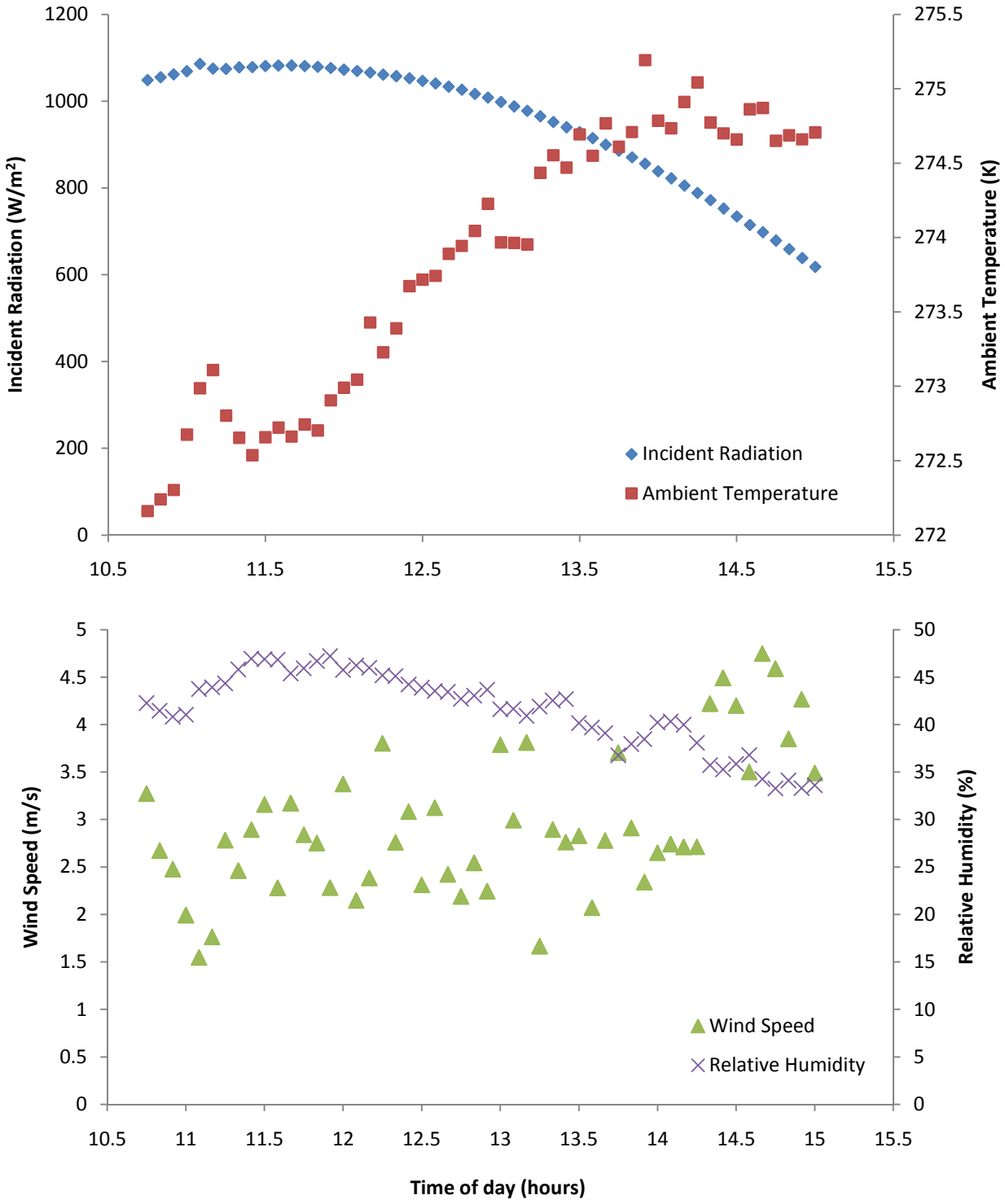

FIGURE 5.22 MARCH 4 WEATHER DATA

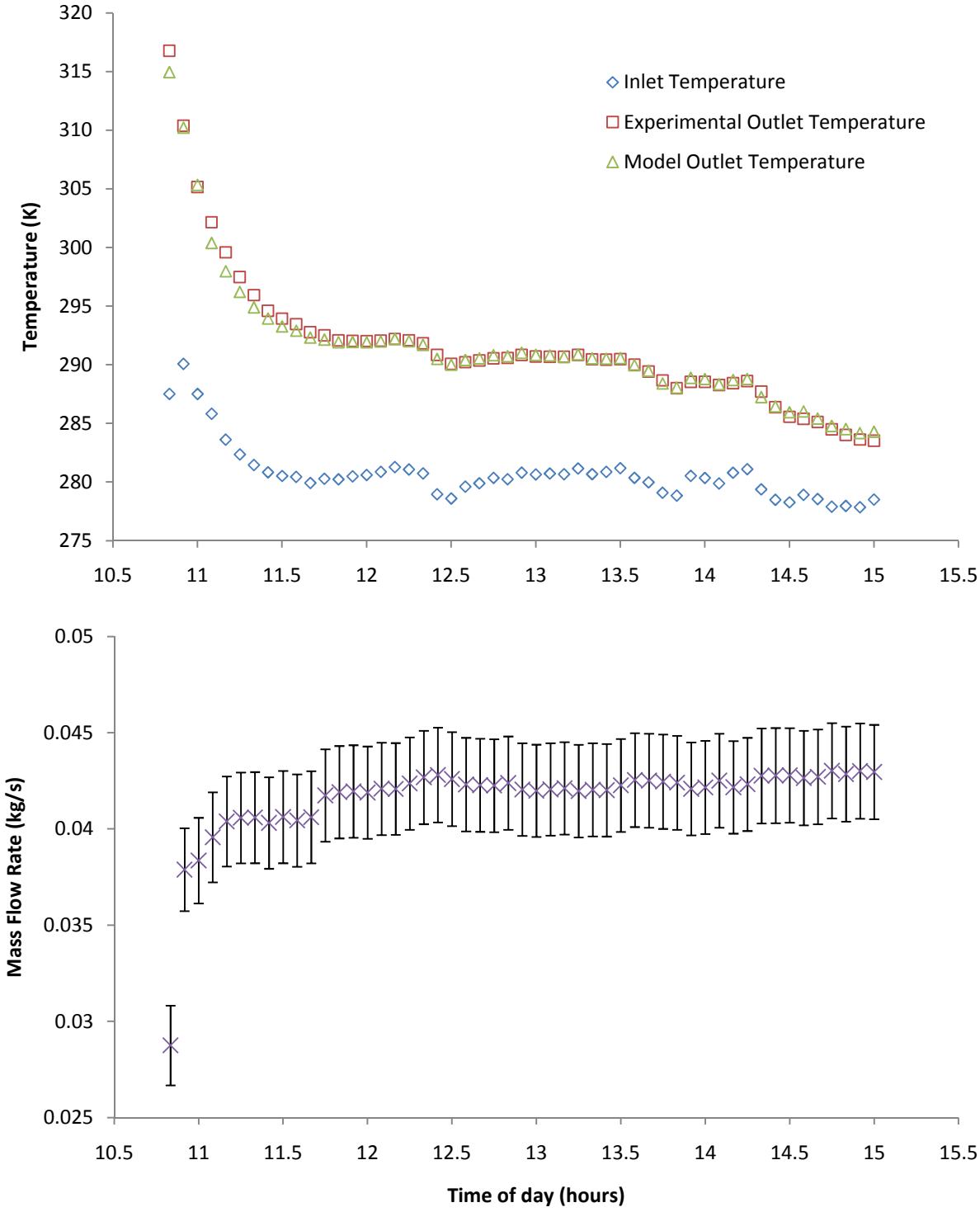

FIGURE 5.23 MARCH 4 TEMPERATURES AND MASS FLOW RATE

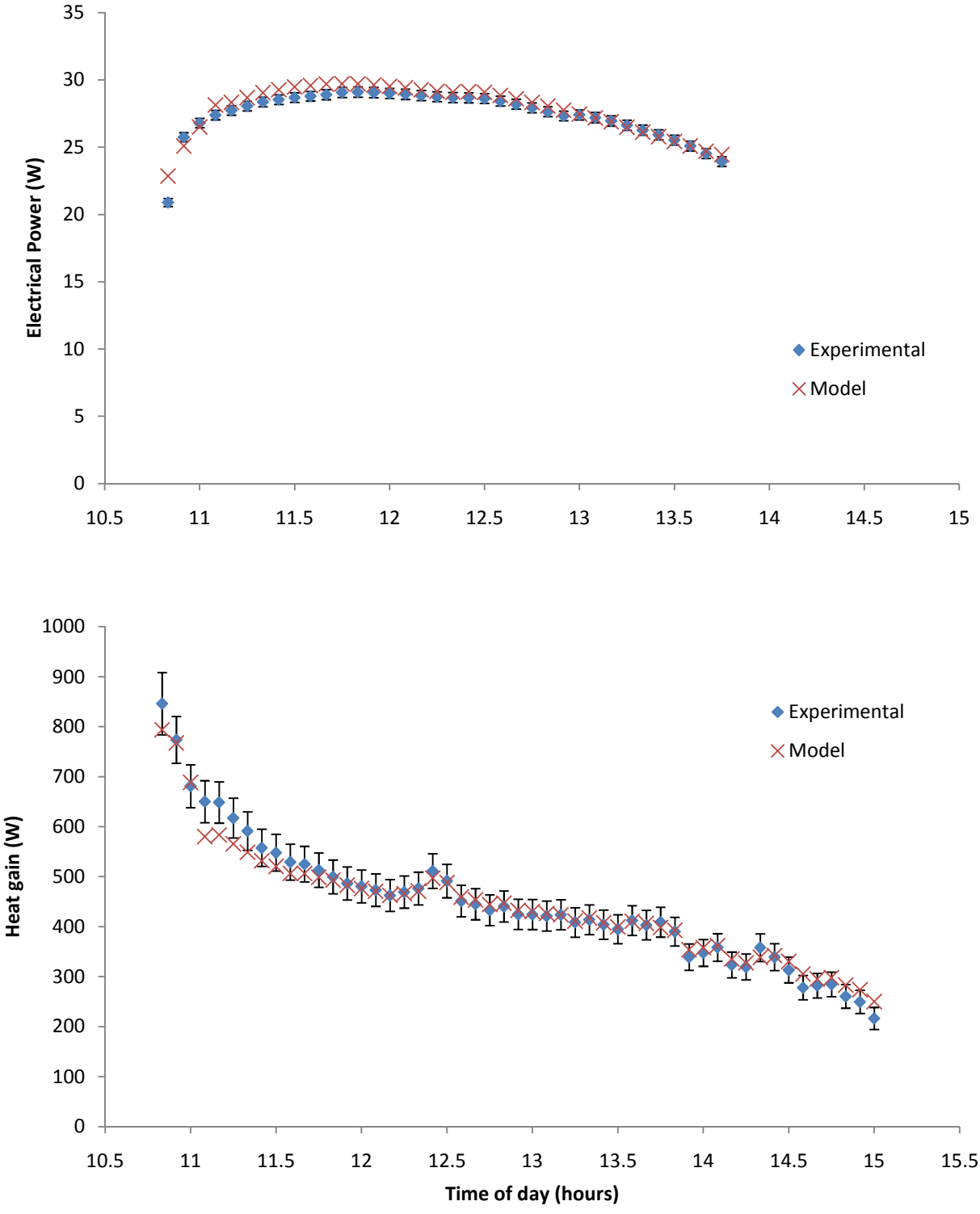

FIGURE 5.24 MARCH 4 PV OUTPUT AND HEAT GAIN

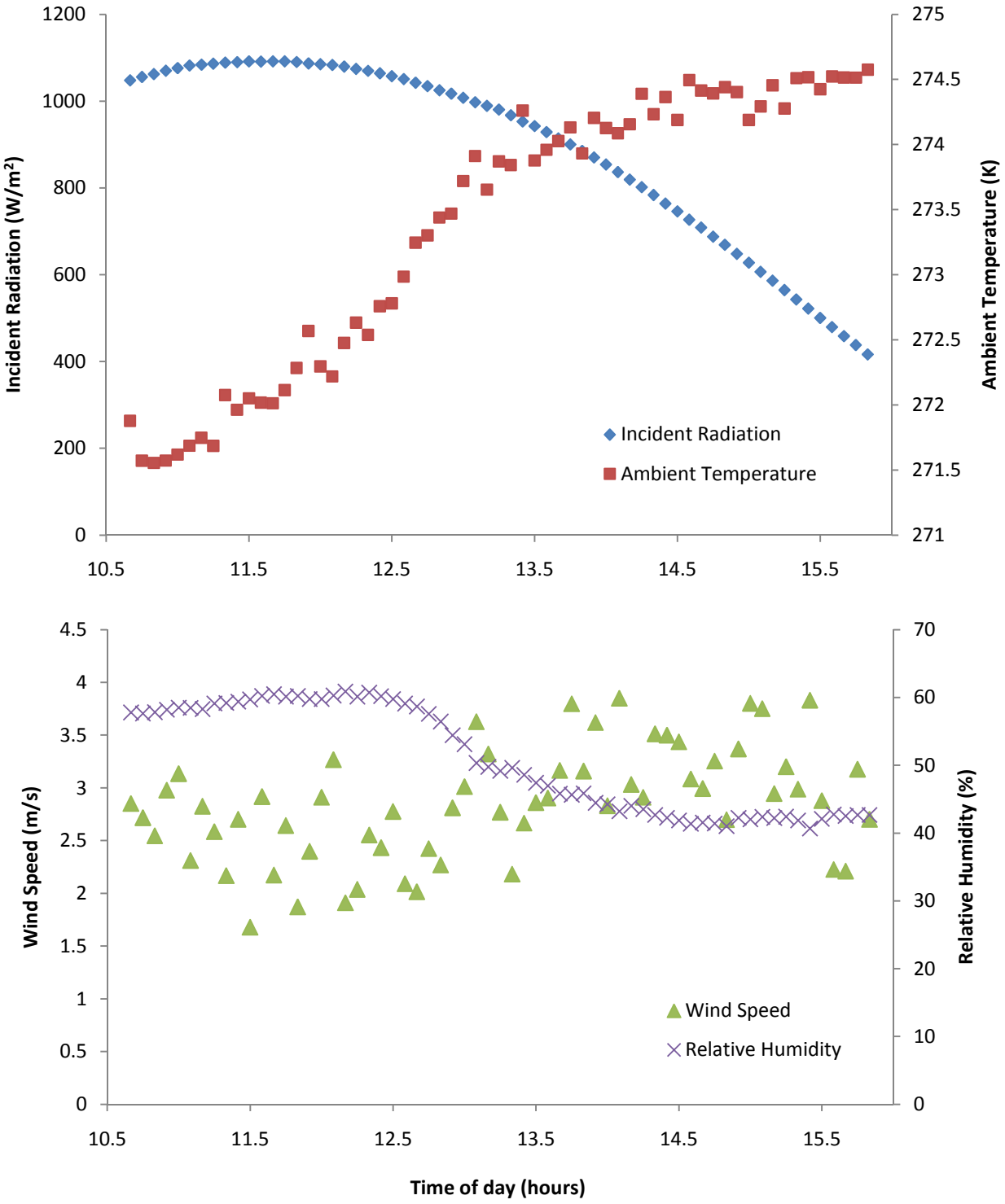

FIGURE 5.25 MARCH 5 WEATHER DATA

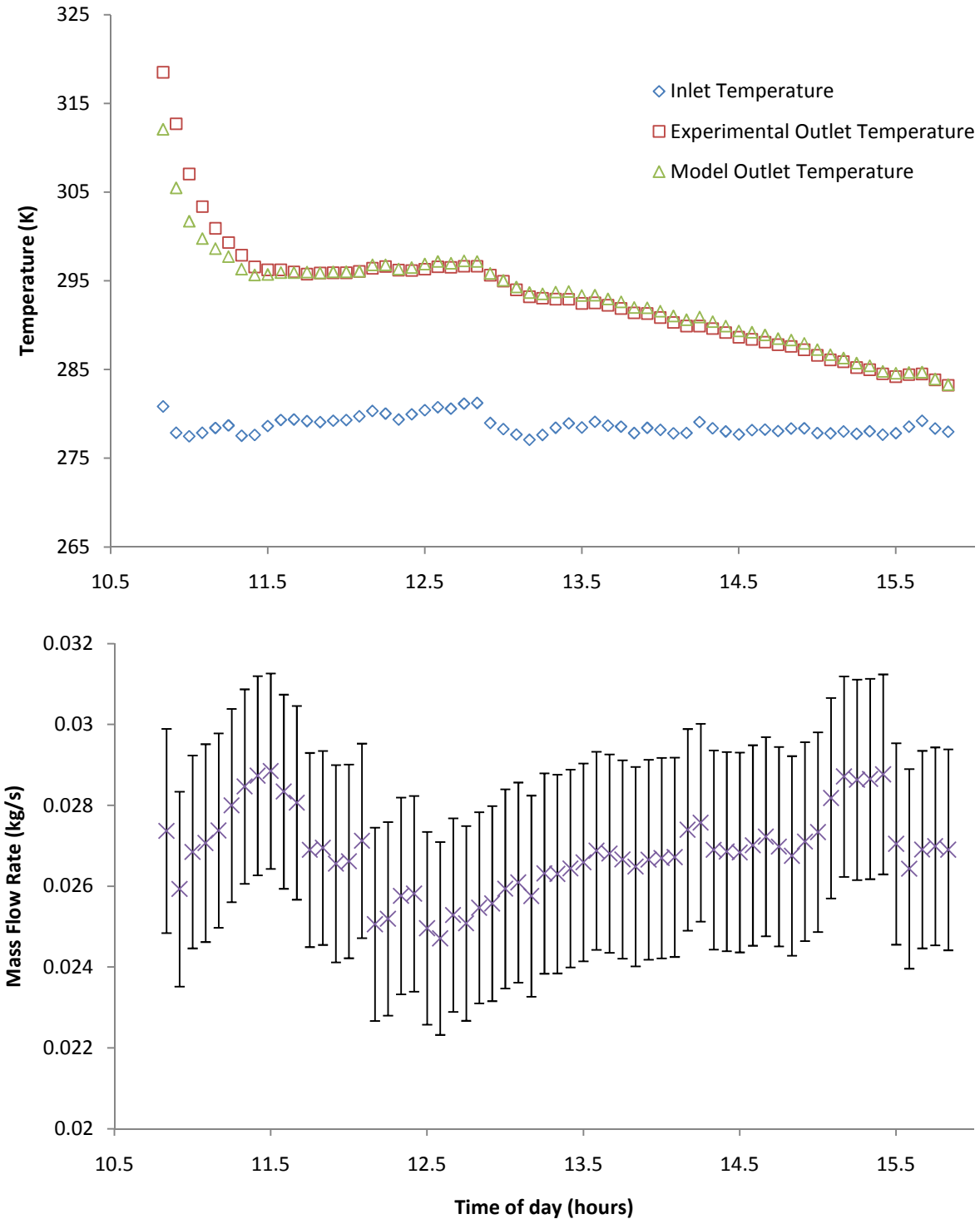

FIGURE 5.26 MARCH 5 TEMPERATURES AND MASS FLOW RATE

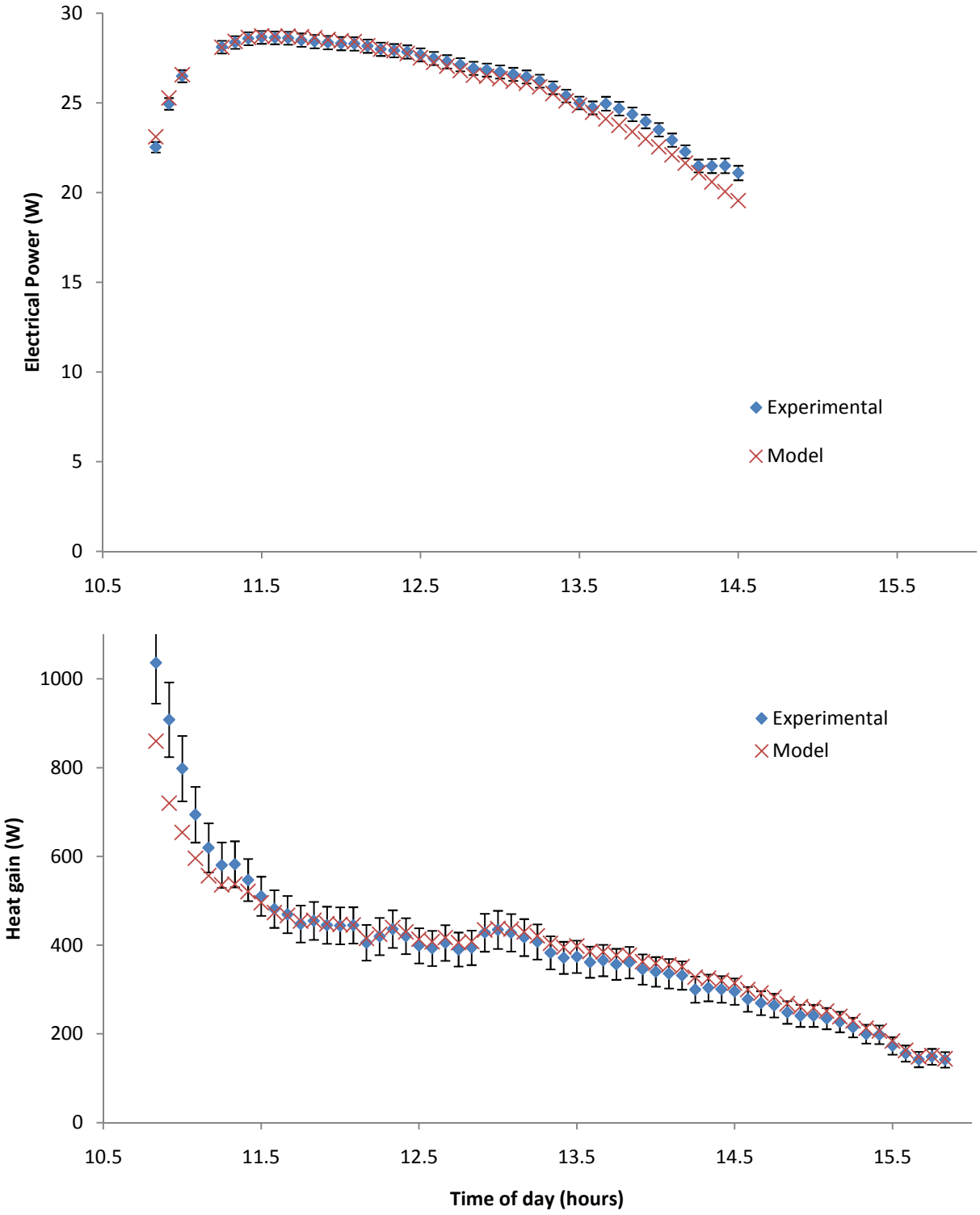

FIGURE 5.27 MARCH 5 PV OUTPUT AND HEAT GAIN

5.3.5 OTHER

February 4th was the second day of testing. There were difficulties in holding the mass flow rate steady, and there were too many variations to look at the effects of the change in mass flow rate.

The mass flow rate was kept between 0.02 kg/s and 0.03 kg/s for most of the day but varied very quickly and often. The dampers on the ducts were kept closed the whole day so that the heated air could recirculate to the collector, bringing the average temperature of the collector up, but the ducts had very little insulation so some of the heat got lost to the environment.

The heat gain was overestimated by the model until 14:00. This coincides with a slight increase in mass flow rate and a decrease in inlet temperature. The electrical output was well predicted for the whole day. The weather data for March 3rd is shown in Figure 5.28. Figure 5.29 shows the temperatures and mass flow rate. The heat gain and electrical output are shown in Figure 5.30.

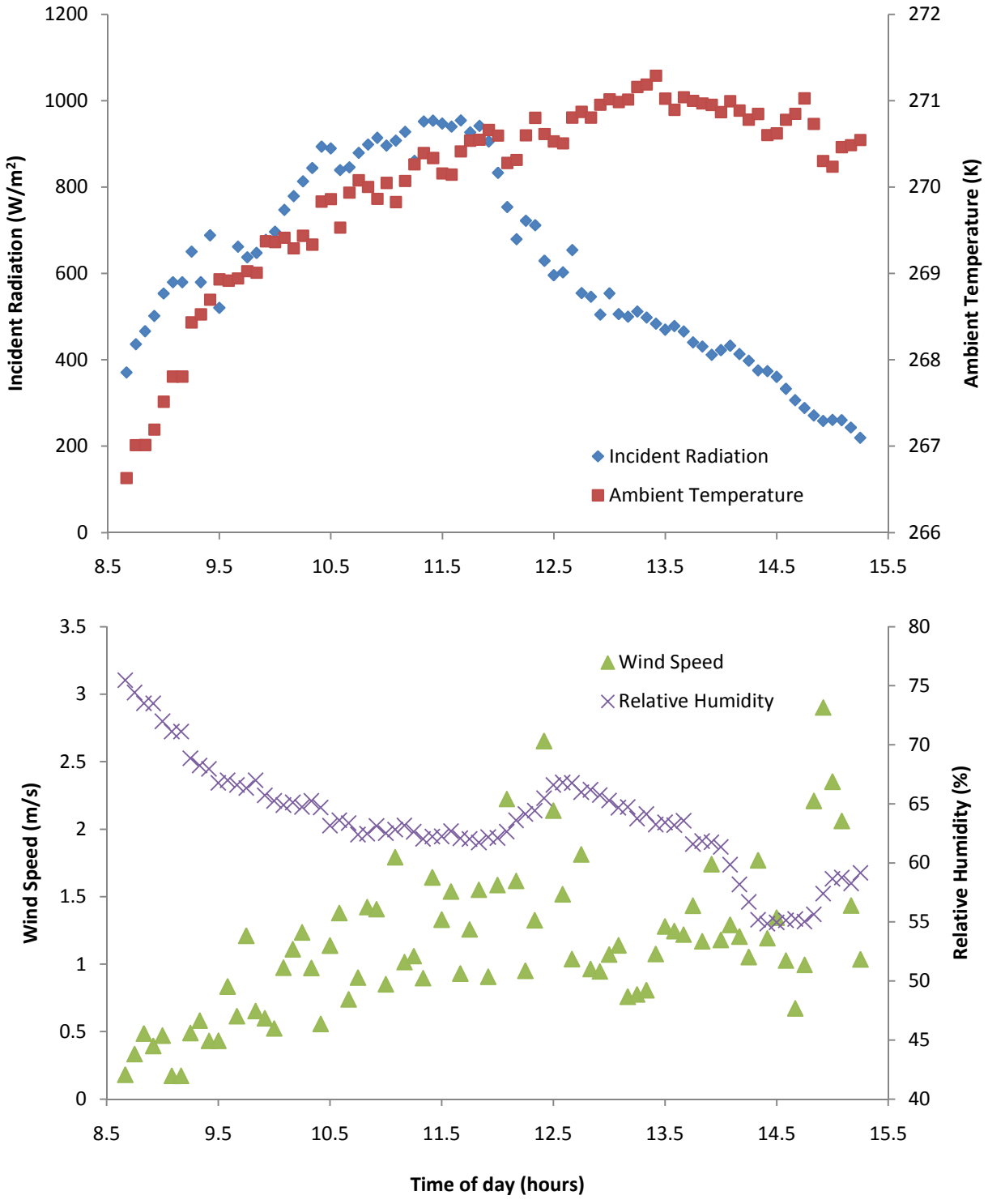

FIGURE 5.28 FEBRUARY 4 WEATHER DATA

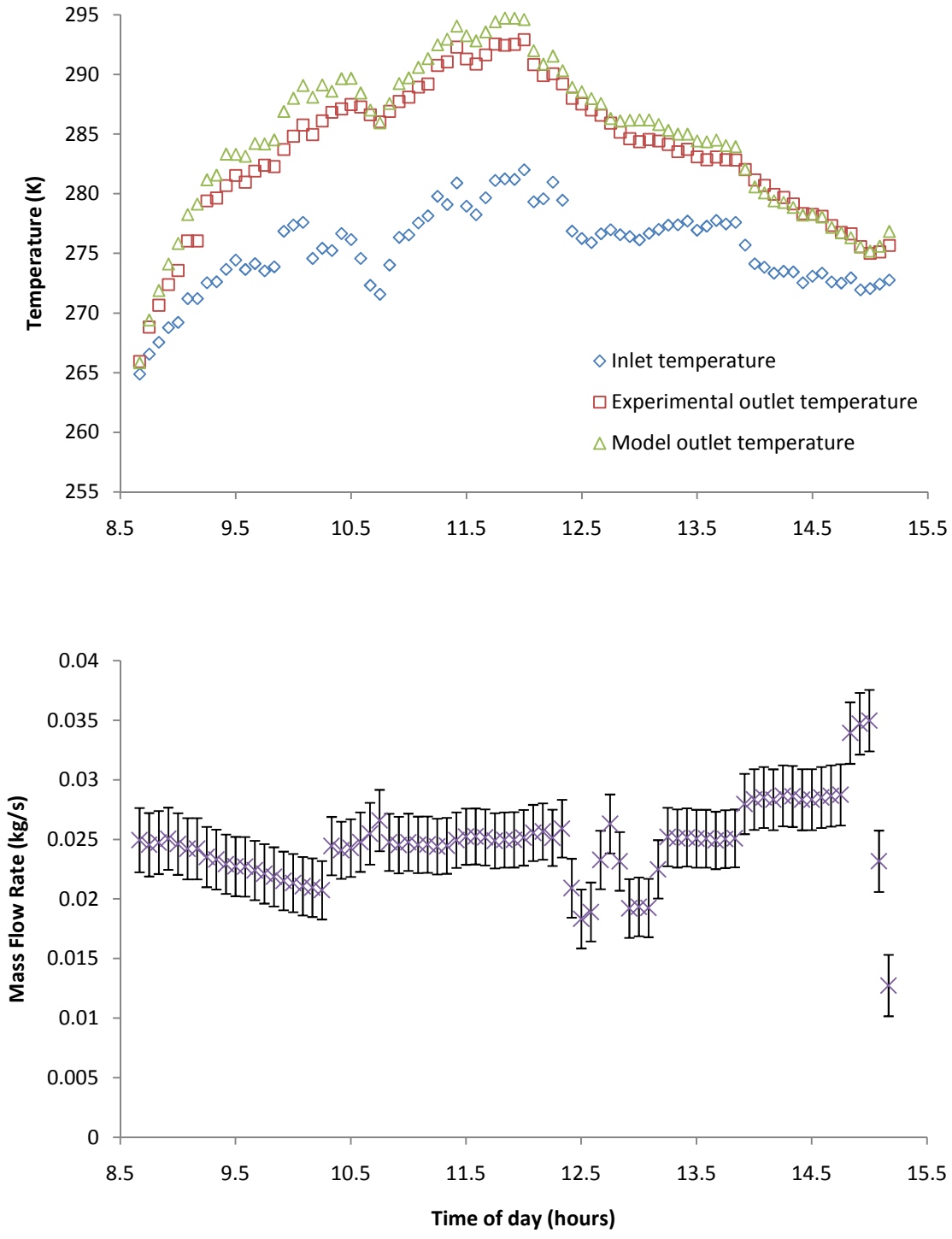

FIGURE 5.29 FEBRUARY 4 TEMPERATURES AND MASS FLOW RATE

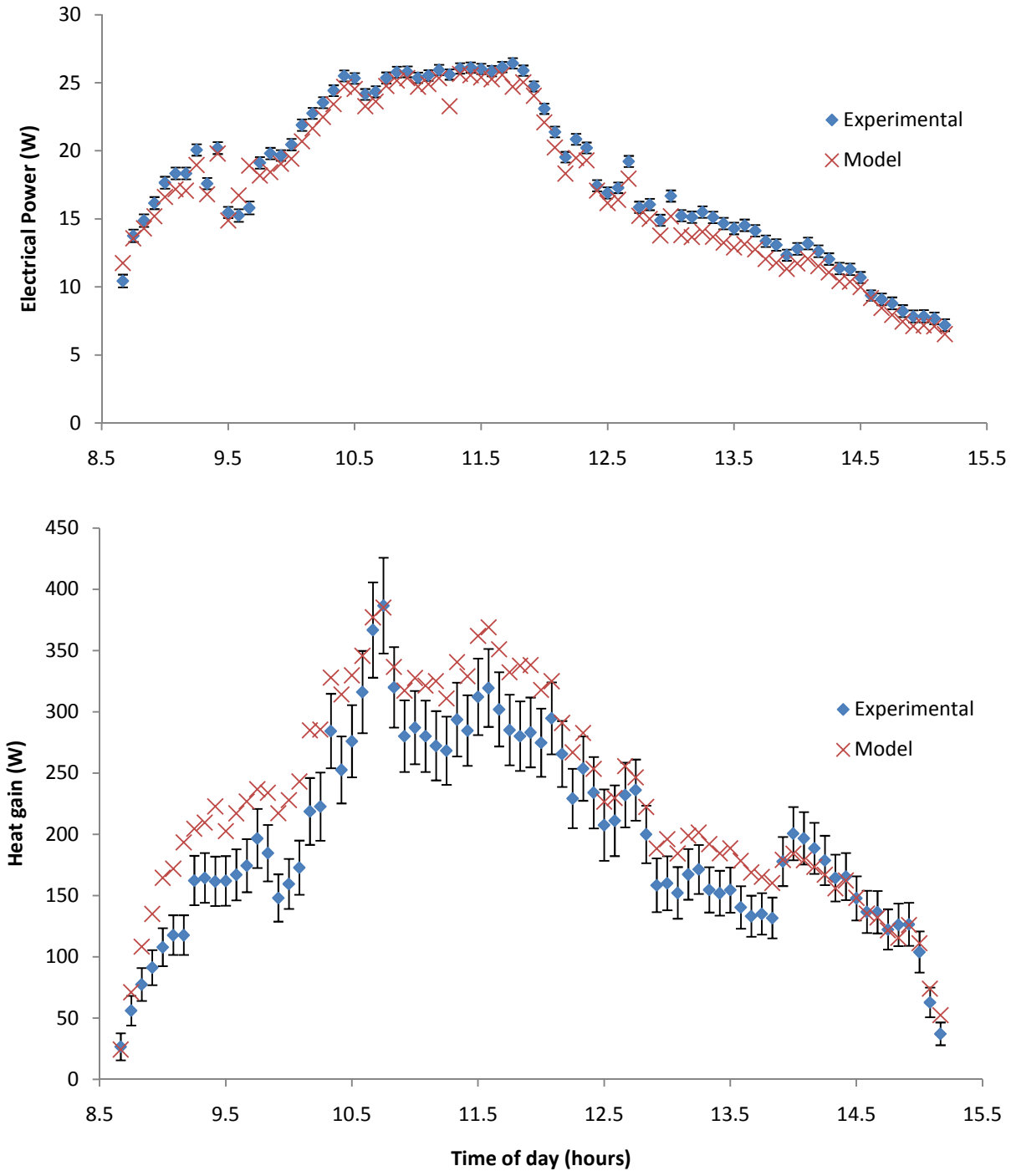

FIGURE 5.30 FEBRUARY 4 PV OUTPUT AND HEAT GAIN

5.4 DISCUSSION

5.4.1 MODEL VALIDATION

Figure 5.31 shows a plot of the model vs experimental heat gain for the modeled days. The RMSD for all data points was 35.4 W. Nineteen (19) points with larger values than 500 W were left out of the graph. A graph with those 19 data points is included in Appendix G. A major deviation can be seen in Appendix G for 3 points on March 5th. That deviation can also be seen in Figure 5.27 as the first 3 data points of March 5th. It is difficult to know why there is such a large deviation. On March 5th, the collector was allowed to stagnate and then the fans were turned on. The deviation may be due to the very transient nature of the first few minutes.

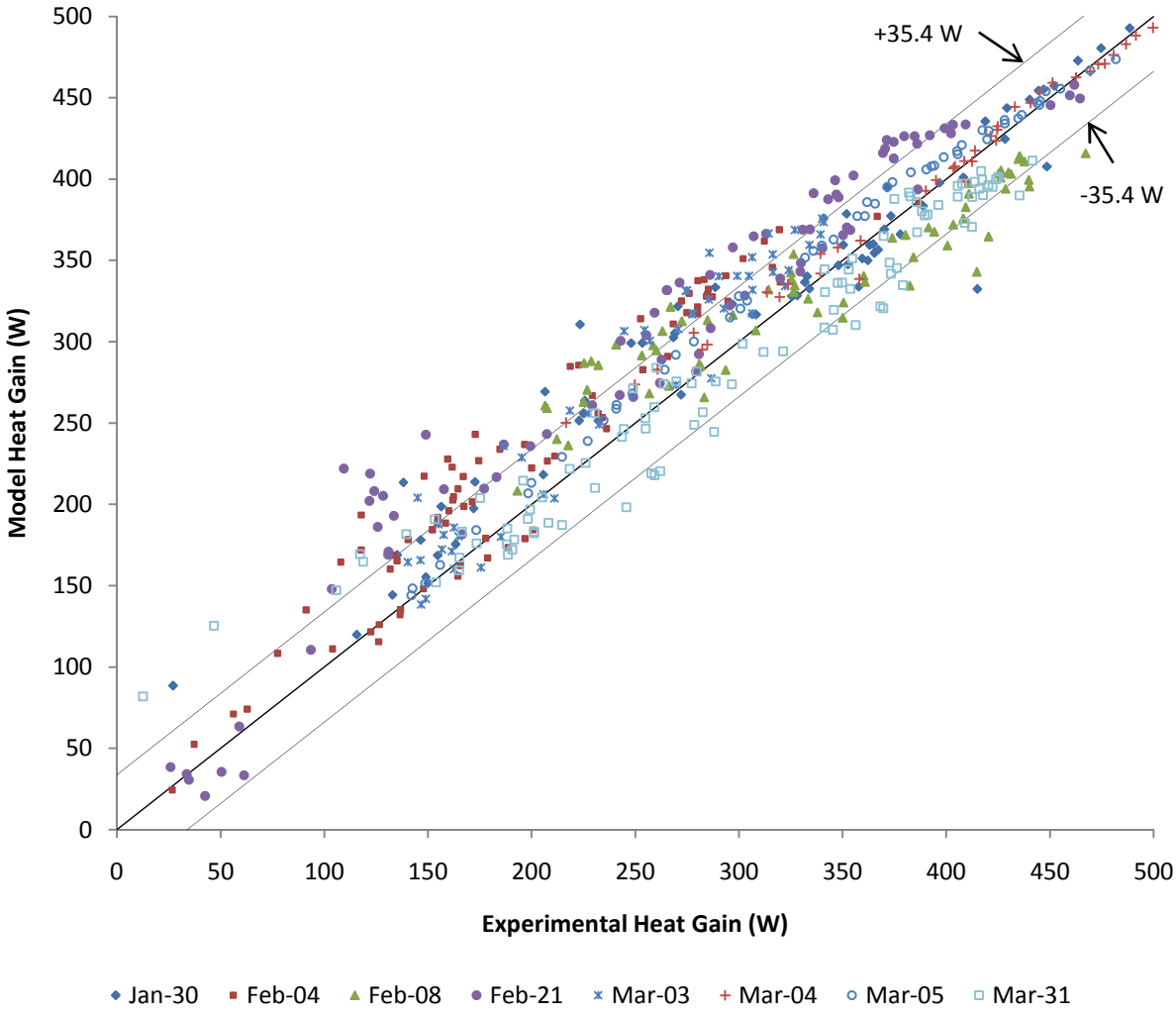

FIGURE 5.31 MODELED VS EXPERIMENTAL HEAT GAIN

Figure 5.32 shows a plot of the model vs experimental PV output for all of the modeled days, The RMSD for all the data points was 1.26 W. There appears to be a second order element missing from the electrical model. This may be due to the model not taking into account the irradiance level as having an effect on the cell efficiency. A sample of the raw input data (as collected during the experiment) and the model output for March 31st can be found in Appendix G.

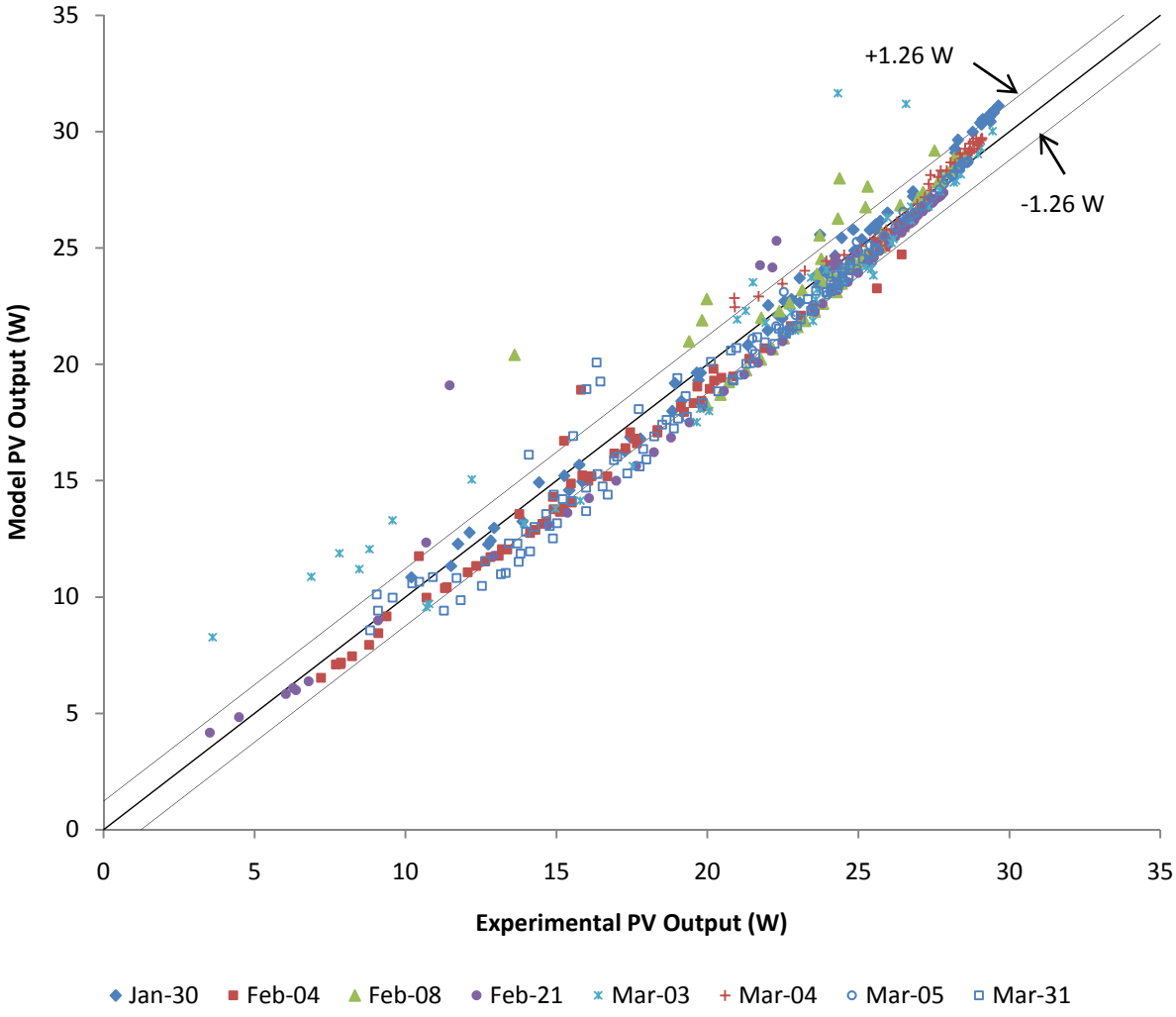

FIGURE 5.32 MODELED VS EXPERIMENTAL PV OUTPUT

5.4.2 PERFORMANCE

In order to quantify how well the collector works, its efficiency can be calculated. Because the experiment was always stopped before the collector completely cooled down at the end of the day, the thermal efficiency of the collector would be underestimated if the efficiency for the full day was to be calculated. Knowing this, it is still possible to evaluate the efficiency of the collector for March 31st. A total of 4515.3 W·h was incident on the collector between 8:05 and 16:25. For that same time period, the model predicted 2311.5 W·h of heat gain and 148.3 W·h of electrical energy produced. This means that the collector converted 54.5% of incident solar radiation in either heat or electrical energy.

Figure 5.33 show the total modeled thermal and electrical energy output for March 31st and different configurations of the collector.

- The first case is the collector that was built for the experiment (see Chapter 4) and extensively studied in Chapter 5.
- The second case is a thermal collector with the same dimensions as case 1. Plate 2 (P_2) is an opaque absorber with the same optical properties as P1 (see Section 4.2.3).
- The third case is for a PV/Thermal collector like the first case, but with an opaque Plate 2 (P_2).
- The fourth case is for a collector with 100% PV coverage. For the particular conditions on March 31st, the thermal collector without PV produces the most energy of all the cases.
- The fifth case is for a PV module using the same PV cells as the ones used in the collector, and with the same area as the collector. This module was modelled using type 94a in TRNSYS. Some assumptions had to be made regarding the nominal operating cell temperatures and conditions. This case produces slightly more electrical output than for case 4.
- The last case is for no flow conditions. The collector is stagnating, and the only electrical PV energy is gained. Even though there is roughly 3 times the amount of PV area compared to case 1, the PV output is only increased by 70%. This is due to the high temperature of the cells in stagnating conditions (around 370K). It is important to note that a typical PV module, like in case 5, would not be built in such way that very little heat losses would occur. In reality, a PV module would most likely be much cooler (around 330K), and therefore produce more electricity, than the stagnating collector. That same

module would most likely be slightly less efficient than a PV/Thermal collector with a large enough flow rate.

These results are not necessarily true for all conditions and parameters. For example, a larger $\frac{T_{in}-T_{ambient}}{S}$ would yield greater losses in the opaque P_2 case with possibly less impact on the transparent case because the collector effectively becomes a double glazed collector in the case of a transparent P_2. It is impossible to generalise the behaviour of the collector from only a few test cases. A full parametric study would be required in order to know more about the effects of changing certain parameters in the collector.

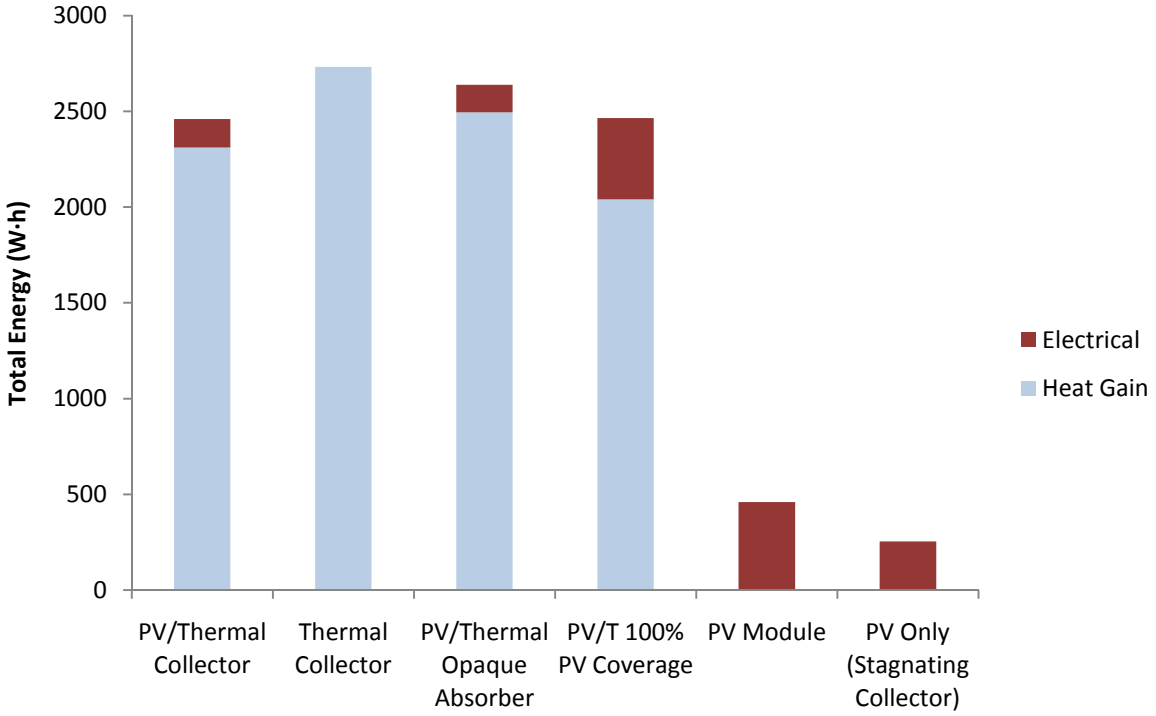

FIGURE 5.33 TOTAL ENERGY OUTPUT FOR DIFFERENT CONFIGURATIONS OF COLLECTOR ON MARCH 31

Figure 5.34 shows the effects of varying the PV coverage for the first case of Figure 5.33. For the conditions that were present on that day, the total energy of the collector does not vary significantly if the PV coverage is changed. Figure 5.35 shows the effects of varying the PV coverage for the third case in Figure 5.33. In this case, the total energy gained is larger with no PV coverage (third case in Figure 5.33) and goes down with increasing PV coverage. There is a 10% increase in total energy gain from the 100% PV coverage to the 0% PV coverage. This may be due to

the relatively low absorptivity of solar cells (0.80) compared to the absorber plate (0.91).

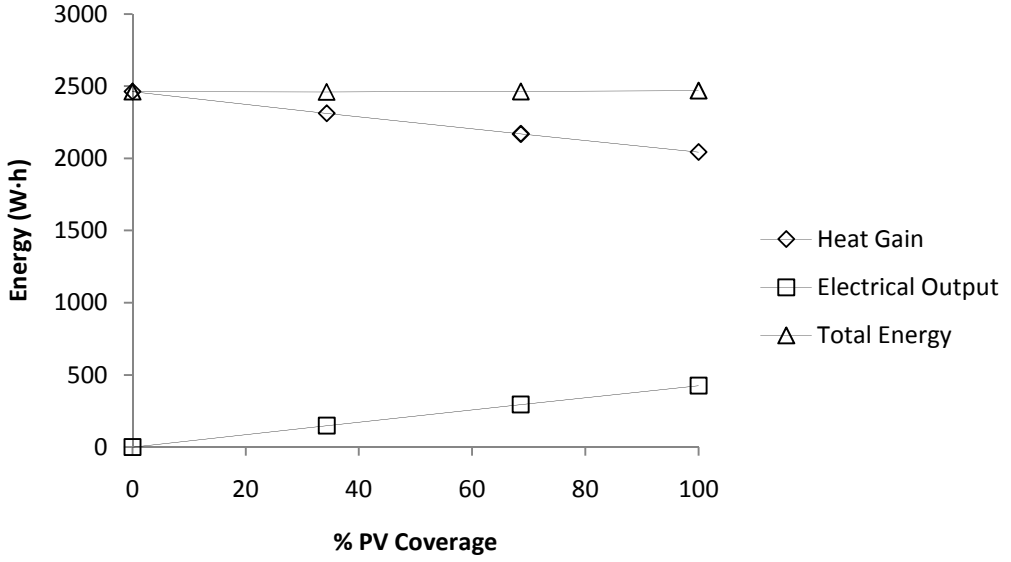

FIGURE 5.34 EFFECTS OF % PV COVERAGE ON ENERGY GAINED BY COLLECTOR FOR TRANSPARENT P2 ON MARCH 31

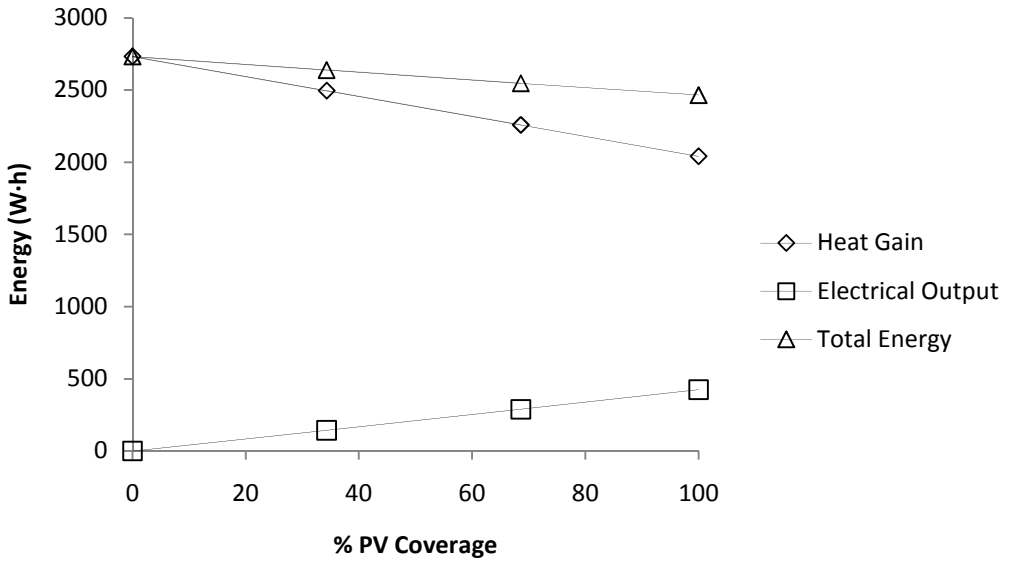

FIGURE 5.35 EFFECTS OF % PV COVERAGE ON ENERGY GAINED BY COLLECTOR FOR OPAQUE P2 ON MARCH 31

Chapter 6
CONCLUSIONS AND RECOMMENDATIONS

6.1 CONCLUSIONS

A model for a PV/Thermal impinging jet collector has been developed. An experiment was conducted at the University of Waterloo ERC building in an attempt to validate the model. Results of the experiment and the model were compared. In general, the heat gain and the PV output were well predicted by the model.

The PV output was very well predicted most of the time. Some of the discrepancies between the model and the experiment may be due to the error in adjusting the maximum power point tracking manually. The heat gain was slightly less well predicted, but the model results were still deemed acceptable. The thermal model is much more sensitive to a number of variables than the electrical model. The electrical model is only very sensitive to irradiance, angle of incidence and to a lesser extent, temperature. The thermal model is sensitive to temperature, wind speed, quality of insulation, irradiance, angle of incidence, and many more variables. Also complicating things are the transient effects due to thermal mass that are much more present in the thermal output than the PV output. There are also multiple convective heat transfer coefficients used in the model that are not perfectly accurate (as are most convective heat transfer coefficients).

The time constant for the collector was found to be roughly 15 minutes. It was also found that there can be a significant increase in PV output (up to 40%) when the collector is running compared to when it is stagnating.

6.2 RECOMMENDATIONS

In the future, it would be very interesting to do a parametric analysis using the model and the experimental setup. The collector frame was designed in such a way that some geometry changes are possible. Parameters that could be varied range from the PV cells coverage to the spacing of the holes in the perforated plate. A

parametric study would be important because it would help learn a lot about this type of collector. As mentioned in Section 5.4.2, it is impossible to state with certainty that the collector always behaves in a certain way (for example, the collector always outputs more total energy with an opaque P_2) without a detailed parametric study. It may well be that the collector demonstrates certain behaviours under specific conditions but not others.

It would also be good to look at how the model works with P_2 being opaque and with a high solar absorptivity. The PV cells could also be removed to look at the thermal collector like the one discussed by Choudhury and Garg (1991).

The model assumed that the mass flow rate was equal in all holes of the collector. One modification to the model could be to include the flow distribution model presented by Floerschutz et al. (1981). This might make the thermal part of the model more accurate.

This model has not been used to look at how this type of collector would perform when integrated with a building HVAC system. It would be interesting to see how the use of a collector like this would affect the energy consumption of the building. It would also be nice to look at whether it would be viable to sell in the market, and how to design the collector frame properly.

Appendix A
FORTRAN CODE FOR TRANSIENT MODEL

```
                        SUBROUTINE TYPE196 (TIME,XIN,OUT,T,DTDT,PAR,INFO,ICNTRL,*)
C**********************************************************************
C Object: Impinging Jet PV/T air collector
C Simulation Studio Model: type196
C
C Author: Sebastien Brideau
C Editor:
C Date:   last modified: April 17,2010
C
C
C ***
C *** Model Parameters
C ***
C

C                       initialTa        K [0;+Inf] (initial guess ambient temperature)
C                       amountofx        - [1;+Inf] (amount of discrete "elements" along the length of
C                       collector)
C                       w        m [0;+Inf] (width of collector)
C                       L        m [0;+Inf] (Length of collector)
C                       Ac       m^2 [0;+Inf] (Area of collector)
C                       Apv      m^2 [0;+Inf] (PV area)
C                       zB       m [0;+Inf] (thickness of back plate)
C                       eB       - [0;1] (emissivity of bacl plate)
C                       zP1      m [0;+Inf] (thickness of Plate 1)
C                       eP1up    - [0;1] (Emissivity of Plate 1, facing towards P2)
C                       eP1down  - [0;1] (Emissivity of Plate 1, facing towards back plate)
C                       zP2      m [0;+Inf] (thickness of plate 2)
C                       eP2      - [0;1] (emissivity of plate 2)
C                       eg       - [0;1] (emissivity of glass cover)
C                       zg       m [0;+Inf] (thickness of glass cover)
C                       es       - [0;1] (emissivity of PV cells)
C                       zs       m [0;+Inf] (thickness of PV cells)
C                       Zb1      m [0;+Inf]  (distance between back plate and P1)
C                       D        m [0.001;+Inf] (Diameter of holes in perforated plate)
C                       Xn       m [0.06;+Inf] (Distance between holes in perforated plate)
C                       Zn       m [0.05;+Inf] (distance between P1 and P2)
C                       ZgP2     m [0;+Inf] (distance between P2 and cover)
C                       Kg       m^-1 [-Inf;+Inf] (Extinction coefficient of glass cover)
C                       ng       - [-Inf;+Inf] (index of refraction of glass cover)
C                       KP2      m^-1 [-Inf;+Inf] (Extinction coefficient of P2 if opaque)
C                       nP2      - [-Inf;+Inf] (index of refraction of P2 if opaque)
C                       taoP1    - [-Inf;+Inf] (not used)
C                       alphaP1  - [-Inf;+Inf] (solar absorptivity of P1)
C                       Cf1      J/kg.K [-Inf;+Inf] (not used)
C                       Cf2      J/kg.K [-Inf;+Inf] (not used)
C                       kB       W/m.K [-Inf;+Inf] (conductivity of insulation)
C                       NOCTeff  - [-Inf;+Inf] (NOCT efficiency of PV cells)
C                       tempCoef - [-Inf;+Inf] (PV cells temperature coefficient in %efficiency per deg C)
C                       theta    - [0;1] (not used)
C                       AbsorberPlateCheck       - [-Inf;+Inf] (if P2 opaque = 1, if P2 clear = 0)
C                       eAbsorberPlateup - [-Inf;+Inf] (emissivity of P2 towards cover)
C                       eAbsorberPlatedown       - [-Inf;+Inf] (emissivity of P2 towards back plate)
C                       alphaAbsorberPlate       - [-Inf;+Inf] (solar absorptivity of P2)
C                       npv      - [-Inf;+Inf] (equivalent index of refraction Parretta et al 1999)
C                       alphapvnormal - (absorptivity of PV cells at 0 degree incidence angle)
```

```
C                       kside - (conductivity of side insulation)
C                       zside - (thickness of side insulation)
C                       Cg - (specific heat of cover)
C                       CP1 - (specific heat of Plate 1)
C                       CP2 - (specific heat of Plate 2)
C                       CB - (specific heat of back plate)
C                       Cs - (specific heat of PV cells)
C                       rhos - density of PV cells)
C                       rhog - (density of cover)
C                       rhoP1 - (density of P1)
C                       rhoP2 - (density of P2)
C                       rhoB - (density of back plate)
C                       zBplate - (thickness of back plate)
C ***
C *** Model Inputs
C ***
C                       mdot    kg/s [0;+Inf]
C                       Beta    rads [-Inf;+Inf]
C                       S       W/m^2 [0;+Inf]
C                       Tin     K [0;+Inf]
C                       Ta      K [0;+Inf]
C                       Tsky    K [-Inf;+Inf]
C                       V       - [-Inf;+Inf]
C                       incidentangle    - [-Inf;+Inf]
C                       Sdiffuse - [-Inf;+Inf]
C                       Sground  - [-Inf;+Inf]
C ***
C *** Model Outputs
C ***
C                       Toutofcollector  - [-Inf;+Inf]
C                       thermalefficiency- [-Inf;+Inf]
C                       elecpower        - [-Inf;+Inf]
C                       eleceff  - [-Inf;+Inf]
C                       totaleff - [-Inf;+Inf]
C                       test1    - [-Inf;+Inf]
C                       test2    - [-Inf;+Inf]
C                       test3    - [-Inf;+Inf]
C                       test4    - [-Inf;+Inf]
C                       test5    - [-Inf;+Inf]
C                       test6    - [-Inf;+Inf]
C                       test7    - [-Inf;+Inf]


C ***
C *** Other
C ***

C       ztotal - total thickness of collector
C       alphagdiffuse - absorptivity of glass cover, sky diffuse radiation
C       alphagground - absorptivity of glass cover, ground diffuse radiation
C       taoalphasdiffuse - tao-alpha product for PV cell, sky diffuse
C       taoalphasgdiffuse - not used
C       taoalphaP2diffuse - tao-alpha product of P2, sky diffuse radiation
C       taoalphaP1diffuse - tao-alpha product of P1, sky diffuse radiation
C       incidentanglediffuse - equivalent incident angle of sky diffuse radiation
C       incidentangleground - equivalent incident angle of ground diffuse radiation
C       taoalphasground - tao-alpha product for PV cell, ground diffuse
C       taoalphasgground - not used
C       taoalphaP2ground - tao-alpha product of P2, ground diffuse radiation
C       taoalphaP1ground - tao-alpha product of P1, ground diffuse radiation
C       ElecPowerTotal - total amount of energy produced by the PV cells
C       alphasg - not used
C       reflP2_perp - reflectivity of P2, perpendicular component
C       reflP2_para - reflectivity of P2, paralell component
```

```
C       pveff - actual PV efficiency at operating conditions
C       taoalphas - tao-alpha product for PV cell, beam radiation
C       taoalphasg - not used
C       taoalphaP2 - tao-alpha product of P2, beam radiation
C       taoalphaP1 - tao-alpha product of P1, beam radiation
C       reflm - not used
C       refld - equivalent diffuse reflectance of P2 and glass cover (from P1 at 60 degrees)
C       taom_perp - perpendicular component of transmissivity of glass cover and P2 (with PV cells included)
C       taom_para - parallel component of transmissivity of glass cover and P2 (with PV cells included)
C       taom - total transmissivity of glass cover and P2 (with PV cells included)
C       taoP2s - total transmissivity of P2 (with PV cells included)
C       taoP2s_perp - perpendicular component of transmissivity of P2 (with PV cells included)
C       taoP2s_para - parallel component of transmissivity of P2 (with PV cells included)
C       alphaP2s - absorptivity of P2 and PV cells
C       refls_perp - perpendicular component of reflectivity of PV cells
C       refls_para - parallel component of reflectivity of PV cells
C       refls - total reflectivity of PV cells
C       reflP2 - total reflectivity of P2
C       taos_perp - not used
C       taos_para - not used
C       alphaP2_perp - perpendicular component of absorptivity of P2
C       alphaP2_para - parallel component of absorptivity of P2
C       hr_P1_B - radiative heat transfer coefficient between P1 and back plate
C       icountInitialTemp - not used
C       ElecPower - PV power at specific element
C       Tavgcrossflow - not used
C       Tcrossflow - not used
C       fTf1 - function used to find temperature of fluid between P1 and back plate
C       hw - wind heat transfer coefficient
C       hr_g_sky - heat transfer coefficient between cover and sky
C       hc_s_g - convective heat transfer coefficient between PV cell and cover
C       Nu_g_s - Nusselt number glass to PV cell
C       variable1pv - to calculate Nu_g_s
C       variable2pv - to calculate Nu_g_s
C       variable3pv - to calculate Nu_g_s
C       Rapv - Raleigh number to calculate Nu_g_s
C       deltaTpv - difference in temp between PV cell and glass cover
C       BetaPrimepv - inverse of average temperature of PV cell and glass cover
C       hr_s_g - radiative heat transfer between PV and glass cover
C       hr_P2_s - not used
C       hcond_P2_s - conductive heat transfer between P2 and PV cell
C       hc_P2_g - convective heat transfer between P2 and cover
C       Nu_g_P2 - Nusselt number between P2 and cover
C       variable1 - to calculate Nu_g_P2
C       variable2 - to calculate Nu_g_P2
C       variable3 - to calculate Nu_g_P2
C       phi2 - to calculate Nu_f2_P2
C       m - to calculate Nu_f2_P2
C       Nu_f2_P2 - Nusselt number for impinging jet
C       hc_f2_P2 - impinging jet heat transfer coefficient
C       hc_B_f1 - parallel flow heat transfer coefficient on back plate
C       hc_P1_f1 - parallel flow heat transfer coefficient on bottom side of P1
C       hc_P1_f2 - parallel flow heat transfer coefficient on top side of P1
C       UB - conductivity of back insulation
C       hr_P1_P2 - radiative heat transfer coefficient between P1 and P2
C       BetaPrime - inverse of average temperature of P2 and glass cover
C       deltaT - difference in temp between P2 and glass cover
C       phi1 - to calculate Nu_f2_P2
C       xvarphi2 - to calculate phi2
C       Re - reynolds number
C       mu - viscosity
C       rg_para - reflectance of glass cover at air-glass interface, parallel component
C       taog_perp - transmissivity of cover, perpendicular component
C       rg_perp - reflectance of glass cover at air-glass interface, perpendicular component
```

```
C       taog_a - transmissivity through cover only looking at the extinction coefficient, not the air-glass
C       interface
C       theta2 - Snell's law angle
C       angle60 - 60 degrees in radians
C       Pr - Prandtl number
C       ka - conductivity of air
C       icountConverge - not used
C       x - distance from begining of collector of element being analysed
C       icountx - number of element being analysed
C       Tg - temperature of cover
C       Tf2out - temperature of fluid coming out of element being analysed (between P1 and P2)
C       Tf1out - temperature of fluid coming out of element being analysed (between P1 and back plate)
C       TB - back plate temperature
C       TP1 - P1 temperature
C       TP2 - P2 temperature
C       Tf1 - temperature of fluid in element being analysed (between P1 and back plate)
C       Tf2 - temperature of fluid in element being analysed (between P1 and P2)
C       Ts - PV cell temperature
C       sigma - Stefan-Boltzmann constant
C       hr_P2_g - radiative heat transfer coefficient P2 to cover
C       Ra = Raleigh number
C       convergecheckTemp - test variable to see wether solution has converged
C       alphag - absorptivity of cover
C       p1f1_100 - nost used
C       f2P2_100 - not used
C       P1f2 - not used
C       Timp - impinging jet temperature
C       Tf2in - average temperature of air coming in the specific element between P2 and P1
C       Tf1f2avg - not used
C       hfree - free convection heat transfer coefficient on cover (ambient air)
C       Rafree - Raleigh number for calculating hfree
C       airdiff - diffusivity of air
C       kinvisc - kinematic viscosity of air
C       Us - condictivity of side insulation
C       initialcounter - counter to set temperatures at begining of model
C       timestep - size of time step in seconds
C       icountstorage - counter to store temperatures for the next time step
C       incidentangledeg - incident angle in degrees
C       A - Variable for correlation by Floerschutz (impinging jet) not used
C       B - Variable for correlation by Floerschutz (impinging jet) not used
C       n - Variable for correlation by Floerschutz (impinging jet) not used
C       Gj - Variable for correlation by Floerschutz (impinging jet) not used
C       Gc - Variable for correlation by Floerschutz (impinging jet) not used
C       hr_g_ground - radiative heat transfer coefficient between cover and ground

C ***
C *** Model Derivatives
C ***

C (Comments and routine interface generated by TRNSYS Studio)
C*************************************************************************

C    TRNSYS acess functions (allow to acess TIME etc.)
      USE TrnsysConstants
      USE TrnsysFunctions

C-------------------------------------------------------------------------------------------------------------
C    REQUIRED BY THE MULTI-DLL VERSION OF TRNSYS
      !DEC$ATTRIBUTES DLLEXPORT :: TYPE196                          !SET THE CORRECT TYPE NUMBER HERE
C-------------------------------------------------------------------------------------------------------------
C-------------------------------------------------------------------------------------------------------------
C    TRNSYS DECLARATIONS
      IMPLICIT NONE                       !REQUIRES THE USER TO DEFINE ALL VARIABLES BEFORE USING THEM
```

```
        DOUBLE PRECISION XIN      !THE ARRAY FROM WHICH THE INPUTS TO THIS TYPE WILL BE RETRIEVED
        DOUBLE PRECISION OUT      !THE ARRAY WHICH WILL BE USED TO STORE THE OUTPUTS FROM THIS TYPE
        DOUBLE PRECISION TIME     !THE CURRENT SIMULATION TIME - YOU MAY USE THIS VARIABLE BUT DO NOT SET IT!
        DOUBLE PRECISION PAR      !THE ARRAY FROM WHICH THE PARAMETERS FOR THIS TYPE WILL BE RETRIEVED
        DOUBLE PRECISION STORED !THE STORAGE ARRAY FOR HOLDING VARIABLES FROM TIMESTEP TO TIMESTEP
        DOUBLE PRECISION T                !AN ARRAY CONTAINING THE RESULTS FROM THE DIFFERENTIAL EQUATION
SOLVER
        DOUBLE PRECISION DTDT     !AN ARRAY CONTAINING THE DERIVATIVES TO BE PASSED TO THE DIFF.EQ. SOLVER
        INTEGER*4 INFO(15)                !THE INFO ARRAY STORES AND PASSES VALUABLE INFORMATION TO AND FROM
THIS TYPE
        INTEGER*4 NP,NI,NOUT,ND   !VARIABLES FOR THE MAXIMUM NUMBER OF PARAMETERS,INPUTS,OUTPUTS AND
DERIVATIVES
        INTEGER*4 NPAR,NIN,NDER   !VARIABLES FOR THE CORRECT NUMBER OF PARAMETERS,INPUTS,OUTPUTS AND
DERIVATIVES
        INTEGER*4 IUNIT,ITYPE     !THE UNIT NUMBER AND TYPE NUMBER FOR THIS COMPONENT
        INTEGER*4 ICNTRL          !AN ARRAY FOR HOLDING VALUES OF CONTROL FUNCTIONS WITH THE NEW SOLVER
        INTEGER*4 NSTORED         !THE NUMBER OF VARIABLES THAT WILL BE PASSED INTO AND OUT OF STORAGE
        CHARACTER*3 OCHECK                !AN ARRAY TO BE FILLED WITH THE CORRECT VARIABLE TYPES FOR THE
OUTPUTS
        CHARACTER*3 YCHECK                !AN ARRAY TO BE FILLED WITH THE CORRECT VARIABLE TYPES FOR THE
INPUTS
C-------------------------------------------------------------------------------------------------------------------
C-------------------------------------------------------------------------------------------------------------------
C    OUTPUTS (NOUT), AND DERIVATIVES (ND) THAT MAY BE SUPPLIED FOR THIS TYPE
      PARAMETER (NP=54,NI=10,NOUT=12,ND=0,NSTORED=3000)
C-------------------------------------------------------------------------------------------------------------------
C-------------------------------------------------------------------------------------------------------------------
C    REQUIRED TRNSYS DIMENSIONS
      DIMENSION XIN(NI),OUT(NOUT),PAR(NP),YCHECK(NI),OCHECK(NOUT),
        1   STORED(NSTORED),T(ND),DTDT(ND)
      INTEGER NITEMS
C-------------------------------------------------------------------------------------------------------------------
C-------------------------------------------------------------------------------------------------------------------
C    ADD DECLARATIONS AND DEFINITIONS FOR THE USER-VARIABLES HERE
C    PARAMETERS
        DOUBLE PRECISION initialTa
        DOUBLE PRECISION amountofx
        DOUBLE PRECISION w
        DOUBLE PRECISION L
        DOUBLE PRECISION Ac
        DOUBLE PRECISION Apv
        DOUBLE PRECISION zB
        DOUBLE PRECISION eB
        DOUBLE PRECISION zP1
        DOUBLE PRECISION eP1up
        DOUBLE PRECISION eP1down
        DOUBLE PRECISION zP2
        DOUBLE PRECISION eP2
        DOUBLE PRECISION eg
        DOUBLE PRECISION zg
        DOUBLE PRECISION es
        DOUBLE PRECISION zs
        DOUBLE PRECISION Zb1
        DOUBLE PRECISION D
        DOUBLE PRECISION Xn
        DOUBLE PRECISION Zn
        DOUBLE PRECISION ZgP2
        DOUBLE PRECISION Kg
        DOUBLE PRECISION ng
        DOUBLE PRECISION KP2
        DOUBLE PRECISION nP2
        DOUBLE PRECISION taoP1
        DOUBLE PRECISION alphaP1
        DOUBLE PRECISION Cf1
        DOUBLE PRECISION Cf2
        DOUBLE PRECISION kB
```

```
          DOUBLE PRECISION NOCTeff
          DOUBLE PRECISION tempCoef
          DOUBLE PRECISION theta
          DOUBLE PRECISION AbsorberPlateCheck
          DOUBLE PRECISION eAbsorberPlateup
          DOUBLE PRECISION eAbsorberPlatedown
          DOUBLE PRECISION alphaAbsorberPlate
          DOUBLE PRECISION npv
          DOUBLE PRECISION alphapvnormal
          DOUBLE PRECISION kside
          DOUBLE PRECISION zside
          DOUBLE PRECISION Cg
          DOUBLE PRECISION CP1
          DOUBLE PRECISION CP2
          DOUBLE PRECISION CB
          DOUBLE PRECISION Cs
          DOUBLE PRECISION rhos
          DOUBLE PRECISION rhog
          DOUBLE PRECISION rhoP1
          DOUBLE PRECISION rhoP2
          DOUBLE PRECISION rhoB
          DOUBLE PRECISION zBplate


C     INPUTS
          DOUBLE PRECISION mdot
          DOUBLE PRECISION Beta
          DOUBLE PRECISION S
          DOUBLE PRECISION Tin
          DOUBLE PRECISION Ta
          DOUBLE PRECISION Tsky
          DOUBLE PRECISION V
          DOUBLE PRECISION incidentangle
          DOUBLE PRECISION Sdiffuse
          DOUBLE PRECISION Sground

C         others
          DOUBLE PRECISION ztotal
          DOUBLE PRECISION alphagdiffuse
          DOUBLE PRECISION alphagground
          DOUBLE PRECISION taoalphasdiffuse
          DOUBLE PRECISION taoalphasgdiffuse
          DOUBLE PRECISION taoalphaP2diffuse
          DOUBLE PRECISION taoalphaP1diffuse
          DOUBLE PRECISION incidentanglediffuse
          DOUBLE PRECISION incidentangleground
          DOUBLE PRECISION taoalphasground
          DOUBLE PRECISION taoalphasgground
          DOUBLE PRECISION taoalphaP2ground
          DOUBLE PRECISION taoalphaP1ground
          DOUBLE PRECISION ElecPowerTotal
          DOUBLE PRECISION alphasg
          DOUBLE PRECISION reflP2_perp
          DOUBLE PRECISION reflP2_para
          DOUBLE PRECISION pveff
          DOUBLE PRECISION taoalphas
          DOUBLE PRECISION taoalphasg
          DOUBLE PRECISION taoalphaP2
          DOUBLE PRECISION taoalphaP1
          DOUBLE PRECISION reflm
          DOUBLE PRECISION refld
          DOUBLE PRECISION taom_perp
          DOUBLE PRECISION taom_para
          DOUBLE PRECISION taom
```

```
DOUBLE PRECISION taoP2s
DOUBLE PRECISION taoP2s_perp
DOUBLE PRECISION taoP2s_para
DOUBLE PRECISION reflP2s
DOUBLE PRECISION reflP2s_perp
DOUBLE PRECISION reflP2s_para
DOUBLE PRECISION alphaP2s
DOUBLE PRECISION refls_perp
DOUBLE PRECISION refls_para
DOUBLE PRECISION refls
DOUBLE PRECISION reflP2
DOUBLE PRECISION taos_perp
DOUBLE PRECISION taos_para
DOUBLE PRECISION alphaP2_perp
DOUBLE PRECISION alphaP2_para
DOUBLE PRECISION hr_P1_B
DOUBLE PRECISION icountInitialTemp
DOUBLE PRECISION ElecPower(400)
DOUBLE PRECISION Tavgcrossflow
DOUBLE PRECISION Tcrossflow
DOUBLE PRECISION fTf1
DOUBLE PRECISION hw
DOUBLE PRECISION hr_g_sky
DOUBLE PRECISION hc_s_g
DOUBLE PRECISION Nu_g_s
DOUBLE PRECISION variable1pv
DOUBLE PRECISION variable2pv
DOUBLE PRECISION variable3pv
DOUBLE PRECISION Rapv
DOUBLE PRECISION deltaTpv
DOUBLE PRECISION BetaPrimepv
DOUBLE PRECISION hr_s_g
DOUBLE PRECISION hr_P2_s
DOUBLE PRECISION hcond_P2_s
DOUBLE PRECISION hc_P2_g
DOUBLE PRECISION Nu_g_P2
DOUBLE PRECISION variable1
DOUBLE PRECISION variable2
DOUBLE PRECISION variable3
DOUBLE PRECISION phi2
DOUBLE PRECISION m
DOUBLE PRECISION Nu_f2_P2
DOUBLE PRECISION hc_f2_P2
DOUBLE PRECISION hc_B_f1
DOUBLE PRECISION hc_P1_f1
DOUBLE PRECISION hc_P1_f2
DOUBLE PRECISION UB
DOUBLE PRECISION hr_P1_P2
DOUBLE PRECISION BetaPrime
DOUBLE PRECISION deltaT
DOUBLE PRECISION phi1
DOUBLE PRECISION xvarphi2
DOUBLE PRECISION Re
DOUBLE PRECISION mu
DOUBLE PRECISION rg_para
DOUBLE PRECISION taog_perp
DOUBLE PRECISION rg_perp
DOUBLE PRECISION taog_a
DOUBLE PRECISION theta2
DOUBLE PRECISION angle60
DOUBLE PRECISION Pr
DOUBLE PRECISION ka
DOUBLE PRECISION icountConverge
DOUBLE PRECISION x
```

```
        DOUBLE PRECISION icountx
        DOUBLE PRECISION Tg(400)
        DOUBLE PRECISION Tf2out(400)
        DOUBLE PRECISION Tf1out(400)
        DOUBLE PRECISION TB(400)
        DOUBLE PRECISION TP1(400)
        DOUBLE PRECISION TP2(400)
        DOUBLE PRECISION Tf1(400)
        DOUBLE PRECISION Tf2(400)
        DOUBLE PRECISION Ts(400)
        DOUBLE PRECISION sigma
        DOUBLE PRECISION hr_P2_g
        DOUBLE PRECISION Ra
        DOUBLE PRECISION convergecheckTemp
        DOUBLE PRECISION alphag
        DOUBLE PRECISION p1f1_100
        DOUBLE PRECISION f2P2_100
        DOUBLE PRECISION P1f2
        DOUBLE PRECISION Timp
        DOUBLE PRECISION Tf2in
        DOUBLE PRECISION Tf1f2avg(400)
        DOUBLE PRECISION hcP1f1
        DOUBLE PRECISION hcP2f2
        DOUBLE PRECISION hcP1f2
        DOUBLE PRECISION hcBf1
        DOUBLE PRECISION hcsg
        DOUBLE PRECISION hcP2g
        DOUBLE PRECISION hrgsky
        DOUBLE PRECISION hrP2g
        DOUBLE PRECISION hrsg
        DOUBLE PRECISION hrP1P2
        DOUBLE PRECISION hrP1B
        DOUBLE PRECISION hfree
        DOUBLE PRECISION Rafree
        DOUBLE PRECISION airdiff
        DOUBLE PRECISION kinvisc
        DOUBLE PRECISION Us
        DOUBLE PRECISION initialcounter
        DOUBLE PRECISION timestep
        DOUBLE PRECISION icountstorage
        DOUBLE PRECISION incidentangledeg
        DOUBLE PRECISION A
        DOUBLE PRECISION B
        DOUBLE PRECISION n
        DOUBLE PRECISION Gj
        DOUBLE PRECISION Gc
        DOUBLE PRECISION hr_g_ground
C-----------------------------------------------------------------------------------------------------------------
C       READ IN THE VALUES OF THE PARAMETERS IN SEQUENTIAL ORDER
      initialTa=PAR(1)
      amountofx=PAR(2)
      w=PAR(3)
      L=PAR(4)
      Ac=PAR(5)
      Apv=PAR(6)
      zB=PAR(7)
      eB=PAR(8)
      zP1=PAR(9)
      eP1up=PAR(10)
      eP1down=PAR(11)
      zP2=PAR(12)
      eP2=PAR(13)
      eg=PAR(14)
      zg=PAR(15)
```

```
       es=PAR(16)
       zs=PAR(17)
       Zb1=PAR(18)
       D=PAR(19)
       Xn=PAR(20)
       Zn=PAR(21)
       ZgP2=PAR(22)
       Kg=PAR(23)
       ng=PAR(24)
       KP2=PAR(25)
       nP2=PAR(26)
       taoP1=PAR(27)
       alphaP1=PAR(28)
       Cf1=PAR(29)
       Cf2=PAR(30)
       kB=PAR(31)
       NOCTeff=PAR(32)
       tempCoef=PAR(33)
       theta=PAR(34)
       AbsorberPlateCheck=PAR(35)
       eAbsorberPlateup=PAR(36)
       eAbsorberPlatedown=PAR(37)
       alphaAbsorberPlate=PAR(38)
       npv=PAR(39)
       alphapvnormal=PAR(40)
       kside=PAR(41)
       zside=PAR(42)
       Cg=PAR(43)
       CP1=PAR(44)
       CP2=PAR(45)
       CB=PAR(46)
       Cs=PAR(47)
       rhos=PAR(48)
       rhog=PAR(49)
       rhoP1=PAR(50)
       rhoP2=PAR(51)
       rhoB=PAR(52)
       zBplate=PAR(53)
       hcond_P2_s=PAR(54)
C-------------------------------------------------------------------------------------------------------------------
C    RETRIEVE THE CURRENT VALUES OF THE INPUTS TO THIS MODEL FROM THE XIN ARRAY IN SEQUENTIAL ORDER

       mdot=XIN(1)
       Beta=XIN(2)
       S=XIN(3)
       Tin=XIN(4)
       Ta=XIN(5)
       Tsky=XIN(6)
       V=XIN(7)
       incidentangle=XIN(8)
       Sdiffuse=XIN(9)
       Sground=XIN(10)
            IUNIT=INFO(1)
            ITYPE=INFO(2)

C-------------------------------------------------------------------------------------------------------------------
C    SET THE VERSION INFORMATION FOR TRNSYS
       IF(INFO(7).EQ.-2) THEN
            INFO(12)=16
            RETURN 1
          ENDIF
C-------------------------------------------------------------------------------------------------------------------
C-------------------------------------------------------------------------------------------------------------------
C    DO ALL THE VERY LAST CALL OF THE SIMULATION MANIPULATIONS HERE
```

```
      IF (INFO(8).EQ.-1) THEN
            RETURN 1
         ENDIF
C-----------------------------------------------------------------------------------------------------------------------

C-----------------------------------------------------------------------------------------------------------------------
C    PERFORM ANY 'AFTER-ITERATION' MANIPULATIONS THAT ARE REQUIRED HERE
C    e.g. save variables to storage array for the next timestep
      IF (INFO(13).GT.0) THEN
            NITEMS=0
C           STORED(1)=... (if NITEMS > 0)
C        CALL setStorageVars(STORED,NITEMS,INFO)
            RETURN 1
         ENDIF
C
C-----------------------------------------------------------------------------------------------------------------------
C-----------------------------------------------------------------------------------------------------------------------
C    DO ALL THE VERY FIRST CALL OF THE SIMULATION MANIPULATIONS HERE
      IF (INFO(7).EQ.-1) THEN
C       SET SOME INFO ARRAY VARIABLES TO TELL THE TRNSYS ENGINE HOW THIS TYPE IS TO WORK
         INFO(6)=NOUT
         INFO(9)=1
            INFO(10)=0    !STORAGE FOR VERSION 16 HAS BEEN CHANGED
C       SET THE REQUIRED NUMBER OF INPUTS, PARAMETERS AND DERIVATIVES THAT THE USER SHOULD SUPPLY IN THE INPUT
C        FILE
C       IN SOME CASES, THE NUMBER OF VARIABLES MAY DEPEND ON THE VALUE OF PARAMETERS TO THIS MODEL....
         NIN=NI
            NPAR=NP
            NDER=ND

C       CALL THE TYPE CHECK SUBROUTINE TO COMPARE WHAT THIS COMPONENT REQUIRES TO WHAT IS SUPPLIED IN
C       THE TRNSYS INPUT FILE
            CALL TYPECK(1,INFO,NIN,NPAR,NDER)

C       SET THE NUMBER OF STORAGE SPOTS NEEDED FOR THIS COMPONENT
         NITEMS=3000
            CALL setStorageSize(NITEMS,INFO)

C       RETURN TO THE CALLING PROGRAM
         RETURN 1

      ENDIF
C-----------------------------------------------------------------------------------------------------------------------
C-----------------------------------------------------------------------------------------------------------------------
C    DO ALL OF THE INITIAL TIMESTEP MANIPULATIONS HERE - THERE ARE NO ITERATIONS AT THE INTIAL TIME
      IF (TIME .LT. (getSimulationStartTime() +
     . getSimulationTimeStep()/2.D0)) THEN

C       SET THE UNIT NUMBER FOR FUTURE CALLS
         IUNIT=INFO(1)
         ITYPE=INFO(2)

C       CHECK THE PARAMETERS FOR PROBLEMS AND RETURN FROM THE SUBROUTINE IF AN ERROR IS FOUND
C         IF(...) CALL TYPECK(-4,INFO,0,"BAD PARAMETER #",0)

C       PERFORM ANY REQUIRED CALCULATIONS TO SET THE INITIAL VALUES OF THE OUTPUTS HERE
C                 Toutofcollector
                        OUT(1)=Ta
C                 thermalefficiency
                        OUT(2)=0
C                 elecpower
                        OUT(3)=0
C                 eleceff
                        OUT(4)=0
```

```
C                totaleff
                        OUT(5)=0
C                test1
                        OUT(6)=0
C                test2
                        OUT(7)=0
C                test3
                        OUT(8)=0
C                test4
                        OUT(9)=0
C                test5
                        OUT(10)=0
C                test6
                        OUT(11)=0
C                test7
                        OUT(12)=0
C       PERFORM ANY REQUIRED CALCULATIONS TO SET THE INITIAL STORAGE VARIABLES HERE
         NITEMS=3000
                DO initialcounter = 1,amountofx*5
                        STORED(initialcounter)= Ta
                ENDDO

C       PUT THE STORED ARRAY IN THE GLOBAL STORED ARRAY
         CALL setStorageVars(STORED,NITEMS,INFO)

C       RETURN TO THE CALLING PROGRAM
         RETURN 1

      ENDIF
C-------------------------------------------------------------------------------------------------------------------
C-------------------------------------------------------------------------------------------------------------------
C    *** ITS AN ITERATIVE CALL TO THIS COMPONENT ***
C-------------------------------------------------------------------------------------------------------------------


C-------------------------------------------------------------------------------------------------------------------
C    RETRIEVE THE VALUES IN THE STORAGE ARRAY FOR THIS ITERATION
      NITEMS=3000
         CALL getStorageVars(STORED,NITEMS,INFO)

C-------------------------------------------------------------------------------------------------------------------
C-------------------------------------------------------------------------------------------------------------------
C    CHECK THE INPUTS FOR PROBLEMS
C      IF(...) CALL TYPECK(-3,INFO,'BAD INPUT #',0,0)
C       IF(IERROR.GT.0) RETURN 1
C-------------------------------------------------------------------------------------------------------------------
C-------------------------------------------------------------------------------------------------------------------
C    *** PERFORM ALL THE CALCULATION HERE FOR THIS MODEL. ***
C-------------------------------------------------------------------------------------------------------------------
C                ADD YOUR COMPONENT EQUATIONS HERE; BASICALLY THE EQUATIONS THAT WILL
C                CALCULATE THE OUTPUTS BASED ON THE PARAMETERS AND THE INPUTS.       REFER TO
C                CHAPTER 3 OF THE TRNSYS VOLUME 1 MANUAL FOR DETAILED INFORMATION ON
C                WRITING TRNSYS COMPONENTS.

C234567890
         sigma = 5.67d-8
         timestep = 3600*getsimulationtimestep()

C        Calculate back and side losses
         ztotal = zg+zP2+zP1+Zn+Zg+Zb1;
         UB = (kB/zB)
         Us = kside/zside

C        Properties for beam radiation
```

```
          call solarproperties (incidentangle,Kg,ng,zg,KP2,nP2,zP2,
     >taoP1,alphaP1,Apv,Ac,taoalphaP1,taoalphaP2,taoalphasg
     >,taoalphas,alphag,AbsorberPlateCheck,alphaAbsorberPlate,npv
     >,alphapvnormal)
C         Properties for ground radiation
          incidentangleground = (3.141592654/180.0)*(90.0-0.5788*
     >(Beta*180.0/3.141592654)+0.002693*(Beta*180.0/3.141592654)**2)
          call solarproperties (incidentangleground,Kg,ng,zg,KP2,nP2,zP2,
     >taoP1,alphaP1,Apv,Ac,taoalphaP1ground,taoalphaP2ground
     >,taoalphasgground,taoalphasground, alphagground,AbsorberPlateCheck
     >,alphaAbsorberPlate,npv,alphapvnormal)
C         Properties for sky diffuse radiation
          incidentanglediffuse = (3.141592654/180.0)*(59.7-0.1388*
     >(Beta*180.0/3.141592654)+0.001497*(Beta*180.0/3.141592654)**2)
          call solarproperties (incidentanglediffuse,Kg,ng,zg,KP2,nP2,zP2,
     >taoP1,alphaP1,Apv,Ac,taoalphaP1diffuse,taoalphaP2diffuse
     >,taoalphasgdiffuse,taoalphasdiffuse,alphagdiffuse,
     >AbsorberPlateCheck,alphaAbsorberPlate,npv,alphapvnormal)

          ElecPowerTotal = 0

C         Calculations for Temperature start HERE*********************************************
          do icountx = 1,amountofx
          x = ((icountx-0.5)*L/amountofx)
          convergecheckTemp = 0

          if (icountx.eq.1) then
          TB(icountx) = 330
          TP1(icountx) = 330
          Tf1(icountx) = Tin
          Tf2(icountx) = Tin
          TP2(icountx) = 330
          Ts(icountx) = 330
          Tg(icountx) = 330
          end if

          if (icountx.gt.1) then
          TB(icountx) = TB(icountx-1)
          TP1(icountx) = TP1(icountx-1)
          Tf1(icountx) = Tf1(icountx-1)
          Tf2(icountx) = Tf2(icountx-1)
          TP2(icountx) = TP2(icountx-1)
          Ts(icountx) = Ts(icountx-1)
          Tg(icountx) = Tg(icountx-1)

          end if

          do while (abs(convergecheckTemp - Tf2(icountx)).ge.0.00000025)
          convergecheckTemp = Tf2(icountx)

C         wind heat transfer coefficient
          hw=(3.83*V**0.5)*(L**-0.5)

          airdiff = (1.4614d-07)*(((Ta+Tg(icountx))/2)-273.15)
     >+ 1.8343d-05

          kinvisc = (9.7506d-08)*(((Ta+Tg(icountx))/2)-273.15)
     >+ 1.3118d-05
          ka = ((7.5714d-5)*(((Ta+Tg(icountx))/2)-273.15)) + 2.4181d-2

          hfree = (ka*0.15*(9.8*2*abs(Tg(icountx)-Ta)/((Tg(icountx)+Ta)*
     >airdiff * kinvisc))**0.333)/((4*Ac)/(2*(W+L)))

          if (hw.lt.hfree) then
```

```
                hw = hfree
            endif
C           %%%%%%%calc. hc_f2_P2 See paper by Kercher and Tabakoff.

            ka = ((7.5714d-5)*(((Tf1(icountx)+TP2(icountx))/2)-273.15))
     >+ 2.4181d-2

            Pr = ((-9.8398d-10)*(((Tf1(icountx)+TP2(icountx))/2)-273.15)**4)
     >+((1.8486d-7)*(((Tf1(icountx)+TP2(icountx))/2)-273.15)**3)-
     >((8.5713d-6)*(((Tf1(icountx)+TP2(icountx))/2)-273.15)**2)
     >-((2.2359d-4)*(((Tf1(icountx)+TP2(icountx))/2)-273.15))+0.7157

            mu = (4.614d-8)*(((Tf1(icountx)+TP2(icountx))/2)-273.15) +1.718d-5

            Re = mdot*4*(Xn**2)/(3.141592654d0*D*mu*L*w)

            xvarphi2 = ((mdot*(x/L)/(w*Zn))/(mdot/(amountofx*w*(L/amountofx)
     >*3.141592654d0*(D**2)/(4*(Xn**2)))))*(Zn/D)

            if (Re.lt.3d3) then

            phi1 = 2.8055*((Xn/D)**-2.255)
            phi2 = 0.9582*exp(-0.302*xvarphi2)
            m =(-0.0000023674*((Xn/D)**4))+(0.00016098*((Xn/D)**3))
     >-(0.0042898*(Xn/D)**2)+ (0.059113*(Xn/D))+0.49957

            else

            phi1 = 3.3588*(Xn/D)**(-2.789)
            phi2 = 0.9699*exp(-0.363*xvarphi2)
            m = -(0.0024*((Xn/D)**2)) + 0.0696*(Xn/D) + 0.4969

            if (Xn/D.gt.15) then
            m = 1.0
            endif

            endif

C           Florschuetz correlation  (for future studies)
C           Gc = mdot*(x/L)/(w*Zn)
C           Gj = mdot/(amountofx*w*(L/amountofx)
C       >*3.141592654d0*(D**2)/(4*(Xn**2)))
C           A=1.18*((Xn/D)**-0.944)*((Xn/D)**-0.642)*((Zn/D)**0.169)
C           m=0.612*((Xn/D)**0.059)*((Xn/D)**0.032)*((Zn/D)**-0.022)
C           B=0.437*((Xn/D)**-0.095)*((Xn/D)**-0.219)*((Zn/D)**0.275)
C           n=0.092*((Xn/D)**-0.005)*((Xn/D)**0.599)*((Zn/D)**1.04)
C           Nu_f2_P2 = A*(Re**m)*(1-B*((Zn/D)*(Gc/Gj))**n)*Pr**1./3.

            Nu_f2_P2 = phi1*phi2*(Pr**(1./3.))*(Re**m)*((Zn/D)**0.091)
            hc_f2_P2 = Nu_f2_P2*ka/D
C
            ka = ((7.5714d-5)*(((Tf1(icountx)+TB(icountx))/2)-273.15))
     >+ 2.4181d-2

            mu = (4.614d-8)*(((Tf1(icountx)+TB(icountx))/2)-273.15) +1.718d-5

            hc_B_f1 = (ka*(w+Zb1)/(2*(w*Zb1)))*0.0158*(2*mdot*(1-(x/L))/
     >((w+Zb1)*mu))**0.8 !see example 3.14.2

            mu = (4.614d-8)*(((Tf1(icountx)+TP1(icountx))/2)-273.15) +1.718d-5

            ka = ((7.5714d-5)*(((Tf1(icountx)+TP1(icountx))/2)-273.15))
     >+ 2.4181d-2
```

```
          hc_P1_f1 = (ka*(w+Zb1)/(2*(w*Zb1)))*0.0158*(2*mdot*(1-(x/L))/
     >((w+Zb1)*mu))**0.8 !see example 3.14.2

          ka = ((7.5714d-5)*(((Tf2(icountx)+TP1(icountx))/2)-273.15))
     >+ 2.4181d-2


          mu = (4.614d-8)*(((Tf2(icountx)+TP1(icountx))/2)-273.15) +1.718d-5

          hc_P1_f2 = (ka*(w+Zn)/(2*(w*Zn)))*0.0158*(2*mdot*(x/L)/
     >((w+Zn)*mu))**0.8

          hr_P1_B = sigma*((TP1(icountx)**2) + (TB(icountx)**2))*
     >(TP1(icountx)+ TB(icountx))/((eB**-1)+(eP1down**-1)-1)

          hr_P1_P2 = sigma*((TP1(icountx)**2)+(TP2(icountx)**2))*
     >(TP1(icountx)+ TP2(icountx))/((eP2**-1)+(eP1up**-1)-1)

          if (AbsorberPlateCheck.eq.1) then
          hr_P1_P2 = sigma*((TP1(icountx)**2)+(TP2(icountx)**2))*
     >(TP1(icountx)+ TP2(icountx))/((eAbsorberPlatedown**-1)+
     >(eP1up**-1)-1)
          endif

C         %%%%%calc. hc_P2_g%%%%%%%%% use equation 3.11.4 in Duffie Beckman
          BetaPrime = ((TP2(icountx)+Tg(icountx))/2)**-1
          deltaT = abs(TP2(icountx)-Tg(icountx))

          airdiff = (1.4614d-07)*(((TP2(icountx)+Tg(icountx))/2)-273.15)
     >+ 1.8343d-05

          kinvisc = (9.7506d-08)*(((TP2(icountx)+Tg(icountx))/2)-273.15)
     >+ 1.3118d-05

          ka = ((7.5714d-5)*(((TP2(icountx)+Tg(icountx))/2))) + 2.4181d-2

          Ra = (9.81*BetaPrime*deltaT*(ZgP2**3))/(kinvisc*airdiff)

          if (Ra.ne.0) then

         variable1 = (1-((1708*(sin(1.8*Beta))**1.6)/(Ra*cos(Beta))))
         variable2 = (1-(1708/(Ra*cos(Beta))))
         variable3 = (((Ra*cos(Beta))/5830)**(1./3.))-1
         if (variable2.lt.0) then
             variable2 = 0
         endif

         if (variable3.lt.0) then
             variable3 = 0
         endif

         Nu_g_P2 = 1 + (1.44*variable1*variable2)+variable3

         hc_P2_g = Nu_g_P2*ka/ZgP2
          else

         hc_P2_g = 0
          endif

          hr_P2_g = sigma*(TP2(icountx)**2 + Tg(icountx)**2)*(TP2(icountx)+
     >Tg(icountx))/(((1-eP2)/eP2)+1+((1-eg)*(Ac-Apv)/(eg*Ac)))

          if (AbsorberPlateCheck.eq.1) then
          hr_P2_g = sigma*(TP2(icountx)**2 + Tg(icountx)**2)*(TP2(icountx)+
```

```
     >Tg(icountx))/(((1-eAbsorberPlateup)/eAbsorberPlateup)+1+((1-eg)*
     >(Ac-Apv)/(eg*Ac)))
         endif

         hr_s_g = sigma*(Ts(icountx)**2 + Tg(icountx)**2)*(Ts(icountx)
     >+Tg(icountx))/(((1-es)/es)+1+((1-eg)*(Apv)/(eg*Ac)))
C        hr_s_g=0

C        %%%%%calc. hc_s_g%%%%%%%%% use equation 3.11.4 in Duffie Beckman

         airdiff = (1.4614d-07)*(((Ts(icountx)+Tg(icountx))/2)-273.15)
     >+ 1.8343d-05

         kinvisc = (9.7506d-08)*(((Ts(icountx)+Tg(icountx))/2)-273.15)
     >+ 1.3118d-05

         BetaPrimepv = ((Ts(icountx)+Tg(icountx))/2)**-1
         deltaTpv = abs(Ts(icountx)-Tg(icountx))
         Rapv = (9.81*BetaPrimepv*deltaTpv*(ZgP2**3))/(kinvisc*airdiff)

         if (Rapv.ne.0) then

        variable1pv = (1-((1708*(sin(1.8*Beta))**1.6)/(Rapv*cos(Beta))))
        variable2pv = (1-(1708/(Rapv*cos(Beta))))
        variable3pv = (((Rapv*cos(Beta))/5830)**(1./3.))-1
        if (variable2pv.lt.0) then
            variable2pv = 0
        endif

        if (variable3pv.lt.0) then
            variable3pv = 0
        endif
         ka = ((7.5714d-5)*(((Ts(icountx)+Tg(icountx))/2))) + 2.4181d-2
        Nu_g_s = 1 + (1.44*variable1pv*variable2pv)+variable3pv

        hc_s_g = Nu_g_s*ka/ZgP2
         else

        hc_s_g = 0

         endif

         hr_g_sky=eg*((Tg(icountx)**2)+(Tsky**2))*
     >(Tg(icountx)+Tsky)*sigma*(1+cos(Beta))/2

         hr_g_ground = eg*((Tg(icountx)**2)+(Ta**2))*
     >(Tg(icountx)+Ta)*sigma*(1-cos(Beta))/2

C        fluid1

       Cf1=0.0006*((Tf1(icountx)-273.15)**2)
     >-(0.0011*(Tf1(icountx)-273.15))+1005.9


         if (icountx.eq.1) then
        fTf1 = hc_P1_f1*(TB(icountx)+TP1(icountx)-(2*Tin))*w/
     >((mdot*(1-x/L))*Cf1)
        Tf1out(icountx) = (fTf1*L/amountofx) + Tin
        Tf1(icountx)= (Tf1out(icountx)+Tin)/2
        fTf1 = hc_P1_f1*(TB(icountx)+TP1(icountx)-(2*Tf1(icountx)))*w/
     >((mdot*(1-x/L))*Cf1)
        Tf1out(icountx) = (fTf1*L/amountofx) + Tin
        Tf1(icountx)= (Tf1out(icountx)+Tin)/2
```

```
          else
          fTf1 = ((hc_P1_f1*(TB(icountx)+TP1(icountx)
     >-(2*Tf1out(icountx-1)))
     >*w)+Us*2*(Zb1/L)*(L+w)*(Ta-Tf1out(icountx-1)))/((mdot*(1-x/L))
     >*Cf1)

            Tf1out(icountx) = (fTf1*L/amountofx) + Tf1out(icountx - 1)

            Tf1(icountx)= (Tf1out(icountx-1)+Tf1out(icountx))/2

            fTf1 = ((hc_P1_f1*(TB(icountx)+TP1(icountx)-(2*Tf1(icountx)))
     >*w)+Us*2*(Zb1/L)*(L+w)*(Ta-Tf1(icountx)))/((mdot*(1-x/L))*Cf1)

            Tf1out(icountx) = (fTf1*L/amountofx) + Tf1out(icountx - 1)

            Tf1(icountx) = (Tf1out(icountx-1)+Tf1out(icountx))/2

          endif

C         fluid2 calculations

       Cf2=0.0006*((Tf2(icountx)-273.15)**2)
     >-(0.0011*(Tf2(icountx)-273.15))+1005.9

          if (icountx.eq.1) then

          Timp = Tf1(icountx)

       Tf2in= Timp

          Tf2out(icountx) =  ((hc_f2_P2*(TP2(icountx)-Timp)+hc_P1_f2
     >*(TP1(icountx)-Tf2in))*(L/amountofx)*w/
     >(Cf2*(mdot*(((icountx-1)*L/amountofx)/L)+(mdot/amountofx))))+
     >Tf2in

          Tf2(icountx) = (Tf2out(icountx)+Tf2in)/2

          Tf2out(icountx) =  ((hc_f2_P2*(TP2(icountx)-Timp)+hc_P1_f2
     >*(TP1(icountx)-Tf2(icountx)))*(L/amountofx)*w/
     >(Cf2*(mdot*(((icountx-1)*L/amountofx)/L)+(mdot/amountofx))))+
     >Tf2in

          else
          Timp = theta*(Tf1(icountx)-Tf2out(icountx-1))+Tf2out(icountx-1)


       Tf2in= (mdot*(((icountx-1)*L/amountofx)/L)*
     >Tf2out(icountx-1)+((mdot/(amountofx))*Tf1(icountx)))/
     >(mdot*(((icountx-1)*L/amountofx)/L)+(mdot/(amountofx)))

          Tf2out(icountx) =  ((((hc_f2_P2*(TP2(icountx)-Timp)+hc_P1_f2
     >*(TP1(icountx)-Tf2out(icountx-1)))*(L/amountofx)*w)
     >+Us*(Ta-Tf2out(icountx-1))*2*Zn*((L+w)/amountofx))/
     >(Cf2*(mdot*(((icountx-1)*L/amountofx)/L)+(mdot/amountofx))))+
     >Tf2in

          Tf2(icountx) = (Tf2out(icountx)+Tf2out(icountx-1))/2

          Tf2out(icountx) =  ((((hc_f2_P2*(TP2(icountx)-Timp)+hc_P1_f2
     >*(TP1(icountx)-Tf2(icountx)))*(L/amountofx)*w)
     >+Us*(Ta-Tf2out(icountx-1))*Zn*2*((L+w)/amountofx))/
     >(Cf2*(mdot*(((icountx-1)*L/amountofx)/L)+(mdot/amountofx))))+
     >Tf2in
```

```
          endif


          TB(icountx) = ((timestep/(rhoB*zBplate*CB))*(hr_P1_B*TP1(icountx)
     >+hc_B_f1*Tf1(icountx)+UB*Ta)+STORED(icountx))/
     >(1+(timestep/(rhoB*zBplate*CB))*(hr_P1_B+hc_B_f1+UB))


          TP1(icountx) = ((timestep/(rhoP1*zP1*CP1))*(hc_P1_f1*Tf1(icountx)+
     >hc_P1_f2*Tf2(icountx)+hr_P1_B*TB(icountx)+
     > hr_P1_P2*TP2(icountx)
     >+S*taoalphaP1+Sground*taoalphaP1ground+Sdiffuse*taoalphaP1diffuse)
     > + STORED(icountx + amountofx))/
     >(1+(timestep/(rhoP1*zP1*CP1))*
     >(hc_P1_f1+hr_P1_B+hr_P1_P2+hc_P1_f2))

C         Plate 2... with Timp
          TP2(icountx) =(((timestep/(rhoP2*zP2*CP2))*(hr_P1_P2*TP1(icountx)+
     >((S*taoalphaP2+Sground*
     >taoalphaP2ground+Sdiffuse*taoalphaP2diffuse)*(1-(Apv/Ac)))
     >+ hcond_P2_s*(Apv/Ac)*Ts(icountx) + (1-(Apv/Ac))
     >*hr_P2_g*Tg(icountx) + hc_f2_P2*Timp + hc_P2_g*Tg(icountx)
     >*(1-(Apv/Ac))))+STORED(icountx+2*amountofx))/
     >(1+(timestep/(rhoP2*zP2*CP2))*(
     >+hr_P1_P2+hcond_P2_s*(Apv/Ac)+(1-(Apv/Ac))
     >*hr_P2_g+hc_f2_P2+hc_P2_g*(1-(Apv/Ac))))


C         Electrical Power calcs    ***************************************************************
          pveff = NOCTeff-tempCoef*(Ts(icountx)-298.15)
          ElecPower(icountx) = (S*taoalphas+Sdiffuse*taoalphasdiffuse+
     >Sground*taoalphasground)*pveff/alphapvnormal

C         ********************************************************************************


          Ts(icountx) = ((timestep/(rhos*zs*Cs))*(hr_s_g*Tg(icountx)
     >+ (S*taoalphas+Sdiffuse*
     >taoalphasdiffuse+Sground*taoalphasground)+hcond_P2_s*
     >TP2(icountx) +hc_s_g*Tg(icountx) - ElecPower(icountx))
     >+STORED(icountx+3*amountofx))/(1+(timestep/(rhos*zs*Cs))*((hr_s_g
     >+ hcond_P2_s + hc_s_g)))

          Tg(icountx) = ((timestep/(rhog*zg*Cg))*((Apv/Ac)*Ts(icountx)*
     >hr_s_g + S*alphag + Sground*alphagground+Sdiffuse*alphagdiffuse+
     >(1-(Apv/Ac))*hr_P2_g*TP2(icountx)+ Tsky*hr_g_sky
     > + (hr_g_ground+hw)*Ta + hc_s_g
     >*Ts(icountx)*(Apv/Ac) + hc_P2_g*TP2(icountx)*(1-(Apv/Ac)))
     >+STORED(icountx+amountofx*4))/(1+(timestep/(rhog*zg*Cg))
     >*(((Apv/Ac)*hr_s_g)+((1-(Apv/Ac))*hr_P2_g)+hr_g_sky+
     >hr_g_ground+hw+
     >(hc_s_g*(Apv/Ac))+(hc_P2_g*(1-(Apv/Ac)))))

          enddo
          ElecPowerTotal = ElecPower(icountx)/amountofx+ElecPowerTotal
          enddo

C-------------------------------------------------------------------------------------------------------------------
C-------------------------------------------------------------------------------------------------------------------
C-------------------------------------------------------------------------------------------------------------------
C     SET THE STORAGE ARRAY AT THE END OF THIS ITERATION IF NECESSARY
       NITEMS=3000
       DO icountstorage = 1,amountofx
```

```
                  STORED(icountstorage) = TB(icountstorage)
                  STORED(icountstorage+amountofx)=TP1(icountstorage)
                  STORED(icountstorage+2*amountofx)=TP2(icountstorage)
                  STORED(icountstorage+3*amountofx)=Ts(icountstorage)
                  STORED(icountstorage+4*amountofx)=Tg(icountstorage)
         ENDDO

         CALL setStorageVars(STORED,NITEMS,INFO)
C-------------------------------------------------------------------------------------------------------------------
----------
C-------------------------------------------------------------------------------------------------------------------
----------
C    REPORT ANY PROBLEMS THAT HAVE BEEN FOUND USING CALLS LIKE THIS:
C      CALL MESSAGES(-1,'put your message here','MESSAGE',IUNIT,ITYPE)
C      CALL MESSAGES(-1,'put your message here','WARNING',IUNIT,ITYPE)
C      CALL MESSAGES(-1,'put your message here','SEVERE',IUNIT,ITYPE)
C      CALL MESSAGES(-1,'put your message here','FATAL',IUNIT,ITYPE)
C-------------------------------------------------------------------------------------------------------------------
----------
C-------------------------------------------------------------------------------------------------------------------
----------
C    SET THE OUTPUTS FROM THIS MODEL IN SEQUENTIAL ORDER AND GET OUT
      Cf2=0.0006*((0.5*(Tf2out(amountofx)+Tin)-273.15)**2)
     >-(0.0011*(0.5*(Tf2out(amountofx)+Tin)-273.15))+1005.9
C                 Toutofcollector
                         OUT(1)=Tf2out(amountofx)
C                 efficiency

                         if (S+Sground+Sdiffuse.eq.0) then
                         OUT(2)=0
                         else
                         OUT(2)=mdot*(Tf2out(amountofx)-Tin)*Cf2/
     >((S+Sground+Sdiffuse)*Ac)
                         endif
C                 elecpower

                         OUT(3)=ElecPowerTotal*Apv
C                 eleceff
                         if (S+Sground+Sdiffuse.eq.0) then
                         OUT(4)= 0
                         else
                         OUT(4)=ElecPowerTotal*Apv/((S+Sground+Sdiffuse)*Ac)
                         endif

C                 totaleff

                         if (S+Sground+Sdiffuse.eq.0) then
                         OUT(5)=0
                         else
                         OUT(5)=(mdot*(Tf2out(amountofx)-Tin)
     >*Cf2/((S+Sground+Sdiffuse
     >)*Ac))+ElecPowerTotal*Apv/((S+Sground+Sdiffuse)*Ac)

                         endif


C                 Thermal Power

                         OUT(6)=mdot*(Tf2out(amountofx)-Tin)*Cf2

C                 Variable that can be used for troubleshooting
                         OUT(7)=0
C                 Variable that can be used for troubleshooting
                         OUT(8)=0
C                 Variable that can be used for troubleshooting
```

```
                        OUT(9)=0
C                   Variable that can be used for troubleshooting
                        OUT(10)=0
C                   Variable that can be used for troubleshooting
                        OUT(11)=0
C                   Variable that can be used for troubleshooting
                        OUT(12)=0
C-------------------------------------------------------------------------------------------------------------
C    EVERYTHING IS DONE - RETURN FROM THIS SUBROUTINE AND MOVE ON
      RETURN 1
      END
C-------------------------------------------------------------------------------------------------------------
         subroutine solarproperties(incidentangle,Kg,ng,zg,KP2,nP2,zP2,
     >taoP1,alphaP1,Apv,Ac,taoalphaP1,taoalphaP2,taoalphasg
     >,taoalphas, alphag,AbsorberPlateCheck,alphaAbsorberPlate,npv
     >,alphapvnormal)
         implicit none

C        Calculate solar spectrum properties*************************************************

         double precision incidentangle,Kg,ng,zg,KP2,nP2,zP2,taoP1,alphaP1
         double precision Apv,Ac,taoalphaP1,taoalphaP2,taoalphasg
         double precision taoalphas,alphag,angle60,theta2,taog_a,rg_perp
         double precision taog_perp,rg_para,taog_para,taog,alphag_perp
         double precision alphag_para,reflg_para,reflg_perp
         double precision reflg,reflg60,taoP2_a,rP2_perp,taoP2_perp
         double precision rP2_para,taoP2_para,taoP2,alphaP2_perp
         double precision alphaP2_para,alphaP2,reflP2_para,reflP2_perp
         double precision reflP2,taos_perp,taos_para,refls,refls_perp
         double precision refls_para,alphaP2s,reflP2s_para,reflP2s_perp
         double precision reflP2s,taoP2s_para,taoP2s_perp,taoP2s,taom
         double precision taom_para,taom_perp,refld,alphas,alphasg
         double precision AbsorberPlateCheck,alphaAbsorberPlate,thetapv
         double precision thetapv0degrees,npv,alphas_para,alphas_perp
         double precision alphapvnormal,incidentangledeg

C        Calculation of refld from P1 (60 degrees)


         angle60 = 1.047197551
C        glass cover
C        eqn. 5.1.4
         theta2 = asin(sin(angle60)/ng)
C        eqn 5.2.2
         taog_a = exp(-Kg*zg/cos(theta2))
C        eqn 5.1.1
         rg_perp = ((sin(theta2-angle60))**2)/((sin(theta2+angle60))**2)
C        eqn 5.3.1
         taog_perp = (taog_a*(1-rg_perp)**2)/(1-(rg_perp*taog_a)**2)
C        eqn 5.1.2
         rg_para = ((tan(theta2-angle60))**2)/((tan(theta2+angle60))**2)
C        eqn 5.3.1
         taog_para = (taog_a*(1-rg_para)**2)/(1-(rg_para*taog_a)**2)

         taog = (taog_para + taog_perp)/2

C        eqn 5.3.3
         alphag_perp = (1-taog_a)*((1-rg_perp)/(1-rg_perp*taog_a))
         alphag_para = (1-taog_a)*((1-rg_para)/(1-rg_para*taog_a))
         alphag = (alphag_para+alphag_perp)/2

C        eqn 5.3.2
         reflg_para = rg_para*(1+taog_a*taog_para)
         reflg_perp = rg_perp*(1+taog_a*taog_perp)
```

```
          reflg = (rg_para*(1+taog_a*taog_para)+rg_perp*
     >(1+taog_a*taog_perp))/2
          reflg60 = reflg

C         pv backing
          theta2 = asin(sin(angle60)/nP2)

          taoP2_a = exp(-KP2*zP2/cos(theta2))

          rP2_perp = ((sin(theta2-angle60))**2)/((sin(theta2+angle60))**2)

          taoP2_perp = (taoP2_a*(1-rP2_perp)**2)/(1-(rP2_perp*taoP2_a)**2)

          rP2_para = ((tan(theta2-angle60))**2)/((tan(theta2+angle60))**2)

          taoP2_para = (taoP2_a*(1-rP2_para)**2)/(1-(rP2_para*taoP2_a)**2)

          taoP2 = (taoP2_para + taoP2_perp)/2

          alphaP2_perp = (1-taoP2_a)*((1-rP2_perp)/(1-rP2_perp*taoP2_a))
          alphaP2_para = (1-taoP2_a)*((1-rP2_para)/(1-rP2_para*taoP2_a))

          alphaP2 = (alphaP2_para+alphaP2_perp)/2
          reflP2_para = rP2_para*(1+taoP2_a*taoP2_para)
          reflP2_perp = rP2_perp*(1+taoP2_a*taoP2_perp)
          reflP2 = (rP2_para*(1+taoP2_a*taoP2_para)+rP2_perp*
     >(1+taoP2_a*taoP2_perp))/2


          theta2 = asin(sin(angle60)/npv)

          taos_perp = 0.
          taos_para = 0.

C         solar cells

C         aprrox. reflectance
          refls = 0.5*(((sin(theta2-angle60))**2)/((sin(theta2+angle60))**2)
     >+((tan(theta2-angle60))**2)/((tan(theta2+angle60))**2))
          refls_perp = ((sin(theta2-angle60))**2)/((sin(theta2+angle60))**2)
          refls_para = ((tan(theta2-angle60))**2)/((tan(theta2+angle60))**2)

C         PV and P2 combined

          alphaP2s = (1-(Apv/Ac))*alphaP2 + taoP2*(Apv/Ac)*1

          reflP2s_para = reflP2_para
          reflP2s_perp = reflP2_perp
          reflP2s = 0.5*(reflP2s_para + reflP2s_perp)

          taoP2s_para = ((1-(Apv/Ac))*taoP2_para + (Apv/Ac)*taos_para)
          taoP2s_perp = ((1-(Apv/Ac))*taoP2_perp + (Apv/Ac)*taos_perp)
          taoP2s = 0.5*(taoP2s_perp+taoP2s_para)

C         eqns 5.3.7 for glass and P2s cover... need to know transmittance and
C         reflectance) of the cover.

          taom  = 0.5*((taog_para*taoP2s_para)/(1-reflg_para*reflP2s_para)
     >+(taog_perp*taoP2s_perp)/(1-reflg_perp*reflP2s_perp))
          taom_para = (taog_para*taoP2s_para)/(1-reflg_para*reflP2s_para)
          taom_perp = (taog_perp*taoP2s_perp)/(1-reflg_perp*reflP2s_perp)

C         rhod from equ. 5.5.1 is found with eqn 5.3.8
          refld = 0.5*((reflP2s_para+(taom_para*reflg_para*taoP2s_para)
```

```
     >/taog_para)+(reflP2s_perp+(taom_perp*reflg_perp*taoP2s_perp)
     >/taog_perp))

C        Calcultations of actual properties with incident angle

         if (incidentangle.le.0) incidentangle = 0.000001
         if (incidentangle.gt.1.570796327) incidentangle=1.57

         theta2 = asin(sin(incidentangle)/ng)

         taog_a = exp(-Kg*zg/cos(theta2))

         rg_perp = ((sin(theta2-incidentangle))**2)/
     >((sin(theta2+incidentangle))**2)

         taog_perp = (taog_a*(1-rg_perp)**2)/(1-(rg_perp*taog_a)**2)

         rg_para = ((tan(theta2-incidentangle))**2)/
     >((tan(theta2+incidentangle))**2)

         taog_para = (taog_a*(1-rg_para)**2)/(1-(rg_para*taog_a)**2)

         taog = (taog_para + taog_perp)/2

         alphag_perp = (1-taog_a)*((1-rg_perp)/(1-rg_perp*taog_a))
         alphag_para = (1-taog_a)*((1-rg_para)/(1-rg_para*taog_a))

         alphag = (alphag_para+alphag_perp)/2
         reflg_para = rg_para*(1+taog_a*taog_para)
         reflg_perp = rg_perp*(1+taog_a*taog_perp)
         reflg = (rg_para*(1+taog_a*taog_para)+
     >rg_perp*(1+taog_a*taog_perp))/2

         theta2 = asin(sin(incidentangle)/nP2)

         taoP2_a = exp(-KP2*zP2/cos(theta2))

         rP2_perp = ((sin(theta2-incidentangle))**2)/
     >((sin(theta2+incidentangle))**2)

         taoP2_perp = (taoP2_a*(1-rP2_perp)**2)/(1-(rP2_perp*taoP2_a)**2)

         rP2_para = ((tan(theta2-incidentangle))**2)/
     >((tan(theta2+incidentangle))**2)

         taoP2_para = (taoP2_a*(1-rP2_para)**2)/(1-(rP2_para*taoP2_a)**2)

         taoP2 = (taoP2_para + taoP2_perp)/2

         alphaP2_perp = (1-taoP2_a)*((1-rP2_perp)/(1-rP2_perp*taoP2_a))
         alphaP2_para = (1-taoP2_a)*((1-rP2_para)/(1-rP2_para*taoP2_a))

         alphaP2 = (alphaP2_para+alphaP2_perp)/2
         reflP2_para = rP2_para*(1+taoP2_a*taoP2_para)
         reflP2_perp = rP2_perp*(1+taoP2_a*taoP2_perp)
         reflP2 = (rP2_para*(1+taoP2_a*taoP2_para)
     >+rP2_perp*(1+taoP2_a*taoP2_perp))/2

         theta2 = asin(sin(incidentangle)/npv)

         taos_perp = 0
         taos_para = 0

C        from equation 5.12.4
```

```
          thetapv = asin(sin(incidentangle)/npv)

          thetapv0degrees = asin(sin(0.0000000001)/npv)

C         approx.absorption in solar cell (silicon)
          alphas = alphapvnormal*(1.0-0.5*(((sin(thetapv-
     >incidentangle))**2)/((sin(thetapv+incidentangle))**2)+
     >((tan(thetapv-incidentangle))**2)/((tan(thetapv+
     >incidentangle))**2)))/(1.0-0.5*(((sin(thetapv0degrees-
     >0.0000000001))**2)/((sin(thetapv0degrees+0.0000000001))**2)+
     >((tan(thetapv0degrees-
     >0.0000000001))**2)/((tan(thetapv0degrees+0.0000000001))**2)))

          alphas_para = alphapvnormal*(1-(((tan(thetapv-
     >incidentangle))**2)/((tan(thetapv+incidentangle))**2)))/
     >(1.0-0.5*(((sin(thetapv0degrees-0.0000000001))
     >**2)/((sin(thetapv0degrees+0.0000000001))**2)+
     >((tan(thetapv0degrees-
     >0.0000000001))**2)/((tan(thetapv0degrees+0.0000000001))**2)))

          alphas_perp = alphapvnormal*(1-(((sin(thetapv-
     >incidentangle))**2)/((sin(thetapv+incidentangle))**2)))/
     >(1.0-0.5*(((sin(thetapv0degrees-0.0000000001))
     >**2)/((sin(thetapv0degrees+0.0000000001))**2)+
     >((tan(thetapv0degrees-
     >0.0000000001))**2)/((tan(thetapv0degrees+0.0000000001))**2)))

C         aprrox. reflectance
          refls = 1-alphas
          refls_perp = 1-alphas_perp
          refls_para = 1-alphas_para

C         PV and P2 combined

          alphaP2s = (1-(Apv/Ac))*alphaP2 + (Apv/Ac)*alphas

          reflP2s_para = (1-(Apv/Ac))*reflP2_para + (Apv/Ac)*refls_para
          reflP2s_perp = (1-(Apv/Ac))*reflP2_perp + (Apv/Ac)*refls_perp
          reflP2s = 0.5*(reflP2s_para + reflP2s_perp)

          taoP2s_para = ((1-(Apv/Ac))*taoP2_para + (Apv/Ac)*taos_para)
          taoP2s_perp = ((1-(Apv/Ac))*taoP2_perp + (Apv/Ac)*taos_perp)
          taoP2s = 0.5*(taoP2s_perp+taoP2s_para)


C         eqns 5.3.7 for glass and P2s cover... need to know transmittance (and
C         maybe reflectance) of the cover.

          taom  = 0.5*((taog_para*taoP2s_para)/(1-reflg_para*reflP2s_para)+
     >(taog_perp*taoP2s_perp)/(1-reflg_perp*reflP2s_perp))
          taom_para = (taog_para*taoP2s_para)/(1-reflg_para*reflP2s_para)
          taom_perp = (taog_perp*taoP2s_perp)/(1-reflg_perp*reflP2s_perp)


C         transmittance-absorptance product (p.215)

          incidentangledeg=incidentangle*180/3.14159265

          alphaP1=alphaP1*(1-(0.0015879*incidentangledeg)+(0.00027314*
     >incidentangledeg**2)-(0.000023026*incidentangledeg**3)+
     >(0.00000090244*incidentangledeg**4)-(0.000000018*
     >incidentangledeg**5)+(0.00000000017734*incidentangledeg**6)-
     >(0.00000000000069937*incidentangledeg**7))
```

```
        taoalphaP1 = taom*alphaP1/(1-(1-alphaP1)*refld)

C
        if (AbsorberPlateCheck.eq.1) then
        alphaP2 = alphaAbsorberPlate
        taoalphaP1 = 0
        endif
        taoalphaP2 = taog*alphaP2/(1-(1-alphaP2)*reflg60)

        taoalphas  = taog*alphas/(1-(1-alphas)*reflg60)


        end
```

Appendix B
COLLECTOR FRAME FABRICATION DRAWINGS

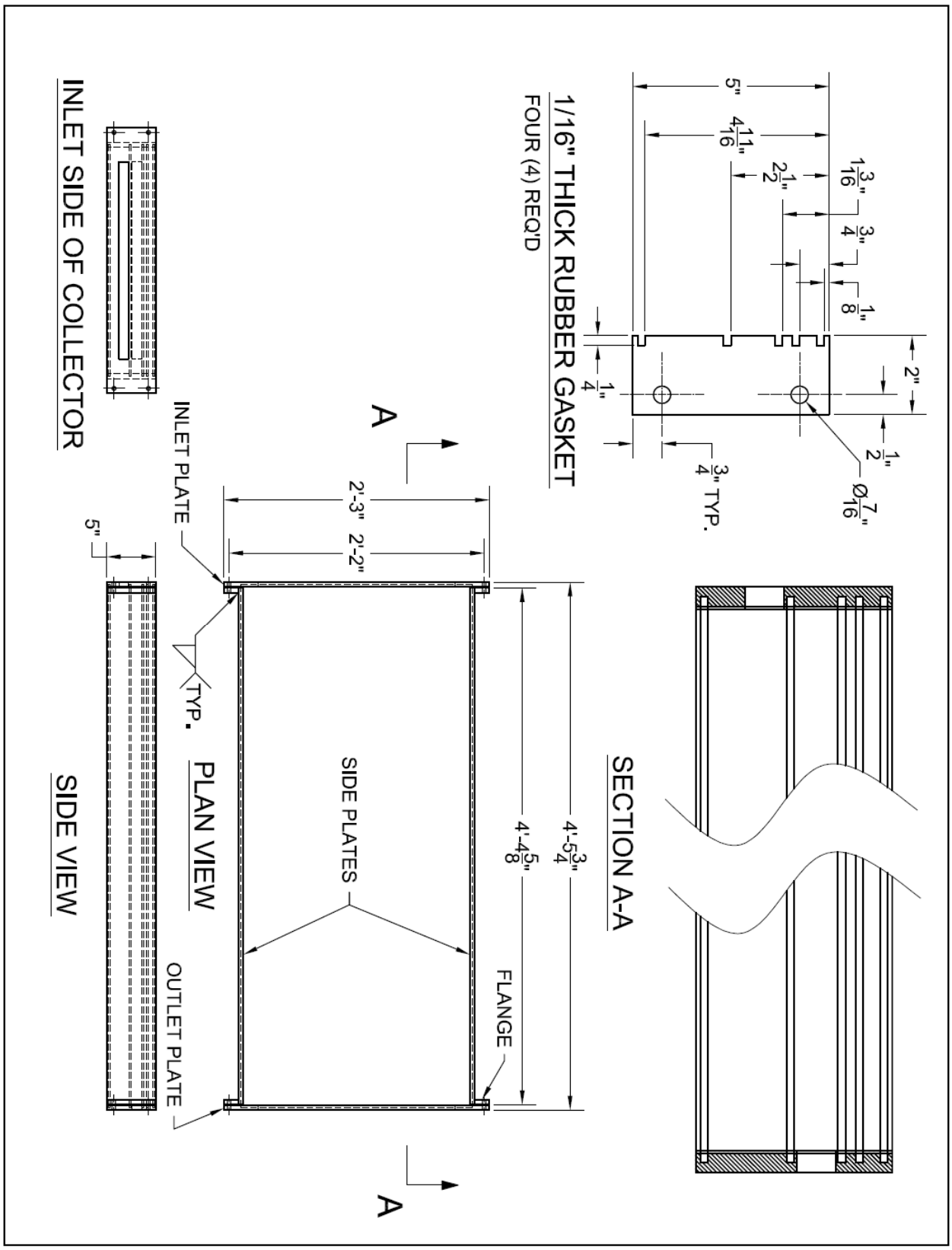

FIGURE B.1 COLLECTOR FRAME GENERAL ASSEMBLY DRAWING

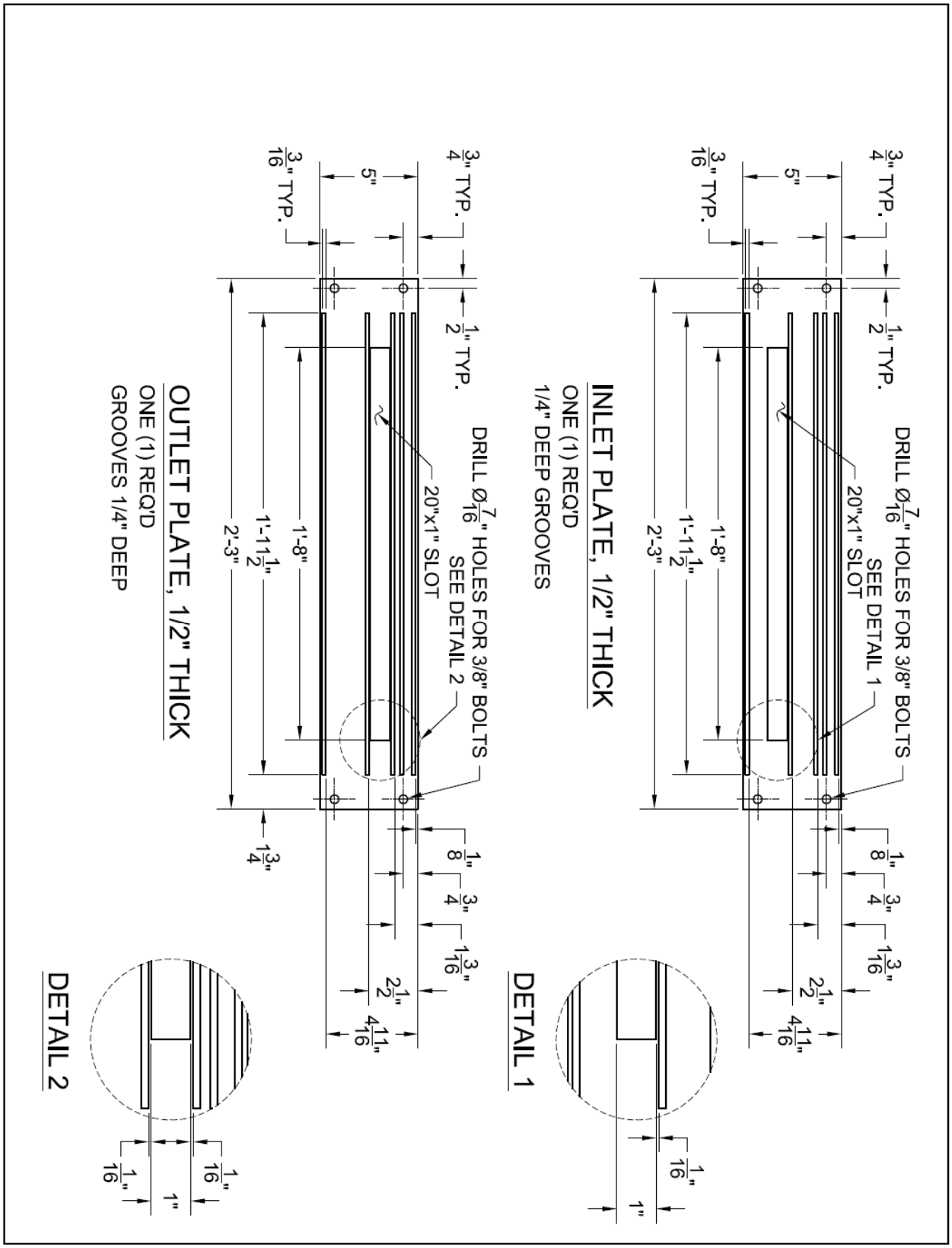

FIGURE B.2 COLLECTOR FRAME INLET AND OUTLET PLATE DETAIL

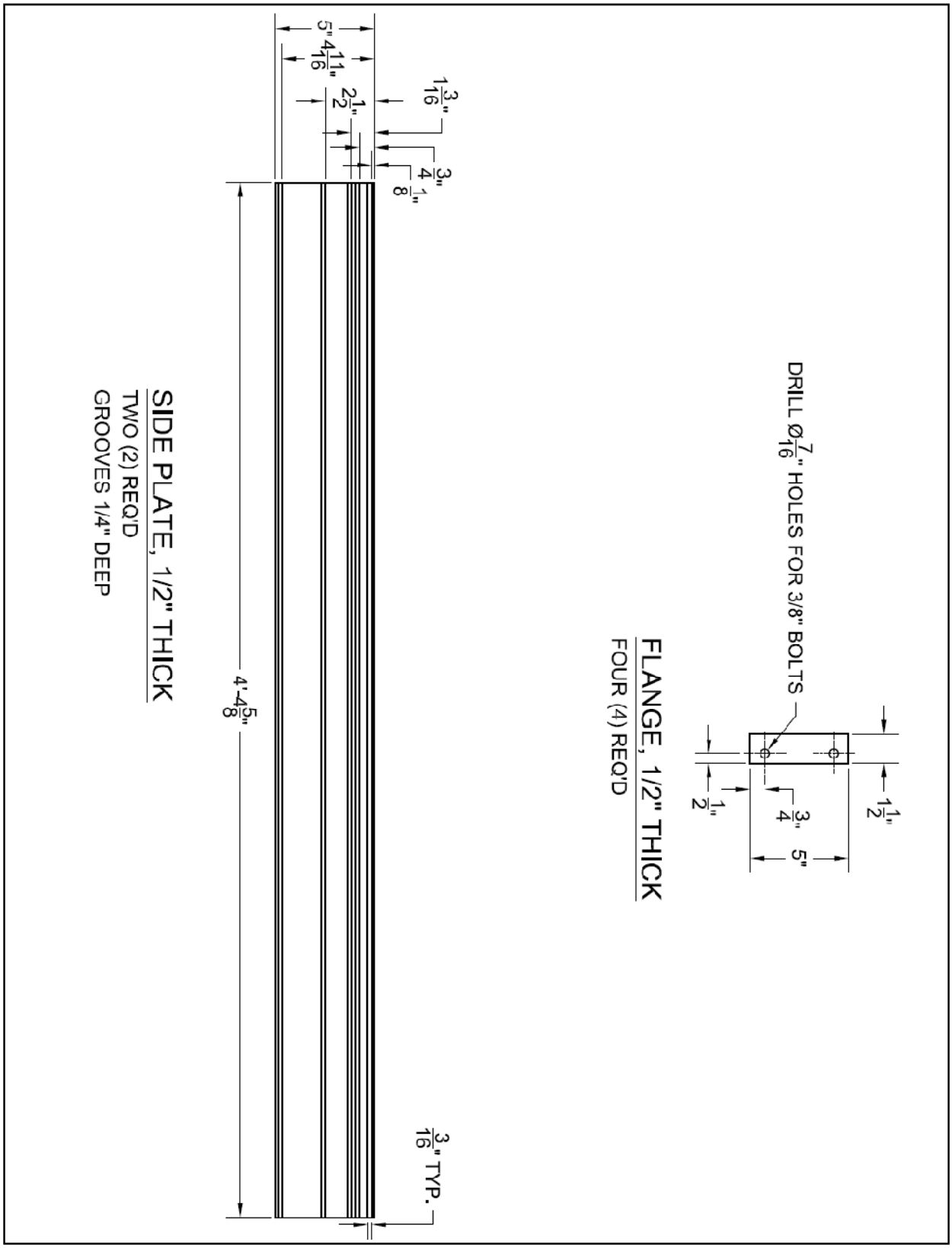

FIGURE B.3 COLLECTOR FRAME SIDE PLATE DETAIL

Appendix C
LABVIEW FRONT PANEL

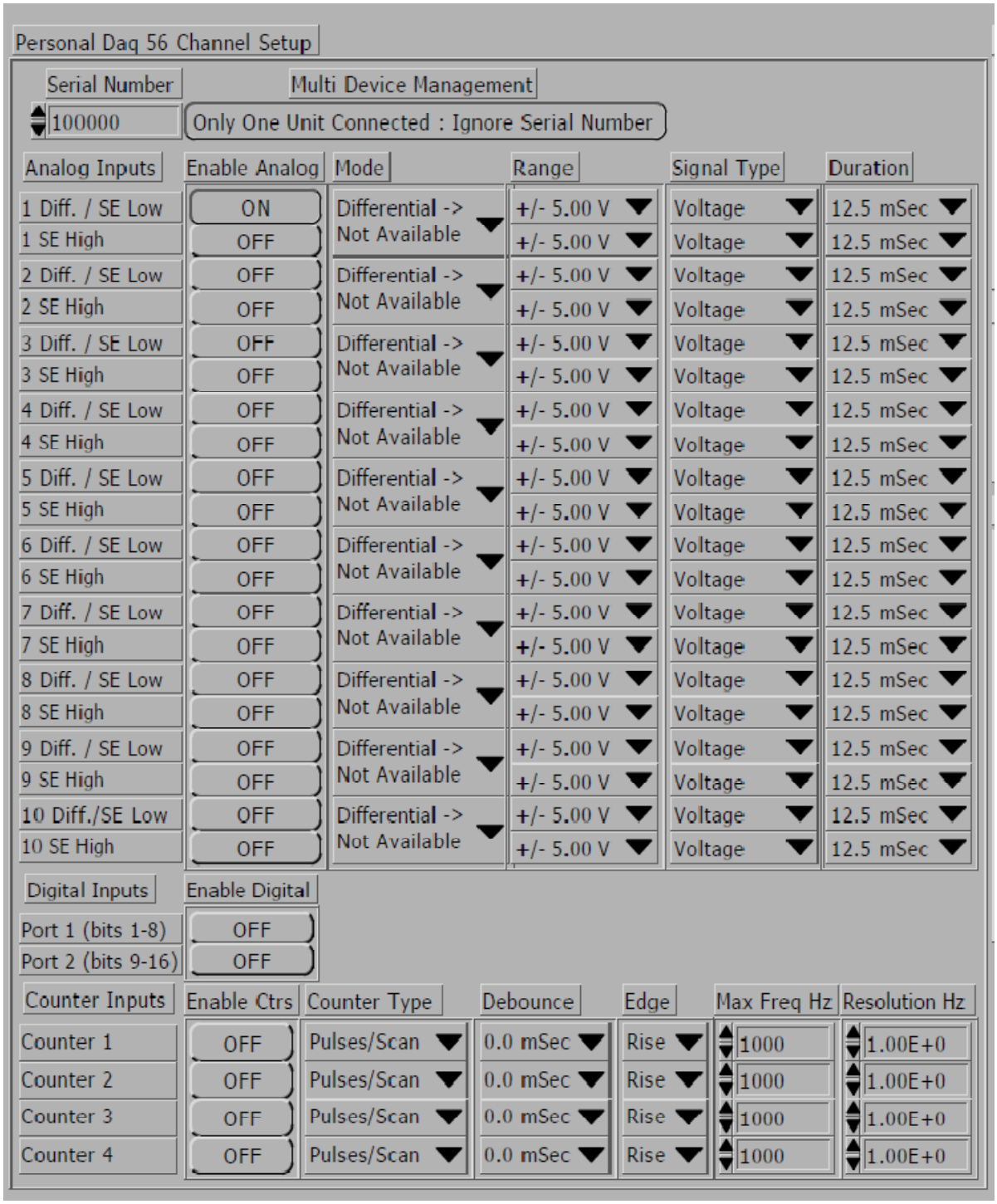

FIGURE C.1 LABVIEW FRONT PANEL CHANNEL SETUP

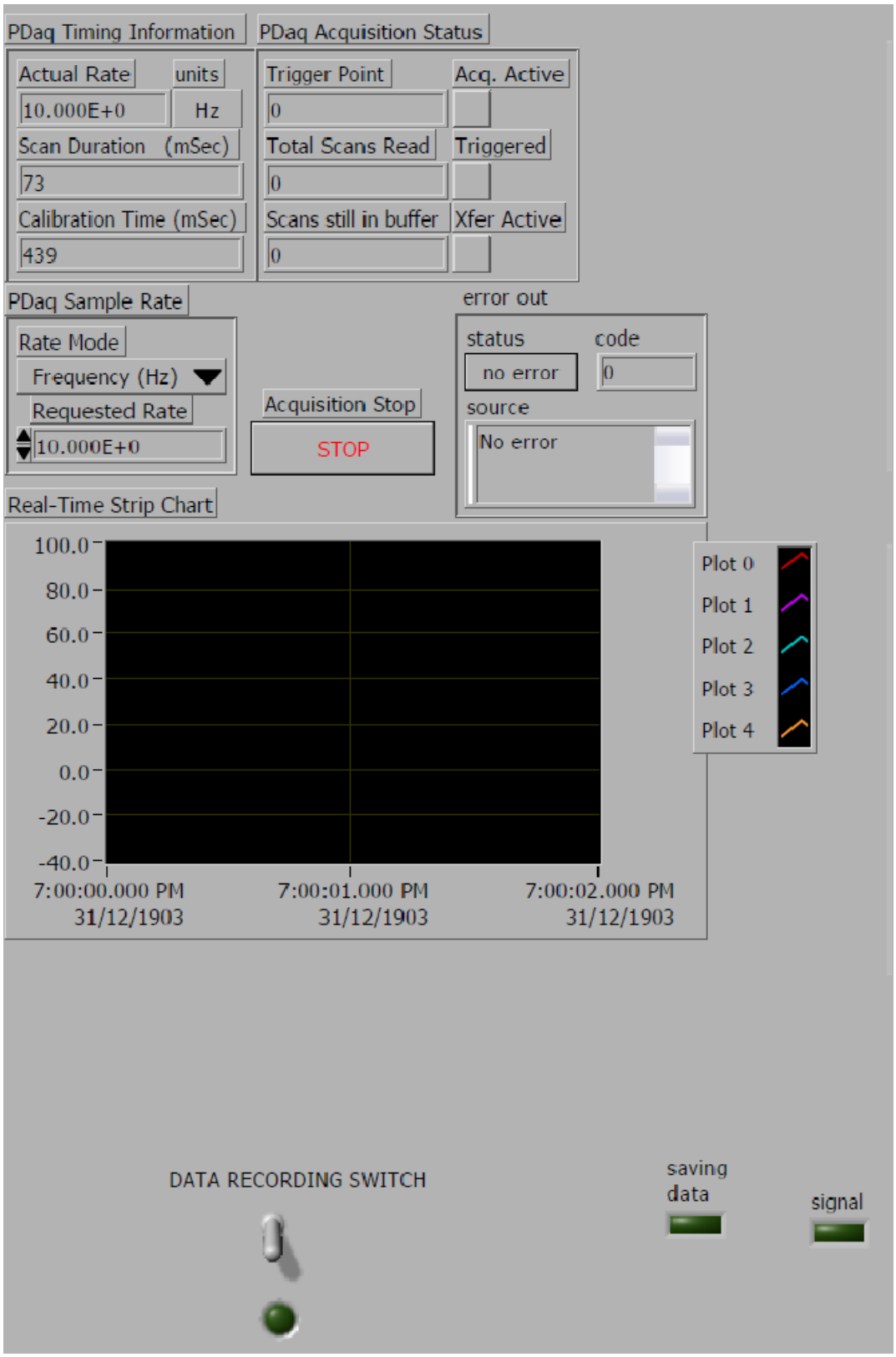

FIGURE C.2 LABVIEW FRONT PANEL SAMPLING RATE AND DATA RECORDING SWITCH

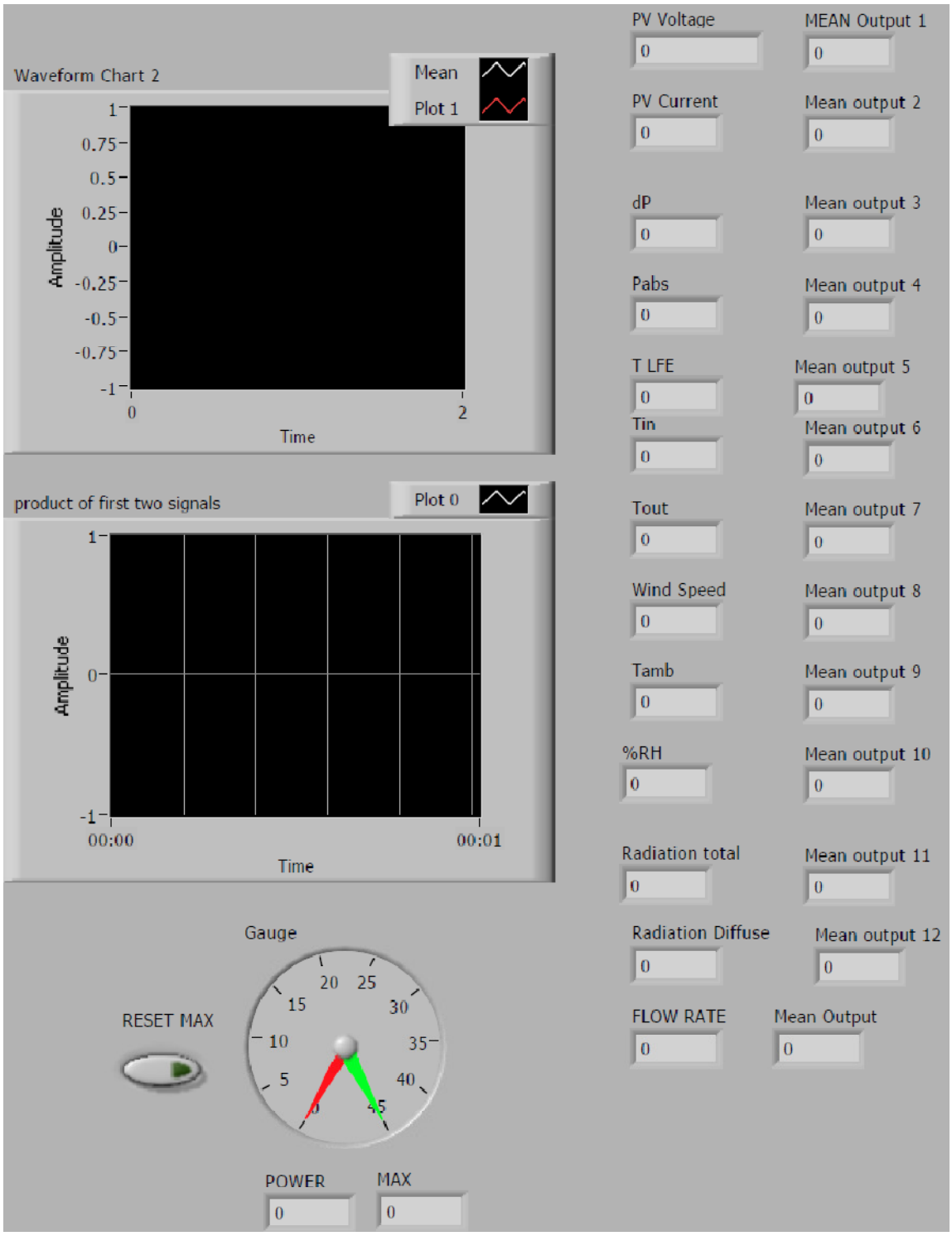

FIGURE C.3 LABVIEW FRONT PANEL OUTPUT VISUALISATION

Appendix D
UNCERTAINTY ANALYSIS

D.1 INTRODUCTION

When measuring the uncertainty of a measurement, bias and precision errors must be accounted for. The bias error is related to the accuracy of the measurement as well as the calibration. The precision error relates to the repeatability of the measurements. As this experiment was performed outdoors, it was very difficult to get measurements at different times with the exact same conditions. Therefore, only the bias error will be taken into consideration in the uncertainty analysis.

Kline and McClintock (1953) developed a method to calculate the bias error of calculated variables. For a calculated variable R, which is a function of n variables v_i, the uncertainty of R, δ_R can be found using

$$\delta_R = \left[\left(\frac{\partial R}{\partial v_1}\delta_{v_1}\right)^2 + \left(\frac{\partial R}{\partial v_2}\delta_{v_2}\right)^2 + \cdots + \left(\frac{\partial R}{\partial v_n}\delta_{v_n}\right)^2\right]^{\frac{1}{2}} \tag{4.1}$$

D.2 MEASURED VALUES

D.2.1 THERMOCOUPLE READINGS

The thermocouples used are type T thermocouples. They were calibrated with a thermistor of ±0.1°C accuracy. The calibration yielded an accuracy of ±0.2°C.

D.2.2 VOLTAGE AND CURRENT MEASUREMENTS FROM PV ARRAY

The DAQ's user manual reports an accuracy of 0.01% of reading + 0.002% of range. For the voltage measurements, the range was set to -10V to 10V. The maximum expected voltage is around 9V. The uncertainty for this particular voltage can be calculated with

$$\begin{aligned}\delta_V &= (0.0001 \times reading + 0.00002 * range) \\ &= (0.0001 \times 9V + 0.00002 * 20V) = 0.0013V\end{aligned} \tag{4.2}$$

To measure the current, a voltage reading is taken across a known resistance. The current is calculated from I=V/R. R is 1 ± 0.01 Ω. A maximum voltage measurement by the DAQ of 5V is expected (equivalent to 5A current across the resistor). The measurement range is set to -10V to 10V. Using equation D.2, the voltage measurement has an uncertainty of ±0.0009V. For this measurement, the uncertainty of the current can be calculated the usual way with

$$\delta_I = \left[\left(\frac{\partial I}{\partial V}\delta_V\right)^2 + \left(\frac{\partial I}{\partial R}\delta_R\right)^2\right]^{\frac{1}{2}} = \left[\left(\frac{1}{R}\delta_V\right)^2 + \left(-\frac{V}{R^2}\delta_R\right)^2\right]^{\frac{1}{2}}$$
$$= \left[\left(\frac{1}{1\Omega}0.0009V\right)^2 + \left(-\frac{5V}{(1\Omega)^2}0.01\Omega\right)^2\right]^{\frac{1}{2}} = 0.05A \tag{4.3}$$

D.2.3 IRRADIANCE

Eppley lab pyranometers were used to measure the total and diffuse incident radiation. They output a voltage proportional to the incident radiation with 10.26μV/Wm^{-2} and 8.04μV/Wm^{-2}.

For the 10.26μV/Wm^{-2} pyranometer, the maximum expected output is 10.26mV (for 1000W/m^2). For a range of -31 to 31mV, this gives a DAQ error of 2.266μV. The pyranometer has a 5% error. The total measurement error is

$$\frac{\delta_G}{G} = \left[\left(\frac{\delta_V}{V}\right)^2 + \left(\frac{\delta_{V_{DAQ}}}{V_{DAQ}}\right)^2\right]^{\frac{1}{2}} = \left[(0.05)^2 + \left(\frac{2.266\mu V}{10.26mV}\right)^2\right]^{\frac{1}{2}} = 0.050 \tag{4.4}$$

Therefore, the pyranometer uncertainty is $\delta_G = 1000\ W/m^2 \times 0.05 = 50\ W/m^2$.

D.2.4 PRESSURE DIFFERENTIAL

An Omega PX277 differential pressure transmitter was used to measure the pressure drop across the laminar flow element. Its accuracy is ±1% of the full range. The pressure transmitter was set for a range of 0 – 7.5" H2O at a voltage of

0 - 10VDC. At a typical pressure differential of 1.35" H2O, the error can be calculated.

If the DAQ range is set at -10V to 10V, and the voltage output from the pressure transmitter is 1.8V, this gives a DAQ error of 580μV.

$$\frac{\delta_{\Delta P}}{\Delta P} = \left[\left(\frac{\delta_V}{V}\right)^2 + \left(\frac{\delta_{V_{DAQ}}}{V_{DAQ}}\right)^2\right]^{\frac{1}{2}} = \left[\left(\frac{7.5"H2O \times 0.01}{1.35"H2O}\right)^2 + \left(\frac{580\mu V}{1.8V}\right)^2\right]^{\frac{1}{2}} = 0.056 \quad (4.5)$$

Therefore, the pressure differential uncertainty is $\delta_{\Delta P} = 1.35"H2O \times 0.056 = 0.076"H2O$.

D.2.5 ABSOLUTE PRESSURE

An Omega PX209 solid state pressure transducer was used to measure the absolute pressure of the air coming in the LFE. Its accuracy is 0.25% of full scale. The transducer gave a 0 – 5VDC signal for a 0 – 30PSIA pressure. At a typical pressure of 14.6PSIA, the error can be calculated.

If the DAQ range is set at -5V to 5V, and the voltage output from the pressure transmitter is 2.43V, this gives a DAQ error of 443μV.

$$\frac{\delta_P}{P} = \left[\left(\frac{\delta_V}{V}\right)^2 + \left(\frac{\delta_{V_{DAQ}}}{V_{DAQ}}\right)^2\right]^{\frac{1}{2}} = \left[\left(\frac{30PSIA \times 0.0025}{14.6PSIA}\right)^2 + \left(\frac{443\mu V}{2.43V}\right)^2\right]^{\frac{1}{2}} = 0.0051 \quad (4.6)$$

Therefore, the pressure absolute pressure uncertainty is $\delta_P = 14.6PSIA \times 0.0051 = 0.074PSIA$.

D.2.6 WIND SPEED

The anemometer had an accuracy of 0.3m/s + 1% of reading. The anemometer gave a 0-1V signal for a 0-50m/s wind speed. For a typical value of 4m/s, the signal is 0.08V.

$$\frac{\delta_{V_{wind}}}{V_{wind}} = \left[\left(\frac{\delta_V}{V}\right)^2 + \left(\frac{\delta_{V_{DAQ}}}{V_{DAQ}}\right)^2\right]^{\frac{1}{2}} = \left[\left(\frac{0.3 + 0.01 * 4}{4}\right)^2 + \left(\frac{28\mu V}{80mV}\right)^2\right]^{\frac{1}{2}} = 0.085 \tag{4.7}$$

Therefore, $\delta_{V_{wind}} = 0.085 * 4\ m/s = 0.34\ m/s$.

D.2.7 AMBIENT TEMPERATURE

The thermistor used for the ambient air temperature measurements has an accuracy of 0.1°C. The accuracy including the DAQ is:

$$\delta_{T_{amb}} = 100\frac{℃}{V} * \left[(\delta_V)^2 + \left(\delta_{V_{DAQ}}\right)^2\right]^{\frac{1}{2}} = 100\frac{℃}{V} * [(0.001V)^2 + (60\mu V)^2]^{\frac{1}{2}} = 0.1℃ \tag{4.8}$$

D.3 CALCULATED VALUES

D.3.1 VOLUMETRIC FLOW RATE

The volumetric flow rate was calculated with a laminar flow element (LFE). The LFE restricts the flow, and a quadratic equation correlates the standard flow rate and the pressure differential across the LFE. Equation D.9 shows the correlation given by the manufacturing company. The equation has an error of 0.72%.

$$CFM = (B \times \Delta P) + (C \times \Delta P^2) \tag{4.9}$$

Where B = 53.3672, and C = -0.0939819

$$\delta_{CFM} = \left[\left(\frac{\partial CFM}{\partial \Delta P}\delta_{\Delta P}\right)^2 + \left(\delta^{Corrolation}{}_{CFM}\right)^2\right]^{\frac{1}{2}} = \left[\left((B + 2C\Delta P)\delta_{\Delta P}\right)^2 + \left(\delta^{Corr}{}_{CFM}\right)^2\right]^{\frac{1}{2}} \tag{4.10}$$

For a typical value of 72CFM, the pressure differential would be 1.35" H2O. Given these values, we can estimate the error for the volumetric flow rate.

$$\delta_{CFM} = \left[\left((53.3672 + 2 \times -0.0939819 \times 1.35)0.076\right)^2 + (0.0072 \times 72)^2\right]^{\frac{1}{2}} = 4.1\ CFM \tag{4.11}$$

D.3.2 MASS FLOW RATE

The mass flow can be calculated from knowing the volumetric flow rate, the temperature and pressure of the fluid coming in the LFE, and the density of the fluid at standard conditions (0.0745lb/ft^3). A conversion factor is used to convert to SI units.

$$\dot{m} = CFM \times \frac{P}{P_{STD}} \times \frac{T_{STD}}{T} \times \rho_{STD} \times \left[\frac{0.00755987\ {}^{kg}/_{s}}{1\ {}^{lb}/_{minute}}\right] \tag{4.12}$$

The error is dependent on the error of the CFM, the pressure, and the temperature.

$$\delta_{\dot{m}} = \left[\left(\frac{\partial \dot{m}}{\partial P}\delta_P\right)^2 + \left(\frac{\partial \dot{m}}{\partial CFM}\delta_{CFM}\right)^2 + \left(\frac{\partial \dot{m}}{\partial T}\delta_T\right)^2\right]^{\frac{1}{2}} = \left[\frac{0.00755987\ {}^{kg}/_{s}}{1\ {}^{lb}/_{minute}}\right]\left[\left(\frac{CFM}{P_{STD}} \times \frac{T_{STD}}{T} \times \rho_{STD} \times \delta_P\right)^2 + \left(\frac{P}{P_{STD}} \times \frac{T_{STD}}{T} \times \rho_{STD} \times \delta_{CFM}\right)^2 + \left(CFM \times \frac{P}{P_{STD}} \times \frac{T_{STD}}{T^2} \times \rho_{STD} \times \delta_T\right)^2\right]^{\frac{1}{2}} \tag{4.13}$$

For typical values of 72CFM, 0°C, and 14.6 PSI_{abs} , we can solve for the error of the mass flow rate. The standard temperature and pressure were 21.1°C and 14.7PSI.

$$\delta_{\dot{m}} = \left[\frac{0.00755987\,{}^{kg}/_{s}}{1\,{}^{lb}/_{minute}}\right] \times 0.0745\frac{lb}{ft^3} \times \left[\left(\frac{72CFM}{14.7PSI} \times \frac{294.25K}{273.15K} \times 0.074PSIA\right)^2 + \left(\frac{14.6PSI}{14.7PSI} \times \frac{294.25K}{273.15K} \times 4.1CFM\right)^2 + \left(72CFM \times \frac{14.6PSI}{14.7PSI} \times \frac{294.25K}{(273.15K)^2} \times 0.2℃\right)^2\right]^{\frac{1}{2}} = 0.00248kg/s \tag{4.14}$$

The flow rate for those same typical values is:

$$\begin{aligned}\dot{m} &= CFM \times \frac{P}{P_{STD}} \times \frac{T_{STD}}{T} \times \rho_{STD} \times \left[\frac{0.00755987\,{}^{kg}/_{s}}{1\,{}^{lb}/_{minute}}\right] \\ &= 72 \times \frac{14.6PSI}{14.7PSI} \times \frac{294.25K}{273.15K} \times 0.0745\frac{lb}{ft^3} \times \left[\frac{0.00755987\,{}^{kg}/_{s}}{1\,{}^{lb}/_{minute}}\right] \\ &= 0.0434kg/s\end{aligned} \tag{4.15}$$

D.3.3 PV Power

The power from all the PV cells is taken as:

$$P_{elec} = V \times I \tag{4.16}$$

As mentioned earlier, the maximum expected current is 5A, and the maximum expected voltage is 9V. The power will therefore be 45W. Taking the errors for current and voltage calculated earlier, the error can be calculated with:

$$\delta_{P_{elec}} = \left[\left(\frac{\partial P_{elec}}{\partial V}\delta_V\right)^2 + \left(\frac{\partial P_{elec}}{\partial I}\delta_I\right)^2\right]^{\frac{1}{2}} = [(I \times \delta_V)^2 + (V \times \delta_I)^2]^{\frac{1}{2}} \tag{4.17}$$
$$= [(5A \times 0.0013V)^2 + (9V \times 0.05A)^2]^{\frac{1}{2}} = 0.45W$$

D.3.4 USEFUL HEAT GAIN

The useful heat gain is found with:

$$Q = \dot{m}C(T_{out} - T_{in}) \tag{4.18}$$

Typical values for C, mass flow rate, and the inlet and outlet temperatures are: 1009 J/kg K, 0.0434kg/s, 273.15K, and 283.87K.

This would yield a useful heat gain of 469.5W.

Because getting an error for the specific heat C is very difficult, it will be omitted from the calculations.

$$\delta_Q = \left[\left(\frac{\partial Q}{\partial \dot{m}}\delta_{\dot{m}}\right)^2 + \left(\frac{\partial Q}{\partial T_{out}}\delta_{T_{out}}\right)^2 + \left(\frac{\partial Q}{\partial T_{in}}\delta_{T_{in}}\right)^2\right]^{\frac{1}{2}}$$
$$= \left[(C(T_{out} - T_{in})\delta_{\dot{m}})^2 + \left(\dot{m}C\delta_{T_{out}}\right)^2 + \left(-\dot{m}\,C\delta_{T_{in}}\right)^2\right]^{\frac{1}{2}}$$
$$= [(1009\ \text{J/kg K}(283.87K - 273.15K)0.00248kg/s)^2 \tag{4.19}$$
$$+ (0.0434kg/s \times 1009\ \text{J/kg K} \times 0.2K)^2$$
$$+ (-0.0434kg/s \times 1009\ \text{J/kg K} \times 0.2K)^2]^{\frac{1}{2}} = 29.5W$$

Appendix E

RAW DATA SAMPLE

This data is from March 31st. The original data was taken every 0.5 seconds. This is the 5 minutes averaged data. To access all of the original data, contact the Solar Thermal Research Laboratory at the University of Waterloo.

PV Voltage	PV Current	dP [in H2O]	Pabs [PSI]	TLFE [K]	Tin [K]	Tout [K]	W [m/s]	Tamb [K]	%RH	S [W/m^2]	Sbackup [W/m^2]	mdot [kg/s]	PV [W]	Time
-9.628	-0.2409	1.24	14.22	272.71	272.16	270.74	0.81671	272.85	78.29	258.988	254.098	0.04146	2.379	8.0833
-9.1346	-0.9663	1.24	14.23	276.22	276.47	275.82	0.41623	273.1	77.73	315.929	313.029	0.0404	8.823	8.1667
-8.7813	-1.0057	1.23	14.24	276.94	276.94	277.25	0.10244	273.62	75.85	346.39	336.098	0.04007	9.086	8.25
-8.1633	-1.106	1.26	14.23	278.32	278.46	278.25	0.68278	274.11	72.63	366.739	365.683	0.04061	9.57	8.3333
-8.92	-1.3108	1.25	14.22	276.39	277.71	278.84	0.88091	274.45	69.29	394.913	383.768	0.04079	11.69	8.4167
-8.803	-1.4363	1.23	14.22	275.26	277.17	279.76	0.35565	274.78	66.52	418.274	407.843	0.04054	12.64	8.5
-8.6982	-1.5448	1.24	14.22	275.71	276.79	279.71	0.70649	275.23	64.69	442.465	427.965	0.04047	13.42	8.5833
-8.8044	-1.6211	1.24	14.22	276.6	277.51	280.38	0.65928	275.55	63.84	466.911	449.096	0.04051	14.27	8.6667
-8.8999	-1.6479	1.25	14.22	276.79	277.75	281.16	1.2314	275.97	60.33	486.029	469.869	0.04057	14.66	8.75
-8.5235	-1.8178	1.24	14.22	277.05	278.13	282.22	0.82084	276.37	59.12	504.543	486.294	0.04037	15.49	8.8333
-8.6602	-1.8454	1.25	14.22	277.92	279.14	282.92	0.22838	276.93	57.92	526.767	504.741	0.04031	15.98	8.9167
-8.7628	-1.8665	1.25	14.22	278.38	279.7	284.03	0.55329	277.58	56.22	548.351	526.164	0.04021	16.36	9
-8.6619	-1.9544	1.28	14.21	278.73	280.51	285.26	0.6353	277.86	56.14	571.072	543.919	0.04099	16.9	9.0833
-8.4068	-2.126	1.26	14.22	279.83	282.27	287.98	1.14326	278.12	56.27	592.564	561.611	0.04017	17.87	9.1667
-8.4954	-2.1472	1.27	14.22	280.22	282.57	288.92	1.00343	278.35	57.81	612.947	580.585	0.04039	18.24	9.25
-8.5387	-2.1667	1.29	14.21	281.15	283.36	289.76	0.49618	278.78	57.75	632.006	598.26	0.04067	18.5	9.3333
-8.0338	-2.405	1.29	14.2	281.86	284.39	290.77	0.42346	279.35	56.87	647.378	611.583	0.04042	19.32	9.4167
-8.1437	-2.4372	1.28	14.21	282.04	284.43	291.3	0.55014	279.83	56.12	671.936	632.788	0.04031	19.85	9.5
-8.0145	-2.5404	1.27	14.19	282.68	285.38	292.48	0.56445	280.45	55.15	693.855	651.709	0.03956	20.36	9.5833
-7.8873	-2.6456	1.3	14.19	283.41	285.88	293.2	0.80414	280.89	55.27	713.642	670.101	0.04031	20.87	9.6667
-7.8695	-2.6469	1.3	14.19	282.96	285.23	293.13	1.108	281.3	54.99	715.076	670.921	0.04044	20.83	9.75
-7.9569	-2.6756	1.26	14.21	282.51	284.7	293.37	1.5791	281.46	55.43	738.257	690.597	0.03958	21.29	9.8333
-8.0139	-2.6938	1.27	14.2	283.21	285.42	294	1.34155	281.92	54.86	756.643	709.363	0.03956	21.59	9.9167
-8.026	-2.7294	1.28	14.2	283.42	285.66	294.31	1.73149	282.2	54.36	776.844	724.88	0.03974	21.9	10
-7.8622	-2.8608	1.28	14.19	283.98	286.54	295.84	1.75858	282.22	54.43	796.568	742.664	0.03952	22.49	10.083
-7.8702	-2.8642	1.27	14.19	284.4	287.26	296.58	1.89762	282.28	54.21	800.908	747.699	0.03925	22.54	10.167
-7.7565	-2.9774	1.27	14.18	284.53	287.28	296.89	1.95173	282.29	54.02	823.152	766.886	0.03919	23.08	10.25
-7.6452	-3.0715	1.27	14.17	285.62	287.78	296.81	0.72518	282.88	53.02	840.67	783.354	0.03893	23.48	10.333
-7.5358	-3.0274	1.28	14.18	285.75	288.26	297.12	0.79921	283.58	51	816.17	761.12	0.03925	22.81	10.417
-7.5074	-3.0248	1.3	14.17	285.38	288.08	297.46	1.47633	283.23	51.68	811.799	756.39	0.03988	22.71	10.5
-7.4903	-3.0172	1.31	14.17	286.25	288.4	297.7	0.69374	283.39	51.99	807.381	754.608	0.03987	22.6	10.583
-7.428	-2.9917	1.29	14.18	286.84	289.19	297.85	0.52094	284.21	50.16	795.672	742.451	0.03921	22.22	10.667

-7.552	-3.0414	1.29	14.17	287.35	289.8	298.62	0.32934	284.28	50.1	828.499	774.513	0.03917	22.97	10.75
-7.5041	-3.1225	1.28	14.16	287.64	290.22	299	0.76538	284.61	49.31	856.451	798.661	0.03862	23.43	10.833
-7.5871	-3.1579	1.28	14.15	287.61	290.04	299.53	0.74323	285.11	48.8	888.34	824.122	0.03871	23.96	10.917
-7.5814	-3.2287	1.29	14.16	287.64	290.14	300.06	1.23305	285.04	48.78	922.51	854.821	0.03889	24.46	11
-7.0097	-3.5268	1.38	14.16	286.98	289.65	300.14	1.49377	284.97	48.86	931.419	863.926	0.04185	24.72	11.083
-6.9212	-3.481	1.38	14.17	287.69	290.15	300.19	1.02197	285.28	48.03	906.387	845.007	0.04186	24.09	11.167
-6.8491	-3.4449	1.38	14.16	287.36	290.1	300.07	2.0827	285.23	47.4	890.816	829.513	0.04167	23.6	11.25
-6.9569	-3.3562	1.37	14.17	286.86	289.63	299.99	2.07243	285.09	47.27	875.659	816.925	0.04178	23.33	11.333
-7.4291	-3.2693	1.37	14.17	287.27	289.41	299.37	1.97069	285.13	46.58	901.729	838.638	0.04153	24.3	11.417
-7.4591	-3.2805	1.37	14.18	287.92	290.18	300.07	1.21903	285.54	46.37	913.444	852.835	0.04146	24.47	11.5
-7.4638	-3.2836	1.38	14.18	287.95	290.33	300.18	1.6747	285.71	45.93	930.994	866.876	0.04174	24.54	11.583
-7.4557	-3.2794	1.37	14.17	287.79	290.33	300.51	1.39213	286.03	44.93	927.707	864.611	0.04151	24.46	11.667
-7.2441	-2.882	1.37	14.16	287.91	290.31	300.22	1.76516	286.09	43.83	802.704	753.883	0.04138	20.96	11.75
-7.1604	-3.3952	1.38	14.16	288.76	290.54	299.56	0.82194	286.41	43.68	920.343	854.003	0.04132	24.27	11.833
-7.0727	-3.5565	1.33	14.15	289.11	291.39	300.93	0.97322	286.9	43.37	955.395	893.824	0.03987	25.15	11.917
-6.931	-3.4888	1.31	14.16	289.63	292.48	302.38	1.20568	286.93	42.17	920.155	864.48	0.03925	24.19	12
-6.8959	-3.471	1.33	14.16	289.77	292.59	302.53	1.08398	286.89	41.45	910.709	854.215	0.03963	23.94	12.083
-6.9175	-3.4805	1.33	14.16	290.29	293.12	302.89	0.72186	287.21	40.93	913.627	859.009	0.03964	24.08	12.167
-6.928	-3.4861	1.32	14.15	289.68	292.77	302.96	1.15703	287.57	38.12	916.479	858.216	0.03954	24.15	12.25
-6.9794	-3.5111	1.32	14.16	289.88	292.48	303.1	0.84835	287.47	36.88	930.002	871.988	0.03934	24.51	12.333
-7.0038	-3.5237	1.32	14.15	289.84	292.66	303.16	0.64159	287.9	37.36	939.645	881.642	0.03949	24.68	12.417
-6.9789	-3.5106	1.33	14.16	290.24	292.97	303.19	1.08031	287.55	37.92	933.1	873.031	0.03964	24.5	12.5
-6.9242	-3.4834	1.32	14.15	289.77	292.44	303.13	1.31091	287.68	34.45	918.456	859.179	0.0394	24.12	12.583
-6.5576	-3.3001	1.31	14.14	290.58	293.14	303.03	0.89662	287.82	32.96	842.051	793.775	0.03878	21.65	12.667
-6.32	-3.1821	1.31	14.17	291.03	293.93	302.95	0.82031	288.23	31.77	803.336	762.025	0.03891	20.12	12.75
-6.6621	-3.3546	1.31	14.16	290.84	294.26	303.35	1.03801	288.45	33.49	859.7	811.065	0.03878	22.37	12.833
-7.1114	-3.5777	1.31	14.16	290.7	293.7	303.45	0.89996	288.31	34.34	974.009	911.339	0.03899	25.44	12.917
-7.1375	-3.5897	1.32	14.15	291.87	294.59	304.49	0.83621	288.77	33.2	995.5	934.74	0.03872	25.62	13
-7.128	-3.584	1.32	14.14	291.68	294.79	305.19	0.91894	289.03	31.95	1001.42	940.517	0.03877	25.55	13.083
-7.1002	-3.5699	1.33	14.13	291.48	294.83	305.43	1.36691	288.94	31.57	994.769	934.493	0.0391	25.35	13.167
-6.4172	-3.2282	1.37	14.14	291.63	295.22	305.3	0.61919	289.24	31.31	831.966	794.13	0.04031	20.77	13.25
-6.1142	-3.0767	1.37	14.15	291.73	295.2	304.36	1.54619	289.2	30.7	784.021	747.303	0.04047	19.01	13.333
-5.3322	-2.6133	1.37	14.14	291.22	294.44	303.19	1.79174	288.63	30.18	652.461	622.063	0.0405	14.08	13.417
-8.304	-2.0473	1.37	14.13	291.4	294.55	302.21	1.7306	288.81	30.27	648.271	618.211	0.04044	17.01	13.5
-8.5064	-2.0826	1.38	14.13	291.52	294.54	301.9	1.5789	289.03	29.43	724.194	688.326	0.04071	17.72	13.583
-7.5317	-1.8438	1.38	14.13	291.53	294.71	301.73	1.61033	289.14	30.17	523.152	507.581	0.04076	13.98	13.667
-7.6396	-1.5493	1.38	14.14	291.21	294.34	300.33	1.94731	288.83	29.1	405.82	396.495	0.04079	11.83	13.75
-7.476	-1.5071	1.38	14.14	290.97	293.96	299.17	1.98869	288.69	27.85	386.965	378.054	0.04093	11.28	13.833
-8.1255	-1.6378	1.38	14.14	290.87	293.94	298.61	1.73119	288.68	28.81	448.439	435.102	0.04083	13.32	13.917
-8.4043	-1.7902	1.35	14.14	291.07	293.91	298.83	2.1156	288.74	29.9	530.047	513.388	0.03999	15.02	14
-8.0328	-1.852	1.37	14.12	291.15	294.22	299.34	1.28423	288.97	29.55	506.682	491.378	0.04042	14.88	14.083

-7.9579	-1.7287	1.38	14.13	291.01	294.08	298.98	1.74557	289.28	29.64	467.748	455.512	0.04078	13.75	14.167
-7.7913	-1.6087	1.38	14.14	290.95	293.74	298.36	2.13154	288.81	30.87	426.619	416.498	0.04095	12.54	14.25
-7.9831	-1.6483	1.38	14.14	290.77	293.66	298.25	2.16377	288.91	29.32	445.158	434.741	0.04084	13.16	14.333
-8.2713	-1.7072	1.38	14.13	290.89	293.74	298.31	1.63765	288.99	30.76	483.201	470.521	0.04085	14.12	14.417
-8.4576	-1.7459	1.39	14.13	291.2	294.17	298.73	1.4265	289.24	29.81	526.398	510.312	0.04102	14.77	14.5
-8.1776	-1.6878	1.39	14.12	290.95	293.99	298.86	2.61575	289	29.15	480.733	469.16	0.04105	13.82	14.583
-8.5779	-1.7705	1.39	14.12	290.85	293.73	298.69	3.04872	288.81	30.49	570.038	548.457	0.0411	15.2	14.667
-8.9287	-1.8426	1.39	14.11	291.53	294.15	299.74	2.41401	289	30.42	765.451	732.308	0.04099	16.45	14.75
-8.896	-1.8353	1.39	14.11	291.82	294.66	301	2.46101	289.22	28.48	804.609	769.92	0.0408	16.33	14.833
-8.8044	-1.8165	1.39	14.12	292.11	295.06	301.87	2.58446	289.53	28.61	763.622	736.584	0.04084	15.99	14.917
-8.6811	-1.7907	1.4	14.12	291.85	294.79	301.76	2.78623	289.44	29.3	685.432	665.189	0.04115	15.55	15
-8.4965	-1.7534	1.41	14.12	292.4	295.11	300.98	1.52969	289.91	29.94	588.773	570.914	0.04139	14.91	15.083
-7.3272	-2.6474	1.36	14.11	292.14	295.38	301.58	2.46587	289.97	29.7	759.384	732.607	0.03992	19.28	15.167
-6.779	-2.7304	1.37	14.11	292.35	295.28	301.95	2.10233	289.78	29.75	721.046	698.923	0.04018	18.65	15.25
-6.8721	-2.7663	1.38	14.11	292.53	295.51	301.99	2.47861	290.25	28.84	726.538	706.496	0.04048	19.03	15.333
-7.1415	-2.6503	1.38	14.12	292.37	295.43	302.23	2.58945	290.2	29.31	712.754	694.917	0.04048	18.89	15.417
-7.4226	-2.4207	1.39	14.12	292.48	295.49	301.82	2.47122	290.3	29.96	660.024	646.23	0.04072	17.98	15.5
-7.4159	-2.3946	1.4	14.12	292.3	295.26	301.46	2.97902	290.31	29.11	649.426	637.599	0.04087	17.76	15.583
-7.328	-2.3665	1.4	14.12	292.21	295	301.19	2.6489	290.07	27.4	639.022	629.768	0.04091	17.34	15.667
-7.1989	-2.2967	1.4	14.12	292.04	294.91	300.8	3.45741	289.95	26.9	619.261	611.287	0.04108	16.53	15.75
-7.9108	-2.1107	1.41	14.12	292.29	295.29	300.73	2.44689	290	24.95	609.241	605.558	0.0413	16.7	15.833
-7.7552	-2.0606	1.41	14.12	292.11	295.1	300.35	2.46676	290.13	25.03	583.004	581.491	0.04131	15.98	15.917
-7.1622	-1.903	1.41	14.12	292.51	295.43	300.22	1.93173	290.46	25.81	527.622	531.785	0.04133	13.71	16
-6.3959	-1.7006	1.43	14.12	292.38	295.54	299.67	2.27026	290.49	26.85	467.113	472.978	0.04179	10.91	16.083
-6.2613	-1.6661	1.44	14.12	292.22	295.36	299.26	2.41723	290.29	29.12	461.318	467.017	0.0421	10.45	16.167
-6.1919	-1.648	1.39	14.12	291.92	295.08	299.09	3.09997	289.96	29.99	463.728	470.256	0.0409	10.22	16.25
-5.8247	-1.551	1.38	14.12	292.14	295.11	298.9	2.22203	290.15	28.82	448.117	457.355	0.04034	9.048	16.333
-4.9242	-1.3111	1.38	14.12	291.62	294.84	298.55	2.7888	289.91	29.18	384.37	394.991	0.04047	6.492	16.417

Appendix F
TRNSYS OUPUT SAMPLE

This sample of the TRNSYS output is for the same data as found in Appendix E. To access all of the original output data, contact the Solar Thermal Research Laboratory at the University of Waterloo.

TIME	elecexp	elecss	electransient	angle	elecexp	Tss	Texp	Ttransient	QuExp	QuTransient
0.00	0.00	0.00	0.00	0.00	258.99	0.00	270.74	275.00	-0.14	0.00
0.08	2.38	7.07	7.09	60.30	258.99	274.58	270.74	274.02	-58.98	77.82
0.17	8.82	8.48	8.57	59.05	315.93	279.22	275.82	277.71	-26.27	50.43
0.25	9.09	9.36	9.42	57.81	346.39	280.07	277.25	278.97	12.54	81.89
0.33	9.57	9.91	9.97	56.56	366.74	281.71	278.25	280.68	-8.53	90.59
0.42	11.69	10.78	10.82	55.31	394.91	281.37	278.84	280.76	46.72	125.35
0.50	12.64	11.52	11.55	54.06	418.27	281.21	279.76	280.77	105.70	147.14
0.58	13.42	12.28	12.30	52.82	442.47	281.21	279.71	280.84	118.78	164.76
0.67	14.27	12.96	13.01	51.57	466.91	282.19	280.38	281.67	117.21	169.41
0.75	14.66	13.53	13.57	50.32	486.03	282.67	281.16	282.20	139.48	181.68
0.83	15.49	14.06	14.13	49.07	504.54	283.31	282.22	282.64	166.39	183.14
0.92	15.98	14.63	14.70	47.83	526.77	284.56	282.92	283.85	153.27	190.81
1.00	16.36	15.21	15.28	46.58	548.35	285.41	284.03	284.75	175.08	203.95
1.08	16.90	15.81	15.88	45.33	571.07	286.34	285.26	285.72	195.83	214.64
1.17	17.87	16.25	16.36	44.08	592.56	288.33	287.98	287.47	230.56	210.14
1.25	18.24	16.80	16.91	42.84	612.95	288.85	288.92	287.96	257.70	219.01
1.33	18.50	17.27	17.40	41.59	632.01	289.78	289.76	288.74	262.02	220.35
1.42	19.32	17.59	17.76	40.34	647.38	290.99	290.77	289.75	259.23	217.88
1.50	19.85	18.25	18.35	39.09	671.94	291.38	291.30	290.57	278.44	248.85
1.58	20.36	18.72	18.83	37.85	693.86	292.68	292.48	291.83	282.45	256.70
1.67	20.87	19.21	19.30	36.60	713.64	293.28	293.20	292.63	296.61	273.75
1.75	20.83	19.32	19.36	35.35	715.08	292.75	293.13	292.46	321.28	294.09
1.83	21.29	19.98	20.02	34.11	738.26	292.70	293.37	292.42	345.37	307.32
1.92	21.59	20.38	20.45	32.86	756.64	293.62	294.00	293.18	341.21	308.67
2.00	21.90	20.88	20.95	31.61	776.84	294.06	294.31	293.66	345.75	319.67
2.08	22.49	21.29	21.37	30.37	796.57	295.12	295.84	294.60	369.58	320.54
2.17	22.54	21.30	21.38	29.12	800.91	295.88	296.58	295.41	368.16	321.78
2.25	23.08	21.87	21.93	27.87	823.15	296.14	296.89	295.77	379.06	334.84
2.33	23.48	22.23	22.35	26.63	840.67	296.94	296.81	296.27	353.64	332.41
2.42	22.81	21.52	21.59	25.38	816.17	297.13	297.12	296.78	349.80	336.42
2.50	22.71	21.46	21.47	24.13	811.80	296.77	297.46	296.69	376.13	345.28

2.58	22.60	21.30	21.32	22.89	807.38	297.02	297.70	296.91	373.25	341.73
2.67	22.22	20.84	20.88	21.64	795.67	297.80	297.85	297.57	341.55	330.55
2.75	22.97	21.59	21.66	20.40	828.50	298.75	298.62	298.33	347.64	336.26
2.83	23.43	22.21	22.30	19.15	856.45	299.61	299.00	299.09	341.29	344.58
2.92	23.96	23.02	23.09	17.91	888.34	299.85	299.53	299.41	369.78	364.92
3.00	24.46	23.85	23.93	16.66	922.51	300.30	300.06	299.85	388.30	380.16
3.08	24.72	24.28	24.24	15.42	931.42	299.32	300.14	299.42	441.60	411.45
3.17	24.09	23.56	23.56	14.18	906.39	299.53	300.19	299.54	422.36	395.13
3.25	23.60	23.16	23.15	12.94	890.82	299.34	300.07	299.41	417.70	390.08
3.33	23.33	22.84	22.80	11.70	875.66	298.71	299.99	298.91	435.31	389.99
3.42	24.30	23.52	23.52	10.46	901.73	298.86	299.37	298.84	415.93	393.98
3.50	24.47	23.68	23.72	9.22	913.44	299.75	300.07	299.51	412.50	389.00
3.58	24.54	24.10	24.14	7.99	930.99	300.03	300.18	299.81	413.73	398.24
3.67	24.46	23.99	24.02	6.77	927.71	300.07	300.51	299.94	425.09	401.23
3.75	20.95	20.79	20.70	5.56	802.70	298.64	300.22	299.22	412.39	370.59
3.83	24.27	23.74	23.81	4.37	920.34	300.25	299.56	299.86	374.93	387.72
3.92	25.15	24.40	24.53	3.22	955.39	301.76	300.93	301.10	382.71	389.34
4.00	24.19	23.33	23.41	2.18	920.15	302.48	302.38	302.05	391.03	378.29
4.08	23.94	23.09	23.12	1.51	910.71	302.37	302.53	302.22	396.22	384.09
4.17	24.08	23.07	23.14	1.71	913.63	302.91	302.89	302.59	389.57	377.59
4.25	24.15	23.18	23.20	2.58	916.48	302.67	302.96	302.55	405.45	389.06
4.33	24.51	23.55	23.56	3.68	930.00	302.60	303.10	302.50	420.29	396.39
4.41	24.68	23.74	23.77	4.85	939.64	302.87	303.16	302.71	417.32	399.63
4.50	24.50	23.55	23.56	6.05	933.10	303.00	303.19	302.92	407.69	397.04
4.58	24.12	23.25	23.23	7.27	918.46	302.41	303.13	302.52	423.95	399.81
4.66	21.65	21.22	21.17	8.50	842.05	302.25	303.03	302.55	385.94	367.24
4.75	20.12	20.14	20.11	9.73	803.34	302.48	302.95	302.73	353.02	344.42
4.83	22.37	21.48	21.53	10.96	859.70	303.52	303.35	303.26	354.64	351.10
4.91	25.44	24.36	24.47	12.20	974.01	304.31	303.45	303.69	382.00	391.70
5.00	25.62	24.70	24.90	13.44	995.50	305.48	304.49	304.49	385.72	385.92
5.08	25.55	24.79	24.96	14.68	1001.42	305.74	305.19	304.94	405.44	395.72
5.16	25.35	24.64	24.74	15.93	994.77	305.59	305.43	305.13	416.83	404.92
5.25	20.77	20.70	20.60	17.17	831.97	303.78	305.30	304.41	408.97	372.95
5.33	19.01	19.50	19.42	18.41	784.02	303.16	304.36	303.76	372.70	348.62
5.41	14.08	16.27	16.11	19.66	652.46	300.82	303.19	302.06	356.36	310.18
5.50	17.01	16.14	16.03	20.90	648.27	300.88	302.21	301.76	311.81	293.67
5.58	17.72	18.08	18.07	22.15	724.19	301.76	301.90	301.83	301.71	298.71
5.66	13.98	12.91	12.81	23.39	523.15	299.53	301.73	300.67	288.07	244.62
5.75	11.83	9.96	9.86	24.64	405.82	297.82	300.33	299.17	245.76	198.17
5.83	11.28	9.51	9.42	25.89	386.96	297.23	299.17	298.51	214.73	187.41
5.91	13.32	11.06	11.03	27.13	448.44	297.92	298.61	298.28	191.55	178.27

6.00	15.02	13.15	13.17	28.38	530.05	298.89	298.83	298.65	198.13	190.95
6.08	14.88	12.52	12.52	29.63	506.68	298.91	299.34	298.86	208.08	188.65
6.16	13.75	11.54	11.52	30.87	467.75	298.31	298.98	298.54	201.28	183.28
6.25	12.54	10.51	10.48	32.12	426.62	297.47	298.36	297.91	190.70	172.19
6.33	13.16	10.99	10.98	33.37	445.16	297.62	298.25	297.77	188.61	169.06
6.41	14.12	11.95	11.96	34.61	483.20	298.15	298.31	298.01	188.05	175.42
6.50	14.77	13.02	13.05	35.86	526.40	299.04	298.73	298.65	188.19	185.14
6.58	13.82	11.87	11.86	37.11	480.73	298.28	298.86	298.40	201.23	182.18
6.66	15.20	14.18	14.21	38.36	570.04	299.02	298.69	298.67	205.10	204.28
6.75	16.45	19.08	19.26	39.60	765.45	301.66	299.74	300.36	230.45	256.05
6.83	16.33	19.94	20.08	40.85	804.61	302.56	301.00	301.57	260.21	283.94
6.91	15.99	18.87	18.94	42.10	763.62	302.42	301.87	301.91	279.61	281.62
7.00	15.55	16.94	16.92	43.35	685.43	301.30	301.76	301.44	288.72	275.53
7.08	14.91	14.45	14.41	44.59	588.77	300.57	300.98	301.03	244.43	246.28
7.16	19.28	18.55	18.64	45.84	759.38	302.82	301.58	302.14	248.92	271.25
7.25	18.65	17.61	17.61	47.09	721.05	302.19	301.95	302.09	269.90	275.49
7.33	19.03	17.65	17.67	48.34	726.54	302.42	301.99	302.24	263.75	273.95
7.41	18.89	17.26	17.25	49.58	712.75	302.14	302.23	302.16	277.24	274.49
7.50	17.98	15.95	15.91	50.83	660.02	301.53	301.82	301.83	259.17	259.76
7.58	17.76	15.65	15.62	52.08	649.43	301.13	301.46	301.41	254.82	252.96
7.66	17.34	15.35	15.31	53.33	639.02	300.70	301.19	300.99	255.06	246.57
7.75	16.53	14.81	14.75	54.57	619.26	300.30	300.80	300.75	243.60	241.42
7.83	16.70	14.43	14.41	55.82	609.24	300.47	300.73	300.71	226.01	225.41
7.91	15.98	13.74	13.69	57.07	583.00	299.96	300.35	300.43	218.28	221.72
8.00	13.71	12.34	12.31	58.32	527.62	299.80	300.22	300.16	199.31	196.86
8.08	10.91	10.90	10.87	59.56	467.11	299.25	299.67	299.72	173.49	175.98
8.16	10.45	10.68	10.65	60.81	461.32	298.93	299.26	299.31	165.20	167.22
8.25	10.22	10.61	10.59	62.06	463.73	298.65	299.09	298.95	164.95	159.45
8.33	9.05	10.13	10.11	63.30	448.12	298.53	298.90	298.85	153.94	152.01

Appendix G
MODEL VS EXPERIMENTAL HEAT GAIN

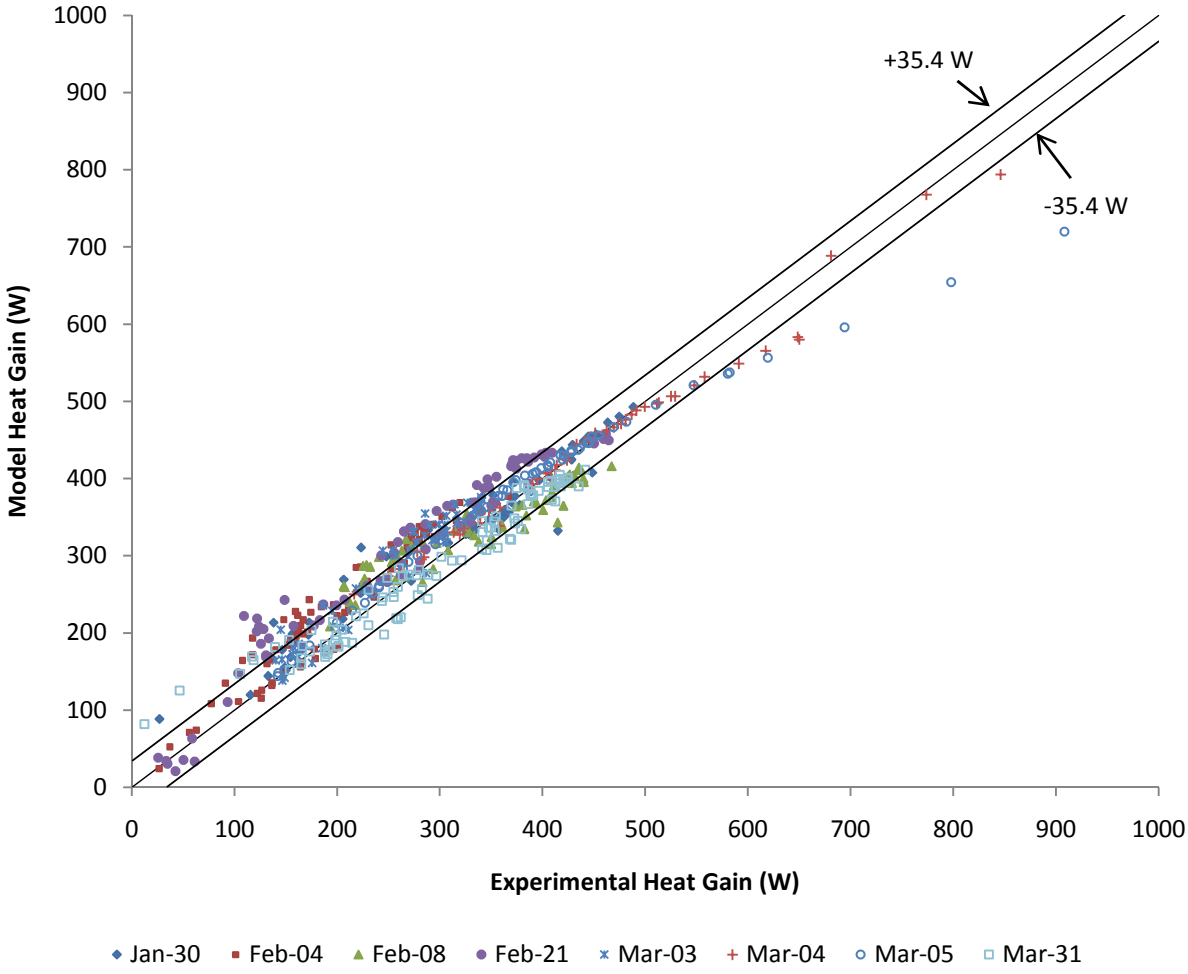

FIGURE G.1 MODELED VS EXPERIMENTAL HEAT GAIN FULL SCALE

BIBLIOGRAPHY

Aste N., Chiesa G., Verri F., Design, Development and Performance Monitoring of a Photovoltaic-Thermal (PVT) Air Collector, Renewable Energy, Volume 33, 2008

Assoa Y.B., Menezo C., Fraisse G., Yezou R., Brau J., Study of a New Concept of Photovoltaic-Thermal Hybrid Collector, Solar Energy, Volume 81, 2007

Belusko M., Saman W., Bruno F., Performance of Jet Impingement in Unglazed Air Collectors, Solar Energy, Volume 82, 2008

Bhargava A.K., Garg H.P., Agarwal R.K., Study of a Hybrid Solar System – Solar Air Heater Combined with Solar Cells, Energy Conversion and Management, Volume 31, 1991

Choudhury C., Garg H.P., Evaluation of a Jet Plate Solar Air Heater, Solar Energy, Volume 46, 1991

Dampney, Solar Selective Coating, http://www.dampney.com/Products/Products.asp?ProductID=28, retrieved on April 17, 2010.

De Soto W., Klein S.A., Beckman W.A., Improvement and Validation of a Model for Photovoltaic Array Performance, Solar Energy, Volume 80, 2006

Dow Corning, Dow Corning® 3-6753 Thermally Conductive Adhesive Kit, http://www.dowcorning.com/applications/search/products/details.aspx?prod=04031931&type=PROD, retrieved on April 17, 2010.

Duffie J.A., Beckman W.A., Solar Engineering of Thermal Processes, 3rd edition, John Wiley & Sons, New Jersey, 2006

Energy Information Agency, International Energy Outlook 2009, http://www.eia.doe.gov/oiaf/ieo/world.html, retrieved October 10 2009

Eppley Lab, Precision Spectral Pyranometer, http://www.eppleylab.com/PrdPrecSpectralPyrmtr.htm, retrieved on April 17, 2010.

Florschuetz L.W., Extension of the Hottel-Whillier Model to the Analysis of Combined Photovoltaic/Thermal Flat Plate Collectors, Solar Energy, Volume 22, 1979

Florschuetz, Metzger, and Truman, Jet Array Impingement With Crossflow - Correlation of Streamwise Resolved Flow and Heat Transfer Distributions, NASA Contractor Report 3373, 1981

Florschuetz, Metzger, Su, Isoda, and Tseng, Jet Array Impingement Flow Distributions and Heat Transfer Characteristics Effects of Initial Crossflow and Nonuniform Array Geometry, NASA Contractor Report 3630, 1982

Florschuetz L.W., Su C.C., Effects of Crossflow Temperature on Heat Transfer within an Array of Impinging Jets, ASME Journal of Heat Transfer, Volume 109, 1987

Gao L., Ekkad S.V., Bunker R.S., Impingement Heat Transfer, Part 1: Linearly Streched Arrays of Holes, Journal of Thermophysics and Heat Transfer, Volume 19, 2005

Garg H.P., Adhikari R.S., Conventional Hybrid Photovoltaic/Thermal (PV/T) Air Heating Collectors: Steady-State Simulation, Renewable Energy, Volume 11, 1997

Garg H.P., Adhikari R.S., Transient Simulation of Conventional Hybrid Photovoltaic/Thermal (PV/T) Air Heating Collectors, International Journal of Energy Research, Volume 22, 1998

Gier Dunkle Instruments, Inc., Infrared Reflectometer DB100 Operating Instructions, Santa Monica, California.

Gier Dunkle Instruments, Inc., Mobile Solar Reflectometer MS-251 Operating Instructions, Santa Monica, California.

Hollands K.G.T, Unny T.E., Raithby G.D., Konicek L., Free Convective Heat Transfer Across Inclined Air Layers, ASME Journal of Heat Transfer, Volume 96, 1976

International Energy Agency, Statistics for Renewables, http://www.iea.org/Textbase/stats/prodresult.asp?PRODUCT=Renewables, retrieved on April 17, 2010.

IPCC, Climate Change 2007: Synthesis Report, http://www.ipcc.ch/pdf/assessment-report/ar4/syr/ar4_syr.pdf, retrieved on April 17, 2010.

Kays W.M., Crawford M.E., Convective Heat and Mass Transfer, 2nd edition, McGraw-Hill, New York, 1980

Kercher D.M., Tabakoff W., Heat Transfer by a Square Array of Round Air Jets Impinging Perpendicular to a Flat Surface Including the Effects of Spent Air, ASME Journal of Engineering for Power, Volume 92, 1970

Klein S.A., Duffie J.A., Beckman W.A., Transient Considerations of Flat-Plate Solar Collectors, ASME Journal of Engineering for Power, Volume 96, 1974

Lloyd J.R., Moran W.P., Natural Convection Adjacent to Horizontal to Horizontal Surface of Various Planforms, ASME Journal of Heat Transfer, Volume 96, 1974

Meriam Process Technologies, Laminar Flow Elements, Installation & Operations Instructions, 2009

Metzger D.E., Florschuetz L.W., Takeuchi D.I., Behee R.D., Berry R.A., Heat Transfer Characteristics for Inline and Staggered Arrays of Circular Jets with Crossflow of Spent Air, ASME Journal of Heat Transfer, Volume 101, 1979

Moffat, R.J., Using uncertainty analysis in the planning of an experiment, Journal of Fluids Engineering, Transactions of the ASME, v107, n 2, p 173-178, 1985

NASA Atmospheric Science Data Center, Educational Resources, http://eosweb.larc.nasa.gov/EDDOCS/Teacher_Notes/resources.html, retrieved on January 14, 2010.

National Renewable Energy Laboratory, Parabolic Trough Solar Field Technology, http://www.nrel.gov/csp/troughnet/solar_field.html, retrieved on January 14 2010.

Natural Resources Canada, Office of Energy Efficiency, Canada's secondary energy use by sector, end-use and sub-sector, http://oee.nrcan.gc.ca/corporate/statistics/neud/dpa/tableshandbook2/aaa_ca_2_e_3.cfm?attr=0, retrieved on April 17, 2010

Omega, Differential Pressure Transmitter with Field Selectable Range, http://www.omega.com/ppt/pptsc.asp?ref=PX277, retrieved on April 17, 2010.

Omega, Solid State Pressure Transducer, http://www.omega.com/pptst/PX209_PX219.html, retrieved on April 17, 2010.

Othman M.Y., Yatim B., Sopian K., Bakar M.N.A., Double-Pass Photovoltaic-Thermal Solar Collector, Journal of Energy Engineering, Volume 132, 2006

Parretta A., Sarno A., Vicari L.R.M., Effects of Solar Irradiation Conditions on the Outdoor Performance of Photovoltaic Modules, Optics Communications, Volume 153, 1998

Parretta A., Sarno A., Yakubu H., Non-Destructive Optical Characterization of Photovoltaic Modules by an Integrating Sphere. Part I: Mono-Si Modules, Optics Communications, Volume 161, 1999a

Parretta A., Sarno A., Tortora P., Yakubu H., Maddalena P., Zhao J., Wang H., Angle-Dependent Reflectance Measurements on Photovoltaic Materials and Solar Cells, Optics Communications, Volume 172, 1999b

PPG, Starphire Table of Contents, http://corporateportal.ppg.com/NA/IdeaScapes/productInfo/glass/StarGlassTOC.htm , retrieved on April 17, 2010.

Rask D.R., Mueller L.J., Pejsa J.H., Low-Cost Solar Air Heater: Final Report, Prepared for U.S. Energy Research and Development Administration COO-2929-13, 1977

R.M. Young, Wind Monitor Model 05103, http://www.youngusa.com/products/7/5.html, retrieved on April 17, 2010.

Rubin, M. Optical properties of soda lime silica glasses, Solar Energy Materials Volume 12, p. 275-288, 1985

SAIC, Survey of active solar thermal collectors, Industry and markets in Canada 2006 and 2007, March 2008

Sartori E., Convection Coefficient Equations for Forced Air Flow Over Flat Surfaces, Solar Energy, Volume 80, 2006

Sjerps-Koomen E.A., Alsema E.A., Turkenburg W.C., A Simple Model for PV Module Reflection Losses Under Field Conditions, Solar Energy, Volume 57, 1996

U.S. Department of Energy, Solar Collectors, http://www1.eere.energy.gov/solar/sh_basics_collectors.html, retrieved on January 14, 2010.a

U.S. Department of Energy, Transpired Collectors, http://www1.eere.energy.gov/femp/pdfs/FTA_trans_coll.pdf, retrieved on January 14, 2010.b

Vaisala, Vaisala Humicap® Humidity and Temperature Probe HMP155, http://www.vaisala.com/weather/products/hmp155.html, retrieved on April 17, 2010.

Wijeysundera N.E., Response Time of Solar Collectors, Solar Energy, Volume 18, 1976